NMR SPECTROSCOPY FOR CHEMISTS

Martin Dračínský

NMR SPECTROSCOPY FOR CHEMISTS

Martin Dračínský

Praha 2025

IOCB
PRAGUE

This textbook aims to familiarize students of chemistry-related fields with the basic principles of nuclear magnetic resonance (NMR) and the use of NMR spectroscopy in structural analysis. The greatest emphasis is placed on explaining the relationships between molecular structure and their hydrogen (^{1}H) and carbon (^{13}C) NMR spectra. The content is primarily focused on the structure determination of "small" organic molecules. Therefore, this textbook is likely to be most useful for synthetic chemists, for whom the correct interpretation of NMR spectra is often crucial for the successful preparation of both new and known compounds. Separate chapters are also dedicated to the use of NMR spectroscopy for other nuclei (^{19}F, ^{31}P, ^{15}N), monitoring chemical reactions using NMR spectroscopy, and the measurement and interpretation of solid-state NMR spectra.

This textbook was originally published in Czech under the title *NMR Spektroskopie pro chemiky*. The Czech hardcover edition was made possible by the Chemistry Library of the Faculty of Science, Charles University, with the kind support of IOCB Tech s.r.o.

IOCB TECH Charles University

This textbook is based on my experience teaching NMR spectroscopy at the Faculty of Science, Charles University. Its form has been greatly shaped by interaction with students—their suggestions for discussion and their curious questions.

I would like to thank everyone who contributed to the creation of this textbook, whether for the Czech version or the English translation. In particular, I wish to thank my colleagues from the nmr-challenge.com project Ondřej Socha and Zuzana Osifová, scientific editor Miloš Buděšínský, Czech language editor Eva Juláková, and English language editor Kateřina Millerová.

Special thanks go to graphic designer Tomáš Belloň for his excellent professional work. Thanks to him, this textbook is not only informative but also beautiful.

My deepest gratitude goes to my wife Helena and to my entire family for their constant support and love.

CONTENT

LIST OF SYMBOLS AND ABBREVIATIONS

Symbol	Meaning	Unit
A	relative intensity of signals	1
Å	angstrom (1 Å = 10^{-10} m = 10 nm)	m
d_1	the delay in the pulse sequence to return to the steady state	s
B ($\boldsymbol{B}$)	magnetic induction	T
E	energy	J
$\hbar$	reduced Planck constant ($\hbar = 1.0546 \cdot 10^{-34}$ J s)	
I	spin quantum number	–
J	coupling constant	Hz
$J_{C,H}$	heteronuclear coupling constant	Hz
k_b	Boltzmann constant ($k_b = 1.3806 \cdot 10^{-23}$ J K^{-1})	
k_c	rate constant of chemical exchange at the moment of coalescence	s^{-1}
L	liter	m^3
m	magnetic quantum number	–
M ($\boldsymbol{M}$)	magnetization	A m^2
N	number of (nuclei)	1
T	temperature	K
T_c	coalescence temperature	K
t	time	s
t_A	acquisition time	s
T_1	spin-lattice relaxation time	s
T_2	spin-spin relaxation time	s
t_{mix}	mixing time	s
α	angle	°
γ	gyromagnetic ratio	rad T^{-1} s^{-1}
δ	chemical shift	1 (ppm)
η	NOE efficiency	1
θ_m	magic angle ($\theta_m = 54.7356°$)	°
μ ($\boldsymbol{\mu}$)	nuclear magnetic moment	A m^2
ν	frequency	Hz ≡ s^{-1}
$\Delta\nu$	spectral window range	Hz
$\Delta\nu_{DR}$	digital resolution	Hz
π	Ludolph number	–
σ	shielding constant	–
τ	delay	s
τ_C	effective correlation time	s
φ	angle	°
ω_0	angular velocity of Larmor precession	rad s^{-1}

Abbreviation	Meaning
APT	*Attached Proton Test*
AT	*Acqusition Time*
BB	*Broad Band decoupling*
COSY	*COrrelation SpectroscopY*
CP	*Cross Polarization*
CSA	*Chemical Shift Anisotropy*
CW	*Continuous Wave*
DEPT	*Distorsionless Enhancement by Polarization Transfer*
DFT	*Density Functional Theory*
DOSY	*Diffusion-Ordered SpectroscopY*
DR	*Digital Resolution*
FID	*Free Induction Decay*
FT	*Fourier Transform*
FT NMR	*Pulsed NMR spectroscopy*
HETCOR	*HETeronuclear CORrelation*
HMBC	*Heteronuclear Multiple Bond Correlation*
HMQC	*Heteronuclear Multiple Quantum Correlation*
HSQC	*Heteronuclear Single Quantum Correlation*
INEPT	*Insensitive Nuclei Enhancement by Polarization Transfer*
MAS	*Magic-Angle Spinning*
MRI	*Magnetic Resonance Imaging*
MRT	*Magnetic Resonance Tomography*
NMR	*Nuclear Magnetic Resonance*
NOE	*Nuclear Overhauser Effect*
NOESY	*Nuclear Overhauser Effect SpectroscopY*
PFG	*Pulse Field Gradient*
RDC	*Residual Dipolar Coupling*
ROESY	*Rotating frame nuclear Overhauser Effect SpectroscopY*
SW	*Spectral Width*
TOCSY	*TOtal Correlation SpectroscopY*

01

INTRODUCTION

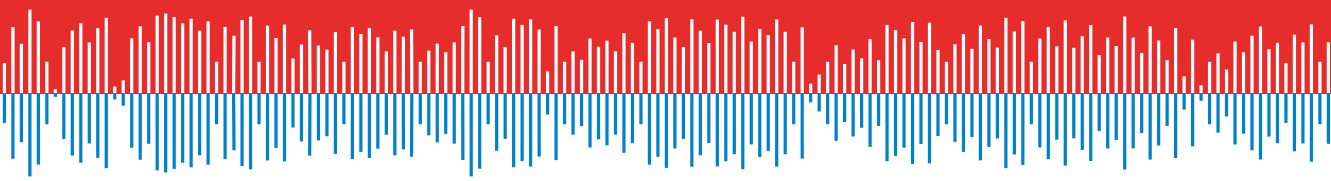

Chapter content

1.1 NMR Spectroscopy

Nuclear magnetic resonance (NMR) spectroscopy is a method that utilizes the magnetic properties of the atomic nuclei of certain isotopes. This method has found applications in various scientific fields, including physics, chemistry and medicine. It is also used in the pharmaceutical industry, for food-quality control, and for the determination of the botanical and geographical origin of semi-synthetic drugs.

In chemistry, NMR spectroscopy is a unique tool for determining the structure of molecules. It has become indispensable especially for synthetic chemists. It is also used to monitor the progress of chemical reactions, to verify the structure of products and intermediates, and to study reaction mechanisms and kinetics. NMR spectroscopy allows us to determine the molecular structure in the broadest sense—besides determining constitution, we can also assess the configuration and conformation of molecules. NMR spectroscopy relatively quickly and easily provides complex structural information, which would otherwise be obtainable only through a complicated combination of other analytical and chemical methods or would be entirely inaccessible. Consequently, NMR spectroscopy plays an irreplaceable role in determining the structure of substances isolated from natural sources. The vast diversity and complexity of naturally occurring compounds are a real challenge for structural analysis, and without NMR spectroscopy, the structure of many natural substances would remain undetermined. A major advantage of NMR spectroscopy is that it is non-destructive, which means that the examined material can be fully recovered.

NMR spectroscopy enables the study of even very complex molecular systems, such as biopolymers (proteins, nucleic acids), and the interactions between them. A significant advantage of NMR spectroscopy in the study of biomolecules is that it allows the determination of their three-dimensional structure under "physiological" conditions (in a solution with a specific pH, temperature, and ionic strength). NMR spectroscopy is also widely used in metabolomics, which is a comprehensive analysis of metabolism at a particular physiological or developmental stage of an organism, tissue or cell. For example, metabolomics examines changes in the concentrations of individual metabolites in body fluids caused by various diseases, potentially revealing the onset of disease even before symptoms appear.

Magnetic resonance imaging (MRI), a method based on magnetic resonance, is now commonly used to study tissues and organs in the human body. NMR spectroscopy also has extensive applications in materials chemistry, the pharmaceutical industry, and solid-state physics. For example, NMR spectroscopy can be utilized to determine the polymorphic purity of pharmaceutical products, which is crucial for the bioavailability and pharmacokinetic properties of drugs and for patent protection of new products.

1.2 For Whom This Textbook Is Intended

This textbook aims to introduce chemistry students to the basic principles of magnetic resonance, particularly the relations between molecular structures and their spectra. The primary focus is on "small" organic molecules. Therefore, the textbook is most useful for synthetic chemists, for whom the correct interpretation of NMR spectra is often crucial for the successful preparation of both new and known compounds. We will only briefly touch on the use of magnetic resonance in physics, medicine and the study of large biomolecules.

1.3 A Historical Introduction

In 1945, signals from hydrogen nuclei in water and paraffin were observed for the first time. In the 1950s, the first commercially produced NMR spectrometers appeared. Although the measurement at that time mainly focused on hydrogen nuclei (^{1}H), the information obtained proved to be invaluable in determining the structure of compounds, particularly organic ones. The first ^{13}C NMR spectra were described in 1957 and the broadband decoupling of hydrogen was introduced in 1965. Since then, NMR spectroscopy has rapidly developed and become an essential part of structural analysis. The introduction of superconducting magnets and their subsequent improvement enabled a gradual increase in the intensity of the magnetic field, thereby improving the sensitivity and resolution of the method. The discovery of two-dimensional (2D) experiments in the 1970s led to techniques capable of providing complete information about the molecular skeleton and the spatial arrangement of atoms. Methods enabling the acquisition of spectra or at least certain information about atomic nuclei in small spatial elements within objects gave rise to NMR imaging (MRI or magnetic resonance tomography, MRT).

The importance of nuclear magnetic resonance is underscored by several Nobel Prizes awarded in this field. In 1943, Otto Stern **(1)** received the Nobel Prize in Physics for the discovery of the magnetic moment of the proton.

In 1944, Isidor Isaac Rabi **(2)** was awarded the Nobel Prize in Physics for his resonance method for determining the magnetic properties of atomic nuclei. In 1952, Felix Bloch **(3)** and Edward Mills Purcell **(4)** received the Nobel Prize in Physics for the development of new methods for precise measurements of nuclear magnetism and the first detection of the NMR signal. In 1991, Richard R. Ernst **(5)** was awarded the Nobel Prize in Chemistry for his contributions to the development of high-resolution nuclear magnetic resonance, the introduction of pulse techniques, the use of Fourier transform, and the development of two-dimensional NMR techniques. In 2002, Kurt Wüthrich **(6)** received the Nobel Prize in Chemistry for the development of NMR methods enabling the determination of the three-dimensional structure of biological macromolecules in solution. In 2003, Paul C. Lauterbur **(7)** and Peter Mansfield **(8)** were jointly awarded the Nobel Prize in Physiology or Medicine for the development of magnetic resonance imaging (MRI) techniques.

02

THE PRINCIPLES OF NMR SPECTROSCOPY

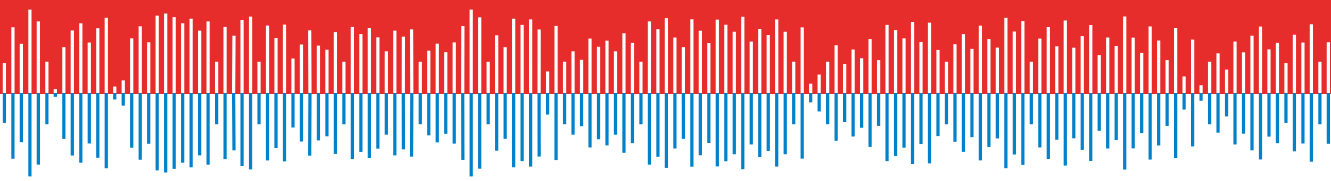

Chapter content

2.1 Introduction

As mentioned above, NMR spectroscopy makes it possible to determine molecular structures. The primary aim of this textbook is to explain the relations between molecular structures and their spectra. NMR spectra can be measured for specific isotopes, such as ^{1}H or ^{13}C. These nuclei are the most important for organic-compound analysis. Examples of their spectra (for 4-ethylbenzoic acid) are shown in **Fig. 2.1**. Although the structure of the substance is not immediately clear from the spectra, the information is encoded within them.

The objective of this book is to explain how the structure of molecules relates to their spectral characteristics. Spectra contain signals characterized by position, intensity, shape and splitting, all of which are connected to the molecular structure. For instance, the number of signals in a carbon spectrum indicates the number of non-equivalent carbon atoms in the molecule, whereas their position reveals in which functional groups these carbon atoms are involved. The carbon spectrum in **Fig. 2.1A** was additionally measured in such a way (**Section 5.2**) that the signals are either positive or negative depending on the number of hydrogen atoms directly attached to the given carbon atom. The intensity of the signals (shown in the hydrogen spectrum below each signal in **Fig. 2.1B**) indicates the relative number of the nuclei represented in the given signal. Signal splitting (for example, the signal of the CH_3 group is split into a triplet in the hydrogen spectrum) provides information about the number of hydrogen atoms attached to neighboring carbon atoms.

In order to understand NMR spectra and deduce molecular structures, we must first grasp the basic principles of NMR spectroscopy. This chapter answers key questions such as: Which nuclei can be measured? How are NMR spectra recorded? How does a molecular structure affect signal position and splitting?

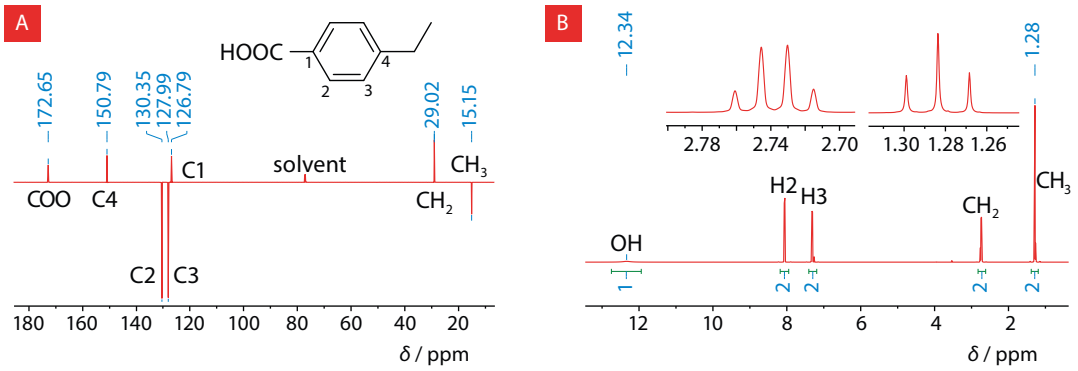

Fig. 2.1: The carbon (A) and proton (B) spectra of 4-ethylbenzoic acid

2.2 Nuclear Spin

In terms of NMR, the atomic nuclei of individual isotopes can be divided into three groups:

1. **Nuclei with a zero spin quantum number $I = 0$** (the term "spin quantum number" is often shortened to "spin" or "nuclear spin"). These nuclei have an even number of protons and neutrons, such as ^{12}C, ^{16}O and ^{32}S. They do not have a nuclear magnetic moment $\boldsymbol{\mu}$ and are not observable by NMR spectroscopy, nor do they influence the spectra of other isotopes.

2. **Nuclei with a spin quantum number $I = ½$** have a nuclear magnetic moment and are easily measurable. Examples include the hydrogen ^{1}H nucleus (proton), which has a high natural abundance and is the most commonly measured isotope, and the carbon ^{13}C, another frequently measured nucleus. However, ^{13}C is less sensitive in NMR spectroscopy and has a low natural abundance (1.11%), which makes its signals approximately 5,700 times weaker than ^{1}H signals. Other nuclei with the spin of ½ include ^{15}N, ^{19}F and ^{31}P.

3. **Nuclei with a spin quantum number $I > ½$** have, in addition to a nuclear magnetic moment, an electric quadrupole moment and are often more difficult to measure. Nuclei with an odd nucleon number (the nucleon number indicates the total number of protons and neutrons) have half-integer spin quantum numbers (½, 3⁄2, 5⁄2…), while nuclei with an even nucleon number but an odd number of protons have integer spin quantum numbers (1, 2, 3…).

Atomic nuclei with non-zero spin have their own nuclear magnetic moment $\boldsymbol{\mu}$. If a nucleus with a non-zero spin quantum number is outside a magnetic field, the nuclear spin does not manifest itself. In a magnetic field with induction $\boldsymbol{B}_0$, the interaction between the magnetic field and the nuclear magnetic moment results in a precessional motion of the nuclear magnetic moment vector $\boldsymbol{\mu}$ around the direction of $\boldsymbol{B}_0$ with a frequency

$$\nu = \gamma B_0 / 2\pi$$

referred to as the **Larmor-precession frequency**, where γ is the **gyromagnetic ratio**, a constant characteristic for each isotope, and B_0 is the magnitude of magnetic induction. In NMR spectroscopy, the projection of the nuclear magnetic moment $\boldsymbol{\mu}$ onto the axis of the magnetic field $\boldsymbol{B}_0$ is particularly important. This projection is quantized and can assume a total of $2I + 1$ values, corresponding to energy levels in a magnetic field with induction B_0 given by the equation:

$$E = -\gamma m \hbar B_0$$

where m is the **magnetic quantum number**, which can take the values $-I$, $-I + 1$, ..., I, and $\hbar$ is the **reduced Planck constant** ($\hbar = 1.0546 \cdot 10^{-34}$ Js). Focusing on the most commonly measured nuclei with a spin quantum number $I = ½$, the magnetic quantum number can take two values, $m = -½$ and $m = ½$. The nuclear magnetic moment can occupy two states in a magnetic field with induction B_0, which are referred to as the α and β states, with the energy levels:

$$E_\alpha = -0{,}5\ \gamma \hbar B_0$$

$$E_\beta = 0{,}5\ \gamma \hbar B_0.$$

The energy difference between these states is:

$$\Delta E = \gamma \hbar B_0$$

This energy difference corresponds to the **transition frequency** $\nu = \gamma B_0 / 2\pi$ (known as the **NMR resonance condition**), which is identical to the Larmor-precession frequency. At the magnetic-field strengths achievable today, this frequency ranges from tens to hundreds of MHz.

The population distribution of nuclei across both energy levels is nearly equal because of the small energy difference between the two levels; the excess in the lower level is on the order of 10^{-5}, depending on the strength of the magnetic field. The ratio of the nuclei in the α and β spin states can be calculated using the **Boltzmann distribution**:

$$N_\alpha / N_\beta = e^{\Delta E / k_b T}$$

where k_b is the **Boltzmann constant** ($k_b = 1.3806 \cdot 10^{-23}$ J/K) and ΔE is the energy difference

between the α and β spin states. For example, for ^{1}H nuclei at room temperature in a field with an induction of 11.74 T, we have $N_\beta \approx 0.99992\ N_\alpha$, which means that for every 100,000 hydrogen nuclei in the α spin state, 99,992 are in the β state. The larger the magnetic induction B_0, the greater the energy difference between the α and β states and the greater the population difference between the two spin states, leading to higher NMR sensitivity.

In NMR spectroscopy, we do not detect individual nuclear magnetic moments but rather their sum in the sample being measured. The vector sum of all nuclear magnetic moments is called **magnetization *M***, which is a macroscopic quantity that can be manipulated and then measured. Because of the small population difference between the spin states, the magnitude of magnetization is small and the resulting NMR signal is weak.

The sensitivity of NMR spectroscopy is the greatest weakness of this spectral method. In comparison with such techniques as mass spectrometry, the amount of the material required for analysis is much higher — for routine measurements of organic compounds, this is on the order of milligrams. However, NMR spectroscopy is a non-destructive method, which means that all the material used for analysis can be recovered. A significant part of the development of NMR spectrometers and measurement techniques is driven by the effort to increase sensitivity.

An important piece of information that can be obtained from NMR spectra is the **intensity of signals** (*A*). It is expressed relative to other signals; ideally (ignoring the factors related to the construction of the NMR spectrometer), it follows the direct proportionality:

$$A \sim \frac{niB_0^2\gamma^3 I(I+1)}{T}$$

where *n* is the number of equivalent nuclei in the sample, *i* is the natural abundance of the given isotope, and *T* is temperature. In one spectrum, we always measure nuclei of the same type, in the same magnetic field and at the same temperature. Therefore, the signal intensity is proportional to the number of equivalent nuclei *n* in the molecule. From the above formula, we can also deduce the relationship between the intensities of signals from different nuclei. For example, if we measure the proton and silicon spectra of a compound containing a $-SiCH_3$ group on the same instrument and at the same temperature, the intensities of the hydrogen and silicon signals are approximately in the ratio of 8,000:1.

In order to achieve the required signal-to-noise ratio for nuclei with low sensitivity or low isotopic abundance, we must use more concentrated samples, samples of compounds enriched with the measured isotope, or extend the measurement time.

From the above formula, it is clear that the signal intensity (and thus the measurement sensitivity) can be significantly increased if NMR experiments are performed on spectrometers with a stronger magnetic field (magnetic induction B_0). Therefore, the construction of magnets with increasingly intense magnetic fields is one of the main trends in the development of NMR spectrometers.

Table 2.1 summarizes the important magnetic properties of selected isotopes. Note that the gyromagnetic ratio *γ* can have both positive and negative signs. Nuclei with a negative *γ* have a precession direction opposite to that of nuclei with a positive *γ*. The penultimate column shows the resonance frequency in a magnetic field with an induction of 11.74 T (tesla, T = kg s^{-2} A^{-1}). In NMR spectroscopy, it is common to express the magnetic induction B_0 of a device as the frequency at which ^{1}H nuclei resonate. Therefore, we often refer to a 500-MHz spectrometer, the field strength of 500 MHz, etc. The last column of the table shows the relative sensitivity of isotopes for NMR

Table 2.1: Magnetic properties of isotopes of the most important elements present in organic compounds

Nucleus	Spin	Natural abundance %	γ 10^7 rad T^{-1} s^{-1}	Frequency in the field of 11.74 T MHz	Sensitivity
^{1}H	½	99.99	26.75	500.0	100
^{2}H	1	0.01	4.11	76.8	0.0001
^{3}H	½	–	28.54	533.3	0
^{12}C	0	98.93	–	–	–
^{13}C	½	1.11	6.73	125.7	0.02
^{14}N	1	99.63	1.93	36.1	0.1
^{15}N	½	0.37	–2.71	50.7	0.0004
^{16}O	0	99.96	–	–	–
^{17}O	⅝	0.037	–3.63	67.8	0.001
^{19}F	½	100	25.18	470.4	83
^{31}P	½	100	10.84	202.4	6.6

measurement. The most sensitive isotope is ^{1}H, which is assigned a value of 100. Other isotopes are less sensitive because they have a smaller gyromagnetic ratio and thus a smaller energy difference between the α and β spin states and a smaller excess of α spin states at equilibrium. The low natural abundance of some isotopes also contributes to their low sensitivity. For example, the natural abundance of ^{13}C is around 1%, with the remaining 99% being magnetically inactive ^{12}C nuclei, which means that only one in a hundred carbon nuclei contributes to the NMR signal.

As mentioned above, the nuclei with $I = ½$ can exist in two spin states. In NMR, the coordinate system is conventionally arranged such that the positive direction of the *z*-axis points along the direction of the magnetic field. In **equilibrium**, outside a magnetic field, the nuclear magnetic

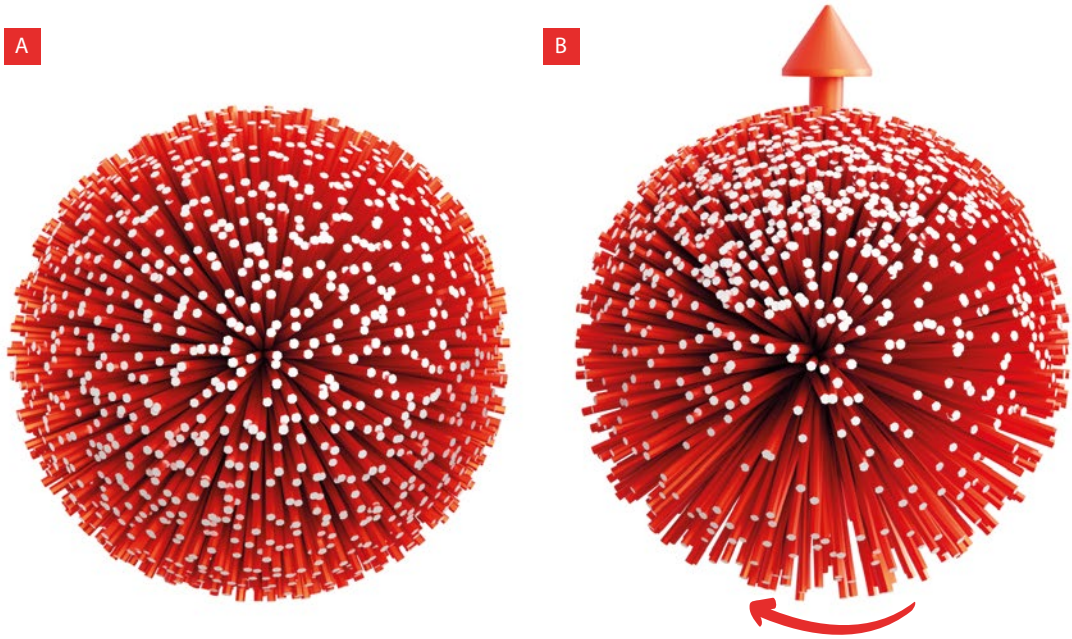

Fig. 2.2: Nuclear magnetic moments in (**A**) zero and (**B**) non-zero magnetic fields

moments have random orientations (**Fig. 2.2**). In a magnetic field, the nuclear magnetic moments also have random orientations, but after some time, there is a slight excess of nuclei with the lower energy state α, which have a positive projection of their nuclear magnetic moment along the *z*-axis. Additionally, in a magnetic field, all nuclear magnetic moments perform a precessional motion around the *z*-axis. A small excess of nuclei in the lower energy state (these are conventionally the spins above the *xy*-plane) causes the overall magnetization ***M*** of the sample (the vector sum of the magnetic moments of all nuclei) to align along the *z*-axis (denoted by the bold arrow in **Fig. 2.2**).

2.3 Chemical Shift

The above-mentioned relation for the energy difference between spin states implies that all nuclei of one isotope, if placed in the same magnetic field, will resonate at the same frequency. If this were the case, it would not make sense to talk about NMR spectra, as these spectra would contain only a single signal for each isotope present in the sample.

However, NMR spectra can be observed because the nuclei of atoms are **shielded** from the magnetic field, in which they are located, by electrons. The movement of electrons generates a magnetic field that opposes the external magnetic field $\boldsymbol{B}_0$. Nuclei of the same isotope that do not share the same chemical environment (i.e. are not **chemically equivalent**) differ in the distribution of the electrons around them, and thus, albeit very slightly, they also differ in the intensity of the shielding. This shielding is proportional to the magnitude of the external magnetic field $\boldsymbol{B}_0$, and it is characterized by the shielding constant σ. The effective magnetic field B_{ef} acting on the nucleus is expressed by the equation:

$$B_{ef} = B_0 - \sigma B_0 = B_0 (1 - \sigma)$$

If different nuclei are subjected to varying effective magnetic fields, they will also have different resonance frequencies. For example, if the nuclei of ^{1}H in tetramethylsilane (TMS) have a resonance frequency of exactly 500,000,000 Hz (500 MHz) in the field of 11.74 T, the hydrogens of the CH_3 group in methanol, which are less shielded, will have a resonance frequency of 500,001,650 Hz in the same magnetic field, whereas the hydrogens in benzene, which are even less shielded, will have a resonance frequency of 500,003,635 Hz. In a magnetic field with half the induction, the hydrogens in TMS will resonate at 250 MHz, the hydrogens in the CH_3 group in methanol at 250,000,825 Hz, and the hydrogens in benzene at 250,001,817.5 Hz. Expressing resonance frequencies in absolute values is inconvenient because they are primarily dependent on the magnetic field B_0. Therefore, the **chemical-shift** scale δ with the dimensionless unit **ppm** (parts per million) has been established to express resonance frequencies. The chemical shift is defined as:

$$\delta_x = 10^6(\nu_x - \nu_{ref}) / \nu_{ref}$$

where δ_x is the chemical shift of atom x, ν_x is the resonance frequency of atom x, and ν_{ref} is the resonance frequency of a reference compound. If TMS is taken as the reference compound and the aforementioned resonance frequencies are substituted into the formula, the chemical shift of the hydrogens in the methyl group in methanol is 3.3 ppm and the chemical shift of the hydrogens in benzene is 7.27 ppm. The main advantage of the chemical shift δ is that it does not depend on the magnitude of the magnetic field, so that it takes the same value on different NMR spectrometers with varying magnetic induction values. The nuclei that are **more shielded** by electrons have a **lower chemical shift**. The direction from higher to lower chemical shifts δ in NMR spectra is also called the direction toward a higher magnetic field (*upfield shift*), a shift to lower frequency, or a diamagnetic shift. The opposite direction, toward higher δ values, is called a paramagnet-

ic shift or a shift toward a lower field (*downfield shift*) or the direction toward higher frequency (**Fig. 2.3**). The terms "*downfield*" and "*upfield*" are historical, but they are still commonly used. We can explain them by saying that in order to achieve the same resonance frequency, we would need to use a higher magnetic field (*upfield*) for more shielded nuclei and a lower magnetic field (*downfield*) for less shielded nuclei. For historical reasons, NMR spectra are also displayed such that the lower values are on the right side of the chemical-shift axis and the higher values are on the left.

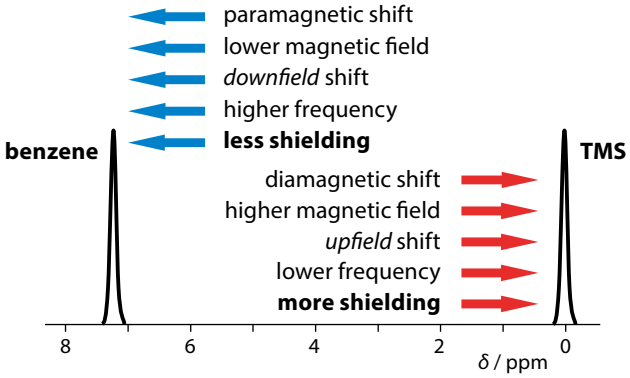

Fig. 2.3: A schematic representation of a ^{1}H NMR spectrum with signals at higher and lower chemical shifts

The nuclei with the same chemical environment are called **chemically equivalent**; they have the same electron shielding and thus the same resonance frequency (a shared signal in the spectrum). For example, the symmetry in the benzene molecule makes all carbon nuclei chemically equivalent, and only one signal is observed in the ^{13}C NMR spectrum of benzene. The same applies to the hydrogen nuclei; in the ^{1}H spectrum of benzene, there is a single signal with the corresponding chemical shift. In contrast, in the toluene molecule, not all carbon nuclei are chemically equivalent; due to the symmetry of the molecule, we expect five signals in the ^{13}C spectrum: one signal for the carbon in the methyl group, one signal for the quaternary aromatic carbon, and three signals for the aromatic CH carbons. The carbons at positions C2 and C6 are chemically equivalent and have a shared signal, while the carbons at positions C3 and C5 are also chemically equivalent and resonate at the same frequency (**Fig. 2.4**). In the hydrogen spectrum of toluene, we expect four signals: one for the hydrogens of the methyl group (the three hydrogens in a methyl group are always equivalent) and three aromatic signals, two of which will have double intensity.

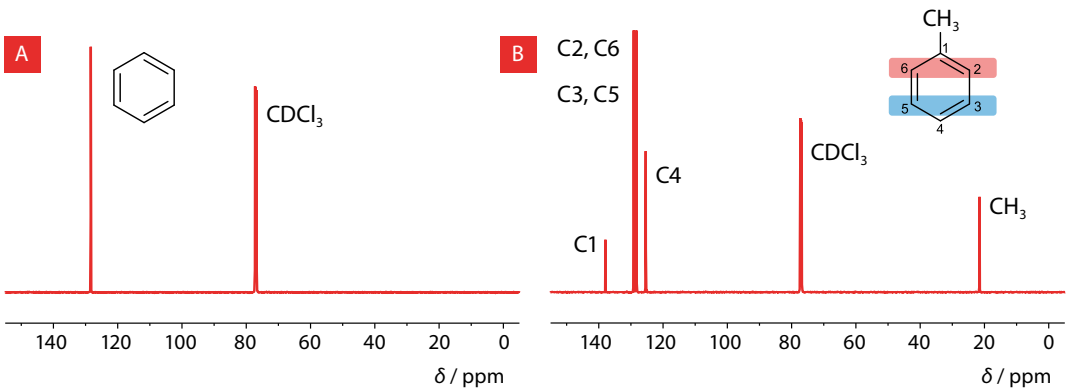

Fig. 2.4: The ^{13}C NMR spectra of benzene (**A**) and toluene (**B**)

Chemically equivalent atoms can best be identified by the fact that, when each of them is successively replaced by a different atom, the same compound is always formed. For example, diethyl ether contains six chemically equivalent protons in the methyl groups and four chemically equivalent protons in the $-CH_2-$ groups. The replacement of any of the first six hydrogen atoms with, for instance, chlorine, produces 1-ethoxy-2-chloroethane, while the replacement of any of the remaining four hydrogens yields 1-ethoxy-1-chloroethane. Therefore, the proton NMR spectrum of diethyl ether will contain two signals with intensities in a ratio of 6:4, i.e. 3:2. However, intensities do not refer to the height of the signals but rather to their area (hence they are often called "integral intensities"). An example of a ^1H NMR spectrum with integral intensities showing the number of chemically equivalent nuclei is shown in **Fig. 2.4B**.

2.4 Recording the NMR Signal

The previous explanation is sufficient to understand classical spectroscopy, known as CW NMR (CW stands for "continuous wave"). In this measurement, the sample containing magnetically active nuclei is placed in a magnetic field, and a coil carrying an alternating current at a frequency on the order of MHz is placed near the sample. Subsequently, the magnetic-field induction B_0 or the frequency of the current in the coil is continuously changed. When the resonance condition mentioned above is met, radiofrequency radiation is absorbed, which can be measured in various ways common in electrical engineering. CW NMR spectrometers were commonly manufactured until the 1970s. Their electronics were relatively simple, and data processing did not require a computer. The frequency generator was controlled by the position of a pen on the *x*-axis of a recorder or oscilloscope, and the amplified signal from the absorption meter was recorded on the *y*-axis.

Most modern spectrometers operate in a different mode, involving Fourier transform (FT, see **Section 2.5**). In this mode, all nuclei of a given isotope are excited by a very short radiofrequency pulse lasting on the order of microseconds. Such a short pulse has some frequency uncertainty and typically covers the frequency range of all nuclei of a given isotope. The pulse causes the magnetization vector $\boldsymbol{M}$ to be displaced from the *z*-axis. During the pulse, the magnetization vector rotates around the axis of the pulse. Depending on the duration and intensity of the pulse, the magnetization vector can rotate by various angles. The most typical is the 90° pulse, which rotates the magnetization vector into the *xy*-plane.

The Larmor precession of individual nuclear magnetic moments $\boldsymbol{\mu}$ leads to the precession of macroscopic magnetization $\boldsymbol{M}$ at the same (Larmor) frequency. If the magnetization points along the *z*-axis (in equilibrium), precession around the same *z*-axis does not manifest itself. However, if the magnetization is in the *xy*-plane, the Larmor precession leads to the rotation of the magnetization vector in this plane. If a coil is placed near the sample, the precessional motion of the magnetization in the *xy*-plane induces an electric current in it. The recording of this induced current (i.e. the NMR signal) is called **FID** (free-induction decay). It takes the form of an exponentially damped periodic function, representing the sum of sinusoids with frequencies corresponding to individual signals, and reflects the **dependence of the electric current induced in the detection coil over time**. The FID signal is stored in digital form in the computer memory and subjected to Fourier transform, resulting in a **spectrum representing the dependence of signal intensities on frequency**.

The advantage of FT NMR spectroscopy is primarily the capability of quickly repeating the same measurements and summing the resulting FID records. This increases the sensitivity of the measurement, making it possible to measure even dilute samples or nuclei with a low gyromagnet-

ic ratio γ or low isotopic abundance. The intensity of the signal increases proportionally to the number of accumulated FID records, but the intensity of noise increases only in proportion to the square root of the number of accumulations. Therefore, if we perform one hundred accumulations, the signal-to-noise ratio improves tenfold. If we want to double the signal-to-noise ratio, we must allow for four times the duration of the experiment (**Fig. 2.5**). Another advantage of FT NMR is the ability to manipulate spin systems or populations at individual energy levels using pulses, thereby obtaining spectra that contain additional valuable information. FT NMR spectroscopy is sometimes also called **pulse NMR spectroscopy**.

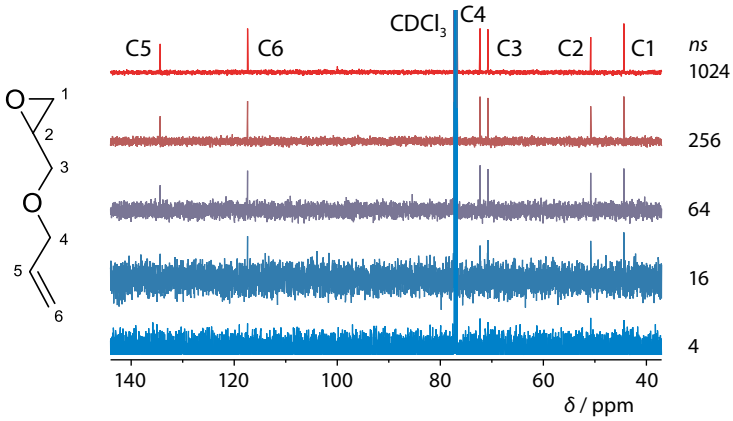

Fig. 2.5: The ^{13}C NMR spectra (with ^{1}H decoupling) of allyl glycidyl ether measured with the number of FID accumulations (ns) indicated to the right of each spectrum

2.5 Fourier Transform

The free-induction decay (FID) signal is a time-based record of the magnitude of the electric current induced in the measuring coil (with time on the *x*-axis), but a spectrum represents the spectral intensity as a function of frequency (with frequency on the *x*-axis). Fourier transform is a mathematical tool that makes it possible to convert a time-domain record (FID) into a spectrum.

Fig. 2.6 shows several examples of time-domain functions and their resulting spectra after Fourier transform. **Fig. 2.6A** on the left represents a non-decaying periodic function (cosine), with two periods occurring in one second. The spectrum on the right has been obtained from the Fourier transform of this function. The line in the spectrum intersects the *x*-axis at 2 Hz (i.e. two periods per second). **Fig. 2.6B** shows a decaying cosine function with the same period as in **Fig. 2.6A**. This resembles the FID measured for a sample with a single signal. Fourier transform of this decaying function results in a signal at 2 Hz. The width of the signal (its half-height width) is related to the rate of decay of the cosine function. The faster the periodic function decays to zero, the wider the resulting signal. This is illustrated in **Fig. 2.6C**, where a periodic function with the same period (two cycles per second) decays more quickly to zero. In the resulting spectrum, there is again a signal at 2 Hz, but it is wider, although its area remains the same (when the signal width increases, its height decreases). **Fig. 2.6D** depicts a decaying cosine function, this time with a period of five cycles per second. The spectrum after Fourier transform contains a single signal at 5 Hz. In **Fig. 2.6E**, the time-domain function results from the sum of two decaying cosine functions with periods of two and five cycles per second. In the resulting spectrum, two signals appear at 2 Hz and 5 Hz.

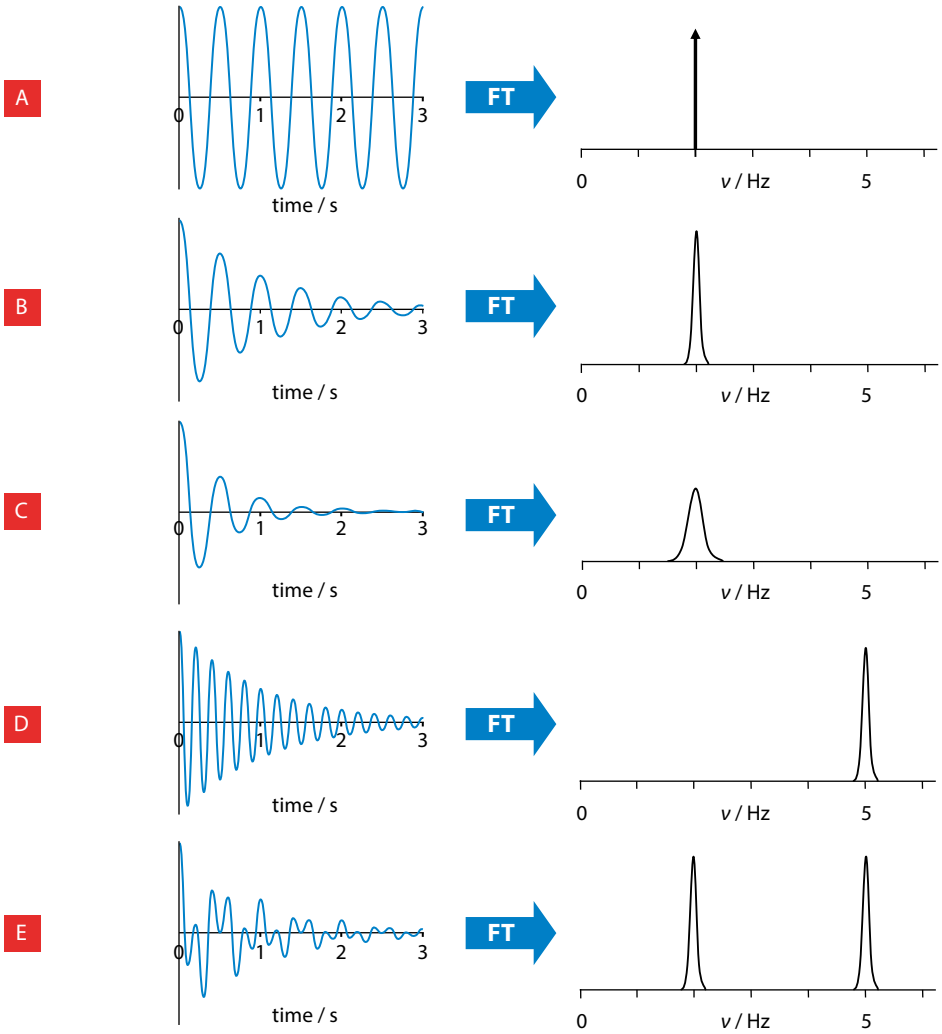

Fig. 2.6: Fourier transform converts FID (time dependence) into a spectrum (frequency dependence)

2.6 Magnetic Interactions of Nuclei

The magnetic moments of atomic nuclei can interact with each other. In NMR spectra, we can observe two types of magnetic interactions between nuclei in molecules:

1. **Direct spin–spin (dipole–dipole, dipolar) interactions** are the result of the interaction between the magnetic moments of nuclei through space. In isotropic environments (liquids, solutions), these interactions are averaged to zero due to rapid molecular reorientations, caused by Brownian motion. Dipolar interactions contribute to the relaxation of the NMR signal (Section 7.3), but they do not affect standard spectra of substances in solution. Dipolar interactions have a significant effect on NMR spectra of solids (Chapter 14).

2. **Indirect spin–spin interactions (scalar interactions, *J*-interactions, *J*-coupling)** are mediated by electrons (because electrons also have spin) and affect the spectra of substances in both solution and solid state. Scalar interactions cause the splitting (multiplicity) of signals

observed in NMR spectra. The magnitude of indirect spin–spin interactions is closely related to molecular structure, providing a valuable tool for structure determination. The following paragraphs briefly outline the mechanism of indirect spin–spin interactions and their effect on spectra. The relationship between molecular structure and the magnitude of these interactions for ^{13}C and ^{1}H nuclei is discussed in detail in **Sections 3.2** and **4.8**.

The mechanism of indirect spin–spin interaction can be illustrated by a simple example of heteronuclear interaction in a chloroform molecule, $^{13}CHCl_3$ (**Fig. 2.7**). The magnetic moment of the hydrogen atom induces a weak magnetic polarization of the bonding electrons (energetically, it is more favorable for the nuclear and electron spins to have opposite orientations). The spins of valence electrons follow Hund's rule and Pauli's exclusion principle. According to the Pauli exclusion principle, electrons in the same orbital always have opposite spins. The interaction with nuclear spins leads to two possible states: When both nuclear spins (^{1}H and ^{13}C) have the same sign, the energy of the entire system is slightly higher than in the case of opposite nuclear-spin signs, where the signs of the nuclear and electron spins alternate.

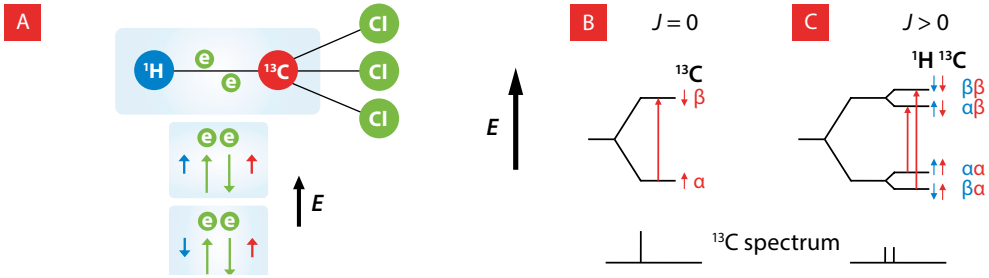

Fig. 2.7: Heteronuclear scalar spin interaction in a chloroform molecule

Fig. 2.7B shows the energy diagram of a ^{13}C nucleus in a magnetic field without spin–spin interaction. For this nucleus, two spin states (α and β) are possible, with an energy difference ΔE, and the spectrum contains a single signal corresponding to this transition (α → β). **Fig. 2.7C** depicts the situation of the ^{13}C nucleus with indirect spin–spin interaction with a hydrogen nucleus. Both spin states of carbon (α and β) are split into two energy levels due to the interaction with the magnetic moments of the hydrogen nucleus. In this diagram, it is possible to observe two different transitions for ^{13}C (α → β). These transitions have different energy differences ΔE, which is reflected in the spectrum by the appearance of two different frequencies. The ^{13}C signal is thus split into two lines of equal intensity (a doublet). The same signal splitting can also be observed in the ^{1}H spectrum (the energy levels of the ^{1}H nucleus are split due to interaction with the ^{13}C nucleus).

The magnitude of an indirect spin–spin interaction is defined by the **coupling constant *J*** (measured in hertz, Hz). The size of the coupling constant determines the difference in the resonance frequencies of individual signal lines. For example, in the ^{13}C spectrum of chloroform, the coupling constant can be obtained by subtracting the resonance frequencies of the two lines in a doublet. This constant is denoted by a left superscript, indicating the number of bonds between the interacting nuclei. Based on the number of bonds, the *J* constants are categorized as one-bond (^{1}J), geminal (^{2}J), vicinal (^{3}J), and long-range interactions (^{4}J, ^{5}J, ...). In our example of the $^{13}CHCl_3$ molecule, the one-bond spin–spin interaction between ^{1}H and ^{13}C has the value of $^{1}J = 209$ Hz. This value can be observed in both the ^{1}H and ^{13}C spectra. The *J*-coupling constant can be positive or negative, but in simple NMR spectra, it is always manifested in the same way, and it is only possible to read the absolute value of *J* from the spectrum.

If a nucleus interacts with multiple magnetic nuclei, the spectrum shows the following effect: Each line created by interaction with one nucleus is further split by interaction with another nucleus. In common nuclei with $I = ½$, each interaction results in the formation of two lines from one original. The signal thus consists of multiple lines, and its overall appearance is referred to as **signal multiplicity**.

For example, nuclei split by interactions with two nuclei having identical coupling constants will form a **triplet** with an intensity ratio of 1 : 2 : 1 (**Fig. 2.8**). The middle line is twice the intensity of the outer lines because it results from the merging of two lines. This situation typically occurs when the signal is split by two chemically equivalent nuclei, for example in the splitting of a ^{13}C signal due to interaction with two directly bonded hydrogen atoms, such as in CH_2Cl_2 or $Cl_2C{=}CH_2$. The coupling constant in the triplet can be determined by subtracting the resonance frequency of the first line from the second, or the second from the third. Both differences are identical in a triplet.

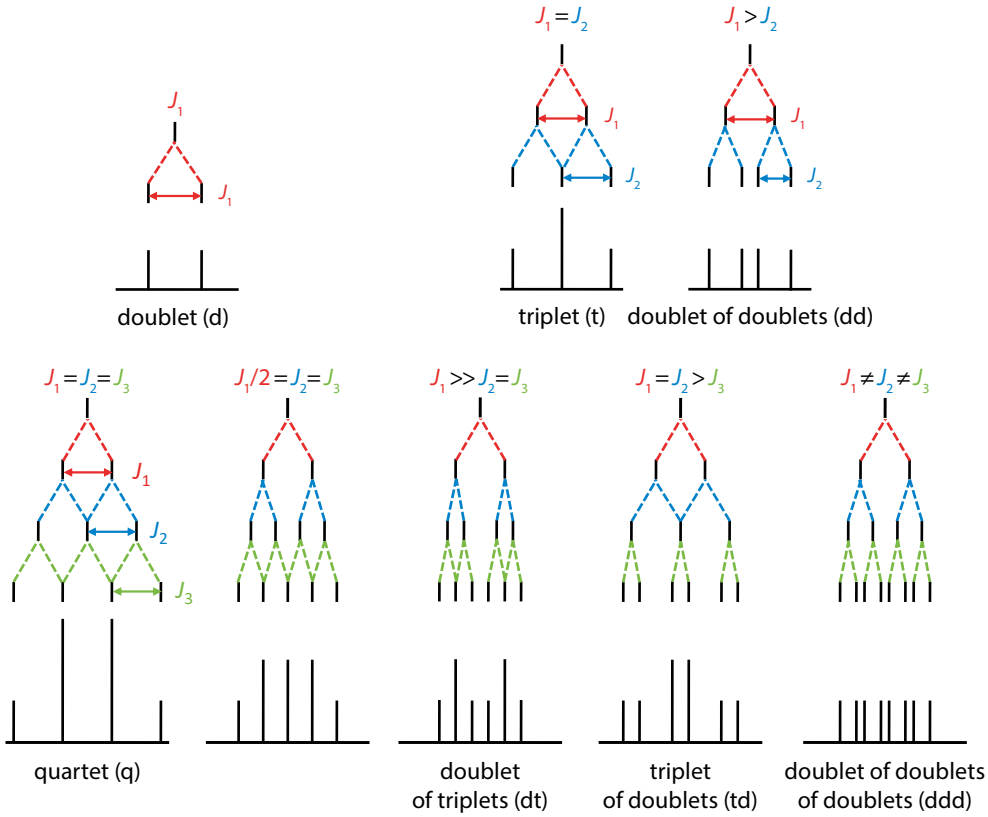

Fig. 2.8: The signal splitting of a nucleus with scalar interaction with one, two or three other nuclei

If a nucleus interacts with two other nuclei but the magnitudes of these two interactions differ, we observe four lines of equal intensity in the spectrum, forming a **doublet of doublets**. The distances between the first and second lines or the third and fourth lines represent one coupling constant, whereas the distances between the first and third or second and fourth lines represent the second constant.

In the case of the splitting by three interacting nuclei, the resulting multiplet may assume various forms. When the coupling constants with all three nuclei are identical, a **quartet** (four lines

with an intensity ratio of 1 : 3 : 3 : 1) appears. A quartet structure typically occurs in the signals of ^{13}C in methyl groups, which contain three equivalent protons, such as in CH_3OH or CH_3Cl.

Other forms of multiplets are named according to their overall appearance, such as a doublet of triplets or a triplet of doublets. If the signal structure is unclear (due to multiple spin–spin interactions, signal overlap, or other complications), it is generally referred to as a **multiplet**.

Concerning signal splitting by scalar interactions with equal coupling constants, the intensity ratio of the lines in the resulting multiplet can be deduced from Pascal's triangle (**Fig. 2.9**). Additionally, scalar interactions are molecular properties, and their magnitude is **independent of the strength of the external magnetic field** (unlike resonance frequency). Scalar interactions **cannot be observed between chemically equivalent nuclei**.

singlet (s)	1						
doublet (d)	1	1					
triplet (t)	1	2	1				
quartet (q)	1	3	3	1			
pentet (p)	1	4	6	4	1		
sextet	1	5	10	10	5	1	
septet	1	6	15	20	15	6	1

Fig. 2.9: Pascal's triangle. Each number is always the sum of the two numbers directly above it. Pascal's triangle can be used to deduce the intensity ratios of lines in multiplets (doublet—two lines with an intensity ratio of 1 : 1, triplet—three lines with an intensity ratio of 1 : 2 : 1, etc.)

Signal splitting caused by spin–spin interactions can complicate the interpretation of ^{13}C NMR spectra (due to more frequent signal overlap), and it also worsens the signal-to-noise ratio (for example, a signal split into a doublet has half the height of a singlet); this reduces the sensitivity of ^{13}C NMR measurements and increases the time required to collect spectra. Heteronuclear (^1H,^{13}C) spin–spin interactions can be removed using **broadband decoupling** (see **Section 5.1**). Throughout the measurement of ^{13}C spectra, hydrogen nuclei are irradiated with an additional electromagnetic field at the resonance frequency of the hydrogen nuclei. This causes rapid transitions between the α and β spin states of the ^1H nuclei, canceling out the spin–spin interactions between hydrogen and carbon nuclei. ^{13}C NMR spectra are generally recorded with decoupling.

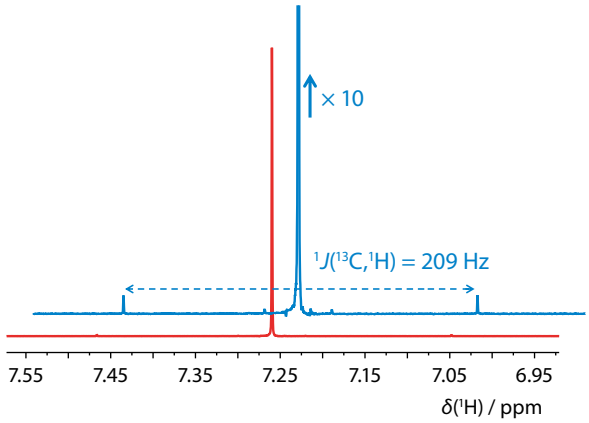

Fig. 2.10: ^{13}C Satellites in the ^1H NMR spectrum of chloroform

Heteronuclear (^{1}H,^{13}C) scalar interactions can be observed as additional signals in ^{1}H NMR spectra, known as **^{13}C satellites**. In compounds with natural isotopic abundance, 99% of the carbon nuclei are composed of the isotope ^{12}C, which is magnetically inactive and does not cause signal splitting resulting from scalar interactions. Therefore, in the ^{1}H NMR spectrum of chloroform ($CHCl_3$), the main signal is a singlet (**Fig. 2.10**). The ^{13}C isotope, which is naturally present in approximately 1% of carbon atoms, causes the hydrogen signal to split into a doublet. In the hydrogen spectrum of chloroform with natural isotopic abundance, it is possible to observe two low-intensity signals, together constituting approximately 1% of the total signal area. These two small signals are located almost symmetrically around the main signal, and the distance between them, measured in Hz, corresponds to the coupling constant $^1J(^{13}C,^1H)$.

In ^{1}H spectra, we can usually observe signal splitting caused by **homonuclear** (^{1}H,^{1}H) interactions. These interactions cannot be removed by broadband decoupling. Nevertheless, they provide crucial information about the molecular structure (see **Section 4.8**).

03

^{13}C NMR SPECTROSCOPY

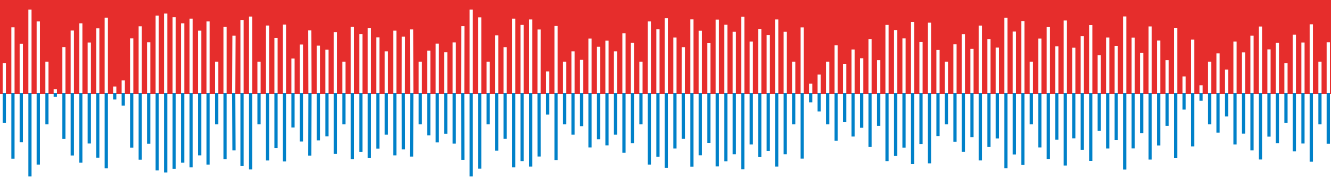

Chapter content

The spectra of ^{13}C nuclei are, after ^{1}H experiments, the second most frequently measured spectra in the structural analysis of organic molecules. These spectra are mostly measured with broadband decoupling (**Section 5.1**), which means that the splitting of signals caused by indirect spin–spin coupling with ^{1}H nuclei is not observed. If there is no spin–spin interaction, the spectrum contains only singlets, which makes ^{13}C spectra relatively easy to interpret. This is also why we first focus on carbon spectra and only then on hydrogen spectra, even though hydrogen spectra are measured much more frequently.

However, the use of broadband decoupling has its drawbacks. The first one is that we lose information about heteronuclear spin–spin interactions (^{13}C, ^{1}H) and thus about the number of hydrogen atoms attached to a given carbon atom. Additionally, broadband decoupling causes changes in the intensity of some carbon signals due to the **nuclear Overhauser effect** (NOE, **Chapter 8**), as a result of which the carbon spectra measured in this way cannot be accurately quantified (the intensities do not correspond to the relative numbers of carbons in the molecule). Another reason why carbon spectra cannot be quantified is the slow return of some carbon-atom magnetizations to equilibrium (slow relaxation, **Chapter 7**).

Therefore, the most important information that can be obtained from ^{13}C spectra concerns the chemical shifts of individual signals. The signals of carbon atoms in common organic compounds are usually found in the spectrum between 0 and 220 ppm. **Fig. 3.1** shows typical regions for signals of various types of carbons, which are discussed in more detail in **Section 3.1**. A simple modification of the carbon experiment can produce spectra where some signals point downward and some upward, depending on the number of the hydrogen atoms directly bonded to the carbon atom (quaternary carbons and CH_2 groups point upward, whereas CH and CH_3 groups point downward). This experiment is referred to as APT (see **Section 5.2**) and it partially compensates for the loss of information caused by the use of decoupling.

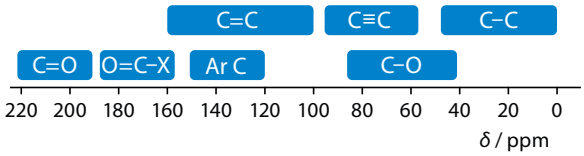

Fig. 3.1: Typical ranges of chemical shifts in ^{13}C spectra of organic molecules

3.1 Chemical Shifts

3.1.1 Alkanes and Cycloalkanes

The chemical shift of carbon atoms in alkanes depends on the branching of the hydrocarbon chain near the observed nucleus. Non-carbon substituents also have a significant effect on ^{13}C chemical shifts, as shown in **Table 3.1**. Electronegative substituents withdraw electron density from the vicinity of the carbon nucleus, making the carbon less shielded, which leads to a higher chemical shift.

The relationship between chemical shift and electronegativity is evident, for example, in the shifts of the carbons adjacent to fluorine, chlorine and bromine. Iodine is an exception to the effect of electronegative substituents. The chemical shift of a carbon directly bonded to an atom with a large atomic number is lower than that of a non-substituted alkane. This phenomenon is known as the heavy-atom effect, and it is most commonly observed in compounds containing iodine. For

example, the chemical shift of a carbon in a CI_4 molecule is –292 ppm, which is well outside the range of commonly measured carbon spectra.

Carbon in the β position to an electronegative substituent is also less shielded, and its signal is shifted to higher chemical-shift values, but this effect is much weaker than in the case of α-carbons (those directly bonded to the substituent). The signals of carbons in the γ position to substituents, on the other hand, are slightly shifted toward lower chemical-shift values. This phenomenon is known as the γ-effect, and it is likely caused by steric interactions.

Table 3.1:
The chemical shifts δ (ppm) of carbon atoms in substituted propane X–$C^{\alpha}H_2$–$C^{\beta}H_2$–$C^{\gamma}H_3$

X	$\delta(C^{\alpha})$	$\delta(C^{\beta})$	$\delta(C^{\gamma})$
H	16.1	16.3	16.1
CH_3	24.9	24.9	13.1
NH_2	44.6	27.4	11.5
OH	64.9	26.9	11.8
NO_2	77.4	21.2	10.8
F	85.2	23.6	9.2
Cl	46.7	26.0	11.5
Br	35.4	26.1	12.7
I	9.0	26.8	15.2

Table 3.2:
The chemical shifts δ (ppm) of carbon atoms in cycloalkanes

Compound	δ
cyclopropane	–2.8
cyclobutane	22.4
cyclopentane	25.8
cyclohexane	27.0
cycloheptane	28.7

The chemical shifts of unsubstituted cycloalkanes appear in the range of 22–29 ppm, with the only exception being cyclopropane, which has a carbon chemical shift of –2.8 ppm (**Table 3.2**). Unusually low chemical shifts are also observed in other three-membered cyclic compounds. For example, the chemical shifts of the carbon atoms in oxirane are around 40 ppm, whereas the chemical shift of the carbon directly bonded to oxygen in larger rings or in acyclic compounds is usually higher than 55 ppm.

3.1.2 Alkenes

The signals of double-bond carbon atoms are most often found in the wide range of 80–150 ppm. If there are only alkyl substituents on the double bond, the range of chemical shifts is narrower, 120–140 ppm. Substituents influence chemical shifts through **inductive** and **mesomeric effects**. Examples of mesomeric effects are shown in **Fig. 3.2**. An electron-donating methoxy substituent increases the electron density on the carbon in the β position (this carbon has a partial negative charge), making it more shielded, as a result of which its chemical shift is lower (84 ppm) than that of unsubstituted ethene (124 ppm). Conversely, an electron-accepting carbonyl group reduces the electron density on the β-carbon, which then has a higher chemical shift (137 ppm).

In iodoethene, the heavy-atom effect is again noticeable—the carbon directly bonded to iodine has an unusually low chemical shift (**Table 3.3**).

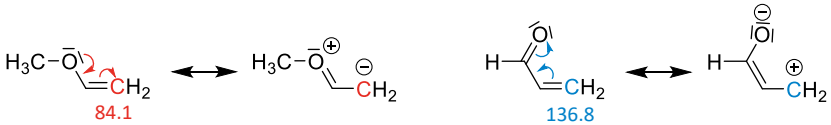

Fig. 3.2: The influence of the mesomeric effect on the electron density and chemical shifts (the values of δ in ppm) of double-bond carbon atoms

Table 3.3: The chemical shifts δ (ppm) of carbon atoms in substituted ethene X–$C^{\alpha}H$=$C^{\beta}H_2$

X	$\delta(C^{\alpha})$	$\delta(C^{\beta})$
H	123.5	123.5
CH_3	133.4	115.9
F	148.2	89.0
Cl	125.9	117.2
Br	115.6	122.1
I	85.2	130.3
OCH_3	153.2	84.1
CHO	139.3	136.8

3.1.3 Alkynes

The signals of carbon atoms in triple bonds generally have lower chemical shifts than the signals of carbon atoms in double bonds, typically observed in the range of 60–90 ppm. However, substituents can significantly alter the position of these signals through inductive and mesomeric effects, as shown in **Table 3.4**.

Table 3.4: The chemical shifts δ (ppm) of carbon atoms in substituted acetylene X–C^{α}≡C^{β}H

X	$\delta(C^{\alpha})$	$\delta(C^{\beta})$
H	71.9	71.9
CH_3	80.1	67.6
OCH_2CH_3	89.6	23.4
CHO	81.8	83.1

3.1.4 Arenes

The signals of aromatic carbon atoms fall roughly within the same range as the signals of carbons in double bonds: 120–140 ppm for unsubstituted or alkyl-substituted arenes, and 100–160 ppm for aromatic compounds with additional substituents (see **Table 3.5**).

Table 3.5: The carbon chemical shifts δ (ppm) of monosubstituted benzenes

X	$\delta(C^{ipso})$	$\delta(C^{ortho})$	$\delta(C^{meta})$	$\delta(C^{para})$
H	128.5	128.5	128.5	128.5
Li	186.6	143.7	124.7	133.9
NO_2	148.4	123.6	129.4	134.6
NH_2	146.7	115.1	129.3	118.5
OH	155.4	115.7	129.9	121.1

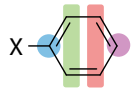

The chemical shifts of aromatic compounds are again significantly influenced by inductive and mesomeric effects. Electron-donating substituents increase the electron density in the aromatic ring. As shown in the possible mesomeric structures for aniline in **Fig. 3.3**, the electron density is highest in the *ortho* and *para* positions relative to the electron-donating substituent. Therefore, the carbons in the *ortho* and *para* positions of these benzene derivatives tend to have lower chemical shifts than those in unsubstituted benzene. The increased electron density also facilitates electrophilic substitution in these positions. Conversely, electron-accepting substituents decrease the electron density in the aromatic ring. As seen in the mesomeric structures for nitrobenzene (**Fig. 3.3**), the electron density is lowest in the *ortho* and *para* positions. For this reason, electro-

philic substitution in these positions is suppressed, and substitution occurs preferentially in the *meta* position relative to the electron-accepting substituent. The chemical shifts of carbons in the *ortho* position to a substituent can also be influenced by steric interactions with the substituent, but the chemical shifts of carbons in the *para* position correlate very well with Hammett constants (**Fig. 3.3B**), which reflect the ability of the substituent to increase or decrease the electron density in the aromatic ring.

A

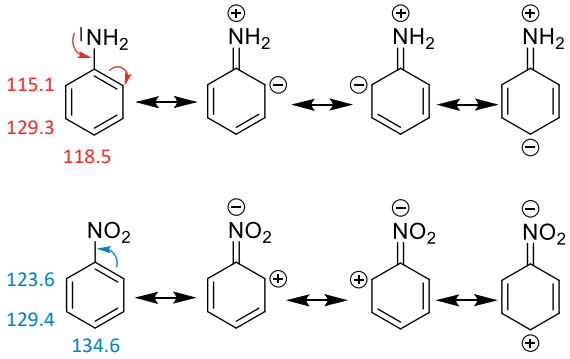

B

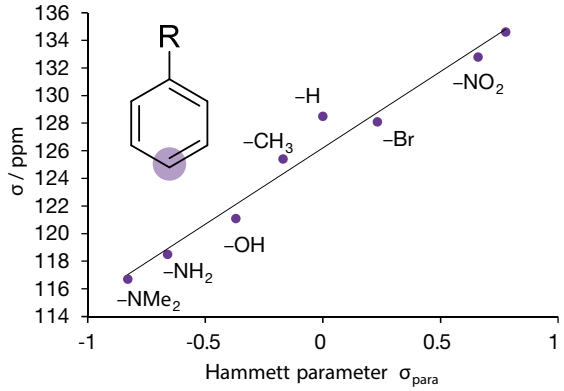

Fig. 3.3: A) The influence of the mesomeric effect on the electron density of carbon atoms and chemical shifts in aromatic compounds (the values of δ in ppm). **B**) The correlation of carbon chemical shifts in the para position to a substituent and Hammett parameters σ_{para}

In **heteroaromatic compounds**, the electron density (and thus the chemical shifts of carbon signals) is significantly influenced by the nature of the heteroatom. The areas of increased or decreased electron density can be determined from the possible mesomeric structures of the given heteroaromatic compound, allowing for an estimation of whether a particular carbon will have a higher or lower chemical shift than the carbons in benzene. For example, the pyridine ring is electron-deficient, and its reactivity toward electrophilic substitution is similar to that of nitrobenzene, with electrophilic substitution most commonly occurring at the 3-position. This correlates well with the chemical shifts of carbon, which are similar to those in nitrobenzene, except for carbon 2, which is directly bonded to the heteroatom (see **Fig. 3.4**).

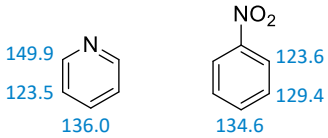

Fig. 3.4: The carbon chemical shifts in pyridine and nitrobenzene (the values of δ in ppm)

3.1.5 Carboxylic-Acid Derivatives

The signals of carbonyl carbons in carboxylic acids, esters, amides, anhydrides and carboxylic-acid halides most commonly occur in the range of 160–180 ppm. When a carboxylic acid is deprotonated in a basic environment, the shielding of the carbonyl carbon is reduced, as a consequence of which its signal appears at higher chemical shifts (approximately 6 ppm higher). Plotting the dependence of chemical shifts on the pH of the environment facilitates the determination of the pK_A of the observed acid (NMR titration, **Section 11.3**).

3.1.6 Aldehydes and Ketones

The signals of carbonyl carbons in aldehydes and ketones usually occur in the range of 190–220 ppm. Conjugated carbonyl carbons (e.g. α,β-unsaturated carbonyl compounds) are more shielded and have a chemical shift approximately 10 ppm lower.

3.2 Coupling Constants

Homonuclear scalar interactions between ^{13}C nuclei in carbon spectra are usually not observed because of the low natural abundance of ^{13}C (1.1%), making it unlikely that a neighboring nucleus will also be ^{13}C. In carbon spectra, homonuclear interactions might appear as ^{13}C satellites around singlet signals; nevertheless, due to the low sensitivity of ^{13}C nuclei, these satellites are often lost in the noise.

Heteronuclear scalar interactions with protons ($^{13}C–^{1}H$) are usually eliminated by decoupling, resulting in spectra that contain only singlets. These spectra are clear and mostly free of overlaps. However, $^{13}C–^{1}H$ interactions can be observed in coupled ^{13}C spectra (measured without decoupling) or in ^{1}H spectra as ^{13}C satellites (**Section 2.6**). It is necessary to know the magnitude of $^{13}C–^{1}H$ scalar interactions for the proper setting of certain experiments, such as APT or INEPT (**Section 5.2**). The magnitude of the interaction through one bond can be estimated by the approximate formula:

$$^{1}J(C,H) = 5 \cdot s\%$$

where s% is the percentage of the s-character of the carbon as determined by its hybridization. Examples are provided in **Table 3.6**. Geminal interactions, $^{2}J(C,H)$, usually range from –10 to +30 Hz, and vicinal interactions, $^{3}J(C,H)$, are typically positive, ranging from 0 to 12 Hz.

Table 3.6: Heteronuclear scalar interactions, $^{1}J(C–H)$, in molecules with various hybridization of carbon atoms

Compound	$H_3C–CH_3$	$H_2C=CH_2$	C_6H_6	HC≡CH
Hybridization	sp^3	sp^2	sp^2	sp
s%	25	33.3	33.3	50
Calculated value of $^{1}J(C,H)$	125	166.5	166.5	250
Experimental value of $^{1}J(C,H)$	124.9	156.4	158.4	249.0

04

^{1}H NMR SPECTROSCOPY

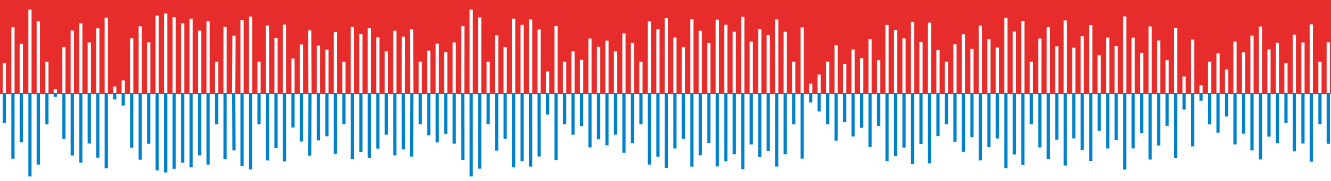

Chapter content

Proton spectra are the most frequently measured NMR spectra because hydrogen nuclei (^{1}H) are the most sensitive in terms of NMR spectroscopy. This is due to the fact that their natural isotopic abundance is nearly 100%. They also have the highest gyromagnetic ratio among all stable isotopes. A typical ^{1}H NMR measurement takes approximately 2–5 minutes, and the resulting spectrum provides very valuable information about the structure of the measured compound. In addition to the chemical shifts of individual signals, we also observe the splitting of signals resulting from homonuclear scalar interactions (most often ^2J(H,H) and ^3J(H,H)) in the spectra. Furthermore, the spectra can be quantified quite accurately, making it possible to determine the number of equivalent hydrogen atoms contributing to each signal. A disadvantage of proton spectra is the small range of chemical shifts (usually from 0 to 10 ppm), which often leads to overlapping signals in the spectrum.

In the following sections, we will first discuss some important concepts and phenomena encountered when interpreting proton spectra. We will also examine the typical chemical shifts of hydrogen atoms in the most common functional groups and the use of homonuclear spin–spin interactions (H,H) for structural analysis.

4.1 Chemical and Magnetic Equivalence

The concept of **chemical equivalence** is intuitive for chemists: Atoms with the same chemical environment (determined by the chemical bonds between these atoms and other atoms in the molecule, as well as the conformation of the molecule) are chemically equivalent. The nuclei of these atoms have the same electronic environment and are shielded by the electrons in the same way, so that they resonate at the same frequency (resulting in a shared signal in the spectrum). However, in order to understand the appearance of signals completely, it is also necessary to introduce the concept of **magnetic equivalence**. Magnetically equivalent nuclei are those that are chemically equivalent and, at the same time, have the same magnitude of scalar interactions with all other magnetically active nuclei in the molecule. For example, the hydrogen nuclei in a molecule of difluoromethane (**Fig. 4.1A**) have the same chemical environment due to the symmetry

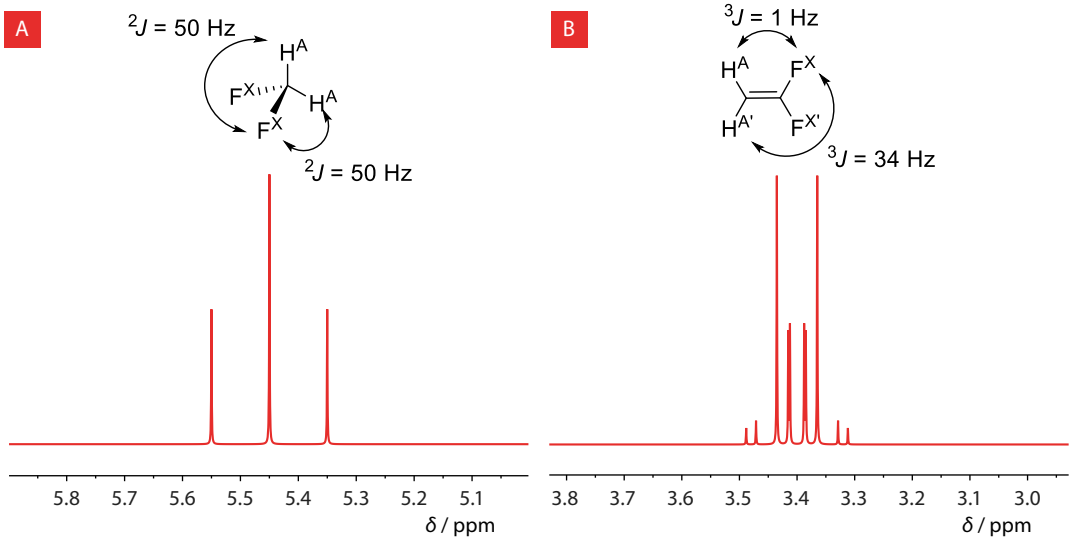

Fig. 4.1: The ^{1}H NMR spectra of difluoromethane (**A**) and 1,1-difluorethene (**B**)

of the molecule and are thus chemically equivalent. Furthermore, both hydrogen nuclei will have the same scalar interaction with both fluorine (^{19}F) nuclei in the molecule, again due to molecular symmetry. Therefore, the two hydrogen nuclei in difluoromethane are both chemically and magnetically equivalent.

In a molecule of 1,1-difluoroethene (**Fig. 4.1B**), both hydrogen nuclei are also chemically equivalent, but the scalar interaction between hydrogen H^A and fluorine F^X differs in magnitude from the scalar interaction between hydrogen $H^{A'}$ and the same fluorine nucleus F^X. Therefore, the hydrogens H^A and $H^{A'}$ are not magnetically equivalent. The magnetic nonequivalence of the H^A and $H^{A'}$ nuclei leads to a more complex appearance of the signal for these nuclei in the spectrum. Since these nuclei are chemically equivalent, their signals have the same chemical shift, but the signal is more complex and contains more lines of varying intensity.

The spin system of difluoromethane is referred to as A_2X_2. The spin system in 1,1-difluoroethene is designated as AA'XX'; this notation indicates that the molecule contains two types of chemically equivalent nuclei, A and X, but the two chemically equivalent A nuclei are not magnetically equivalent and, likewise, the two chemically equivalent X nuclei are not magnetically equivalent either.

Magnetic nonequivalence often occurs in the case of aromatic compounds, where scalar interactions through four or five bonds are frequently observed. For example, in *para*-disubstituted derivatives of benzene, the hydrogen nuclei in the *ortho* position relative to one substituent are

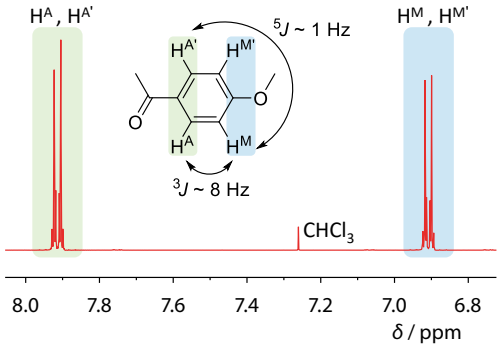

Fig. 4.2: The aromatic region of the ^1H NMR spectrum of a *para*-disubstituted benzene containing signals of magnetically non-equivalent nuclei

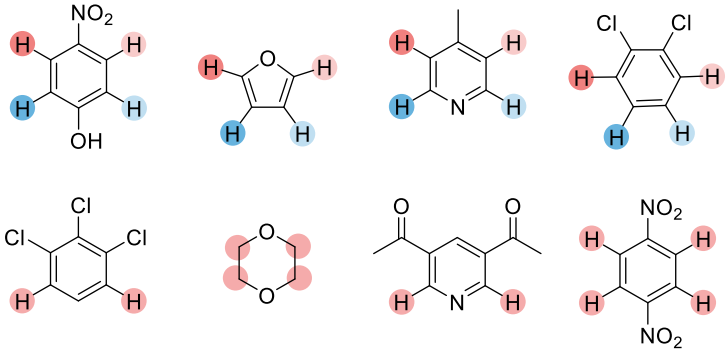

Fig. 4.3: Examples of molecules with magnetically nonequivalent hydrogens: The hydrogens marked with different shades of the same color are chemically equivalent but magnetically nonequivalent. Hydrogens marked with the same color and shade (in the second row) are both chemically and magnetically equivalent.

chemically equivalent. However, due to the unequal magnitude of the scalar interaction with another hydrogen in the *meta* position of the molecule, these nuclei are not magnetically equivalent. This magnetic nonequivalence leads to the formation of multiplets in the spectrum (**Fig. 4.2**). The signals of magnetically nonequivalent nuclei may resemble a doublet, triplet, etc., but they must always be described as multiplets because, upon closer inspection, they consist of more lines of varying intensity.

Other examples of molecules with magnetically equivalent and nonequivalent hydrogen nuclei are shown in **Fig. 4.3**.

4.2 Spin System, the Order of the Spectrum

In the previous text, the spin system in a molecule was denoted by letters, or by letters with primes for magnetically nonequivalent nuclei (A_2X_2, AA'XX'). This method of labeling spin systems is normally used in texts describing NMR spectra. For signals that are far apart in the spectrum, it is common to utilize letters that are distant from each other in the alphabet (e.g. A and X), whereas letters closer together in the alphabet (such as A and B) are used for signals that are close to one another in the spectrum.

The spectra of spin systems with scalar interactions between nuclei are called **first-order spectra** when the difference in resonance frequencies is significantly larger than the size of the spin–spin coupling constant (an example is the AX system in **Fig. 4.4**). First-order spectra can be analyzed according to the rules discussed in **Section 2.6**, for instance the interaction with one other nucleus causes the signal to split into a doublet with a line intensity ratio of 1:1.

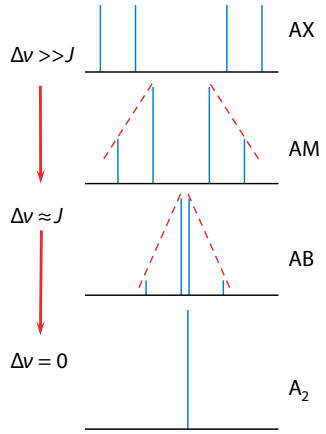

Fig. 4.4: The spectrum of a molecule containing two interacting ^{1}H nuclei. In the AX system, the difference in resonance frequencies is significantly larger than the size of the coupling constant *J*(A,X), which leads to the observation of a first-order spectrum. In the AM and AB spectra, the difference in resonance frequencies is comparable to the size of the coupling constant, and the roof effect is observed. If the difference in resonance frequencies is zero, the coupling between the nuclei is not manifested in the spectrum.

When the difference in the resonance frequencies of the interacting nuclei is comparable to the magnitude of the coupling constant, the intensity ratios of the lines in the multiplets change and no longer match the ratios derived from Pascal's triangle. The intensity of the line that is closer to the signal of the interacting partner in the spectrum becomes higher than the intensity of the line further away. This change in line intensities is called the **roof effect**; when the peaks of individual

lines of one signal are connected, we obtain the first half of a "roof," and the connection of the peaks of the lines of the second signal provides the other half of the "roof." Both parts of the roof always face each other, which means that the connection of the peaks of the lines always forms a roof, not a V-shape.

If the line intensities in the multiplets are not significantly different from the ideal ratios derived from Pascal's triangle, the spectrum is sometimes referred to as a **pseudo-first-order spectrum** (such as the AM-system spectrum in **Fig. 4.4**). If the changes in the line intensities are pronounced, the spectrum is classified as a **higher-order spectrum** (also called a second-order spectrum in some cases), with the AB-system spectrum in **Fig. 4.4** being an example.

4.3 Chirality

A molecule that contains an element of chirality (such as a center, axis, or plane of chirality) is referred to as chiral or optically active (it rotates the plane of polarized light). The mirror image of such a molecule is called an enantiomer. In organic chemistry, we most commonly encounter centers of chirality. For example, a carbon atom that is bonded to four different substituents is chiral (it cannot be superimposed on its mirror image). The configuration of chiral centers is labeled as *R* or *S*, according to the Cahn–Ingold–Prelog rules.

Enantiomers have identical physical and chemical properties unless they interact with another chiral element in the environment (for example with another chiral molecule or polarized light). If a molecule contains multiple elements of chirality, such as two chiral centers, the enantiomer of this molecule has the opposite configuration at all chiral elements. If the configuration is changed at one (or more, but not all) chiral elements, we obtain a diastereomer. Diastereomers have different physical and chemical properties and hence different NMR spectra.

Standard NMR spectroscopy does not involve any chiral element, which means that enantiomers are indistinguishable in typical NMR spectra. Consequently, ordinary NMR spectra cannot be used to determine the optical purity of substances. In order to be able to distinguish between enantiomers in NMR spectra, it is necessary to introduce a chiral element, which transforms the problem of distinguishing between enantiomers into the problem of distinguishing between diastereomers. A common approach is to use **chiral shift reagents** or **chiral solvents**. When a single enantiomer of a chiral solvent is used, the solvation of the chiral substrate and the intermolecular interactions between the substrate and the solvent are different for each enantiomer of the substrate. This results in different signals in the NMR spectrum for each enantiomer. Examples of chiral solvents include 1-phenyl-2,2,2-trifluoroethanol, 1-phenylethanol and 1-phenylethanamine (**Fig. 4.5**). An example of enantiomer differentiation using a chiral solvent is shown in **Fig. 4.6**.

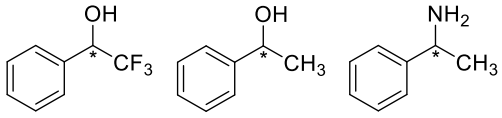

Fig. 4.5: The structures of the most commonly used chiral solvents

The method of using **chiral shift reagents** is based on a principle similar to the use of chiral solvents. Chiral shift reagents are substances that interact with substrate molecules, but this interaction differs depending on the configuration of the substrate. In solution, the interaction leads to the formation of complexes of the substrate and reagent, in which both the substrate and the reagent contain a chiral element. A substrate with the opposite configuration at the chiral center

forms a diastereomeric complex, which results in a different NMR spectrum. A commonly used chiral shift reagent is 1-anthryl-2,2,2-trifluoroethanol (**Fig. 4.7**). For the differentiation between enantiomers using chiral shift reagents, it is necessary to ensure a sufficiently strong interaction between the substrate and the shift reagent. This interaction can be enhanced by using weakly solvating solvents (such as chloroform), increasing the concentration of the shift reagent, or by lowering the temperature during the experiment.

In the past, it was common to utilize shift reagents containing lanthanoid ions, such as the europium complex with a fluorinated diketone derivative of camphor, $Eu(TFC)_3$ or $Eu(HFC)_3$. However, these substances are less frequently used now because, on spectrometers with higher magnetic fields, they often cause significant broadening of the substrate signals.

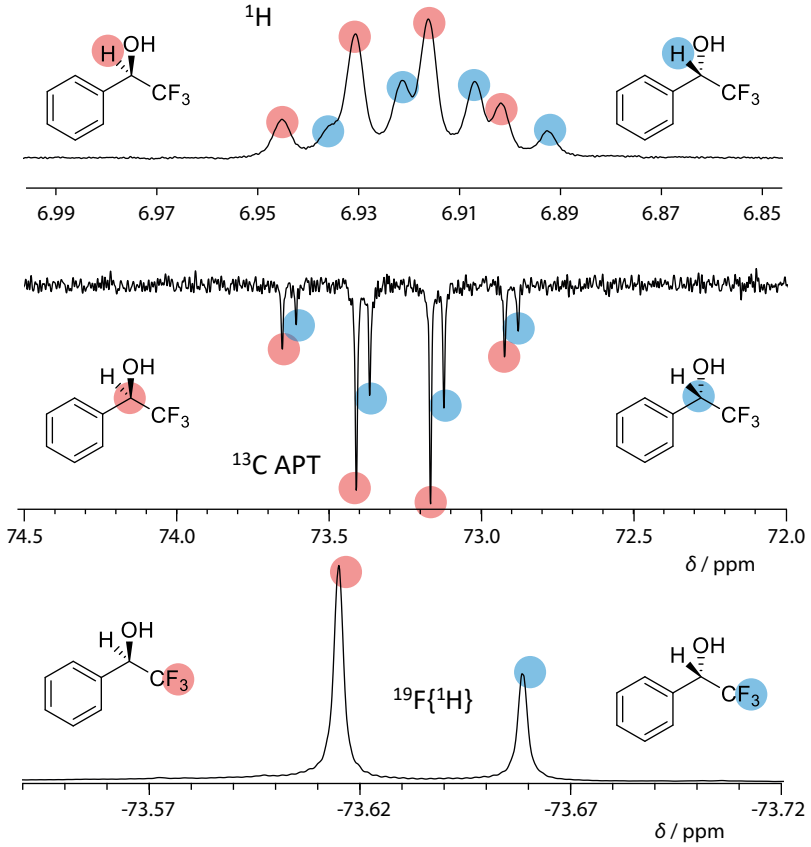

Fig. 4.6: A part of the spectra of ^{1}H, ^{13}C APT and ^{19}F with ^{1}H decoupling, showing a mixture of two enantiomers of 1-phenyl-2,2,2-trifluoroethanol (in an *R* : *S* ratio of 2:1) in the chiral solvent *R*-1-phenylethanamine. The signal in both the hydrogen and carbon spectra is split into a quartet due to coupling with the three ^{19}F nuclei

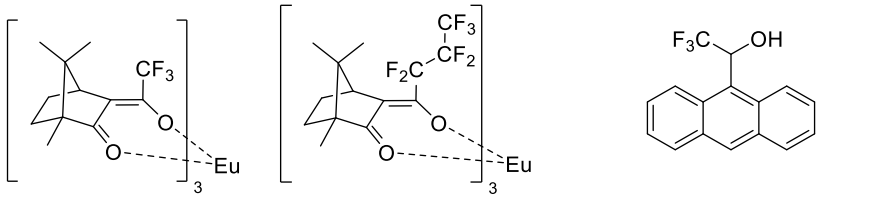

$Eu(TFC)_3$ $Eu(HFC)_3$ 1-anthryl-2,2,2-trifluorethanol

Fig. 4.7: Examples of chiral shift reagents

Another approach to distinguishing between two enantiomers in NMR spectra is chemical **derivatization**. This method introduces an additional chiral center into the molecule, converting enantiomers into diastereomers, which are distinguishable in NMR spectra (**Fig. 4.8**). One of the most commonly used derivatization reagents is 3,3,3-trifluoro-2-methoxy-2phenylpropanoic acid, also known as **Mosher's acid**. The derivatization of chiral alcohols with this acid (forming diastereomeric esters) even enables the determination of the **absolute configuration** of the chiral alcohol based on changes in chemical shifts caused by the proximity of the phenyl ring.

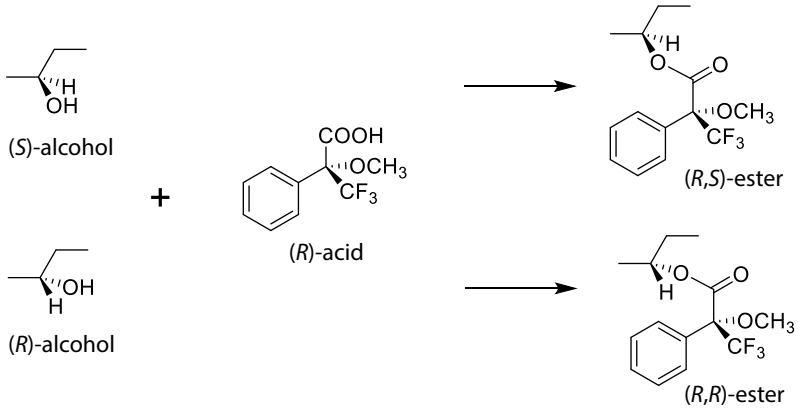

Fig. 4.8: The reaction of one enantiomer of Mosher's acid with two enantiomers of an alcohol leads to the formation of two diastereomeric esters

Chiral elements in a molecule or the possibility of their formation are also important for the chemical equivalence of atomic nuclei. For example, the hydrogens H^A and H^B in the molecule of *cis*-2-methylcyclopentanol (**Fig. 4.9**) are not chemically equivalent because the hydrogen H^A is in the *cis* position relative to both the methyl and hydroxyl substituents, whereas the hydrogen H^B is in the *trans* position. The hydrogens H^A and H^B are referred to as **diastereotopic**; since they are not equivalent, each has its own signal in the spectrum, and we can also observe the geminal interaction ^2J between them.

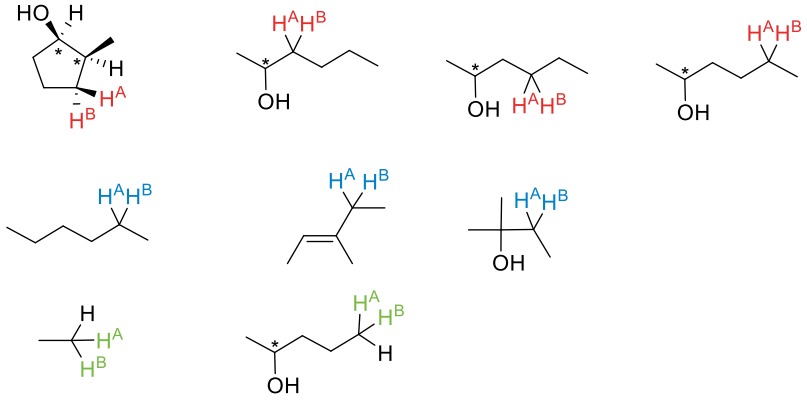

Fig. 4.9: Examples of diastereotopic (**red**), enantiotopic (**blue**) and homotopic (**green**) hydrogen atoms H^A and H^B

Hydrogens (or atoms and molecular fragments in general) can be classified into three types: homotopic, enantiotopic and diastereotopic (**Fig. 4.9**). **Homotopic** hydrogens are indistinguishable by NMR spectroscopy and always give a single, shared signal (for instance, all three hydrogens in

methyl groups are always homotopic). **Enantiotopic** hydrogens can be distinguished in a chiral environment. For example, the measurement of the NMR spectrum of ethanol in a chiral solvent or in the presence of a chiral shift reagent can distinguish between the two hydrogens in the CH_2 group because each has its own signal in the spectrum. However, in the measurement of standard NMR spectra without the presence of chiral interactions, both hydrogens in the CH_2 group of ethanol are equivalent. **Diastereotopic** hydrogens are chemically non-equivalent; each of them can have a separate NMR signal.

In order to determine the topicity of the hydrogens in CH_2 groups, if we consider only chiral centers as possible elements of chirality, we can use the following simple rules:

1. If the replacement of one of the hydrogens with another substituent does not create any chiral center, the hydrogens are homotopic, which means that they are indistinguishable in terms of NMR spectroscopy.
2. If the replacement of one of the hydrogens with another substituent creates a single new chiral center and there are no other chiral centers in the molecule, the hydrogens are enantiotopic. In standard NMR spectra, they are also indistinguishable, and distinguishing between them requires the use of a chiral solvent or a shift reagent.
3. If the replacement of one of the hydrogens with another substituent creates a new chiral center and there is already another chiral center present in the molecule, or multiple chiral centers are formed at once, the hydrogens are diastereotopic. This means they are nonequivalent, each has its own NMR signal, and we can also observe couplings between them.

An example of a hydrogen spectrum that demonstrates the nonequivalence of diastereotopic hydrogens is shown in **Fig. 4.10**. A somewhat more complex case occurs when the replacement of one of the hydrogens results in the formation of multiple chiral centers simultaneously. An example of this is dibenzyl sulfoxide, with its hydrogen spectrum shown in **Fig. 4.11**. The hydrogens in the CH_2 group are diastereotopic because the substitution of one of them creates a chiral center on both the carbon and sulfur atoms (sulfur has a lone electron pair as the fourth substituent). Consequently, each hydrogen has its own signal and it is possible to observe a geminal interaction between them. Nevertheless, the chemical shifts of the two hydrogens are close, so that on

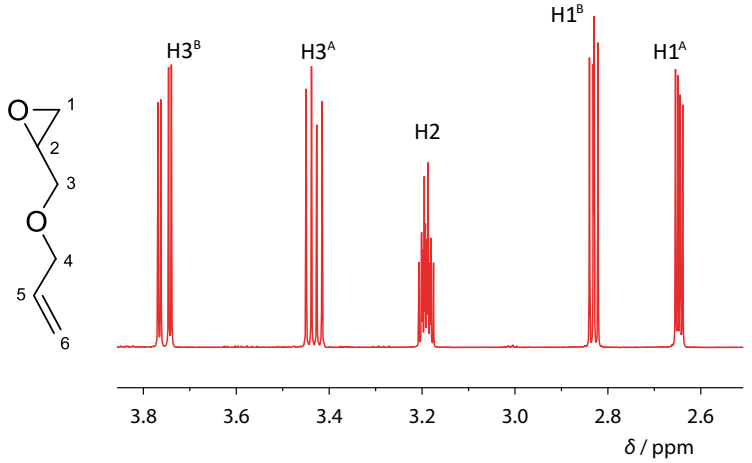

Fig. 4.10: A part of the ^1H spectrum of allylglycidyl ether. The hydrogen atoms in the CH_2 groups at positions 1 and 3 are diastereotopic, which means that they are not equivalent. Each has its own signal, and it is also possible to observe the spin–spin couplings between them

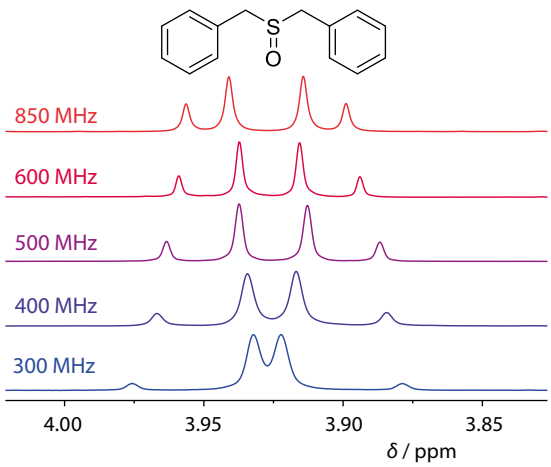

Fig. 4.11: A part of the ^{1}H spectrum of dibenzyl sulfoxide. The hydrogens in the CH_2 group are diastereotopic and each of them has its own signal. It is possible to observe the geminal interaction between them.

spectrometers with low resonance frequency, a higher-order spectrum is observed. Even on an 850-MHz spectrometer, the roof effect is clearly visible. In analogy to dibenzyl sulfoxide, a similar non-equivalence might be expected in debenzyl amine. However, rapid pyramidal inversion of the nitrogen atom causes an effective racemization of the chiral center on this atom. Therefore, the two hydrogen atoms in the CH_2 group in dibenzyl amine are enantiotopic and give rise to a single singlet NMR signal in an achiral environment. At low temperature, however, the pyramidal inversion may be suppressed and the CH_2-hydrogen atoms may become diastereotopic.

Examples of other molecules with diastereotopic hydrogens are provided in **Fig. 4.12**. The case with phosphonates shown in this figure is quite complex. The dimethyl ester of phosphonic acid (the middle structure) does not contain any element of chirality. However, the replacement of one methyl group (for example CH_3^A) results in the simultaneous formation of two new chiral centers (on the CH carbon of isopropyl and on phosphorus). The substitution of the second methyl group from the same isopropyl group (CH_3^B) also creates two new chiral centers, where the configuration of the chiral center on phosphorus is the same as in the previous case, but the configuration on the CH carbon is opposite. The methyl groups A and B are thus diastereotopic. The replacement of one methyl group from the second isopropyl group ($CH_3^{A'}$) again creates two new chiral centers, where the chiral center on phosphorus has the opposite configuration compared to previous cases and the CH carbon has the opposite configuration with respect to the one resulting from the replacement of methyl CH_3^A. Therefore, the methyl groups CH_3^A and $CH_3^{A'}$ are enantiotopic. Similarly, the methyl groups CH_3^B and $CH_3^{B'}$ are also enantiotopic. In achiral solvents, two signals

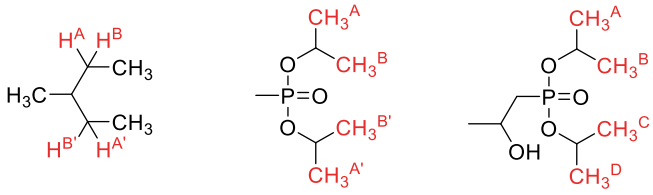

Fig. 4.12: Examples of the diastereotopic hydrogen atoms H^A and H^B. The hydrogens H^A and H^B in 3-methylpentane are diastereotopic because the replacement of one of them creates chiral centers at positions 2 and 3 of the pentane chain. The two H^A hydrogens at positions 2 and 4 are enantiotopic. A similar reasoning explains why the methyl groups in diisopropylphosphonates are not equivalent. In the case of the diisopropyl methylphosphonate, the hydrogen spectrum comprises two signals for diastereotopic methyl groups, CH_3^A and CH_3^B. The spectrum of 2-hydroxypropylphosphonate contains four signals for diastereotopic methyl groups.

for methyl groups can be observed in both the carbon and hydrogen spectra of this substance. The methyl signals in the carbon spectrum are additionally split into doublets due to the interaction with phosphorus, $^{3}J(^{13}C,^{31}P)$. The methyl signals in the hydrogen spectrum are also split into doublets due to the interaction with the CH hydrogen. The phosphonate molecule on the right in **Fig. 4.12** already contains one chiral center. The replacement of any methyl group from the isopropyl residues creates two additional chiral centers. Therefore, all four methyl groups of the isopropyl residues are mutually diastereotopic (i.e. non-equivalent) and the spectra include four different signals belonging to these methyl groups; due to couplings to ^{31}P (in carbon spectra) or to the CH hydrogen (in ^{1}H spectra), these signals are again split into doublets.

4.4 Shielding of Nuclei by Spatially Close Chemical Bonds or Functional Groups

Aromatic molecules contain a system of delocalized π electrons that are positioned above and below the plane of the aromatic skeleton and can move freely within their delocalized orbitals. When an aromatic molecule is placed in a magnetic field, its π electrons move in such a way that they create a circular current, producing an additional magnetic field opposite to the external magnetic field $\boldsymbol{B}_0$ (**Fig. 4.13**). The nuclei that are located close to this molecule, above and below its ring, are additionally shielded by this circular current and their chemical shift is lower than that without the spatial interaction with the aromatic molecule. On the other hand, the nuclei in the plane of the aromatic ring have a higher chemical shift. This additional shielding or deshielding of the nuclei in the vicinity of aromatic molecules is called the "**ring-current effect**."

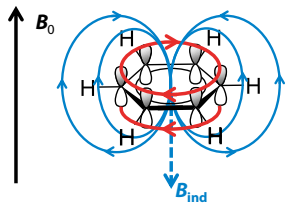

Fig. 4.13: The ring-current effect in the vicinity of aromatic molecules

The ring-current effect is responsible for the characteristic chemical shifts of aromatic hydrogens, which are significantly higher than, for instance, the chemical shifts of hydrogens on a double bond in cyclohexa-1,3-diene (**Fig. 4.14**). In some molecules, the ring-current effect can lead to unusual chemical shifts, examples of which are also provided in **Fig. 4.14**.

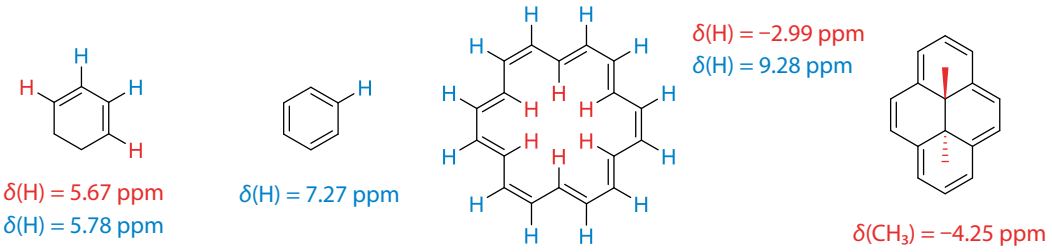

Fig. 4.14: Examples of ^{1}H chemical shifts in molecules where the ring-current effect is present. For comparison, the figure also shows the cyclohexadiene molecule, where a ring-current cannot form.

The ring-current effect can be utilized, for example, when studying the interactions of nucleic acids with small molecules. Planar molecules can often intercalate between two base pairs of a double-stranded DNA. These molecules are then positioned above and below the plane of the aromatic rings of the nucleic-acid bases, and, due to the ring current, their nuclei have lower chemical shifts than if the molecule were freely in solution or interacting with nucleic acids in another way than by intercalation.

Additional shielding or deshielding of nuclei can also be caused by the spatial proximity of various chemical bonds or functional groups. For instance, nuclei located along the axis of a triple bond are shielded by the electrons of the triple bond and have lower chemical shifts. This is also the reason why the hydrogens and carbons of alkynes tend to have lower chemical shifts than the hydrogens and carbons of alkenes.

4.5 Exchangeable Hydrogens

Hydrogens that are bonded to oxygen, nitrogen or sulfur can easily exchange with other hydrogens from the OH, SH or NH groups present in the sample. In deuterated protic solvents, these hydrogens can easily be replaced by deuterium. For example, alcohol dissolved in D_2O can undergo the reaction:

$$R–OH + D_2O \rightarrow R–OD + HDO$$

Therefore, these OH, SH or NH hydrogens are called exchangeable. When measuring the ^1H NMR spectra of compounds with exchangeable hydrogens in aprotic solvents, the exchange with deuterium does not occur and the exchangeable hydrogens can be observed in the spectrum. However, if D_2O, MeOD or another deuterated protic solvent is added to such a sample, these hydrogens are replaced by deuterium and their signal disappears from the ^1H NMR spectrum (**Fig. 4.15**) because the resonance frequency of deuterium nuclei (^2H) is significantly different from that of hydrogen nuclei (^1H) (for instance, on a 500-MHz spectrometer, the resonance frequency of deuterium nuclei is approximately 77 MHz). If the exchangeable hydrogen has indirect spin–spin interactions with other nuclei in the molecule, these interactions are suppressed upon exchange with deuterium.

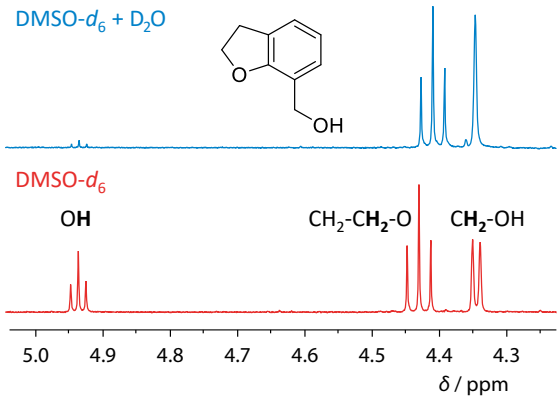

Fig. 4.15: A part of the ^1H NMR spectrum of the displayed molecule in DMSO solution and after adding a drop of D_2O. The addition of D_2O suppresses the hydroxyl-hydrogen signal, and the splitting of the signal of the neighboring CH_2 group disappears. (The slight shift of the signal of the CH_2 group next to the oxygen in the dihydrofuran ring is a result of the change in the solvation of the molecule after the addition of D_2O to the solution.)

In aprotic solvents, the signals of exchangeable hydrogens can be split by indirect interactions with neighboring nuclei. However, a rapid exchange of hydrogens between individual substrate molecules or between the substrate and water, which is often present in trace amounts in solvents, may suppress spin–spin interactions. An example is shown in **Fig. 4.16**, depicting the ^{1}H spectra of methanol measured in DMSO-d_6 at different temperatures. At room temperature, the OH group signal is observed as a quartet (due to interaction with the CH_3 group) and the CH_3 group signal as a doublet. At higher temperatures, the rate of the intermolecular exchange of OH hydrogens increases and the splitting of signals resulting from spin–spin interactions is suppressed. The rate of hydrogen exchange can also increase, for example, in the presence of trace acids or when the sample has low viscosity. Therefore, for instance the splitting of exchangeable hydrogen signals is typically not observed in $CDCl_3$.

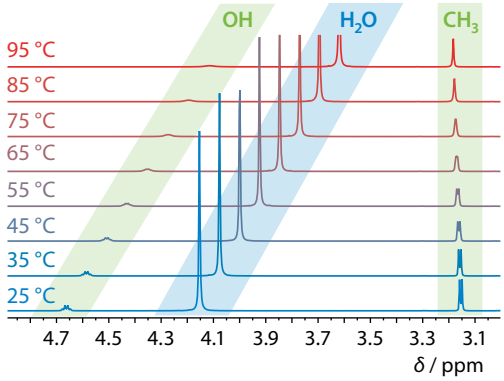

Fig. 4.16: The ^{1}H NMR spectra of methanol with water impurity in DMSO-d_6 measured at different temperatures

Exchangeable hydrogens often participate in hydrogen bonds X–H···Y with other electronegative atoms in the sample. The formation of a hydrogen bond elongates the X–H bond, which reduces the shielding of the hydrogen nuclei by bonding electrons. Signals of these hydrogens then have higher chemical shifts; in the case of strong hydrogen bonds, the chemical shifts can be unusually high. For example, the signal of the OH group in the red azo dye Sudan I is almost at 16 ppm (**Fig. 4.17**).

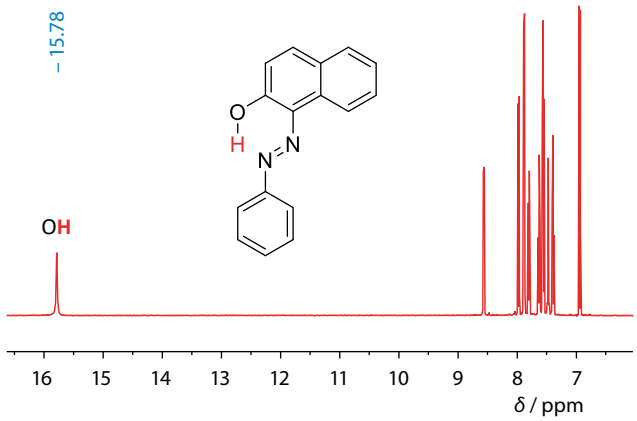

Fig. 4.17: The ^{1}H NMR spectrum of the azo dye Sudan I

By measuring ^{1}H NMR spectra at different temperatures, it is possible to distinguish between intramolecular and intermolecular hydrogen bonds. At higher temperatures, molecules move more

rapidly and intermolecular hydrogen bonds are disrupted. Therefore, the signals of the hydrogens involved in these hydrogen bonds move toward lower chemical shifts as the temperature increases. In contrast, the chemical shifts of the hydrogens involved in intramolecular hydrogen bonds tend to be less temperature-dependent (**Fig. 4.18**). The temperature dependence of the chemical shifts of exchangeable hydrogens is also the reason why it is not advisable to use the water-hydrogen signal as a reference for the chemical-shift scale in ^{1}H spectra (**Chapter 10**). On the other hand, the temperature dependence of OH-hydrogen signals can be used to calibrate the temperature in the NMR tube during experiments (see also **Chapter 10**)

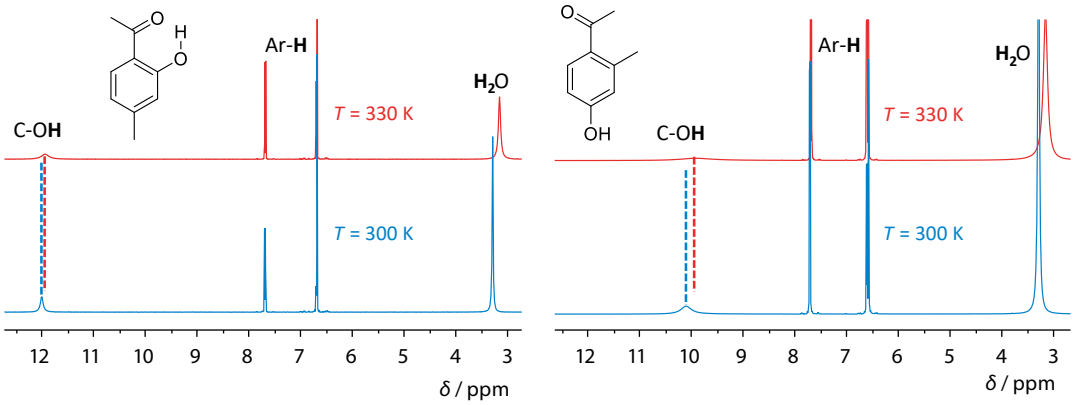

Fig. 4.18: The ^{1}H NMR spectra of two different substituted phenols at 300 K and 330 K. The chemical shifts of the signals of water and OH hydrogens, which are not part of an intramolecular hydrogen bond, are significantly more temperature-dependent.

4.6 The Influence of Magnetic Field, Solvent, Concentration and Temperature

The intensity of the magnetic field in an NMR spectrometer affects both the sensitivity of the measurement and the spectral resolution. The signal intensity increases approximately with the square of the magnetic-field strength (**Section 2.2**). For example, the sensitivity of an NMR experiment on a 600-MHz spectrometer is roughly four times higher than on a 300-MHz spectrometer with a similar probe.

On spectrometers with a stronger magnetic field, the spectral resolution is also higher. It is important to note that the chemical shift (expressed in ppm) is independent of the intensity of the magnetic field. Similarly, scalar coupling constants (expressed in Hz) are molecular properties, independent of the external magnetic field. However, on a spectrometer with a stronger magnetic field, 1 ppm corresponds to a wider frequency range (a "greater number of Hz") than on a spectrometer with a weaker field. For instance, on a 600-MHz spectrometer, 1 ppm = 600 Hz. Two doublets separated by 0.1 ppm (= 60 Hz) and coupled with a coupling constant of 5 Hz would be well resolved, and we would observe a first-order spectrum (**Fig. 4.4**, **Section 4.2**). However, on a 60-MHz spectrometer, 0.1 ppm would correspond to 6 Hz, and the doublet signals would overlap, producing a higher-order spectrum. An example of how the magnetic-field strength affects signal resolution is shown in **Fig. 4.19**, depicting the signals of the diastereotopic hydrogens of the CH_2 group at position 4 of allylglycidyl ether. The chemical shifts of both hydrogens are close.

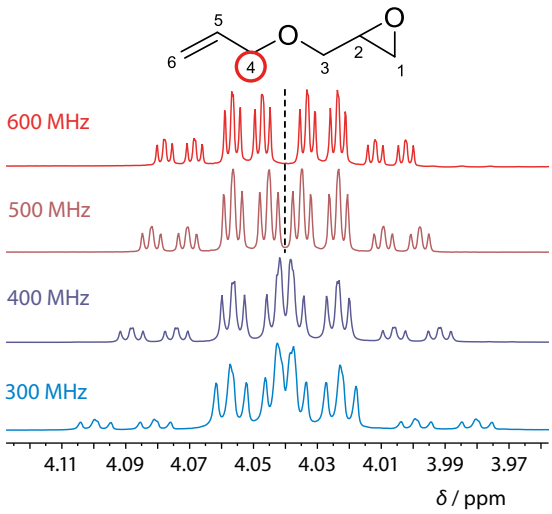

Fig. 4.19: A part of the ^{1}H spectra of allylglycidyl ether showing signals of two nonequivalent hydrogens at position 4; the spectra are measured on spectrometers with different operating frequencies as indicated in the figure. The dashed line separates the two signals in 600-MHz and 500-MHz spectra; at lower fields, the two signals overlap and cannot be separated.

Consequently, on a spectrometer with a lower operating frequency, there is a significant signal overlap and a higher-order spectrum is observed. On a higher-frequency spectrometer, the two signals can be clearly distinguished; each signal is split into a doublet of doublet of triplets (ddt) due to geminal coupling with the other hydrogen in the CH_2 group, vicinal coupling with the neighboring hydrogen at position 5, and two four-bond couplings with the hydrogens at position 6.

Solvents can have a significant effect on NMR spectra, especially if the observed compound interacts (e.g. through hydrogen bonds or π-interactions) with the solvent molecules. An extreme case is water, which has a chemical shift of 0.4 ppm in deuterated benzene and 4.9 ppm in methanol (**Table 4.1**). For hydrogens bonded to carbon, the solvent effect is typically smaller than for exchangeable hydrogens, but chemical-shift changes can still be on the order of several tenths of a ppm. Therefore, when describing an NMR spectrum, it is essential to record the solvent used.

Table 4.1: The chemical shifts δ of water hydrogens in various solvents

Solvent	δ(H_2O)	Solvent	δ(H_2O)
C_6D_6	0.4	$(CD_3)_2SO$	3.3
$CDCl_3$	1.6	D_2O	4.8
$(CD_3)_2CO$	2.8	CD_3OD	4.9

The concentration of the measured compound affects the intensity of the signals and thus the time required to complete the experiment. On the other hand, concentration generally does not have a significant effect on the chemical shifts of the compound. Exceptions occur when substrate–substrate interactions take place at higher concentration, e.g. in the formation of hydrogen-bonded dimers of carboxylic acids.

Temperature significantly affects NMR spectra when dynamic processes (such as a chemical reaction or slow rotation around a partial double bond) occur in the sample. Dynamic processes in NMR spectroscopy, and thus the effect of temperature, are covered in detail in **Chapter 11**.

4.7 Chemical Shifts of Hydrogens

The spectral regions where ^{1}H NMR signals of different types of organic molecules appear (see **Fig. 4.20**) resemble the distribution of typical spectral regions for carbon signals (see **Fig. 3.1**). However, hydrogen chemical shifts are concentrated within a much smaller range, typically from 0 to 13 ppm.

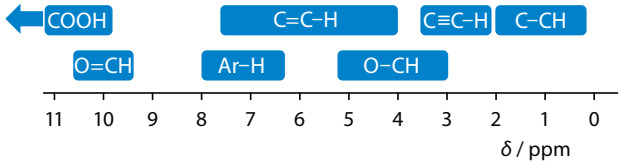

Fig. 4.20: Typical ranges of chemical shifts δ in ^{1}H NMR spectra of organic molecules

4.7.1 Alkanes and Cycloalkanes

The chemical shift of hydrogen in alkanes depends on the substitution of the adjacent carbon (see **Table 4.2**). Electronegative substituents withdraw electron density from the hydrogen nucleus, causing the hydrogen to be less shielded and thus exhibit a higher chemical shift. A comparison of chlorinated methanes shows the additive effect of substituents: The chemical shift of the hydrogens in chloromethane is 3.1 ppm, in dichloromethane 5.2 ppm, and in trichloromethane (chloroform) 7.3 ppm. As expected, the electronegative chlorine withdraws electrons through an inductive effect, deshielding the hydrogen nucleus and shifting its signal to higher ppm values. The chemical shift of unsubstituted cyclopropane is 0.2 ppm, of unsubstituted cyclobutane 1.9 ppm, and other unsubstituted cycloalkanes show signals in the range of 1.4–1.6 ppm.

Table 4.2: The chemical shifts δ (in ppm) of the hydrogens in substituted methane, X–CH_3

X	Li	R_3Si	H	CH_3	NH_2	OH	NO_2	F	Cl	Br	I
δ(H)	–1.0	0.0	0.4	0.8	2.4	3.3	4.3	4.3	3.1	2.7	2.2

4.7.2 Alkenes

The signals of hydrogens on double bonds appear over a wide range of chemical shifts, from 4 to 7.5 ppm. Like carbon chemical shifts, the chemical shifts of hydrogens can be influenced by the inductive and mesomeric effects of substituents. **Fig. 4.21** shows the chemical shifts of ethene substituted with electron-donating methoxy groups and electron-accepting nitro groups. The chemical shift of the hydrogens in unsubstituted ethene is 5.3 ppm.

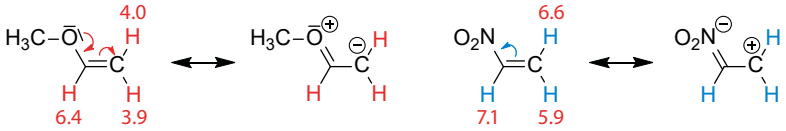

Fig. 4.21: ^{1}H chemical shifts in substituted ethane

4.7.3 Alkynes

The signals of hydrogens on triple bonds appear in the region of 2–3 ppm.

4.7.4 Aromatic Compounds

The chemical shifts of hydrogens in aromatic compounds are mainly influenced by the mesomeric effects of substituents. The signals of the hydrogens in substituted benzenes appear in the region of 6.5–8.2 ppm. The hydrogens in unsubstituted benzene have a chemical shift of 7.3 ppm. **Fig. 4.22** shows the mesomeric structures of aniline and nitrobenzene. The electron-accepting or electron-donating nature of the substituents has a significant effect on the chemical shifts of benzene derivatives.

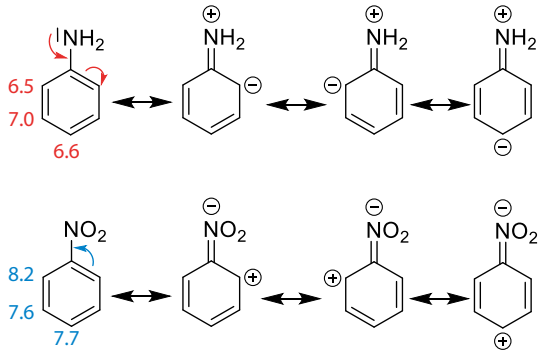

Fig. 4.22: The chemical shifts δ (in ppm) of the hydrogen atoms in aromatic compounds are influenced by the mesomeric effect of the substituents

4.7.5 Aldehydes

The signals of aldehydic hydrogens are usually easily recognizable in the spectrum because they occur in the region of 9.5–10.5 ppm, where no other CH groups are typically observed.

4.7.6 Exchangeable Hydrogens

The signals of exchangeable hydrogens in OH, NH and SH groups can occur over a very wide spectral range, from 1 to 17 ppm, because their chemical shifts are influenced by the acidic nature of these hydrogens. More acidic hydrogens are less shielded by electrons and thus have signals at higher δ values. This is evident, for instance, in the difference between the chemical shifts of hydroxyl hydrogens in phenols and aliphatic alcohols (**Table 4.3**). The chemical shifts of exchangeable hydrogens can also be significantly influenced by hydrogen-bond formation, concentration,

Table 4.3: Chemical-shift ranges for exchangeable hydrogens

Exchangeable hydrogen	Functional group	δ / ppm
OH	aliphatic alcohols	1–5
	phenols	4–10
	carboxylic acids	9–13
	enols	10–17
NH	aliphatic amines	1–5
	amides	5–10
SH	aliphatic thiols	1–3
	thiophenols	3–4

temperature, solvent, the pH of the solution, and the presence of water or other substances containing exchangeable hydrogens. Therefore, the measured chemical shifts of exchangeable hydrogens are reproducible only under identical experimental conditions. The influence of the solvent on the chemical shifts of water hydrogens was demonstrated in **Table 4.1**.

4.8 Scalar Couplings of Hydrogens

Scalar coupling between hydrogens is manifested in NMR spectra as signal splitting, providing highly valuable structural information because the coupling depends on the molecule's geometry and the nature of the substituents. In ^{1}H NMR spectra, we commonly observe interactions over two bonds (geminal) and three bonds (vicinal), but in some cases, interactions over four or more bonds can also be detected.

4.8.1 Geminal Coupling

Geminal coupling occurs between hydrogens in the same CH_2 group when these hydrogens are not equivalent (see **Section 4.3**). Geminal couplings between ^{1}H hydrogens can range from −20 to +40 Hz. However, from standard one-dimensional hydrogen spectra, we cannot determine the sign of the coupling constant and we observe only the absolute value of ^{2}J, which typically ranges from 0 to 40 Hz.

In flexible aliphatic chains, geminal coupling is usually around −12 Hz. The size of geminal coupling depends on the bond angle between the interacting atoms. As the bond angle increases, the value of ^{2}J increases as well. However, since this value is typically below 0 for most substances, the absolute value decreases as the bond angle increases, and thus the observed coupling diminishes. A bond angle of 120°, typical of the hydrogens at the end of a double bond, results in geminal coupling close to 0 Hz. Electronegative substituents in the α-position contribute positively to geminal coupling, as evident in the series cyclopropane–aziridine–oxirane (**Fig. 4.23**). Conversely, proximity to π-electrons leads to a negative contribution, such as in cyclopent-4-en-1,3-dione.

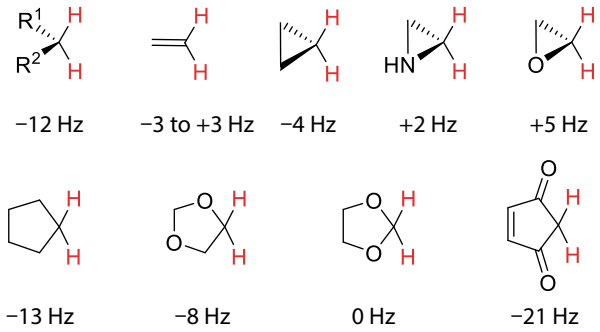

Fig. 4.23: Typical values of the geminal-coupling constants between hydrogen atoms

4.8.2 Vicinal Coupling

Vicinal coupling between hydrogens is crucial for structural analysis, particularly in determining molecular conformation and configuration. The size of the vicinal-coupling constant depends primarily on the dihedral angle between the interacting hydrogens and on the substituents. This dependence on the dihedral angle is known as the **Karplus curve** (**Fig. 4.24**). Vicinal coupling reaches its maximum values at dihedral angles of 0° and 180°, with the maximum at 180° being

higher. For dihedral angles close to 90°, vicinal coupling approaches zero. This relationship can, for instance, be used to determine the positions of substituents on a cyclohexane ring in the chair conformation. When two hydrogens on adjacent carbon atoms are in axial positions, the dihedral angle between them is 180°, and large vicinal coupling (10–13 Hz) is observed. However, when one or both hydrogens are in equatorial positions, the dihedral angle is +60° or –60°, and the vicinal coupling is small (2–4 Hz, see **Fig. 4.25**). In freely rotating aliphatic systems, vicinal coupling is typically in the range of 6–8 Hz.

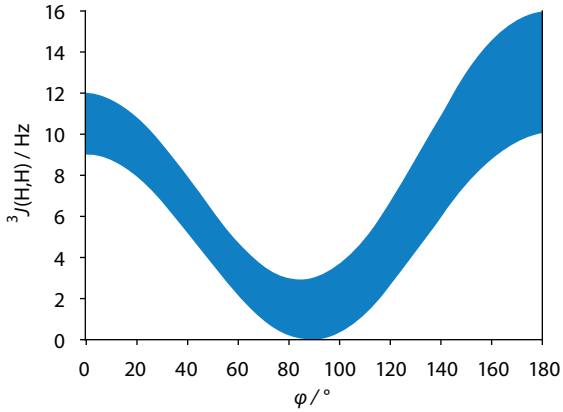

Fig. 4.24: The Karplus curve showing the dependence of the values of vicinal-coupling constants on the dihedral angle φ between the interacting hydrogen atoms

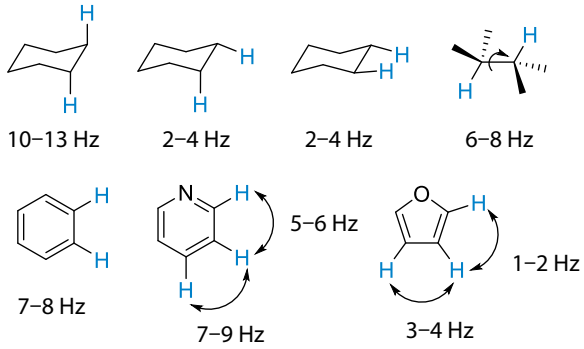

Fig. 4.25: Typical values of vicinal-coupling constants in selected compounds

In benzene derivatives, the vicinal-coupling constant between hydrogens in the *ortho* position is generally 7–8 Hz. The size of the vicinal coupling in aromatic compounds can be significantly affected by the presence of a heteroatom, as shown in **Fig. 4.25**. The vicinal-coupling constant is reduced by electronegative substituents, although this trend is more pronounced in unsaturated compounds than in aliphatic ones (**Tables 4.4** and **4.5**). Vicinal coupling between hydrogens on a double bond is extremely helpful in determining the configuration of the double bond. Hydrogens in a *cis* arrangement have a dihedral angle of 0°, resulting in a smaller vicinal-coupling constant than that of hydrogens in a *trans* arrangement, which have a dihedral angle of 180°.

Table 4.4: Vicinal-coupling constants in substituted ethanes, X–CH_2–CH_3

X	Li	H	CH_3	Cl	OH
^3J(H,H)	8.4	8.0	7.3	7.2	6.9

Table 4.5: Vicinal-coupling constants in substituted ethylenes

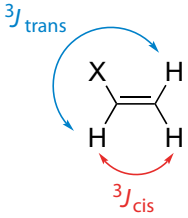

X	Li	H	Cl	OCH_3	F
$^3J_{cis}$	19.3	11.6	7.3	7.1	4.7
$^3J_{trans}$	23.9	19.1	14.6	15.2	12.8

4.8.3 Long-Range Coupling (More than Three Bonds)

The couplings between hydrogens over more than three chemical bonds are usually too small to be observed as signal splitting in one-dimensional hydrogen spectra, because their values are smaller than the half-width of the observed signals. However, there are certain structural motifs where couplings over four or five bonds are larger and thus easily observable in 1D spectra. These motifs include certain bicyclic compounds, structures with multiple bonds between the interacting atoms, aromatic compounds, and structures where the bonds between the interacting atoms form a "W"-like arrangement. Examples of structural motifs that provide observable couplings over four or five bonds are shown in **Fig. 4.26**. Couplings over six or more bonds are rarely observed.

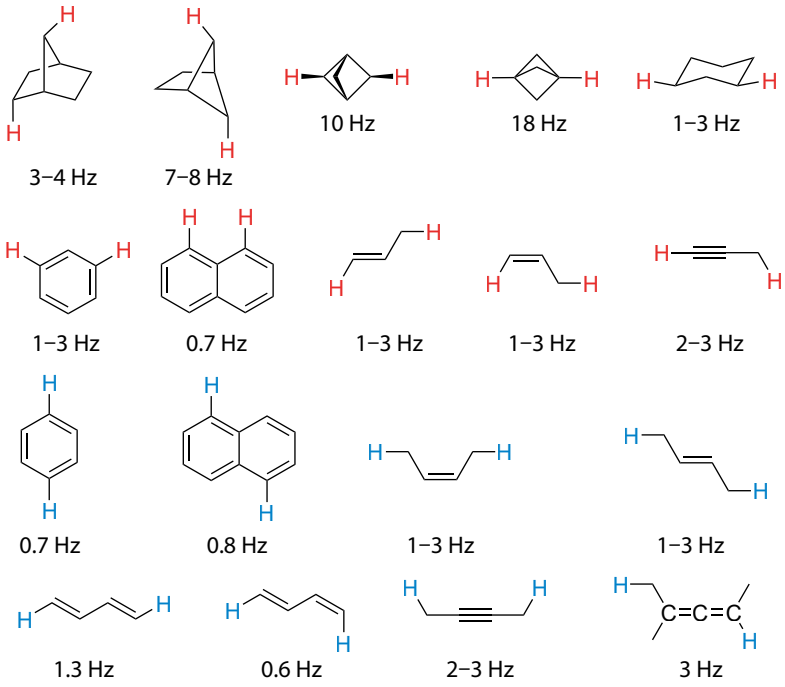

Fig. 4.26: Selected structural motifs where indirect spin–spin coupling across four bonds (^4J) and across five bonds (^5J) can be observed

05

PULSE SEQUENCES AND THEIR ELEMENTS

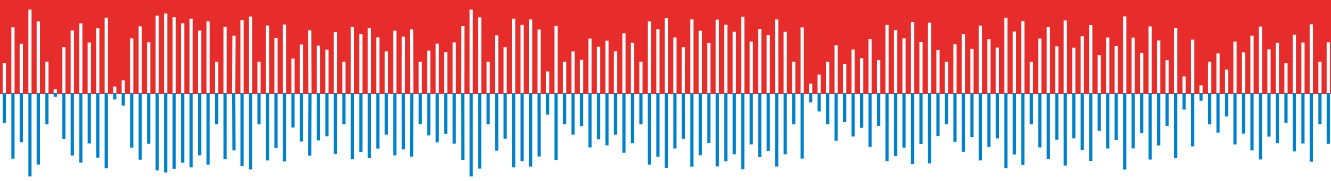

Chapter content

In the previous chapters, we became familiar with the basic principles of NMR spectroscopy and the most commonly measured one-dimensional spectra of ^{1}H and ^{13}C. However, modern NMR spectroscopy enables the acquisition of much more complex structural information than that provided by these basic experiments. Advanced NMR-spectroscopy techniques often manipulate spin systems by means of a series of successive pulses, interspersed with certain delays. This is known as a pulse sequence, which can be graphically represented. The experiment is then clearly defined by the corresponding pulse sequence, including a detailed time description of all events during the experiment. This chapter begins with the introduction of the basic building blocks of pulse sequences, which is followed by a discussion of the most commonly used one- and two-dimensional experiments.

5.1 Elements of Pulse Sequences

A radiofrequency pulse (using the oscillating magnetic field $\boldsymbol{B}_1$, perpendicular to the direction of the $\boldsymbol{B}_0$ field) causes the magnetization vector $\boldsymbol{M}$ to rotate around the axis of the $\boldsymbol{B}_1$ field. In order to understand the development of a spin system during many simple pulse sequences, we can use the vector model, which describes the behavior of magnetization vectors after pulse application. To simplify the description, we use a rotating reference frame that shares the *z*-axis with the regular (laboratory) coordinate system and rotates around this axis at a frequency corresponding to the frequency of the $\boldsymbol{B}_1$ field. The effect of the radiofrequency pulse depends on its power, duration, phase, and the state of the spin system at the moment of the pulse. For example, a pulse along the *x*-axis rotates the magnetization around this axis. If we start from an equilibrium state, where the magnetization vector points along the *z*-axis, a pulse along the *x*-axis will rotate the magnetization vector in the *yz*-plane by a flip angle α, whose value depends on the pulse duration and power. Starting from the equilibrium state, a 90° pulse (or $\pi/2$ pulse) rotates the magnetization by 90° into the *xy*-plane, and a 180° pulse (π pulse) rotates the magnetization to the $-z$ axis. The direction (axis) of the radiofrequency pulse is also called the **phase of the pulse**. Pulse sequences use different (but defined) phases for individual pulses.

In general, the more intense a radiofrequency pulse is, the less selective it becomes (because it excites a broader spectral region). The measurement of one-dimensional NMR spectra most commonly involves very short (on the order of microseconds) and intense pulses, called **hard pulses**, which non-selectively excite the largest possible frequency range of the given nucleus. In graphical representations of pulse sequences, hard pulses are depicted as rectangles (**Fig. 5.1**). The spectral width $\Delta\nu$ excited by a hard 90° pulse can be calculated approximately by the formula:

$$\Delta\nu \approx 0.25/t_{90}$$

where t_{90} is the duration of the 90° pulse. Outside of this spectral width, full excitation does not occur, the flip angle is less than 90°, and the signal intensity in the spectrum is lower.

More distant spectral regions are not excited at all. For example, a 90° pulse with a duration of 5 µs excites a spectral range of about 50 kHz, which is sufficient for measuring, for instance, hydrogen or carbon nuclei on a 500-MHz spectrometer (for the hydrogen-spectrum width of 15 ppm, the required spectral width is 15 × 500 Hz = 7,500 Hz, whereas the spectral width of 200 ppm for a carbon spectrum on the same spectrometer corresponds to 200 × 125 Hz = 25,000 Hz). A problem with exciting the entire spectrum simultaneously may arise when measuring the spectra of fluorine ^{19}F or other nuclei with large ranges of chemical shifts. For example, when measuring ^{19}F nuclei with a chemical-shift range of 400 ppm on a 500-MHz spectrometer, where the resonance

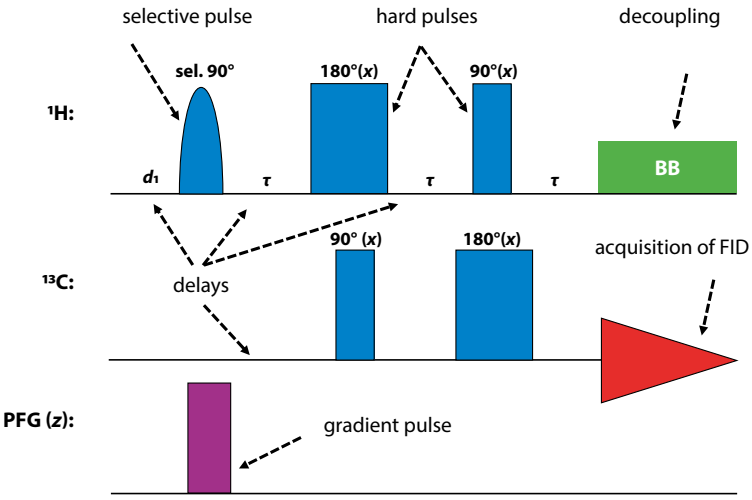

Fig. 5.1: Elements of pulse sequences: delays, pulses, decoupling, data acquisition. The meaning of the abbreviations and terms used is explained in the text.

frequency of ^{19}F nuclei is approximately 470 MHz, one would need to achieve excitation with a spectral width of 400 × 470 Hz = 188 kHz. This would require the use of very short and intense pulses, exceeding the technical limits of standard NMR probes. For this reason, some spectra need to be measured in parts with smaller spectral widths.

The maximum NMR-signal intensity is achieved when the magnetization is flipped by 90° from the equilibrium state (*z*-axis) into the *xy*-plane. In practice, we often use shorter flip pulses, such as a 30° pulse. If we flip the magnetization vector by 30°, we achieve half of the maximum magnetization in the *xy*-plane ($M_{xy} = M_0 \cdot \sin \alpha$) and obtain a signal with half the intensity. However, along the z-axis, there remains 87% of the original magnetization ($M_z = M_0 \cdot \cos \alpha$), allowing for a significantly shorter time before the next repetition of the pulse sequence (**repetition time** t_r). For the optimal flip angle, known as the Ernst angle, the following equation applies for a given repetition time:

$$\cos \alpha = \exp(-t_r/T_1)$$

where T_1 is the relaxation time characterizing the return of magnetization to the *z*-axis (see **Section 7.1**).

Selective pulses excite only a chosen frequency region. The selectivity of a pulse can be achieved by reducing the pulse intensity (power) and extending its duration. For selective excitation, modern NMR spectrometers use shaped pulses, consisting of a sequence of many consecutive pulses varying in power and phase. Shaped pulses can also excite several frequency regions in the spectrum simultaneously. In graphical representations of pulse sequences, selective pulses are depicted as a rounded shape resembling an inverted U (**Fig. 5.1**).

A **gradient pulse** is another possible element of a pulse sequence. It is a short-term creation of a gradient of the magnetic field $\boldsymbol{B}_0$, primarily used in two- and multi-dimensional NMR spectroscopy, in the measurement of diffusion coefficients, and in the suppression of solvent signals. In the graphical representation of pulse sequences, gradient pulses are written in a separate line and marked with the abbreviation PFG (pulsed-field gradient). The use of gradients in NMR spectroscopy is covered in **Chapter 9**.

The measurement of NMR data (the acquisition of FID) is marked with a triangle in pulse sequences (**Fig. 5.1**).

Decoupling is used to suppress spin–spin couplings through the irradiation of selected nuclei (most commonly protons) with another oscillating electromagnetic field, causing rapid transitions between the spin states α and β. Proton decoupling during a carbon experiment is referred to as **heteronuclear decoupling**. If the entire frequency range of the proton spectrum is irradiated in this way, it is called **broadband proton decoupling**. In the pulse sequence, broadband decoupling is represented by a rectangle in the proton channel (**Fig. 5.1**) and marked as BB (short for broadband decoupling). In the text, decoupling is often denoted by curly brackets; for example $^{13}C\{^{1}H\}$ indicates a carbon experiment with broadband proton decoupling. Broadband proton decoupling applied throughout the pulse sequence also leads to an increase in the population differences of the observed ^{13}C nuclei (NOE build-up, see **Chapter 8**), resulting in higher signal intensities.

In **homonuclear decoupling**, both the observed and decoupled nuclei belong to the same isotope. In **selective proton decoupling**, a specific proton signal is selectively irradiated, which removes this signal from the proton spectrum (due to decoupling, the spin states α and β become saturated, as a result of which the overall magnetization of the selected proton is zero) and suppresses all spin–spin interactions of this proton. Selective decoupling thus simplifies multiplets by selectively removing chosen spin–spin couplings. The use of more sophisticated decoupling methods makes it possible to irradiate nuclei with different resonance frequencies simultaneously, allowing multiple signals to be decoupled at once. An example of the carbon spectra of ethanol with the broadband decoupling and selective decoupling of the protons in the CH_2 or CH_3 groups is shown in **Fig. 5.2**.

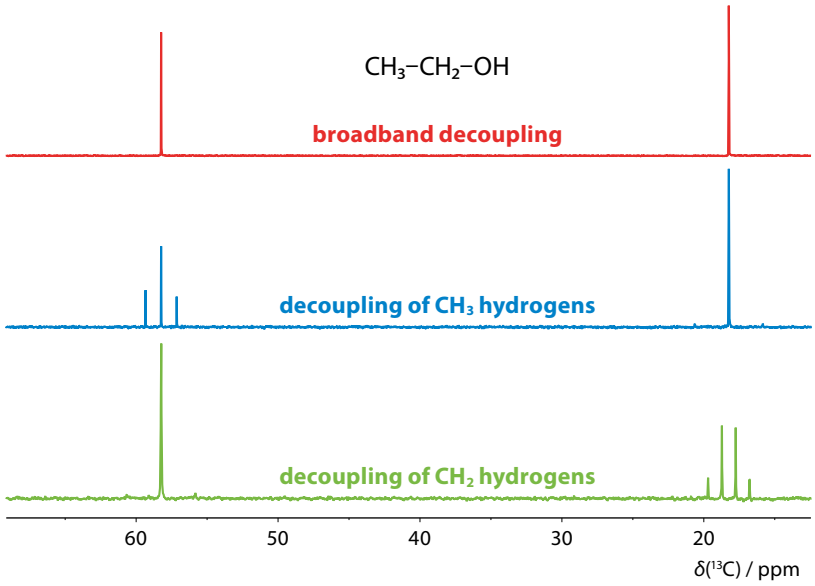

Fig. 5.2: The carbon spectrum of ethanol with the broadband decoupling and selective decoupling of the protons in the CH_3 or CH_2 groups.

5.2 One-Dimensional Pulse Sequences

The simplest-possible pulse sequence contains only one pulse (**Fig. 5.3**). It is suitable for measuring any nucleus without irradiating other nuclei and is commonly used to measure proton spectra. During signal accumulation, this pulse sequence is repeated continuously, and the FIDs obtained during each acquisition (data collection) are summed together. As a specific example, we can imagine measuring the ^{1}H NMR spectrum of a mixture of two substances (e.g. $CHCl_3$ and CH_2Cl_2). In each, the hydrogen nuclei have different chemical environments and hence different resonance frequencies; therefore, we must consider two different magnetization vectors.

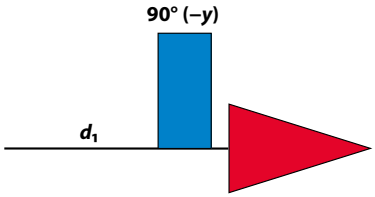

Fig. 5.3: The simplest pulse sequence. The timeline is not uniform; the delay d_1 and the signal acquisition last for several seconds, while the pulse lasts for microseconds.

The graphical representation of the 1D pulse sequence consists of three parts (**Fig. 5.3**). The evolution of the spin system during these three parts proceeds as follows:

1. The **preparation period d_1** usually lasts for several seconds, during which only the external magnetic field $\boldsymbol{B}_0$ acts on the sample. After the pulse from the previous pass through the sequence, the spin populations re-establish equilibrium (**relaxation** occurs) and the magnetization of both components of the mixture aligns along the *z*-axis.

2. This is followed by a **90° pulse**, represented by the rectangle in **Fig. 5.3**. The coil surrounding the sample is connected to the output of a high-frequency source (transmitter). During the pulse, a current with a pulse frequency flows through it. The pulse creates an additional magnetic field that oscillates at the pulse frequency, which is typically centered in the range of the resonance frequencies of the observed nucleus. In the sequence diagram, the pulse phase is shown in parentheses; in our case, it is such that the field $\boldsymbol{B}_1$ points along the –*y*-axis (**Fig. 5.4**). The total magnetization begins to rotate around the –*y*-axis under the influence of the $\boldsymbol{B}_1$ field. The 90° pulse has precisely the intensity and duration required to rotate the magnetization into the *x*-axis direction, but the pulse is so short that the differences in the frequencies of the individual magnetizations have almost no effect. After this pulse, both magnetizations ($\boldsymbol{M}_{CHCl3}$ and $\boldsymbol{M}_{CH2Cl2}$) in the rotating frame are aligned along the *x*-axis and all nuclear magnetic moments, and thus the individual magnetizations $\boldsymbol{M}$, rotate around the *z*-axis at their Larmor frequencies.

3. **Data acquisition** follows. Due to the main magnetic field, the individual magnetizations ($\boldsymbol{M}_{CHCl3}$ and $\boldsymbol{M}_{CH2Cl2}$) now rotate around the *z*-axis at their respective frequencies. At the same time, the spins return to equilibrium, which means that the surplus of spins in the lower-energy state gradually rebuilds. In the rotating model, this process is represented by the magnetization vectors spiraling back to the *z*-axis. During data acquisition, in the *xy*-plane projection, we can observe two rotating magnetization vectors, whose magnitude gradually decreases.

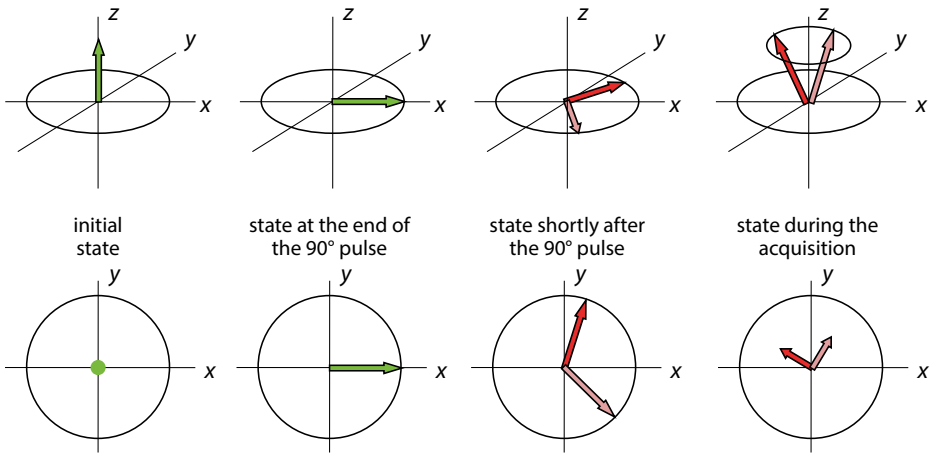

Fig. 5.4: The behavior of magnetizations during a one-pulse sequence. The top shows the overall state, the bottom the projection onto the *xy*-plane. The thick arrows represent the magnetizations contributed by nuclear magnetic moments rotating at the same Larmor frequency.

The electromagnetic field created by the rotating nuclear magnetic moments induces an electric current in the detection coil. The coil is oriented in such a way that it records the components of the magnetization vectors projected onto the *xy*-plane. Typically, **quadrature detection** is used for independent detection of the components along the *x* and *y* axes. The individual magnetizations contribute to the FID signal with sinusoids corresponding to their frequencies. The resulting FID is the sum of these sinusoids, having a complex pattern and reflecting the time evolution of the total sample magnetization, i.e. the vector sum of all partial magnetizations. As the vectors return to equilibrium, the FID-signal intensity decreases (the *z*-axis component increases, and the *xy*-plane projection approaches zero).

Routine ^{13}C NMR spectra are measured with broadband proton decoupling (**Fig. 5.5**). This significantly increases sensitivity for two reasons: **a)** By eliminating all scalar interactions *J*(C,H), all carbon signals appear as singlets. **b)** The nuclear Overhauser effect (NOE, **Chapter 8**) can increase signal intensity up to threefold. However, the information contained in *J*(C,H) is completely lost, as a result of which the signals of CH_3, CH_2, CH and C groups cannot be directly distinguished and the signal intensities become distorted (i.e., the intensity ratios of the signals in the spectrum become non-quantitative). Another reason why the intensities of signals in typical ^{13}C spectra do not correspond to the number of individual carbon atoms is the varying relaxation times of each carbon nucleus (**Chapter 7**). During the delay time, d_1, the complete relaxation of all magnetizations often does not occur, and the subsequent pulse sequence does not begin from the equilibrium state.

In order to obtain **quantitative ^{13}C NMR spectra** with proton decoupling (**Fig. 5.6**), it is necessary to use a sufficiently long delay time d_1, allowing even carbons with long relaxation times T_1 (see **Section 7.1**) to relax fully. The relaxation times can be shortened by adding a relaxation agent, such as chromium(III) acetylacetonate, $Cr(acac)_3$. Additionally, it is important to minimize the nuclear Overhauser effect (NOE) by turning the decoupler on only during the acquisition time.

The ^{13}C NMR spectra including coupling with all *J*(C,H) interactions (**coupled ^{13}C NMR spectra**) can be obtained either by completely omitting proton decoupling or, more effectively, by using

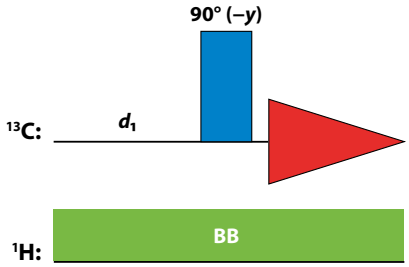

Fig. 5.5: The basic pulse sequence for measuring ^{13}C spectra with proton decoupling

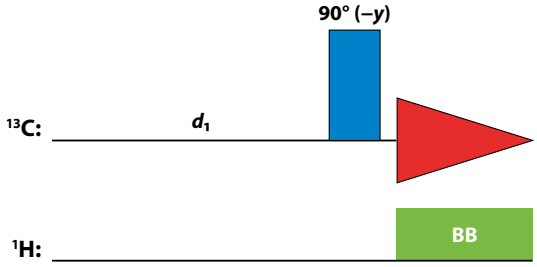

Fig. 5.6: The pulse sequence for measuring quantitative ^{13}C spectra

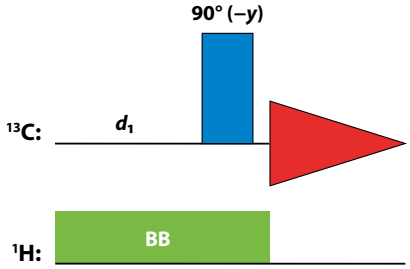

Fig. 5.7: The pulse sequence for measuring coupled ^{13}C spectra

gated decoupling (see **Fig. 5.7**). In this method, the decoupler is turned on only outside the acquisition period, allowing the NOE buildup (which leads to an increase in signal intensity). The carbon signals are split by large ^{1}J(C,H) couplings (of approximately 120–250 Hz) into doublets (CH), triplets (CH_2) or quartets (CH_3), which often involve further splitting by scalar J(C,H) couplings over two or more bonds. An overlap of these multiplets, which are often several ppm wide, can significantly complicate spectral interpretation.

Selective heteronuclear decoupling can be used to assign the individual J(C,H) interactions observed in coupled ^{13}C NMR spectra. During FID acquisition, the signal of a chosen proton is selectively irradiated, which eliminates its interactions with the carbons in the ^{13}C NMR spectrum (see **Fig. 5.2** above).

A simple combination of pulse elements is represented by the **spin echo** (**Fig. 5.8**). It is used in many pulse sequences to refocus chemical shifts and heteronuclear coupling constants as well as to measure relaxation times T_2 (see **Section 7.2**). This sequence begins with a delay time d_1, during which the system returns to equilibrium. Subsequently, a **90° pulse** is applied, which tilts the magnetization from the z-axis into the xy-plane (if the 90° pulse is along the $-y$-axis, the magnetization is tilted into the x-axis). During the time τ, the magnetization precesses around the z-axis at its Larmor frequency and rotates by an angle φ. Afterward, a 180° pulse is applied along the x-axis, keeping the magnetization in the xy-plane but flipping it to the other side of the x-axis. During the second time period τ, the magnetization again precesses around the z-axis at its Larmor frequency. After this time τ, the magnetization returns to the x-axis, although its intensity is reduced due

to the relaxation that occurred during this pulse sequence (see **Section 7.2**). The longer the time τ, the smaller the resulting magnetization in the *x*-axis.

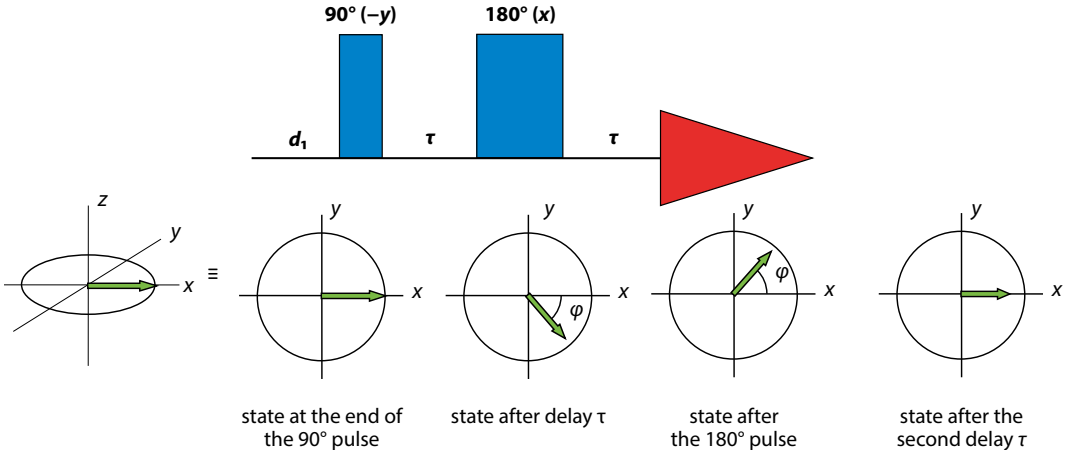

Fig. 5.8: The pulse sequence of the spin echo and its effect on a single-spin system

The return of magnetization vectors to the *x*-axis (**chemical-shift refocusing**) by means of the spin echo can be used to eliminate the effects of **magnetic-field B_0 inhomogeneity**, as shown in **Fig. 5.9**. The first **90° pulse** in the –*y*-axis direction rotates the macroscopic nuclear magnetization from the *z*-axis into the *x*-axis. Due to field inhomogeneity, the vectors of individual nuclear spins move at different rates (a different magnetic field in various parts of the sample leads to different resonance frequencies of equivalent nuclei), causing the total magnetization (the vector sum of all contributions) in the *xy*-plane to decrease. The subsequent **180° pulse** flips the nuclear-spin vectors around the *x*-axis. After the second τ interval, the vectors refocus along the *x*-axis. In the same way, the spin echo refocuses the signals of non-equivalent nuclei. Since individual magnetization vectors perform Larmor precession with a frequency corresponding to their resonance condition, they are not coherent and gradually change their mutual orientation during the delays in pulse sequences. By incorporating the spin echo into the pulse sequence, it can be ensured that at the moment of data acquisition (FID measurement), all magnetization vectors point along the *x*-axis, so that all signals in the spectrum have the same phase.

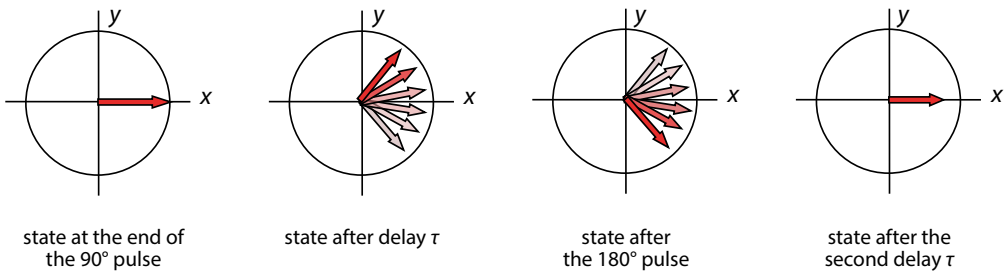

Fig. 5.9: The refocusing of magnetic-field inhomogeneities or nonequivalent signals during the spin echo

Now, let us consider the effect of the spin-echo pulse sequence on a single type of nucleus in a system with **heteronuclear spin–spin coupling**, for example, the carbon nuclei in chloroform, $^{13}CHCl_3$. In a ^{13}C spectrum without decoupling, we would observe a doublet. Therefore, we need to consider two ^{13}C magnetization vectors. After the second τ delay, the magnetization vectors

of the individual components of the multiplet refocus, as shown in **Fig. 5.10**. Both carbon ^{13}C magnetization vectors align along the *x*-axis, which means that the heteronuclear spin–spin coupling has been refocused. If decoupling were started in the proton channel at this moment and FID were measured in the carbon channel, a single peak would be observed in the ^{13}C spectrum. If FID were measured without proton decoupling, a doublet would be observed in the spectrum.

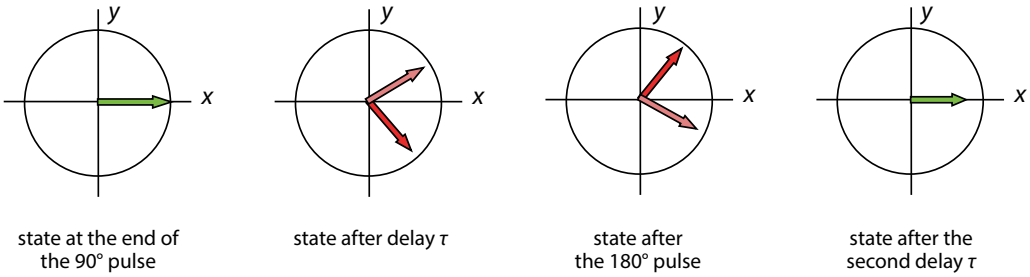

Fig. 5.10: The refocusing of heteronuclear C–H spin–spin coupling during the spin echo applied to the carbon nuclei in chloroform

A somewhat different result is obtained if, during the 180° pulse in the carbon channel, a 180° pulse is simultaneously applied in the proton channel (**Fig. 5.11**). The exchange of the spin states of the hydrogen nuclei causes the "relabeling" of the carbon magnetization vectors and switches their rate of rotation. During the second τ period, instead of refocusing, they thus become further dephased. In the example shown in **Fig. 5.11**, the τ period has been set so that at the end of this pulse sequence, the individual vectors of the ^{13}C magnetization point in opposite directions. If we were to record the ^{13}C FID with proton decoupling at this moment, there would be no signal in the spectrum because the vector sum of both magnetization components would be zero. If we recorded the ^{13}C FID without proton decoupling, there would be two lines in the spectrum with opposite phases. By adjusting the delay τ, it is possible to achieve different phase relationships between the individual magnetization components.

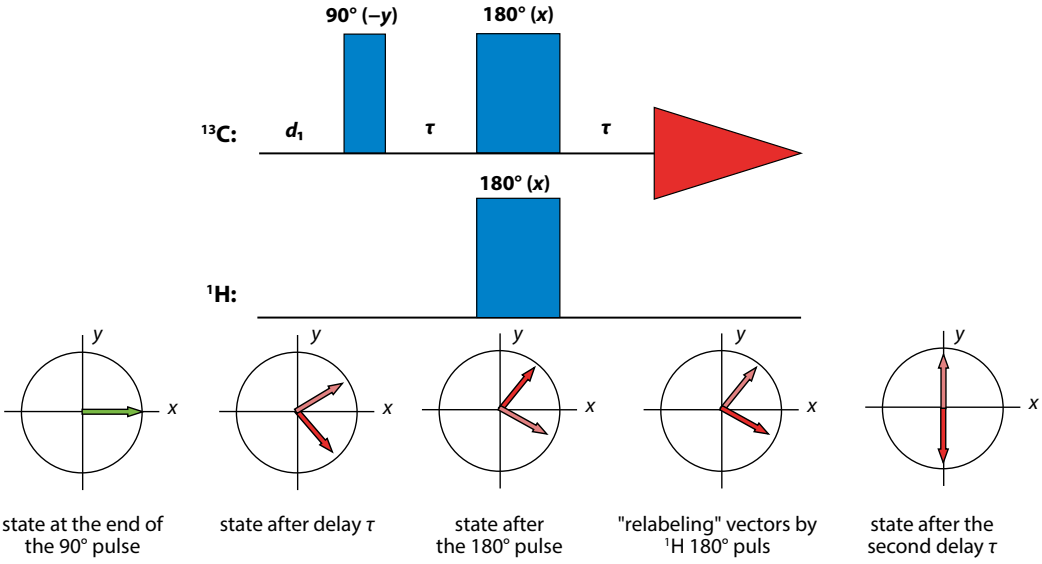

Fig. 5.11: A modified spin echo with a 180° pulse applied simultaneously in both the carbon and hydrogen channels, and the development of the ^{13}C spin system during this sequence

Unlike heteronuclear couplings, spin echo does not result in the refocusing of homonuclear spin–spin couplings. This is because the 180° pulse not only flips the individual magnetization vectors by 180° but also "relabels" them, leading to a change in their rate of rotation. As a result, during the second τ period, the vectors continue to dephase.

^{13}C signals are commonly classified based on the number of directly bonded hydrogens using experiments in which signals in the resulting spectrum are either positive or negative, depending on the type of carbon (C, CH, CH_2, CH_3). The simplest experiment of this type is *J*-modulated spin echo (**Fig. 5.12**). Let us consider two carbon signals: quaternary **a** and tertiary **b**. The first has one line in the ^{13}C spectrum recorded without proton decoupling, while the second has two lines, $\mathbf{b}_1$ and $\mathbf{b}_2$, due to the splitting caused by the directly bonded ^1H atom with coupling constant of, for example, $^1J(C,H) = 140$ Hz. The delay τ in the *J*-modulated spin echo is set to the duration $1 / {}^1J(C,H)$, which is approximately 7 ms. After the first pulse, the individual magnetizations begin to rotate in the *xy*-plane at their Larmor frequencies. Without decoupling, there are interactions with protons. The magnetization of the carbon **a** rotates by an angle corresponding to its chemical shift over 7 ms (in **Fig. 5.12**, this is 45°). The magnetization components corresponding to the lines $\mathbf{b}_1$ and $\mathbf{b}_2$ precess at the chemical shift of the signal **b** and the coupling constant $^1J(C,H)$. If the delay τ is set precisely to the inverse value of this coupling constant, one component of the magnetization rotates by exactly one additional turn around the *z*-axis compared to the other component (in **Fig. 5.12**, the vector $\mathbf{b}_1$ rotates by about 120° and the vector $\mathbf{b}_2$ rotates by about 140° + 360° = 500°).

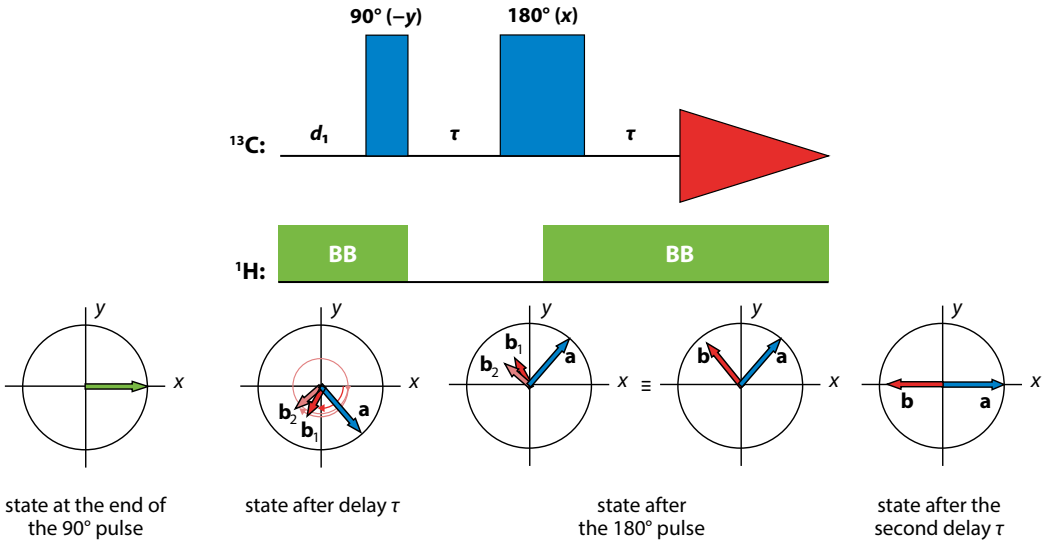

Fig. 5.12: The pulse sequence of the *J*-modulated spin echo and its effect on the magnetization of quaternary and tertiary carbons

This is followed by a 180° pulse along the *x*-axis and the initiation of decoupling. From this moment until the end of the pulse sequence, the influence of interactions with protons is eliminated. The evolution of the magnetization **a** of a quaternary carbon is not influenced by the proton decoupling at all. After the pulse, the magnetization **a** continues to rotate normally and after 7 ms returns to its initial position—pointing in the positive *x*-direction. Both components $\mathbf{b}_1$ and $\mathbf{b}_2$, after decoupling begins, rotate around the *z*-axis at an angular velocity corresponding to the chemical shift of the carbon **b**. Since they now move at the same angular velocity, we can consider their vector sum **b**. The magnetization **b** rotates during the second τ period by an angle

that is the average of the angles covered by the components $\mathbf{b}_1$ and $\mathbf{b}_2$ during the first τ period (in **Fig. 5.12**, the magnetization **b** rotates by (500° + 120°) / 2 = 310° and thus points along the $-x$ semi-axis, resulting in a signal with a phase opposite to that of the carbon **a** in the spectrum. A similar analysis for secondary carbons shows that all three components of the original triplet are now oriented along the $+x$ semi-axis and the primary carbon components (forming a quartet) are oriented along the $-x$ semi-axis.

A slight modification of the *J*-modulated spin echo results in the attached proton test (APT) pulse sequence. The first pulse in this sequence is not a 90° pulse but a shorter one, for example 30°. Such a pulse does not tilt the magnetization fully into the *xy*-plane; the system evolves above this plane, in a plane parallel to it (**Fig. 5.13**). The following 180° pulse flips the magnetization below the *xy*-plane. Since the return from this position to equilibrium after FID acquisition would take a long time, another 180° pulse (a second spin echo) is applied to return the magnetization above the *xy*-plane, where the return to equilibrium is significantly shorter, thus allowing a reduction in the preparation period d_1.

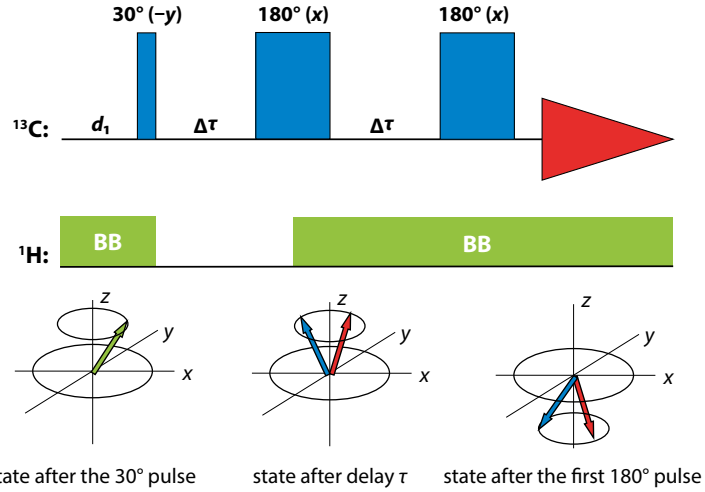

Fig. 5.13: The APT pulse sequence

The magnitude of the coupling constant ^1J(C,H) mainly depends on the hybridization of the carbon atom (**Section 3.2**). For sp^3 carbons, it is around 125 Hz, for sp^2 carbons about 165 Hz, and for sp carbons around 250 Hz. The standard setting of J-modulated echo works with an average value of ^1J(C,H) for sp^2 and sp^3 carbons, 145 Hz, leading to a τ-delay duration of about 7 ms. However, in molecules with larger heteronuclear couplings (e.g. terminal alkynes or certain heteroaromatic compounds), this standard τ delay leads to low or no intensity of CH signals in the spectrum or possibly to signals with positive intensity. Therefore, when studying these substances, it is necessary to adjust the τ delay appropriately, as shown in **Fig. 5.14**.

A frequent element of pulse sequences is **polarization transfer**, related to changes in the populations of nuclear-spin states. The principle of polarization transfer in a simple two-spin heteronuclear system of ^{1}H and ^{13}C nuclei (e.g. in the $^{13}CHCl_3$ molecule) is shown in **Fig. 5.15**. The gyromagnetic ratio γ of ^{1}H nuclei is approximately four times larger than that of ^{13}C nuclei. The energy difference between the α and β spin states, and thus the population difference between these spin states, is also about four times greater for ^{1}H nuclei. The populations are represented by the red beads in **Fig. 5.15**. The population difference between the α and β spin states in the figure is

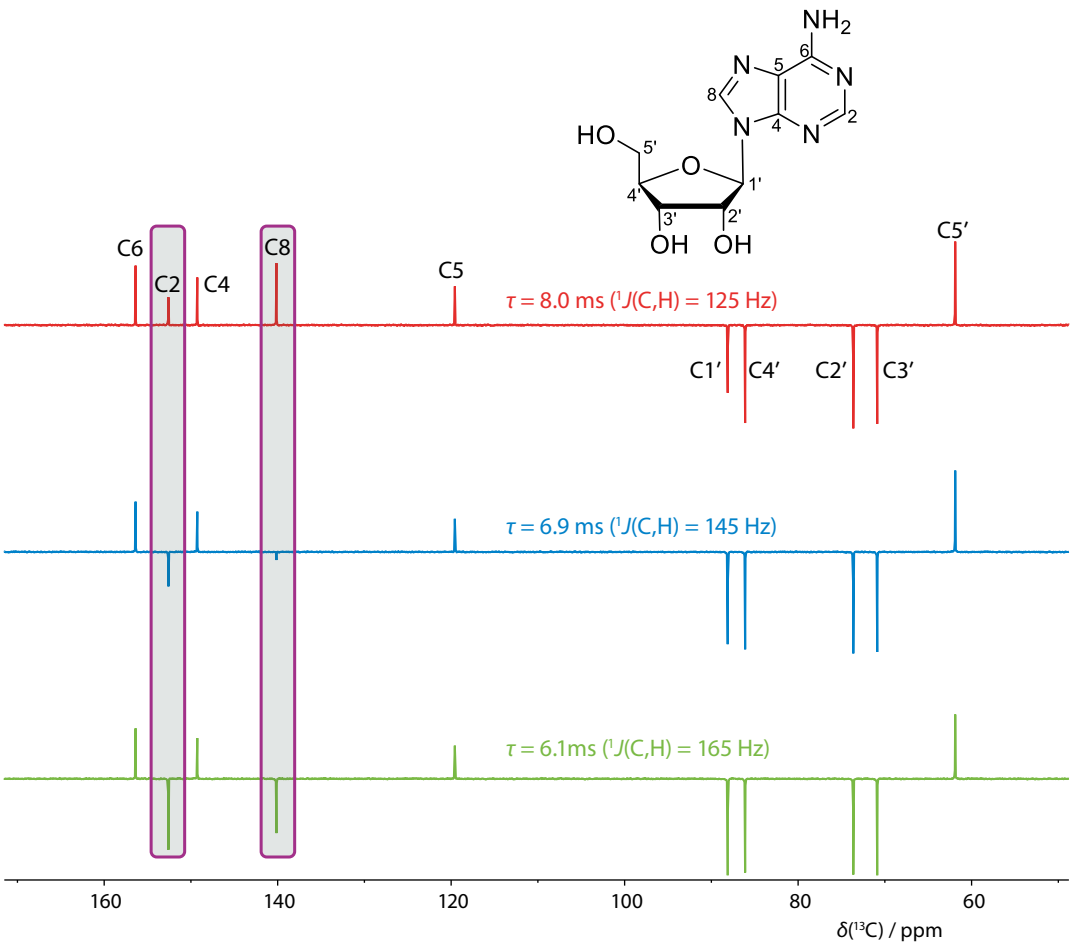

Fig. 5.14: The Influence of the length of delay τ on the APT spectra of adenosine. With the default setting of τ = 6.9 ms, the intensity of the signal of the carbon C8 is close to zero. Therefore, it is advisable to shorten the τ to around 6 ms.

greatly exaggerated for clarity; in reality, at commonly used values of magnetic-field strength, the energy-level difference, and thus the population difference, is very small (see **Section 2.2**). The line intensities in NMR spectra are controlled by the population difference between individual spin states. If an NMR experiment for this two-spin system starts from thermal equilibrium, a doublet is observed in both the ^{1}H and ^{13}C spectra, but the intensity of the lines in the ^{1}H spectrum is approximately four times higher. If no spin–spin interaction existed between the hydrogen and carbon nuclei, the energy difference corresponding to the H^a and H^b transitions as well as the C^a and C^b transitions, would be the same, and thus only a single line (singlet) would be observed in both the carbon and hydrogen spectra.

If we perform a selective inversion of the population corresponding to one hydrogen transition (e.g. H^a, using a selective 180° pulse), changes occur in both the hydrogen and carbon spectra. In the hydrogen spectrum, the H^a line has negative intensity. In the carbon spectrum, one line (C^a) has an intensity of −3 and the other (C^b) has an intensity of +5. If we perform selective inversion of the second hydrogen transition, the situation is reversed, with the carbon line C^a having an intensity of +5 and C^b an intensity of −3. We can then imagine subtracting the resulting carbon

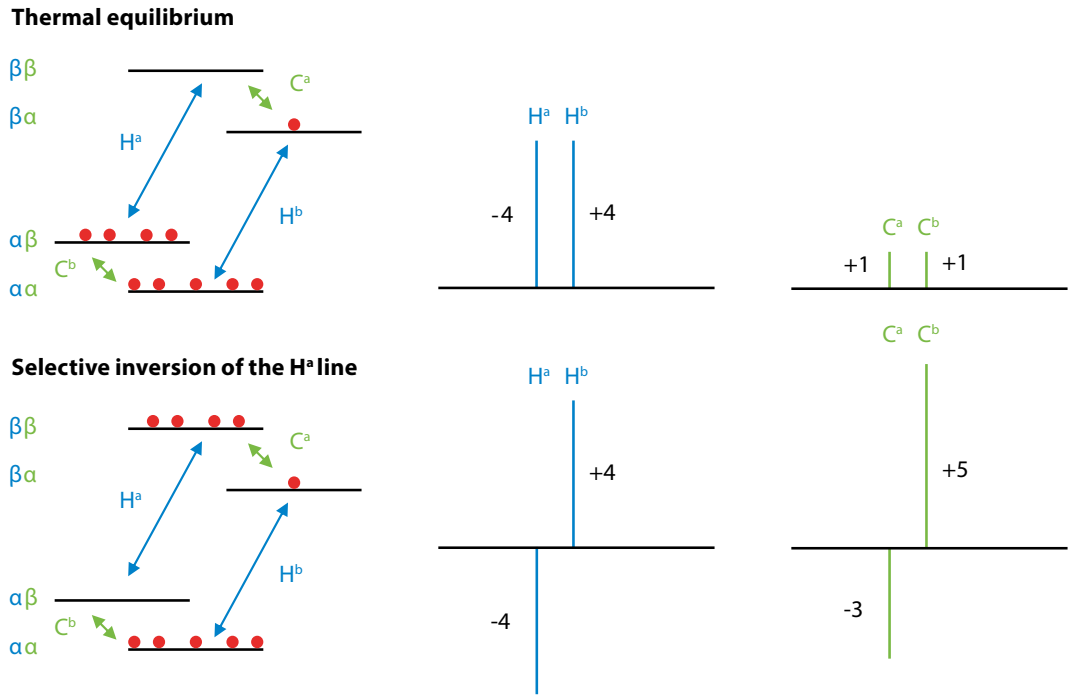

Fig. 5.15: Spin-state populations and polarization transfer

spectra obtained after the selective inversion of the H^a and H^b hydrogen transitions. The resulting carbon spectrum would have line intensities of −8 (= −3 − 5) and +8 (= +5 − (−3)). After two passes through a simple pulse sequence with selective manipulation of the hydrogen transitions, we obtain a spectrum in which the intensity of the carbon lines is four times higher than would correspond to two passes of a standard one-pulse sequence. In this experiment, the polarization transfer from the ^{1}H nuclei to the ^{13}C nuclei has occurred (the greater population difference between the hydrogen spin states means greater polarization). The increase in the sensitivity of the heteronucleus X (e.g. ^{13}C) depends on the ratio between the gyromagnetic ratios γ of hydrogen and the measured nucleus (γ_H / γ_X) and is generally higher than the increase in signal intensity caused by the nuclear Overhauser effect (NOE, see **Chapter 8**). The maximum increase in the intensity of heteronuclear signals through the NOE and polarization transfer is given in **Table 5.1**. The disadvantage of the experiment described above is the need for selective pulses with frequencies corresponding exactly to a specific line in the hydrogen spectrum.

Table 5.1: The maximum increase in NMR signal intensity via the NOE and polarization transfer from ^{1}H nuclei to selected heteronuclei

Nucleus	NOE	Polarization transfer
^{31}P	2.24	2.47
^{13}C	2.99	3.98
^{29}Si	−1.52	5.03
^{15}N	−3.94	9.87

The **INEPT** (insensitive nuclei enhancement by polarization transfer) pulse sequence is also based on polarization transfer from hydrogen nuclei to heteronuclei, but it is not necessary to use selective pulses. This pulse sequence again uses a modified spin echo, in which the time τ corresponds to $1/4J$(C–H) (**Fig. 5.16**). Simultaneously with the 180° pulse on the hydrogen channel, another 180° pulse is applied to the heteronucleus, so that the individual components of the hydrogen magnetization do not refocus; after the second time period τ, these magnetization components are oriented along the $+y$ and $-y$ axes. At this point, a 90° pulse is applied to the hydrogen nuclei along the x-axis. This results in the rotation of the hydrogen magnetization into the positive and negative z-axis, which corresponds to the selective inversion of one hydrogen line and thus the transfer of polarization from the hydrogens to the carbon nuclei. At the same time, a 90° pulse is applied to the carbon nuclei, which causes their magnetization to flip into the xy-plane, and the measurement of the FID signal can begin. As mentioned above, the INEPT pulse sequence can be repeated, but the second 90° pulse in the hydrogen channel is performed with an opposite phase (rotation around the $-x$ axis instead of around the x-axis), which results in the selective inversion of the second hydrogen line. If the resulting carbon spectra are subtracted from each other, we obtain a spectrum with the intensity of the doublet lines −8 and +8. The method of repeatedly running the pulse sequence with different pulse phases is called **phase cycling**. More complex variations of the INEPT experiment lead to the refocusing of the doublet and the presence of only positive singlets in the resulting carbon spectrum.

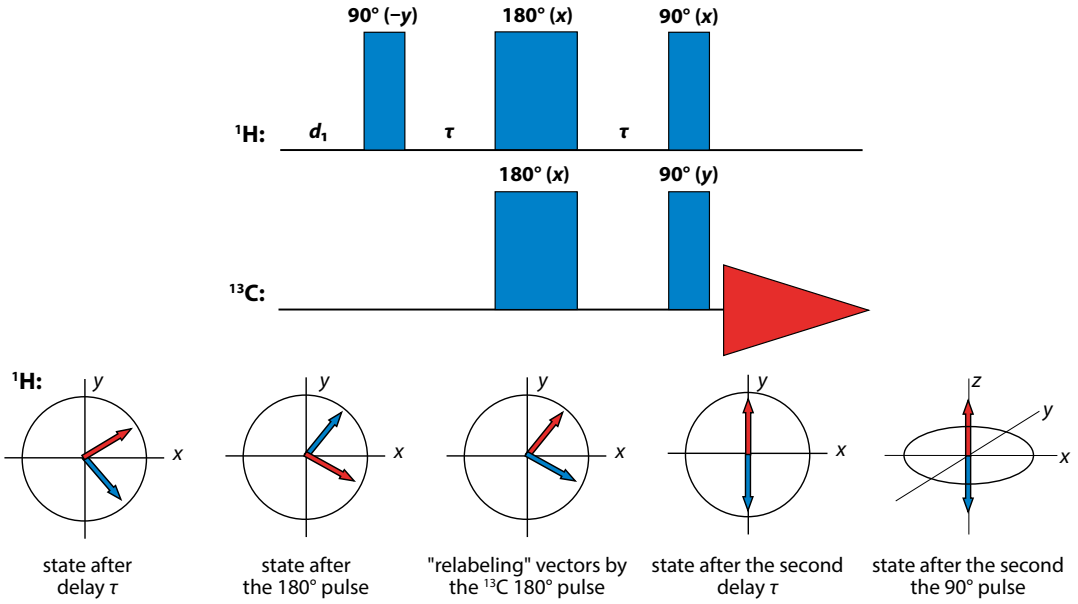

Fig. 5.16: The INEPT pulse sequence and its effect on hydrogen magnetization in the C–H spin system

Another pulse technique for measuring ^{13}C nuclei is the DEPT (distortionless enhancement by polarization transfer) method (**Fig. 5.17**). Its advantage (compared to the INEPT experiment) is a shorter pulse sequence, which reduces signal loss due to relaxation during the evolution period. A process called spectral editing makes it possible to obtain DEPT spectra containing only signals from CH, CH_2 or CH_3. Nevertheless, this requires three different experiments, which differ in the length of the last pulse in the hydrogen channel (**Fig. 5.17**, p3 = 45°, 90° and 135°). The effect of the flip angle of the p3 pulse (determined by its length) on the intensities of the different types of carbon nuclei is shown in **Fig. 5.18**. In the spectrum measured with p3 = 90°, there are only

signals from CH carbons. The spectrum of CH_2 carbons is obtained by subtracting the subspectra with p3 = 45° and p3 = 135°. The spectrum of CH_3 carbons is obtained by adding the spectra with p3 = 45° and p3 = 135° and by subtracting 1.414 times the spectrum with p3 = 90° from this sum. In DEPT spectra, the signals of quaternary carbons are suppressed, so the DEPT experiment must be supplemented by a standard ^{13}C experiment with hydrogen decoupling, where signals from all carbons are observed.

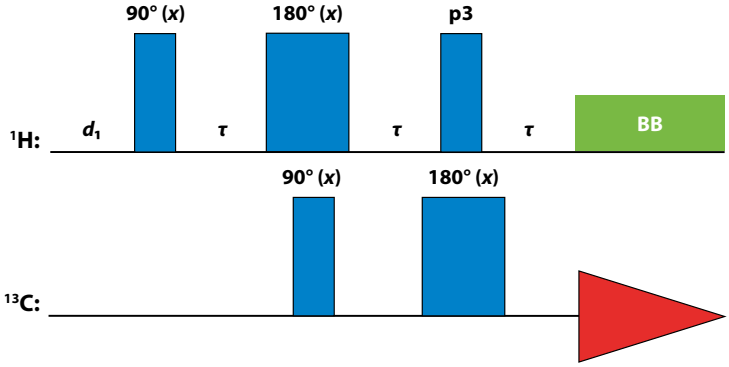

Fig. 5.17: The DEPT pulse sequence

A

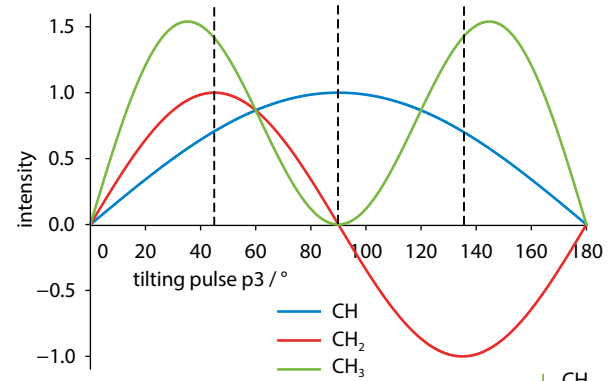

B

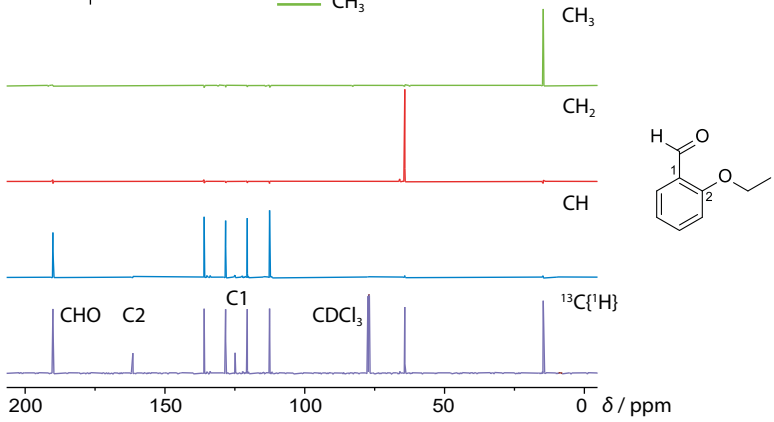

Fig. 5.18: A) The dependence of the signal intensity of carbon nuclei in the DEPT spectrum on the flip angle of the p3 pulse (the dashed lines indicate the commonly used flip angles of 45°, 90° and 135°). **B)** An example of the subspectra of CH_3, CH_2 and CH carbon atoms obtained from a DEPT experiment with 2-ethoxybenzaldehyde and the carbon spectrum of a compound showing all carbon signals

5.3 Two-Dimensional Experiments

In one-dimensional NMR spectra (mainly proton spectra), signal overlap can occur even with relatively small molecules, which complicates or even prevents the interpretation of these spectra. The introduction of a second dimension into the spectra helps bypass this problem because in two-dimensional NMR spectra, signal overlap is less likely. Moreover, pulse techniques are able to manipulate the spin system in such a way that the resulting 2D spectrum reveals new information valuable for structural analysis, which cannot be obtained from regular one-dimensional experiments. For example, from C–H-correlated spectra, we can directly determine the connections between carbon and hydrogen atoms in a molecule via chemical bonds.

In one-dimensional experiments, the free induction decay (FID) is a function of a single time variable, and the spectrum obtained by Fourier transform is a function of frequency. A characteristic feature of two-dimensional experiments is the introduction of an additional time variable—the evolution time. The detected signal then depends on what happened to the spin system during this evolution time. A systematic change in the evolution time (for example its length by an **increment** Δt_1) leads to the acquisition of a series of FID signals during the detection period. After Fourier transform, this provides a series of one-dimensional spectra. A second Fourier transform yields the second frequency dimension (F_1) for the 2D-NMR spectrum. The evolution time is traditionally denoted as t_1 and the detection time as t_2. A double Fourier transform of the series of FIDs yields a two-dimensional spectrum with two frequency axes (F_1 and F_2).

Two-dimensional NMR experiments can be divided into correlated and *J*-resolved experiments. In spectra obtained from **correlated** experiments, the chemical shifts are on both frequency axes (F_1 and F_2); in homonuclear correlated experiments, these are shifts of the same isotope (e.g. ^{1}H), while in heteronuclear correlated experiments, they are the chemical shifts of different isotopes (e.g. ^{1}H and ^{13}C). In the case of heteronuclear correlated experiments, the nucleus whose chemical shifts are observed on the F_2 axis is detected directly (the chemical shifts of this nucleus are obtained by Fourier transform of the FID), while the chemical shifts on the F_1 axis belong to the nucleus that is detected indirectly. In the 2D spectra obtained from ***J*-resolved** experiments, chemical shifts are present on one frequency axis (F_2) and scalar coupling constants on the other axis (F_1). Homonuclear *J*-resolved experiments provide a spectrum where the coupling constants on the F_1 axis correspond to interactions between nuclei of the same isotope, whose chemical shifts can be observed on the F_2 axis (for instance, the F_2 axis shows ^{1}H chemical shifts and the F_1 axis shows ^{1}H–^{1}H coupling constants). In the spectra from heteronuclear *J*-resolved experiments, heteronuclear coupling constants are observable on the F_1 axis (e.g. ^{13}C chemical shifts on the F_2 axis and ^{1}H–^{13}C coupling constants on the F_1 axis).

As an example of a 2D experiment to demonstrate the principle of two-dimensional NMR methods, we use a heteronuclear *J*-resolved experiment. Its pulse sequence (**Fig. 5.19**) schematically shows three increments (three one-dimensional experiments) with progressively increasing t_1 times. The basis of this pulse sequence is a spin echo with hydrogen decoupling only during part of the sequence (like in the APT experiment). **Fig. 5.19B** depicts the evolution of the carbon spin system in a $^{13}C^1HCl_3$ molecule. After the 90° pulse, the magnetization of the carbon nuclei is in the *xy*-plane; during the first $t_1/2$ period, its two components separate due to the spin–spin interaction with hydrogen (at this moment, decoupling is not active). After the 180° pulse, decoupling begins; instead of two magnetization vectors, we observe only one, whose precession frequency corresponds to the average of the original two magnetization components. If the $t_1/2$ period is zero, the magnetization components do not separate, and at the end of the pulse sequence, we

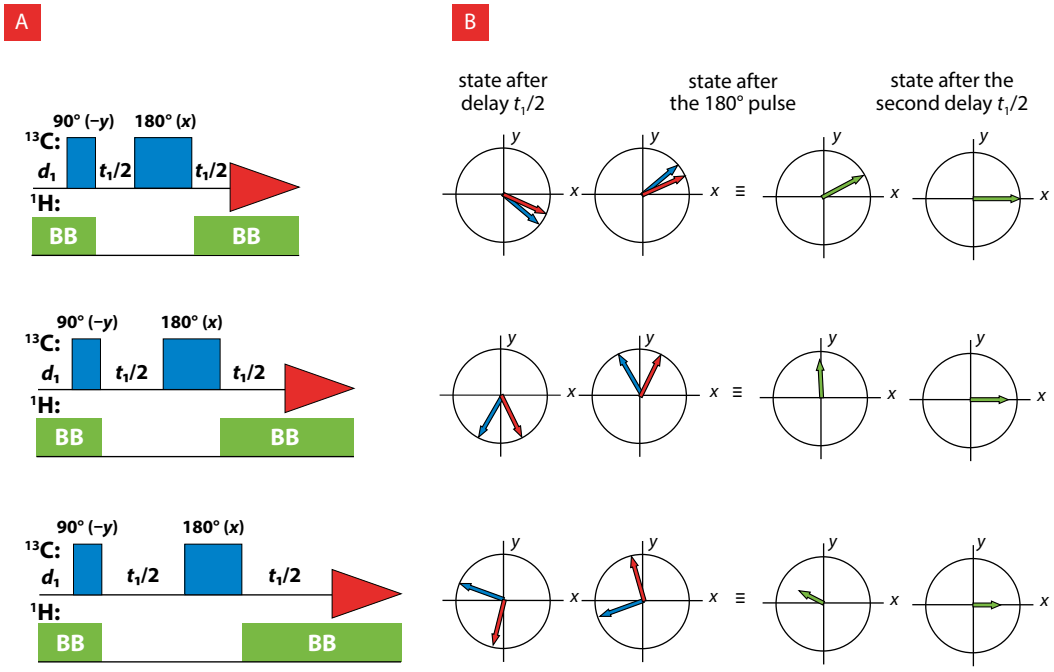

Fig. 5.19: A schematic representation of three increments of the pulse sequence for measuring two-dimensional heteronuclear *J*-resolved spectra **(A)** and the evolution of carbon magnetization in the ^{13}C–^{1}H spin system during this pulse sequence **(B)**

obtain a signal with maximum intensity. If the $t_1/2$ period is not zero, the signal intensity at the end of the pulse sequence depends on how the individual magnetization vectors separate during the first $t_1/2$ period. This is determined by the length of this delay and the magnitude of the C–H coupling (**Fig. 5.20**). For example, if the $t_1/2$ period is equal to one half of the reciprocal value of this heteronuclear coupling constant ($t_1 = 1 / {}^{1}J(C–H)$), the individual magnetization components separate by exactly 180° and their vector sum after the initiation of decoupling is zero. If we plot the dependence of carbon-signal intensity on the time t_1 (**Fig. 5.20B**), we obtain a decaying periodic function resembling a FID, and its Fourier transform yields the frequency corresponding to the coupling constant $^{1}J(C,H)$ (more precisely this constant multiplied by a factor of ¼, which can be easily corrected during spectrum processing). Typical 2D NMR experiments measure hundreds of increments, i.e., one-dimensional experiments with varying evolution times.

The **spectral resolution** in the directly detected dimension (F_2) is determined by the resolution in the 1D spectra obtained during the 2D experiment. The resolution in the indirectly detected dimension (F_1) depends on the number of increments.

Like 1D spectra, which are essentially "two-dimensional" (the second dimension being intensity), 2D spectra have an additional "third" dimension—intensity. Therefore, their graphical representation requires reducing one dimension in some of the ways described below. A perspective display retains complete intensity information, but it is difficult to interpret (due to perspective distortion and potential signal overlap). The most common form of display is the contour plot, which is analogous to topographical maps, representing sections of the three-dimensional spectrum in planes parallel to the F_1-F_2 plane at several different heights (**Fig. 5.21**). The choice of the lowest contour level and the number of levels determines how much intensity information is retained in

the spectrum. The advantage of contour plots is their clarity and ease of interpretation. Another way to display 2D spectra is by using a color scale, where a specific color shade corresponds to a particular signal intensity.

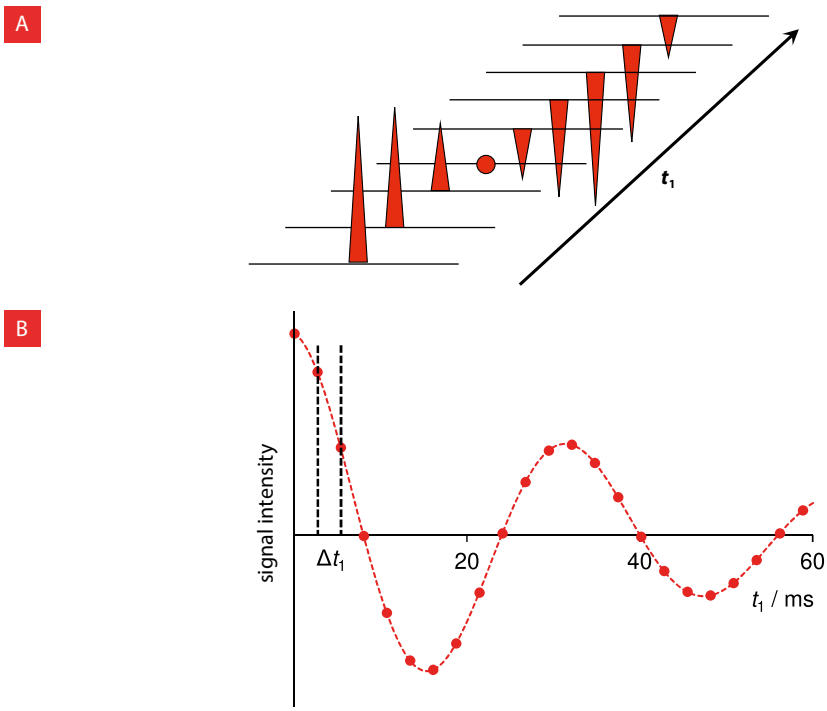

Fig. 5.20: The dependence of ^{13}C signal intensity on the time t_1 in the heteronuclear *J*-resolved experiment shown in **Fig. 5.19**. **A)** A schematic view and **B)** a graph showing the decaying periodic dependence of signal intensity

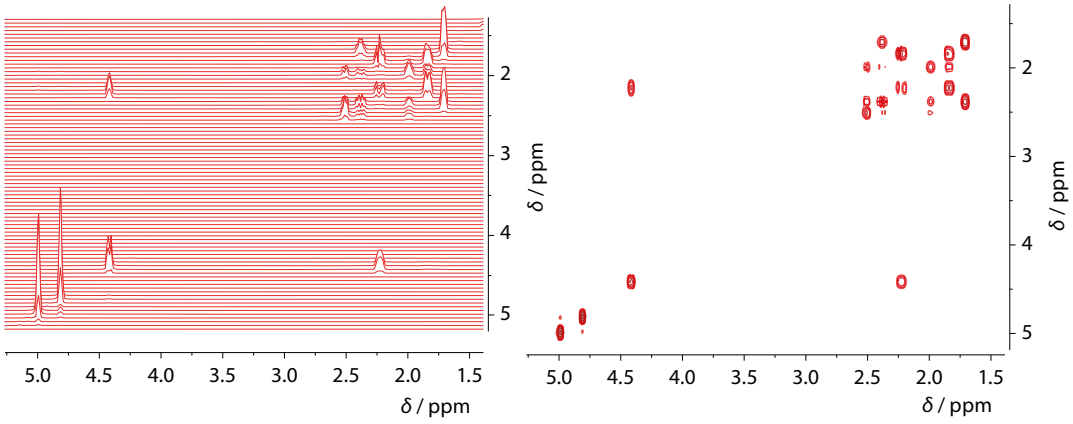

Fig. 5.21: Perspective (left) and contour (right) representations of a 2D spectrum

Inverse techniques involve direct detection of nuclei with high sensitivity (e.g. ^{1}H), while nuclei with lower sensitivity (e.g. ^{13}C and ^{15}N) are detected indirectly. Information about these nuclei is thus encoded in the individual FIDs of the directly detected nucleus. In these experiments, the frequency paths are inverted—the detection path is set to detect ^{1}H, and the decoupling path is tuned to the frequency of the less sensitive nucleus. The development of inverse experiments is

closely linked to advancements in NMR probes. In traditional setups, the probe consists of a coil designed to detect the less sensitive nucleus, placed as close as possible to the sample, whereas the coil for decoupling and detecting hydrogen nuclei is located slightly further away (the sensitivity of ^{1}H nuclei is so good that the loss of part of the signal in this arrangement does not play a crucial role). In contrast, in inverse probes (probes with inverse path arrangements), the coil for detecting ^{1}H nuclei is placed as close to the sample as possible to maximize the sensitivity of inverse experiments, and the second coil allows the decoupling of the indirectly detected nuclei.

Modern NMR techniques often use **magnetic-field gradients** during pulse sequences. This enables the selection of the information to be encoded in the resulting spectrum and the removal of unwanted information (for instance in heteronuclear experiments, it is possible to eliminate the information about hydrogen atoms bonded to magnetically inactive ^{12}C isotopes).

The following overview presents the most common types of 2D NMR experiments. Most of them have several variants that, through modifications of the corresponding pulse sequences, allow the acquisition or suppression of additional information about the studied spin system. The techniques listed below are organized based on the type of information that can be obtained from the spectra, not according to historical development or pulse-sequence type.

One of the most important and longest-used techniques is the homonuclear correlated ^{1}H-^{1}H **COSY** (**CO**rrelation **S**pectroscop**Y**) experiment. The basic version of the pulse sequence for this experiment contains only two 90° pulses separated by the evolution time t_1. The COSY spectrum has chemical shifts of hydrogens in both frequency dimensions, is symmetric along the diagonal, and features two types of signals: Diagonal signals represent the original one-dimensional spectrum (and thus do not provide any additional information) and off-diagonal cross peaks, which indicate scalar interactions between nuclei (**Fig. 5.22**). The chemical shifts of interacting partners can be

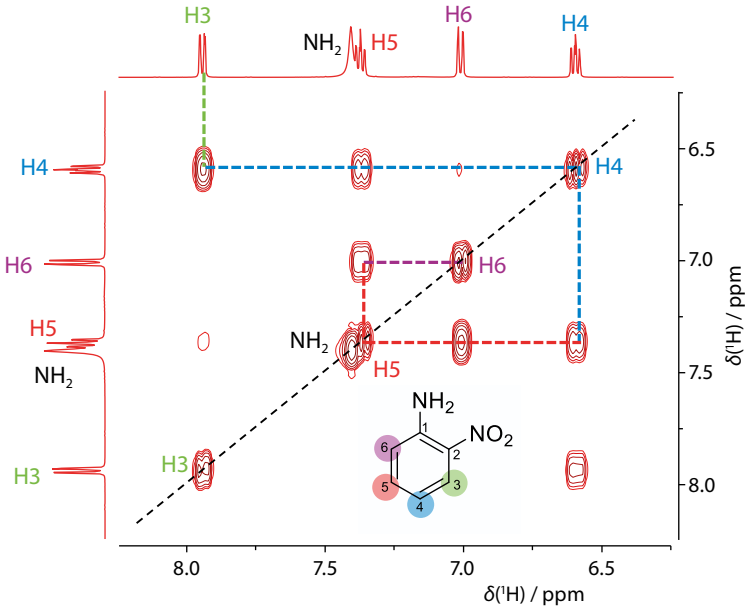

Fig. 5.22: The COSY spectrum of 2-nitroaniline with an indicated signal-assignment procedure. The spectrum is symmetric along the diagonal indicated by the black dashed line. Weak cross peaks corresponding to scalar interactions through four bonds (H3–H5 and H4–H6) are also visible. For comparison, the 1D ^{1}H spectrum is shown at the top and along the vertical left side.

identified using horizontal and vertical lines drawn from the cross peak. Due to the symmetry of the spectrum along the diagonal, this procedure can be performed in both the upper-left and lower-right triangular sections.

The intensity of the cross peaks is related to the magnitude of the scalar coupling between the interacting nuclei. A typical COSY spectrum reliably detects interactions where $|J| \geq 1$ Hz. Very small interactions (< 1 Hz) can be identified using the long-range COSY method, which often reveals interactions that are not resolved in the 1D spectrum.

Total correlation spectroscopy (**TOCSY**) uses a different way to transfer information about *J*(H,H) couplings than the COSY method. In TOCSY, the pulse sequence utilizes a technique called **spinlock**, which "locks" the magnetization vectors in the *xy*-plane using a magnetic field created by a rapid sequence of 180° pulses. During the spinlock, the spin system does not evolve according to the magnetic field $\boldsymbol{B}_0$ (the field of the superconducting magnet), but according to the magnetic field that maintains the magnetization vectors in the *xy*-plane. During the spinlock, spin–spin interactions gradually develop among all hydrogens within a particular **isolated spin system** (**Fig. 5.23**). An isolated spin system refers to a part of the molecule where no hydrogen has scalar interactions with hydrogens from another part of the molecule. Typical examples of isolated spin systems are provided by oligosaccharides or oligopeptides, where each monosaccharide or amino-acid unit forms one isolated spin system. In an ideal TOCSY spectrum, for each hydrogen, there are cross peaks with all other hydrogens of that spin system.

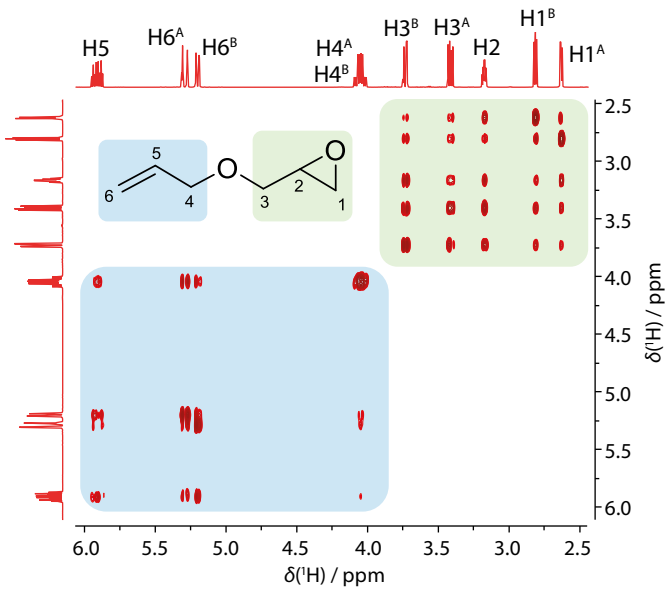

Fig. 5.23: The TOCSY spectrum of allylglycidyl ether. All hydrogens in positions 1–3 form one spin system, and all hydrogens in positions 4–6 form another spin system. The spectrum shows correlations between all hydrogens of a given spin system. Notice the non-equivalence of the CH2 hydrogens in positions 1, 3 and 4. The hydrogens in these positions are diastereotopic (as discussed in **Section 4.3**). The 1D ^{1}H spectrum is included in the figure (above and vertically on the left). For comparison, the COSY spectrum of the same compound is shown in the next figure, **Fig. 5.24**.

Other commonly measured homonuclear correlation 2D experiments are **NOESY** and **ROESY**. The cross peaks in NOESY and ROESY spectra do not indicate scalar interactions between nuclei but reflect the **spatial proximity** of the nuclei. These types of experiments are discussed in more detail in **Chapter 8**.

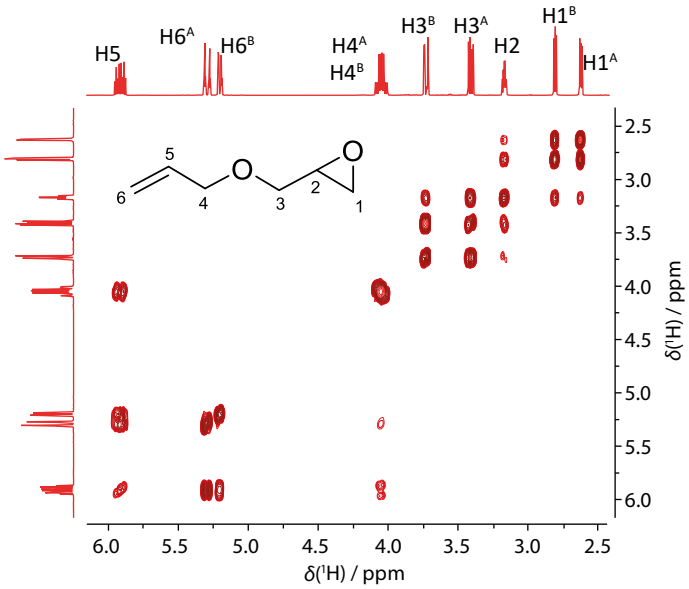

Fig. 5.24: The COSY spectrum of allylglycidyl ether. For comparison, the 1D ^{1}H spectrum is included in the figure (above and vertically on the left).

The variability of pulse sequences can be demonstrated using a heteronuclear correlated experiment that allows the assignment of the signals of connected hydrogen and carbon atoms. The original experiment, which involves direct detection of carbons, is called **C,H COSY** or **HETCOR**. The inverse version of this experiment is called **HMQC**, and another inverse pulse sequence leading to the same information in the spectrum is called **HSQC** (heteronuclear single quantum correlation). An example of an HSQC spectrum of 2-nitroaniline is shown in **Fig. 5.25**. Modern versions

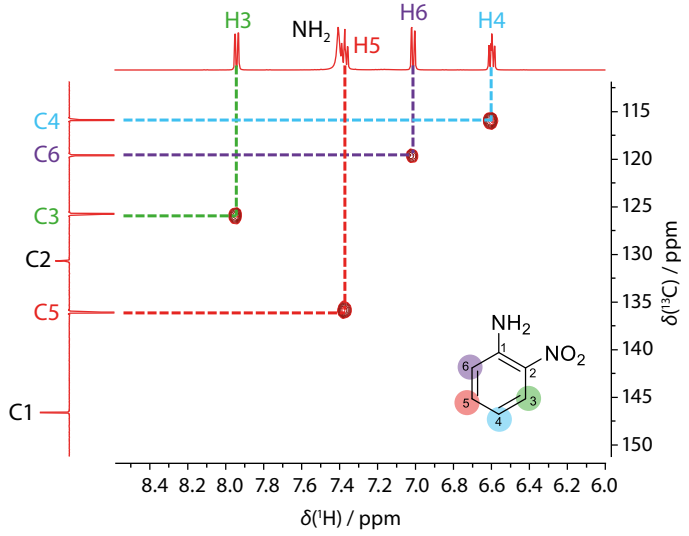

Fig. 5.25: The HSQC spectrum of 2-nitroaniline. The cross peaks connect the signals of bonded hydrogen and carbon atoms. The hydrogens of the NH_2 group do not have any cross peaks because they are directly bonded to nitrogen, not to carbon. Similarly, the quaternary carbon atoms C1 and C2 do not have any cross peaks because no hydrogens are attached to them. The 1D ^{1}H spectrum (above) and the ^{13}C APT spectrum (vertically on the left) are included in the figure for comparison.

of the HSQC experiment also include gradient pulses. Further variants of this experiment may result in positive or negative signals, depending on the number of hydrogen atoms attached to the given carbon atom. The choice of the pulse sequence depends on the operator's preferences and the specific problem being studied. Inverse techniques are much more sensitive than non-inverse ones, which is why they are generally used more frequently. Less sensitive non-inverse HETCOR can be selected, for instance, when the carbon signals are very close to each other and achieving sufficient resolution of the carbon dimension (F_1) in an inverse experiment would require a very high number of increments.

H–C correlations across two or more bonds are obtained using the **HMBC** (heteronuclear multiple-bond correlation) method. The intensity of a cross peak is determined by the magnitude of the heteronuclear C–H coupling, most often showing correlations through two or three bonds. However, it is not possible to determine from the intensity of the cross peak how many bonds separate the interacting atoms. For example, in benzene derivatives, heteronuclear scalar couplings across two bonds are often smaller than those across three bonds. **Fig. 5.26** shows an HMBC spectrum of 2-nitroaniline. For example, the hydrogen H3 in this spectrum has two intense cross peaks with the carbons C1 and C5 (both across three bonds) and one less intense cross peak with the carbon C2 (across two bonds). No cross peak with the carbon C4 is observed. Similarly, the spectrum shows other intense cross peaks across three bonds, such as H5–C3, H5–C1, H6–C4, H6–C2, H4–C6 and H4–C2. In HMBC spectra, it is possible to observe interactions involving hydrogens that are not directly attached to carbon; in the 2-nitroaniline spectrum, for instance, there is a cross peak between the NH_2-group hydrogens and the carbons C2 and C6 (both representing interactions across three bonds). In some cases, it is possible to observe correlations across four or more bonds in HMBC spectra, and it is also common to encounter signals known as HSQC artifacts (highlighted with colored rings in **Fig. 5.26**). These artifacts always appear as doublets, with their center corresponding to the cross peak between directly bonded hydrogen and carbon (e.g. H3–C3).

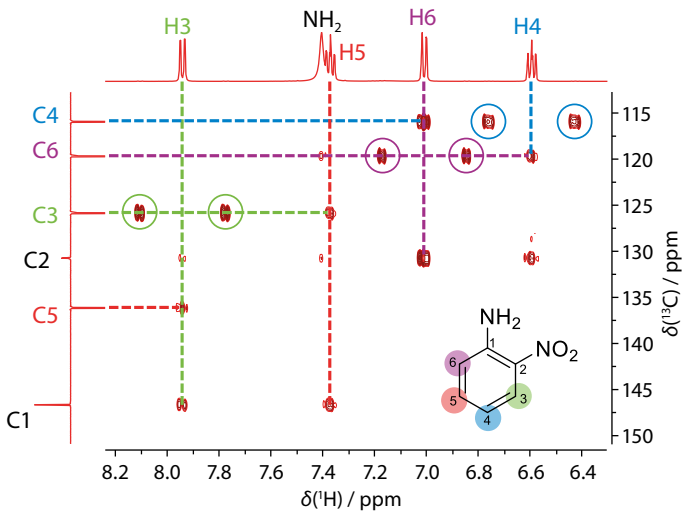

Fig. 5.26: The HMBC spectrum of 2-nitroaniline. The cross peaks connect the signals of the carbon and hydrogen atoms separated by two or three chemical bonds. HSQC artifacts are highlighted with colored circles.

One of the most demanding methods in terms of both time and sample quantity is the **2D-INADEQUATE** experiment (**Fig. 5.27**). This method allows the correlation of directly bonded carbon atoms and thus the determination of the carbon skeleton. Due to the low isotopic abun-

dance of ^{13}C (about 1%, which means that a ^{13}C–^{13}C pair can occur in only 0.01% of cases), this method is very insensitive and requires a significant amount of sample (typically tens to hundreds of milligrams).

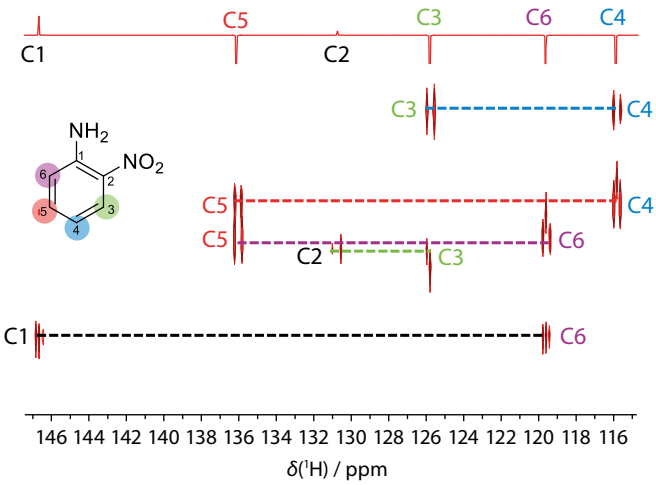

Fig. 5.27: The 2D-INADEQUATE spectrum of 2-nitroaniline with an indicated signal assignment, enabling the determination of C–C bonds in the carbon skeleton of the molecule. For clarity, the 1D ^{13}C APT spectrum is also included at the top of the figure.

Correlated 2D NMR experiments now have much greater practical applications than *J*-resolved experiments, which are only desirable in special cases. The principle of generating heteronuclear *J*-resolved spectra was described earlier, and an example is shown in **Fig. 5.28**. An example of a homonuclear *J*-resolved spectrum is given in **Fig. 5.29**. This experiment enables the separation of hydrogen chemical shifts in the F_2 axis from *J*(H,H) coupling constants in the F_1 axis. The projection along the F_2 axis is equivalent to a ^1H NMR spectrum with "complete hydrogen decoupling" (singlets for each hydrogen) referred to as **pure-shift NMR**, and the slices parallel to the F_1 axis represent the separated multiplets of individual hydrogens.

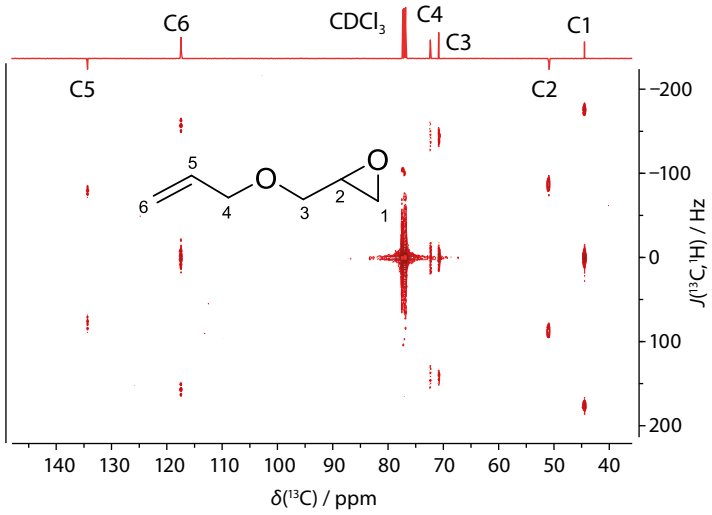

Fig. 5.28: The heteronuclear *J*-resolved spectrum of allylglycidyl ether

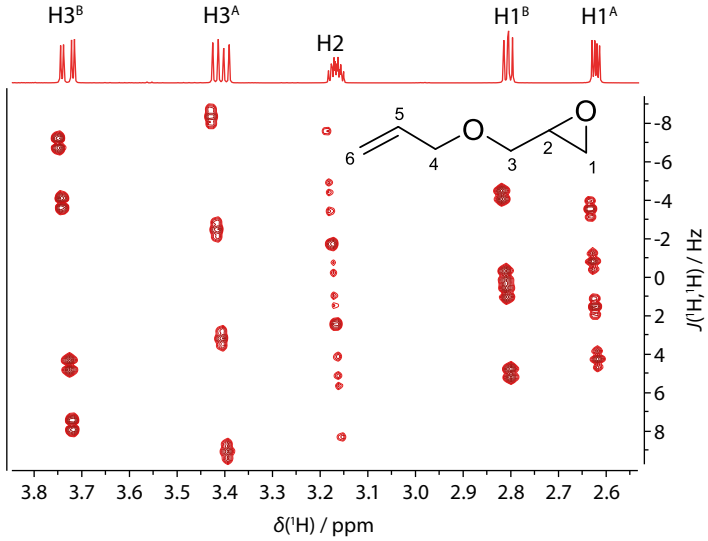

Fig. 5.29: A portion of the homonuclear *J*-resolved spectrum of allylglycidyl ether. The signals in this spectrum are slightly tilted along the F_1 axis (the axis of coupling constants), which can be corrected during spectrum processing.

5.4 Three-Dimensional Experiments

For the structural analysis of organic molecules, a combination of one-dimensional (1D) and two-dimensional (2D) NMR experiments is typically sufficient. However, when studying large molecules such as proteins and nucleic acids, even 2D spectra can have overlapping signals. In these cases, pulse sequences are designed to introduce one or more additional time variables, resulting in three-dimensional (3D) or multi-dimensional spectra. The study of proteins by NMR spectroscopy often uses samples enriched with isotopes such as ^{13}C and ^{15}N. These samples are produced through gene expression in microorganisms grown in media enriched with these isotopes. For these isotopically enriched samples, it is possible to perform 3D correlation experiments, where each axis of the 3D spectrum represents the chemical shifts of ^{1}H, ^{13}C and ^{15}N nuclei.

06

EXAMPLES OF STRUCTURE DETERMINATION USING NMR SPECTRA

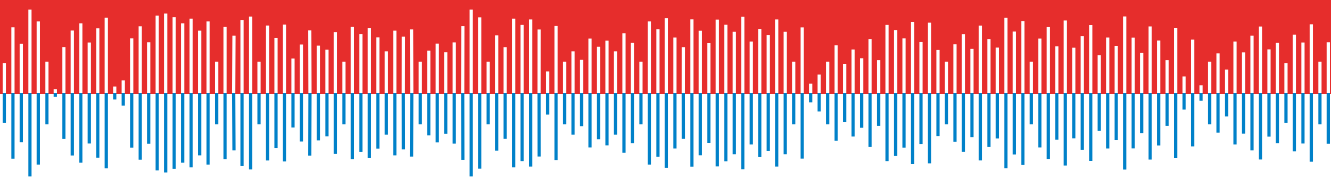

Chapter content

This chapter illustrates how NMR spectra can be used to determine the structure of an unknown compound. Many other examples of NMR spectra for structural analysis can be found at **nmr-challenge.com**, which is an interactive webpage where users can solve NMR spectral assignments of various difficulty, submit their solutions and receive an immediate feedback on the proposed structure.

NMR CHALLENGE
IOCB Prague

6.1 Structure Determination from 1D Spectra

For simplicity, let us assume that the molecular formula of the compound under study is known—it can be determined, for example, by mass spectrometry. Although it is often possible to deduce the structure from NMR spectra without knowing the molecular formula, having this information simplifies the process.

Consider an unknown compound **A** with the molecular formula $C_9H_{10}O_2$. First, examine its proton NMR spectrum (**Fig. 6.1**). The integrals beneath the peaks show the relative intensity of each signal, revealing how many hydrogen atoms correspond to each signal. The spectrum shows a triplet at 1.45 ppm with an intensity corresponding to three hydrogens. This signal could belong to a methyl group adjacent to a CH_2 group. The coupling with the two hydrogens of the CH_2 group splits the methyl signal into a triplet. The coupling constant between the lines of the triplet is 7 Hz, which is a typical value for vicinal coupling in freely rotating chains.

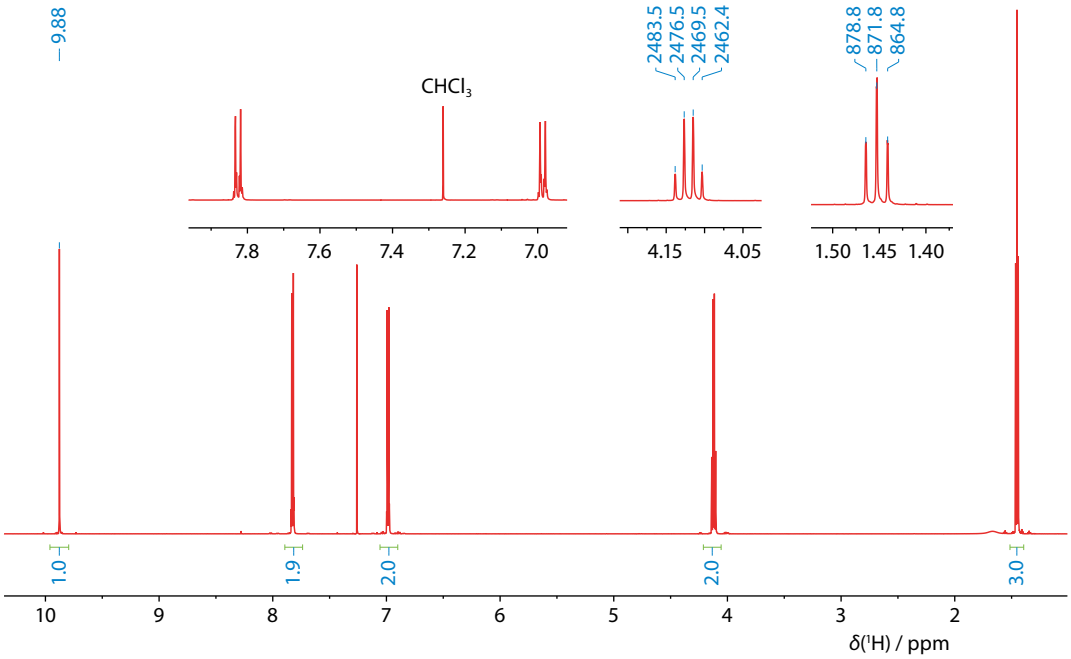

Fig. 6.1: The proton NMR spectrum of an unknown compound **A** with the molecular formula $C_9H_{10}O_2$ in $CDCl_3$

At 4.12 ppm, there is a quartet corresponding to two hydrogens. The coupling constant of 7 Hz again implies that this is probably the CH_2 group next to the methyl group. The chemical shift (4.12 ppm) indicates that the CH_2 group is attached to oxygen, suggesting a fragment like CH_3–CH_2–O– in the molecule. The spectrum also shows two signals in the aromatic region, each corresponding to two hydrogens (the signal at 7.26 ppm belongs to the solvent). The appearance of these aromatic signals is characteristic of magnetically nonequivalent hydrogens in a *para*-disubstituted benzene ring. The final signal at 9.88 ppm appears in the region typical of aldehyde or exchangeable protons.

In the carbon APT spectrum, CH and CH_3 carbon signals point downward, while CH_2- and quaternary-carbon signals point upward. The spectrum in **Fig. 6.2** shows a negative signal at 191 ppm, clearly indicating an aldehyde carbon. In this region, we can encounter only aldehyde or ketone signals. Nevertheless, a ketone signal would point upward, as ketones do not carry any hydrogen (they are quaternary carbons). This confirms that the proton signal at 9.88 ppm also belongs to an aldehyde proton. The carbon spectrum further shows four signals in the aromatic region—two upward and two downward—which aligns with the assumption of a *para*-disubstituted benzene ring. The *para*-disubstituted benzene ring has two quaternary carbons and four CH carbons. Two and two of the CH carbon atoms are equivalent, giving rise to two downward signals. One of the quaternary carbon signals is at a very high shift (164 ppm), indicting that an oxygen is attached to the corresponding carbon atom. The carbon spectrum also shows signals corresponding to the ethoxy group identified in the proton spectrum: The CH_2-carbon signal points up, and its shift is typical of a carbon attached to an oxygen, whereas the CH_3 carbon signal points down at 14.8 ppm.

Combining the information from both the proton and carbon spectra, we can conclude that these spectra correspond to 4-ethoxybenzaldehyde (**Fig. 6.3**).

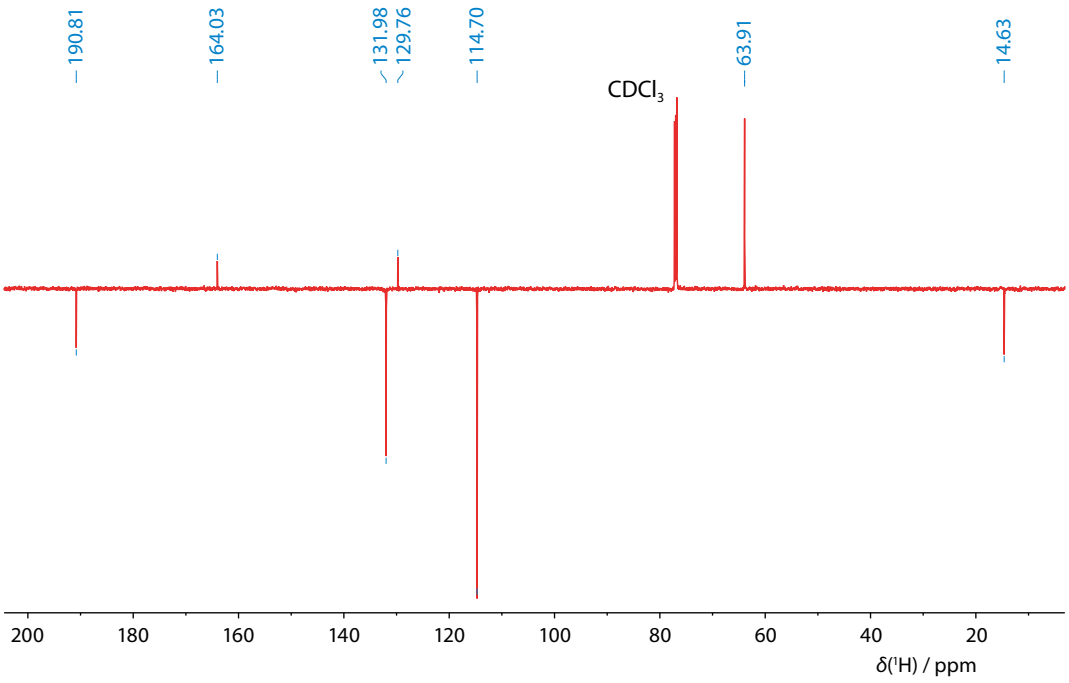

Fig. 6.2: The ^{13}C APT spectrum of an unknown compound **A** with the molecular formula $C_9H_{10}O_2$ in $CDCl_3$

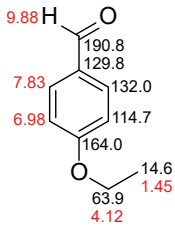

Fig. 6.3: The structure of the compound **A** with the assignment of ^{1}H (**red**) and ^{13}C (**black**) chemical shifts (ppm).

6.2 Structure Determination from 2D Spectra

In this example, an unknown molecule **B** also has the molecular formula $C_9H_{10}O_2$, like the previous one, but its ^{1}H and ^{13}C spectra are different, indicating a different structure. Valuable information about the structure can be obtained from 1D spectra. The proton spectrum (**Fig. 6.4**) shows two singlets near 2.5 ppm, each corresponding to three hydrogens. These are likely to be two nonequivalent methyl groups not attached to oxygen—if they were attached, they would have higher chemical shifts. The spectrum also shows signals for three aromatic hydrogens, although two of them overlap, preventing the determination of coupling constants. The third aromatic hydrogen appears as a doublet with a coupling constant of 8.4 Hz, consistent with vicinal coupling in benzene derivatives. The final signal at 12 ppm is very broad, characteristic of carboxylic acids.

The carbon spectrum (**Fig. 6.5**) confirms the findings from the proton spectrum. The spectrum shows two methyl-group signals, three quaternary aromatic carbons, and three aromatic CH carbons. The final signal at 173 ppm is in the region containing signals of carboxylic acids and their derivatives.

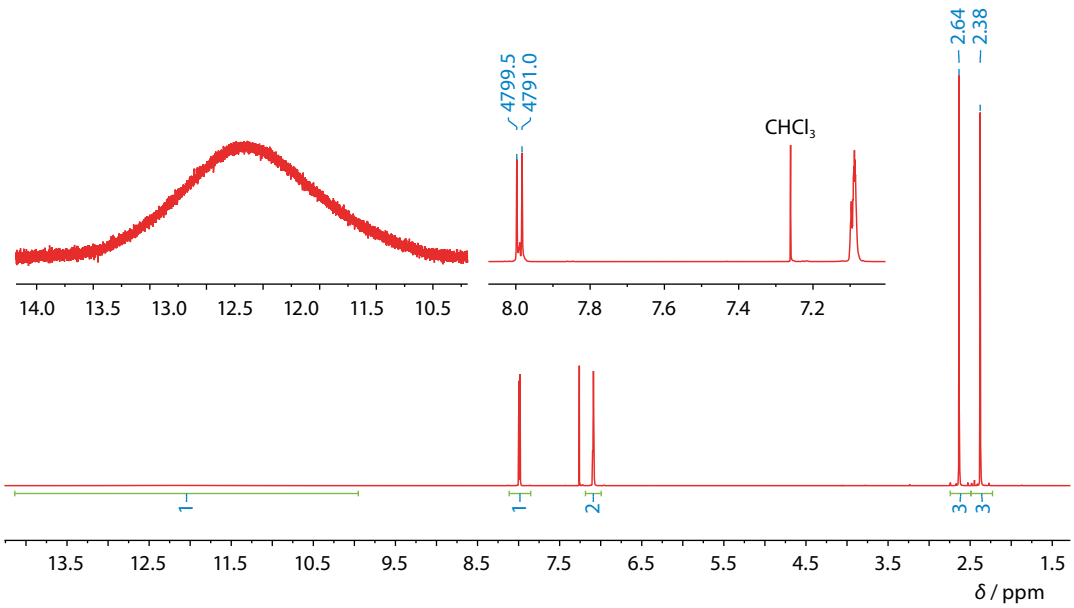

Fig. 6.4: The proton NMR spectrum of an unknown compound **B** with the molecular formula $C_9H_{10}O_2$ in $CDCl_3$

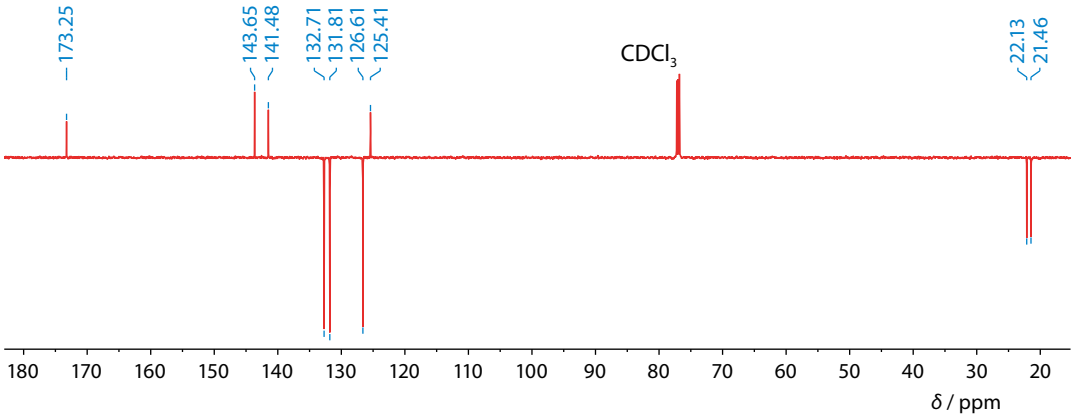

Fig. 6.5: The ^{13}C APT spectrum of an unknown compound **B** with the molecular formula $C_9H_{10}O_2$ in $CDCl_3$

By combining the information from the proton and carbon spectra, we can conclude that the molecule is a trisubstituted benzene with two methyl groups and one –COOH group, making it a dimethylbenzoic acid. However, the spectra alone cannot determine the exact positions of the methyl groups, leaving us with six possible structures (A–F) for this compound (see **Fig. 6.6**). The structures D and F can be immediately excluded because in these structures, the methyl groups are chemically equivalent and would produce only one signal.

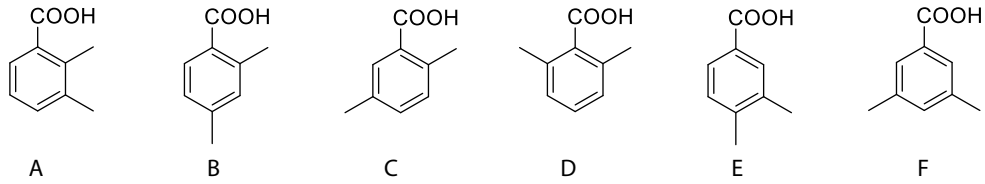

Fig. 6.6: The possible structures of dimethylbenzoic acid

The key to determining the correct structure of compound **B** is the HMBC spectrum, which typically shows correlations between hydrogens and carbons separated by two or three bonds. The most important signals in this case are the correlations between the methyl hydrogens and the aromatic carbons, shown in the inset of **Fig. 6.7**. Each methyl hydrogen has a cross peak with three aromatic carbons—one through two bonds and two through three bonds. In the spectrum, the hydrogen signal at 2.38 ppm, highlighted by a red dashed line in the figure, has cross peaks with one quaternary carbon (143.7 ppm) and two CH carbons (126.6 and 132.7 ppm). This indicates that both *ortho* positions to this methyl group contain CH carbons and the quaternary carbon at 143.7 ppm is directly bonded to this methyl group. This eliminates the structures A and E from **Fig. 6.6** because neither has a methyl group with CH carbons in both *ortho* positions. This leaves us with the structures B and C.

The proton signal at 2.64 ppm (highlighted in blue in **Fig. 6.7**) shows cross peaks (correlations) with two quaternary carbons (125.4 and 141.5 ppm) and with one CH carbon (132.7 ppm). The CH carbon neighboring this methyl group is the same as one of the CH carbons neighboring the other methyl group. This excludes the structure C, in which the methyl groups do not share a common neighbor (a CH carbon), leaving only one possible structure B, i.e. 2,4-dimethylbenzoic acid. In the HMBC spectrum, there is also a weak cross peak between the hydrogen of the methyl

group at position 2 and the carbon of the COOH group, corresponding to a four-bond interaction, which explains its low intensity. **Fig. 6.8** shows the structure of 2,4-dimethylbenzoic acid with the assigned proton and carbon signals and the correlations observed in the HMBC spectrum, which lead to the definitive structural identification of this compound.

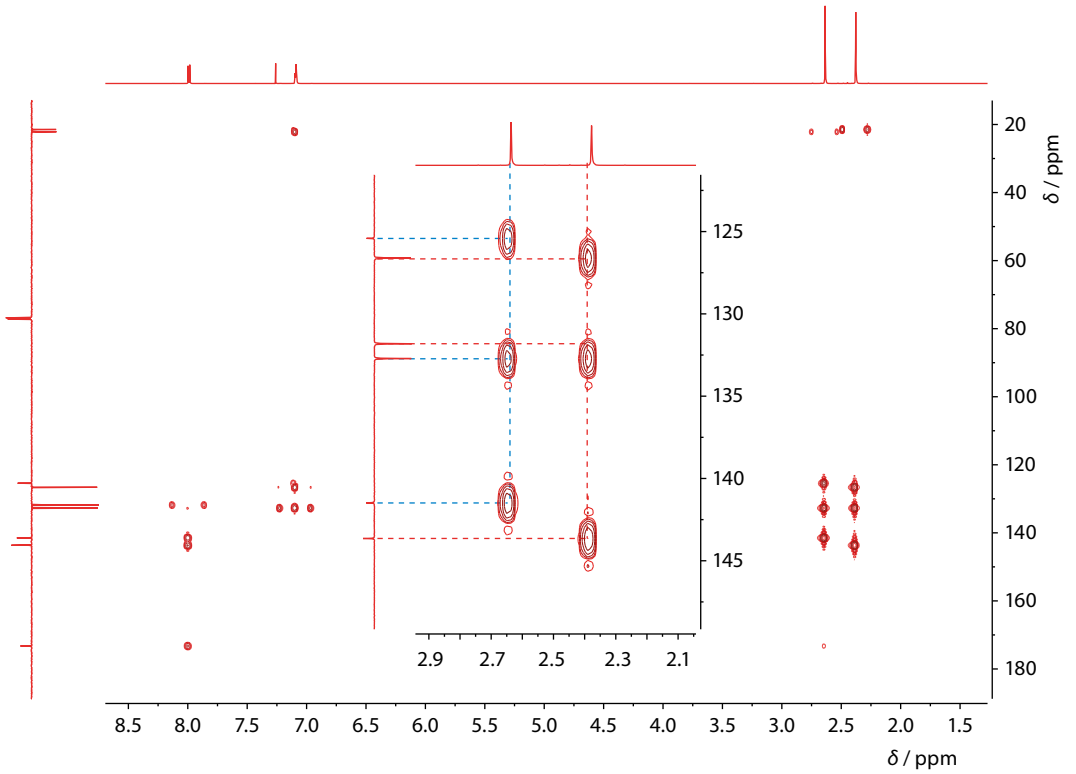

Fig. 6.7: The HMBC spectrum of an unknown compound B with the molecular formula $C_9H_{10}O_2$ in $CDCl_3$. The figure includes the 1D ^1H spectrum (above) and the ^{13}C APT spectrum (vertically on the left).

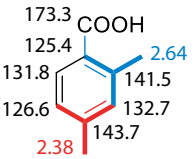

Fig. 6.8: The structure of 2,4-dimethylbenzoic acid with the assigned carbon chemical shifts (in black) and proton chemical shifts of the methyl groups (in **red** and **blue**). The correlations observed in the HMBC spectrum are indicated by colored lines.

07

RELAXATION IN NMR SPECTROSCOPY

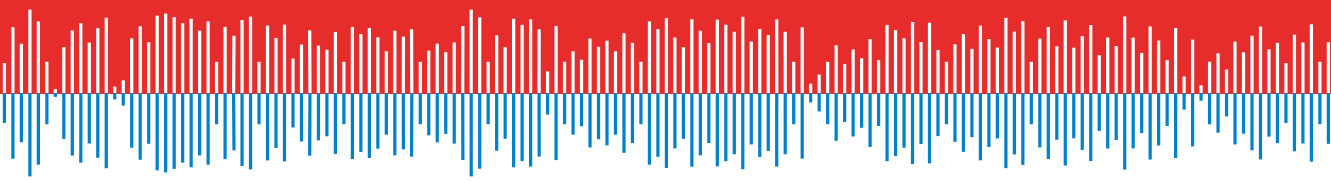

Chapter content

In the equilibrium state, magnetization is aligned along the axis of the magnetic field (the *z*-axis). By applying electromagnetic pulses, we rotate the magnetization away from the z-axis, displacing the nuclear-spin system from equilibrium. The spin system then gradually returns to its equilibrium state, a process known as relaxation. The rate of relaxation is very important for NMR experiments because it influences both the appearance of spectra and the time required to acquire them. This chapter discusses relaxation processes, the methods of measuring relaxation rates, the effect of relaxation on NMR spectra, and the information that the study of relaxation can provide. Two types of relaxation processes are distinguished in NMR spectroscopy: longitudinal relaxation and transverse relaxation.

7.1 Longitudinal Relaxation

During longitudinal relaxation (also known as spin–lattice relaxation), equilibrium magnetization along the *z*-axis is re-established. For example, in the pulse sequence for measuring proton NMR spectra, a 90° pulse is used to rotate the magnetization from the *z*-axis into the *xy*-plane. Immediately after this pulse, the magnetization along the *z*-axis is zero. Longitudinal relaxation gradually rebuilds the equilibrium magnetization along the *z*-axis, and its increase can be described by the equation:

$$M_z = M_0\,(1 - e^{-t/T_1})$$

where M_z is the magnetization along the *z*-axis, M_0 is the equilibrium magnetization, t is the time that has passed since the 90° pulse, and T_1 is the spin–lattice relaxation time (**Fig. 7.1**).

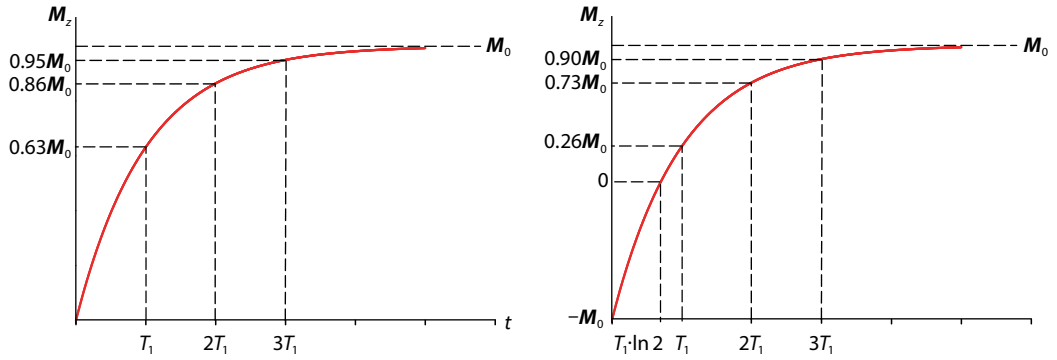

Fig. 7.1: The return of longitudinal magnetization M_z to the equilibrium value M_0 after a 90° pulse (left) and after a 180° pulse (right)

The shorter the T_1, the faster the equilibrium state is reached (typical T_1 values are on the order of hundreds of milliseconds to seconds, but sometimes they can be much shorter or, conversely, much longer, up to several hours). Longitudinal relaxation is also responsible for building up the magnetization $\boldsymbol{M}_0$ after the sample is placed in the magnetic field. The total magnetization of the sample outside the magnetic field is zero, and once placed in the magnetic field, the magnetization gradually builds up with the same characteristic time T_1, like after the excitation of the spin system by electromagnetic pulses. For setting the repetition time in pulse experiments, it is important to have at least an approximate knowledge of the relaxation time T_1. The delay d_1 at the beginning of each pass through a pulse sequence (each scan) must be long enough for the spin system to reach a state close to equilibrium. This is generally not an issue when measuring proton spectra, because protons usually have short relaxation times T_1. However, certain carbon nuclei

(especially those of quaternary carbons) may have longer relaxation times, as a consequence of which their magnetization may not fully reach equilibrium during the typical repetition times of carbon experiments (e.g. 3 seconds). In the next transient of the pulse sequence, after the excitation pulse, the magnetization in the *xy*-plane would be smaller than that of fully relaxed nuclei, with the resulting signal intensities in the spectrum being lower. This is one of the reasons why regular carbon spectra cannot be integrated (another reason is the nuclear Overhauser effect, which is discussed in **Chapter 8**).

Relaxation times T_1 are measured using the **inversion-recovery experiment** (**Fig. 7.2**). This sequence includes a 180° pulse that flips the magnetization to the $-z$ axis, followed by a delay τ, which can be varied. During this delay, the system undergoes longitudinal relaxation, and the magnetization along the $-z$ axis decreases, passes through zero and then begins to build up along the $+z$ axis. After the delay τ, a 90° pulse is applied, and the signal is detected. Depending on the delay τ, the obtained signal changes from negative to positive. An example of measuring carbon relaxation times T_1 is shown in **Fig. 7.3**, and an example of measuring proton relaxation times T_1 is provided in **Fig. 7.4**.

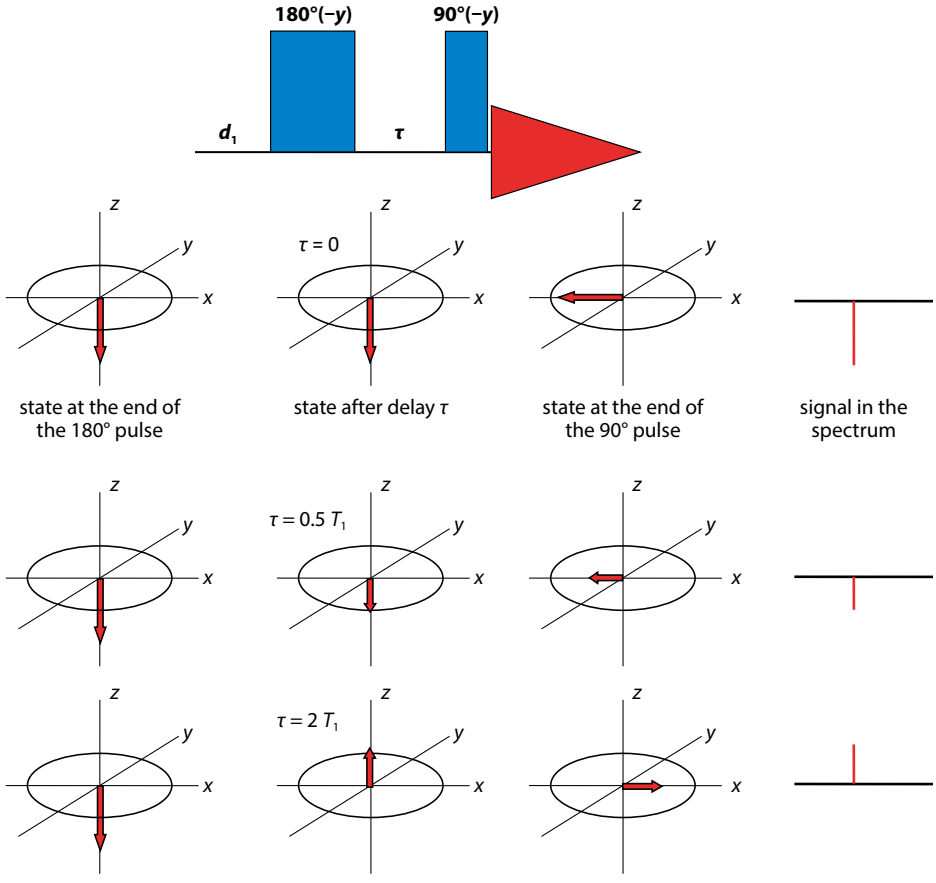

Fig. 7.2: The inversion-recovery pulse sequence and the evolution of the spin system during this sequence as a function of the delay τ

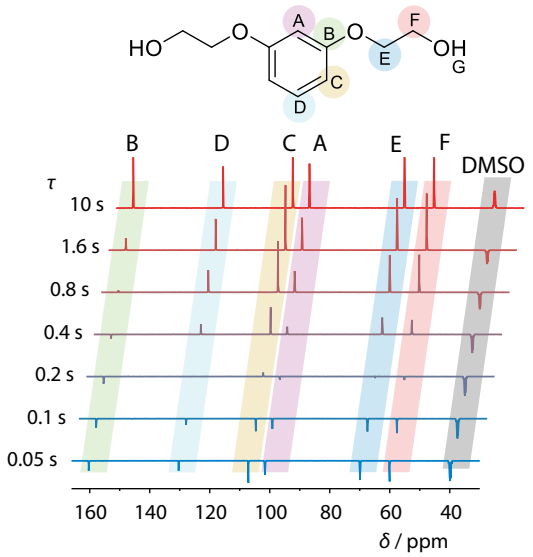

Fig. 7.3: A series of ^{13}C inversion-recovery experiments measured with varying delay τ

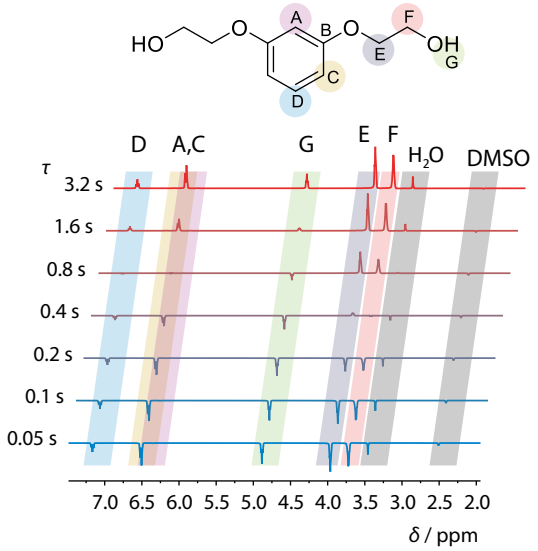

Fig. 7.4: A series of ^{1}H inversion-recovery experiments measured with varying delay τ

7.2 Transverse Relaxation

During transverse relaxation (also known as spin–spin relaxation), the magnetization in the *xy*-plane decays. Transverse relaxation is caused by the interaction between nuclei. Due to molecular collisions and other processes, local magnetic fields fluctuate, leading to fluctuations in the Larmor frequency. These fluctuations cause decoherence (dephasing) of the precessional motion of nuclear magnetic moments, resulting in a reduction of the magnetization vector. The consequence of transverse relaxation is the gradual reduction of the intensity of the detected signal (FID). The decay of magnetization in the *xy*-plane follows the equation:

$$M_{xy} = M_0 \, e^{-t/T_2}$$

where M_{xy} is the magnitude of magnetization in the *xy*-plane, M_0 is the magnetization in the *xy*-plane after the excitation pulse, *t* is the time after the pulse, and T_2 is the spin–spin relaxation time (**Fig. 7.5**). The shorter the T_2, the faster the magnetization in the *xy*-plane decays and the faster the FID decreases. Short T_2 times result in broader signals in the spectrum (see **Section 2.5** on Fourier transform). The value of T_2 typically ranges from hundreds of milliseconds to seconds. Generally, large molecules (e.g. proteins and polymers) have short T_2 relaxation times, as a result of which the signals of these substances are broader. On the other hand, small molecules (e.g. common solvents) have long T_2 times and thus produce narrow signals in the spectrum. In typical samples, the T_2 relaxation time is shorter than or equal to the T_1 relaxation time.

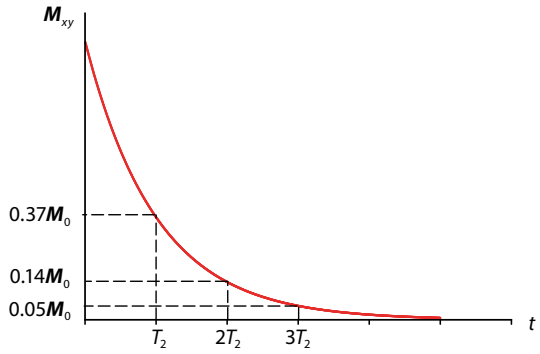

Fig. 7.5: The decay of transverse magnetization M_{xy} to a zero equilibrium value after a 90° pulse

The spin-echo pulse sequence (**Section 5.2**, **Fig. 5.8**) is used to measure T_2 relaxation times. This sequence begins with a delay, during which the system establishes equilibrium. This is followed by a 90° pulse, which flips the magnetization from the *z*-axis to the *xy*-plane. During the time τ, the magnetization undergoes precession around the *z*-axis at its Larmor frequency. In this time τ, the magnetization rotates by an angle φ from its initial position immediately after the 90° pulse (along the *x*-axis). This is followed by a 180° pulse along the *x*-axis, which keeps the magnetization in the *xy*-plane but flips it to the other side of the *x*-axis. During the time τ, the magnetization again undergoes precession around the *z*-axis, rotating by the same angle φ. It thus returns to

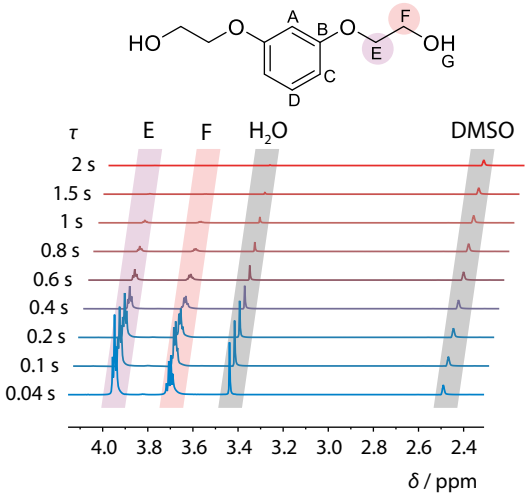

Fig. 7.6: ^{1}H spin echo experiments measured with different delays τ

the *x*-axis, but its intensity is reduced due to the transverse relaxation that occurred during this pulse sequence. The longer the time τ, the smaller the resulting magnetization along the *x*-axis. An example of measuring hydrogen relaxation times T_2 using the spin echo is shown in **Fig. 7.6**.

7.3 Relaxation Mechanisms

Spontaneous relaxation (without external influences) is virtually nonexistent for isolated spin-½ nuclei. For relaxation to occur, the nucleus must be exposed to a fluctuating magnetic field. The primary source of fluctuating magnetic fields is molecular motion, which changes the distances and relative orientations of the nucleus and other magnetically active nuclei in the molecule. Molecular motion can be described by an effective correlation time τ_C, which in the case of translational motion defines the average time between two molecular collisions or, in the case of rotational motion, the average time required for a molecule to rotate by one radian. The value of τ_C is related to the size and symmetry of the molecule, viscosity and temperature. The typical correlation time for small molecules in non-viscous solvents is on the order of 10–12 seconds.

The rate of spin–lattice relaxation ($1/T_1$) is highest when the correlation frequency of the molecular motion ($1/\tau_C$) is close to the resonance frequency of the relaxing nuclei ($\tau_C\omega_0 \approx 1$, where ω_0 is the angular frequency of Larmor precession). The relaxation rate decreases when the molecular motion is significantly faster or slower. In contrast, both low- and high-frequency molecular motion contributes to the rate of spin–spin relaxation ($1/T_2$), so that $1/T_2$ decreases monotonically as τ_C decreases.

The relationship between the relaxation times T_1 and T_2 and the correlation time τ_C is shown in **Fig. 7.7**. Under the conditions of rapid molecular reorientation ($\tau_C\omega_0 << 1$), which are usually fulfilled for most small to medium-sized organic compounds in solution, both relaxation rates, and thus the relaxation times T_1 and T_2, are the same. The condition of rapid reorientation ($\tau_C\omega_0 << 1$) is also referred to as the extreme-narrowing condition because the signal linewidths in spectra obtained under this condition are minimally affected by relaxation times and are primarily determined by magnetic-field inhomogeneity.

The observed relaxation rates $1/T_1$ and $1/T_2$ are the sum of the relaxation rates of several different mechanisms that contribute to the overall relaxation.

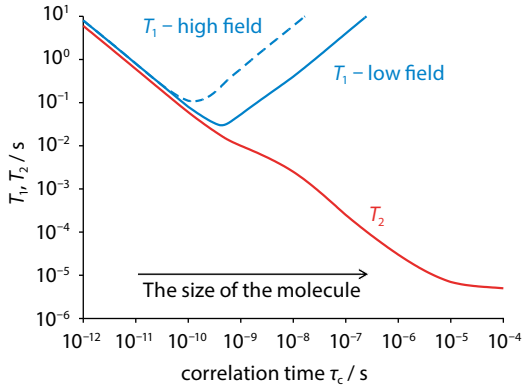

Fig. 7.7: A schematic representation of the relationship between the relaxation times T_1 and T_2 and the correlation time τ_C

Dipole–dipole relaxation is caused by the interaction of nuclear magnetic dipoles. It is the dominant relaxation mechanism for nuclei with spin ½. There are two types of interactions between magnetically active nuclei: indirect (scalar, *J*) interaction, which is mediated by electrons, and direct dipole–dipole (or dipolar) interaction, which depends on the distance between the nuclei and their orientation relative to the magnetic field. Unlike scalar interaction, direct dipole–dipole interaction does not lead to signal splitting in solutions, because the rapid reorientation of molecules averages these interactions to a mean value of zero. However, rapid changes in the magnitude of this interaction during molecular motion contribute to relaxation. The rate of dipole–dipole relaxation decreases with the sixth power of the distance between interacting nuclei, making this type of relaxation most effective in interactions between directly bonded atoms. As a result, quaternary carbon atoms tend to have longer relaxation times than carbons directly bonded to hydrogen atoms. The rate of dipole–dipole relaxation is also directly proportional to the gyromagnetic ratios of the interacting nuclei. Therefore, the relaxation rates of ^{13}C nuclei in deuterated molecules, such as the solvents used for most NMR experiments, are lower than in molecules with ^{1}H, because deuterium (^{2}H) has approximately 6.5 times lower gyromagnetic ratio than hydrogen (^{1}H).

Quadrupolar relaxation is typically the dominant relaxation mechanism for nuclei with spin $I > ½$, which, due to their non-spherical charge distribution, have an electric quadrupole moment. Molecular motion causes fluctuations in the electric field, which can contribute to relaxation. The magnitude of quadrupole interaction depends on the size of the quadrupole moment of the nucleus, which is constant for a given isotope, and the symmetry of the molecule. Some quadrupolar nuclei, such as ^{2}H or ^{6}Li, have small quadrupole moments, and their relaxation is not significantly faster than for nuclei with spin ½, allowing them to be measured in solution without problems. Nuclei with large quadrupole moments tend to have significantly shorter T_1 and T_2 relaxation times, which leads to the broadening of their signals in the spectrum. It is often not possible to distinguish signals from individual nonequivalent nuclei in the molecule. Quadrupolar relaxation can also affect the surrounding magnetically active nuclei, because rapid relaxation may broaden or completely remove scalar interactions with the quadrupolar nucleus, contributing to the relaxation of the observed nucleus (via scalar relaxation, described below). This effect is commonly observed in groups such as $^{14}N–H$, $^{14}N–C$, $^{11}B–H$ and $^{11}B–C$. For example, it is often difficult to observe protons or carbons directly bonded to boron because their signals are broadened by this mechanism. For the same reason, scalar interactions with ^{14}N are usually not observed in hydrogen or carbon spectra, even though ^{14}N is magnetically active and has almost 100% natural isotopic abundance. Scalar interactions with ^{14}N nuclei can only be observed in molecules with tetrahedral symmetry, such as tetraalkylammonium salts or ammonium cations (**Fig. 7.8**).

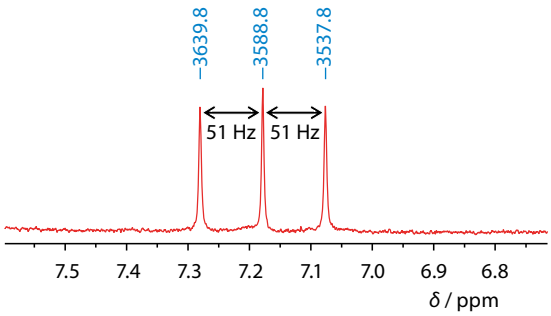

Fig. 7.8: The ^{1}H signal of the ammonium cation of NH_4Cl in DMSO. The signal is split into three equally intense lines due to the scalar interaction of hydrogen nuclei with ^{14}N. Nitrogen-14 has a spin quantum number $I = 1$, giving three possible spin states ($m = –1, 0, 1$).

Spin–rotation relaxation is significant in very small molecules or rapidly rotating groups (e.g. CH_3), especially at higher temperatures and in gases. Rapidly rotating molecules and groups with small moments of inertia generate a rotational magnetic moment, which can interact with the nuclear magnetic moment and lead to nuclear relaxation.

Relaxation can also occur due to **chemical-shift anisotropy (CSA)**. Since the shielding constant σ is generally anisotropic (its value depends on the orientation of the molecule relative to the $\boldsymbol{B}_0$ field), molecular rotation causes random fluctuations in the magnetic field. The reorientation of the molecule averages the shielding of the nucleus (and thus its chemical shift), which leads to the observation of narrow lines in solution NMR spectra. The averaged chemical shift in systems with rapidly reorienting molecules is referred to as **isotropic chemical shift**. However, fluctuating magnetic-field components with suitable frequencies can contribute to nuclear relaxation.

Scalar relaxation may occur when the observed nucleus has a scalar interaction with another nucleus, modulated by either chemical exchange or relaxation of that nucleus. Fluctuations of the scalar spin–spin interaction J can lead to fluctuating magnetic fields at the observed nucleus, contributing to its relaxation.

Like the relaxation contributions from mutual (scalar and dipolar) interactions between nuclei, relaxation times can also be significantly shortened by interactions with unpaired electrons in paramagnetic substances. The presence of paramagnetic ions in the measured solution can cause significant broadening of spectral lines. The relaxation rates increased due to interactions with unpaired electrons are utilized by **relaxation agents**, such as chromium(III) acetylacetonate, which contribute evenly to increasing the relaxation rates of substrate nuclei, allowing for a reduction in the repetition time of pulse sequences (by shortening the d_1 time necessary for the return to equilibrium). If the paramagnetic ion is tightly bound in a complex or molecule (e.g. in metalloproteins), paramagnetic relaxation can be used to obtain structural information, because this relaxation (and thus signal broadening) decreases with the sixth power of the distance between the nucleus and the paramagnetic center. Oxygen molecules (O_2) are also paramagnetic and can shorten the relaxation times of substances in solution. Therefore, before measuring relaxation times, oxygen must be removed from the solution either by vacuum or by bubbling the solution with nitrogen or argon.

Since relaxation rates in NMR are closely related to molecular motion, relaxation-time measurements can be used to study molecular dynamics. For example, the relaxation rate reflects different

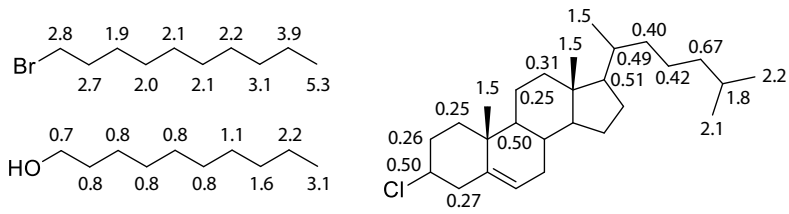

Fig. 7.9: The T_1 values for selected ^{13}C nuclei in 1-bromodecane, decan-1-ol, and cholesterol chloride. In decan-1-ol, carbon T_1 times gradually shorten as the carbon atom approaches the OH group, probably as a result of the "anchoring" of hydroxyl groups by intermolecular hydrogen bonds. The effect of molecular dynamics can also be observed in cholesterol chloride, where all CH carbons in the cyclic skeleton of the molecule have similar T_1 times (0.5 s), while CH_2 carbons in this part of the molecule have the T_1 times around 0.25 s (due to dipole–dipole C–H interaction)—this rigid part of the molecule moves as a single unit. The carbon T_1 times in the side chain are longer as a consequence of increased mobility. Methyl groups typically have longer T_1 times because dipolar interactions are suppressed by the rapid rotation of the methyl group.

molecular-motion rates in different parts (segments) of the molecule. A typical example is provided by the T_1 relaxation times of ^{13}C in 1-bromodecane (**Fig. 7.9**), which are approximately the same for all carbons in the central part of the molecule but become longer near the ends, where conformational flexibility and molecular motion rates are higher. Similarly, it is possible to study the molecular dynamics of biomolecules; for example, the relaxation times in proteins vary significantly between rigid globules and flexible oligopeptide loops.

08

NUCLEAR OVERHAUSER EFFECT

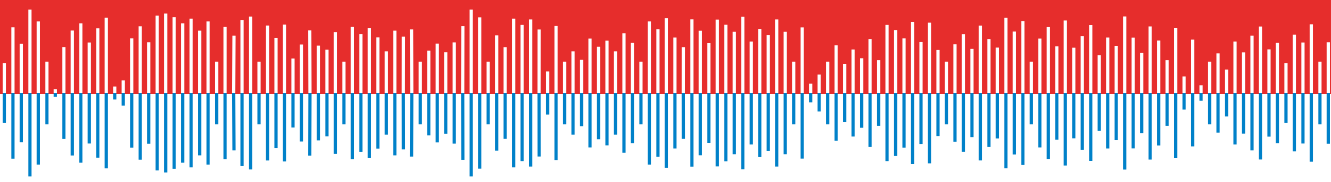

The nuclear Overhauser effect (NOE) is a phenomenon in which irradiation of one nucleus causes a change in the signal intensity of the nuclei in its spatial vicinity. Techniques utilizing NOE can be used, for example, to determine the conformation and configuration of "small" molecules or to determine the three-dimensional structure of biomolecules.

The principle behind the NOE is the cross relaxation of nuclear-spin states (see **Fig. 8.1**). As a model system, we use two ^{1}H atoms that are spatially close but are not coupled via indirect spin–spin interaction. In the hydrogen spectrum of such a system, we would observe two singlets (H1 and H2). A schematic energy diagram of the equilibrium state of such a spin system is shown in **Fig. 8.1**. This system has the lowest energy when both hydrogen nuclei are in the α spin state. Since there is no indirect interaction between the hydrogen nuclei in this model spin system, both transitions of H1 (αα → βα and αβ → ββ) are associated with the same energy change, and we thus observe only one signal line for this hydrogen in the spectrum. The same applies to the H2 signal. If there were indirect spin–spin interactions between the hydrogen nuclei, the energy differences of the individual transitions would change, and we would observe a doublet for each hydrogen in the spectrum (cf. **Fig. 5.15** in **Section 5.2**).

If we perform a selective inversion of the spin state of H1, we swap the populations of its spin states (as shown in **Fig. 8.1** by exchanging the number of beads at the lower and higher energy levels for both transitions of H1). If we measured the spectrum of this spin system after selectively inverting the spin state of H1, we would obtain a signal for this hydrogen with negative intensity. The signal of H2 would not be affected.

However, the spin system after selective inversion of the H1 spin state does not correspond to the

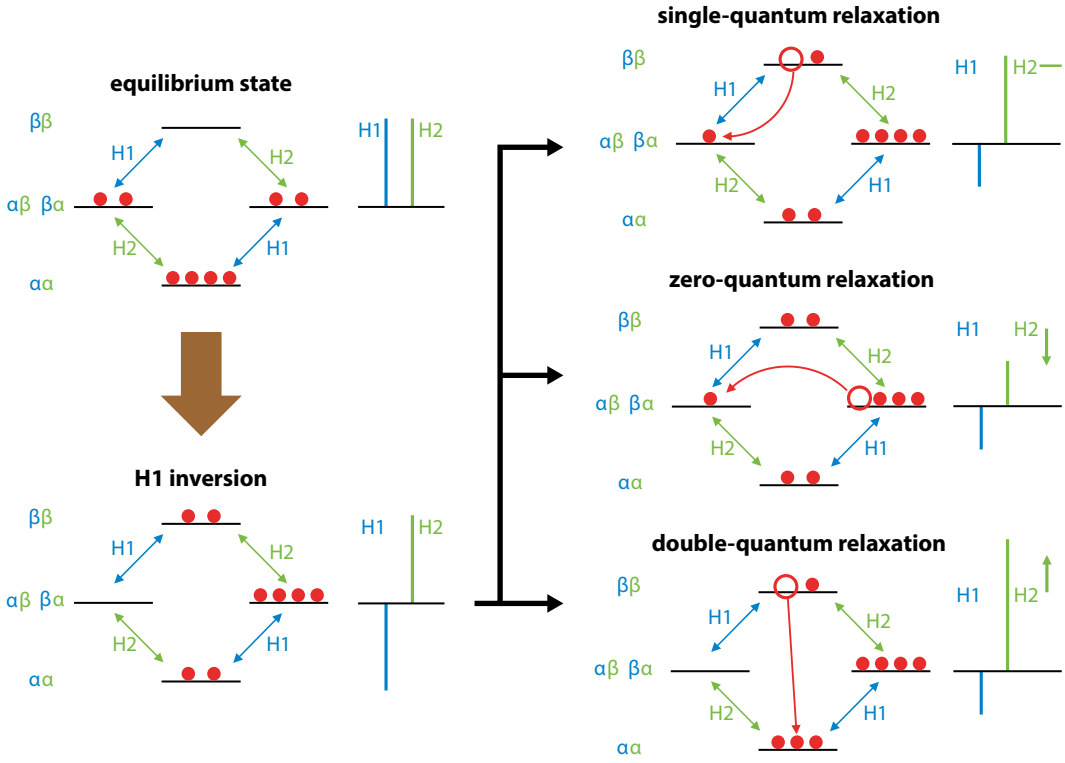

Fig. 8.1: The principle of NOE formation

equilibrium state, and, due to relaxation, it will gradually return to equilibrium. Several processes can lead back to the equilibrium state. A single-quantum relaxation process causes the spin state of one H1 nucleus to change, for example, from ββ to αβ, as shown at the top right of **Fig. 8.1**. Single-quantum relaxation processes lead to the gradual increase of the H1 signal intensity to its original value, corresponding to the equilibrium state of the spin system. The single-quantum relaxation processes of H1 do not affect the H2 signal.

A zero-quantum relaxation process involves no overall change in spin. This means that if the spin state of H1 changes from β to α, the spin state of H2 must simultaneously change from α to β. This process leads to the gradual return of H1 spin-state populations to equilibrium, but it also causes a change in H2 spin-state populations and thus a change in the intensity of H2 signal in the spectrum. Zero-quantum relaxation processes lead to a reduction in H2-signal intensity.

In a double-quantum relaxation process, the spin states of both nuclei change simultaneously (ββ to αα). Through this relaxation process, the spin-state populations of H1 return to equilibrium, while the signal intensity of H2 increases.

The nuclear Overhauser effect can thus be either positive or negative, depending on which cross-relaxation process (zero-quantum or double-quantum) is more likely. The likelihood of these relaxation processes is related to molecular motion. Zero-quantum relaxation processes are more probable when the rate of molecular reorientation is close to the difference in the resonance frequencies of the observed nuclei, which, for ^{1}H nuclei, is on the order of Hz to kHz. Large molecules (such as proteins) reorient at this slow rate. On the other hand, double-quantum relaxation processes are more likely when the rate of molecular reorientation is close to twice the resonance frequency of the observed nuclei, which is on the order of GHz.

The molecular reorientation is quantified by the rotational correlation time (τ_c, see also **Section 7.3**), which gives the average time required for a molecule to rotate by one radian. The NOE is positive when $\omega_0\tau_c$ is less than 1, where ω_0 is the angular velocity of the Larmor precession of the given nucleus. This condition is fulfilled for small molecules. Conversely, the NOE is negative when $\omega_0\tau_c$ is greater than approximately 1 (fulfilled for large molecules). If $\omega_0\tau_c$ is close to 1, the NOE is zero and thus immeasurable, even for nuclei in close spatial proximity (see **Fig. 8.2**). In measurements on a 500-MHz spectrometer at room temperature, the $^{1}H–^{1}H$ NOE is zero for molecules with a relative molecular weight around 1,000.

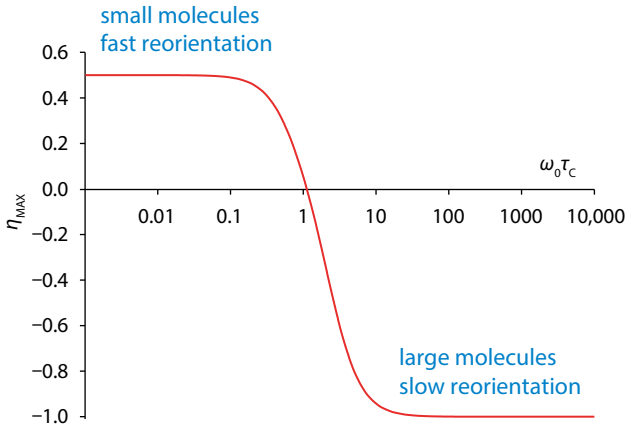

Fig. 8.2: The dependence of the maximum relative NOE intensity on the size of the studied molecules

The relative intensity of the NOE (NOE efficiency, the ratio of the signal amplified with the NOE to the signal without the NOE) is denoted as η. For the maximum NOE (η_{MAX}) in small molecules, it holds that it is equal to $\gamma_A / 2\gamma_B$, where γ_A is the gyromagnetic ratio of the irradiated nucleus and γ_B is the gyromagnetic ratio of the observed nucleus. For the homonuclear $^1H–^1H$ NOE, the maximum possible signal enhancement is 50%. When irradiating hydrogens and observing carbons, the intensity of carbon signals can increase by up to 200%.

The NOE is used in carbon measurements with proton decoupling. During decoupling, hydrogen nuclei are irradiated, which leads to an increase in the intensity of carbon signals. However, this increase is not the same for all carbon atoms because different carbon nuclei have different distances to nearby hydrogen atoms (for instance, quaternary carbons are farther from the nearest hydrogens than other types of carbons). This is one of the reasons why standard carbon spectra cannot be quantified, because the intensities of quaternary carbons are less enhanced by the nuclear Overhauser effect.

Since the NOE is essentially a relaxation process, it is not observable immediately after the initiation of irradiation but develops over time. This can be used in the measurement of quantitative ^{13}C spectra (see **Fig. 5.6** in **Section 5.2**). Decoupling does not occur throughout the experiment but only during FID measurement. Decoupling during data acquisition causes all multiplets arising from C–H interactions to collapse into singlets. At the same time, the NOE does not have time to develop as a consequence of which the carbon-signal intensity is not affected by the distance to ^1H nuclei.

The NOE is inversely proportional to the sixth power of the distance between the irradiated and observed nucleus. Therefore, its magnitude decreases rapidly with increasing internuclear distance and is observable only up to a distance of about 5 Å ($5 \cdot 10^{-10}$ m). This distance dependence of the NOE can be used to determine internuclear distances. If a certain internuclear distance is known (for example, the distance between hydrogens in a CH_2 group is typically 1.6 Å), we can calculate the distance between other nuclei from the ratios of NOE intensities (see **Fig. 8.3**). However, the precise determination of the distances using the NOE is quite complicated, because the irradiated and observed nuclei are never isolated and the proximity of other nuclei leads to changes in NOE magnitude, which must be considered when interpreting measured data.

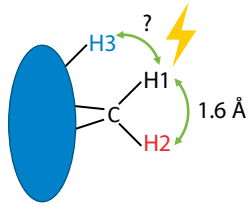

Fig. 8.3: The use of the NOE to measure internuclear distances (r):
The formula $r(H1,H3) = r(H1,H2) \cdot (\eta_{H1,H2}\, \eta_{H1,H3})^{1/6}$ is applied for measuring distances between nuclei.

If one nucleus (e.g. H1 in **Fig. 8.4**) is irradiated and the NOE causes an enhancement in the intensity of the spatially close H2 nucleus, the NOE can propagate further to other nuclei near H2. This phenomenon is called **spin diffusion** and is schematically shown in **Fig. 8.4**. If we irradiate the nucleus H1 and allow the NOE to develop long enough, we may observe enhancement in signals that are not spatially close to the irradiated nucleus but are connected through intermediaries, enabling the NOE to transfer to more distant nuclei. The duration for which the NOE is allowed to develop is called **mixing time** (t_{mix}). The correct choice of the mixing time is crucial for the success

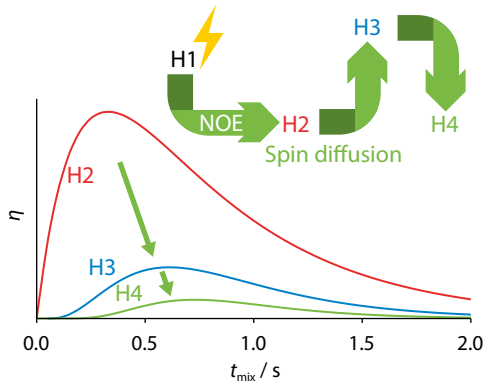

Fig. 8.4: The intensity of the NOE (η) and spin diffusion

of NOE-based experiments. For short t_{mix}, NOE enhancement is minimal, resulting in weak signals; nevertheless, spin diffusion does not occur yet, as a result of which the spectrum only shows interactions between truly spatially close nuclei. If t_{mix} is longer, the signal enhancement becomes higher, but spin diffusion may cause signals from more distant nuclei to be affected as well. In practice, a typical t_{mix} of 200–300 ms is used as a compromise for maximizing NOE enhancement while minimizing spin diffusion. However, when the NOE is used for measuring internuclear distances, it is necessary to apply shorter t_{mix} or a series of t_{mix} to create a NOE-build-up curve.

Experiments using the NOE to track spatial interactions in small molecules can be either one- or two-dimensional. One-dimensional experiments are commonly performed as differential measurements. First, a spectrum is recorded after selective irradiation (causing inversion or saturation) of a chosen signal (the spectrum A in **Fig. 8.5**), where the intensities of other signals are altered due to the NOE, although these changes are often subtle and hard to detect. Subsequently, an identical experiment is conducted, but the irradiation frequency is adjusted so it does not affect any signal in the spectrum (the spectrum B in **Fig. 8.5**). This spectrum will closely resemble a normal 1D spectrum without selective irradiation. When the spectrum B is subtracted from the spectrum A, the resulting differential spectrum highlights the changes in signal intensities caused by the NOE.

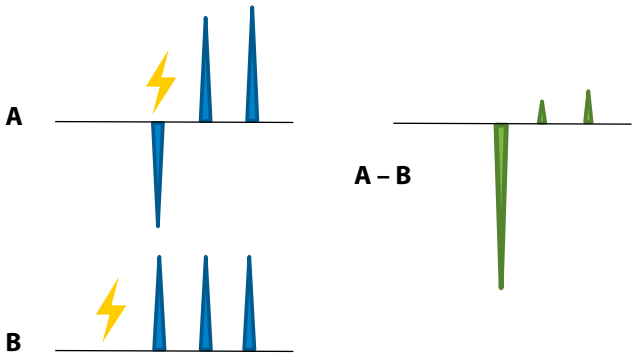

Fig. 8.5: The measurement of differential NOE experiments

A practical example of differential NOE spectra is provided in **Fig. 8.6**, showing three differential spectra after selective irradiation of three different hydrogen nuclei in the molecule of *trans*-pinocarveol. These spectra make it possible to assign all hydrogen signals and to determine the rel-

ative configurations at the carbon C3 or the conformation of the molecule. For example, the first and third spectra in **Fig. 8.6** reveal a close proximity of the hydrogen atom in position 3 and one of the methyl groups in position 6. This observation unequivocally places H3 in the *cis* position with respect to C6; therefore, the OH group in position 3 is *cis* to C7.

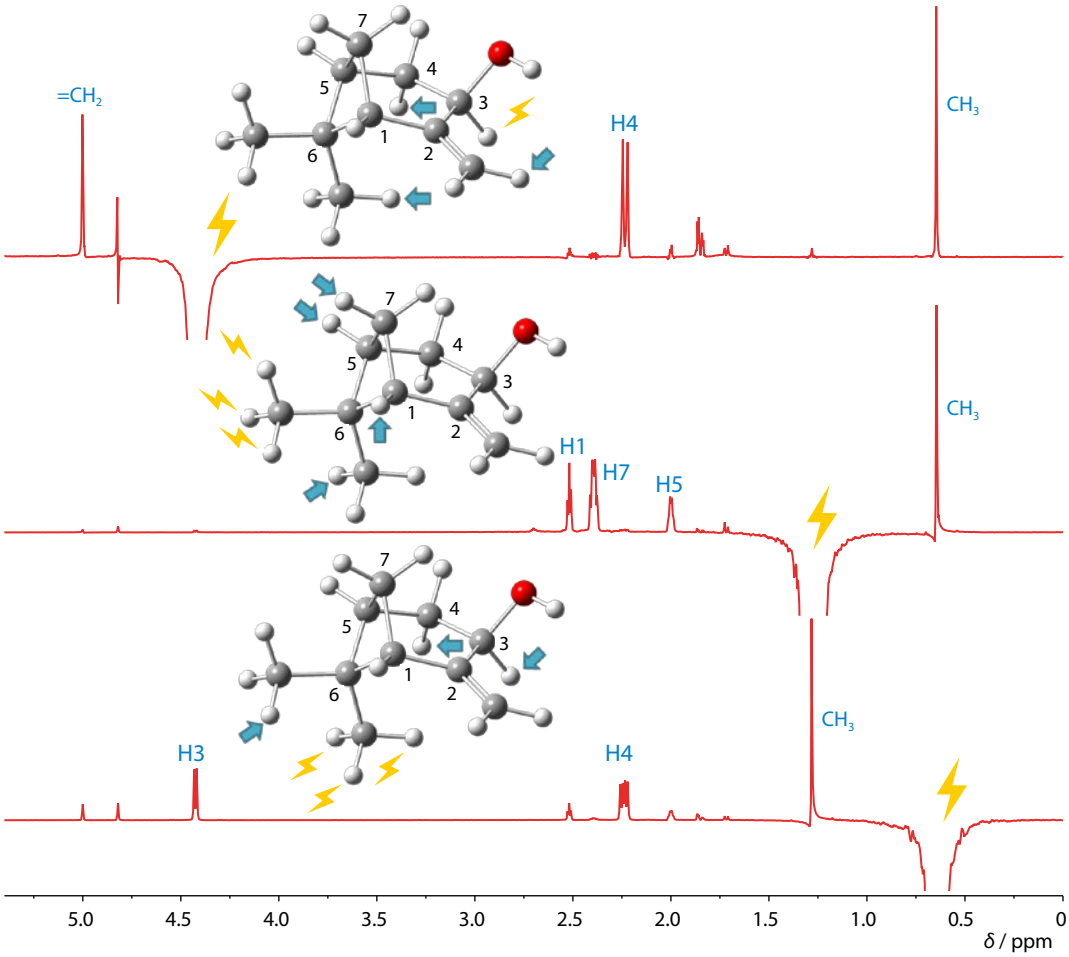

Fig. 8.6: The differential ^{1}H NOE spectra of *trans*-pinocarveol. The arrows indicate the hydrogen nuclei close to the irradiated nucleus, and their signals are observed in the differential NOE spectrum.

Two-dimensional NOE experiments, namely nuclear Overhauser effect spectroscopy (**NOESY**), enable the detection of all spatial contacts in the studied molecule in a single experiment without the need gradually to set selective irradiation frequencies. However, the disadvantages of these experiments are their greater time requirement and the dependence of the resolution in the indirectly detected dimension on the number of increments in the two-dimensional experiment.

Due to the previously described dependence of NOE magnitude on molecular size and the absence of NOE in medium-sized molecules, another type of experiment is commonly used to detect spatial interactions in small and medium-sized molecules. This is called **ROESY** (rotating-frame nuclear Overhauser effect spectroscopy). During this experiment, the magnetization vector is first tilted into the *xy*-plane and then "locked" using a so-called spinlock (also utilized in TOCSY experiment, **Section 5.3**). The development of NOE during the spinlock is not governed by the strength

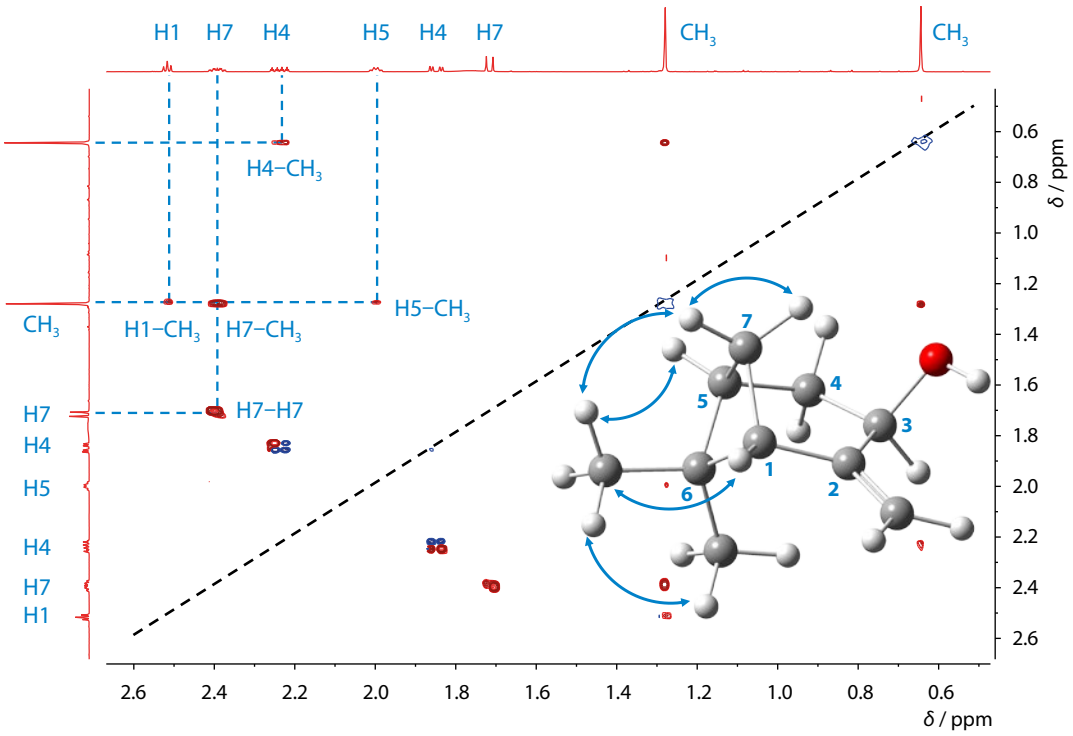

Fig. 8.7: A part of the 2D-ROESY spectrum of *trans*-pinocarveol. The spectrum is symmetrical along the diagonal.

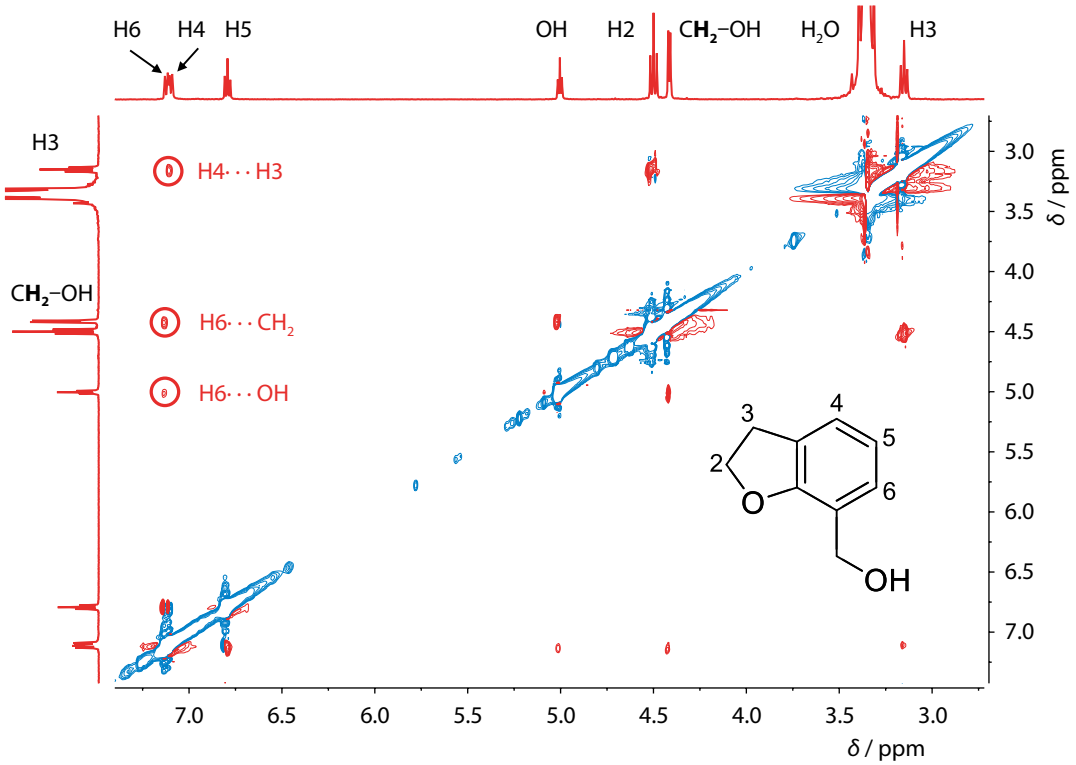

Fig. 8.8: The 2D-ROESY spectrum of the displayed substance

of the magnetic field along the *z*-axis of the spectrometer (the $\boldsymbol{B}_0$ field, with Larmor frequencies in the range of hundreds of MHz), but by the induction of the magnetic field $\boldsymbol{B}_1$, which is applied in the *xy*-plane and serves to lock the magnetization in this plane (in the range of kHz). This results in NOE always being positive. In the two-dimensional ROESY variant, the signals caused by NOE always have the opposite phase (positive vs. negative signals) compared to the diagonal. The maximum signal enhancement in the case of ROESY in a homonuclear ^{1}H–^{1}H experiment ranges from 39 to 68%. Examples of 2D-ROESY spectra are shown in **Figures 8.7** and **8.8**.

If chemical exchange occurs during the mixing time (see **Section 11.2**), cross peaks between the signals of the exchanging nuclei also appear in the resulting 2D spectrum. However, in ROESY spectra, these exchange cross peaks can easily be distinguished from the cross peaks caused by NOE because the exchange signals have the same sign (same phase) as the diagonal. The pulse sequences for measuring NOESY and ROESY spectra can thus also be used to study chemical exchange.

09

MAGNETIC-FIELD GRADIENTS

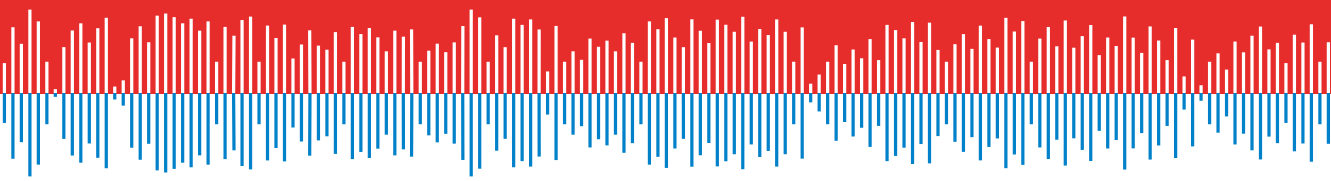

Chapter content

From the previous explanation, it is clear that during NMR-spectroscopy measurements, it is important for the sample to be placed in a homogeneous magnetic field. If different parts of the sample were exposed to different magnetic fields, we would observe different resonance frequencies for equivalent nuclei depending on their location in the sample tube. However, it is sometimes advantageous to disrupt the homogeneity of the magnetic field by creating a magnetic-field gradient, i.e. a field whose intensity linearly depends on the selected axis. In solution-state NMR spectroscopy, we most commonly encounter magnetic-field gradients along the *z*-axis. In magnetic resonance imaging (MRI), gradients are used along all three axes. Gradients are applied for a precisely defined duration during the pulse sequence, which is referred to as a gradient pulse (PFG, **Section 5.1**).

The use of magnetic-field gradients enables, among other things, the selection of the information encoded in the resulting spectrum and the removal of unwanted information (for example, in heteronuclear experiments, C–H information about the hydrogen atoms bound to the magnetically inactive isotope ^{12}C).

9.1 Gradient Echo

The effect of magnetic-field gradients is demonstrated below using the gradient-echo pulse sequence (**Fig. 9.1**). For the sake of simplicity, let us assume that we have a sample tube filled with a sample containing one type of ^{1}H nucleus, for example chloroform ($CHCl_3$). If this sample is placed in a homogeneous magnetic field, all equivalent ^{1}H nuclei have the same Larmor precession frequency, as a result of which the proton spectrum shows a single sharp signal. If a 90° pulse is applied to this sample, the ^{1}H magnetization vectors tilt into the *xy*-plane throughout the sample volume. During the subsequent delay, all nuclear magnetic moments precess with the same Larmor frequency (coherent precession). The vector sum of these magnetic moments, i.e. the magnetization, rotates around the *z*-axis with the same frequency, and the magnitude of the magnetization vector decreases only due to relaxation processes. However, if a magnetic-field gradient is applied along the *z*-axis, the molecules in the sample experience different magnitudes of the total magnetic field depending on their vertical position in the sample tube. It follows from the NMR resonance condition (**Section 2.2**) that the Larmor precession frequency is different in various parts of the sample. During the application of the magnetic-field gradient, the nuclear magnetic moments no longer precess coherently, but they gradually dephase. If the gradient is applied for a sufficiently long time, the magnetic moments at the end of the gradient are uniformly distributed in all directions in the *xy*-plane, and their vector sum is zero. After the gradient is turned off, the magnetic field becomes homogeneous again, and all nuclear magnetic moments once again precess at the same frequency. If we were to start recording the FID at this moment, there would be no signal in the spectrum because the total magnetization vector in the *xy*-plane would be zero. The magnetic-field gradient has no effect on the magnetization along the *z*-axis; the dephasing occurs only in the *xy*-plane. This makes it possible, for example, to suppress unwanted signals in the spectrum.

In a gradient echo, the magnetic-field gradient is followed by a 180° pulse, after which the same magnetic-field gradient is applied once again. After the 180° pulse, the direction of the individual nuclear magnetic moments flips by 180° in the *xy*-plane, but the total magnetization vector remains zero. During the second-gradient pulse, the frequencies of the individual nuclear magnetic moments once again depend on the vertical position of the molecule in the sample tube. If the gradient is of the same intensity and duration as the first gradient, the individual nuclear magnetic moments rotate by the same angle as during the first gradient and thus refocus. At the

end of the second-gradient pulse, all magnetic moments are aligned in the same direction, and the resulting magnetization vector points in the same direction as well. After the second-gradient pulse, the refocused magnetic moments once again precess coherently, and at the end of the second delay τ (if it is the same length as the first τ), the magnetization vector points along the x-axis.

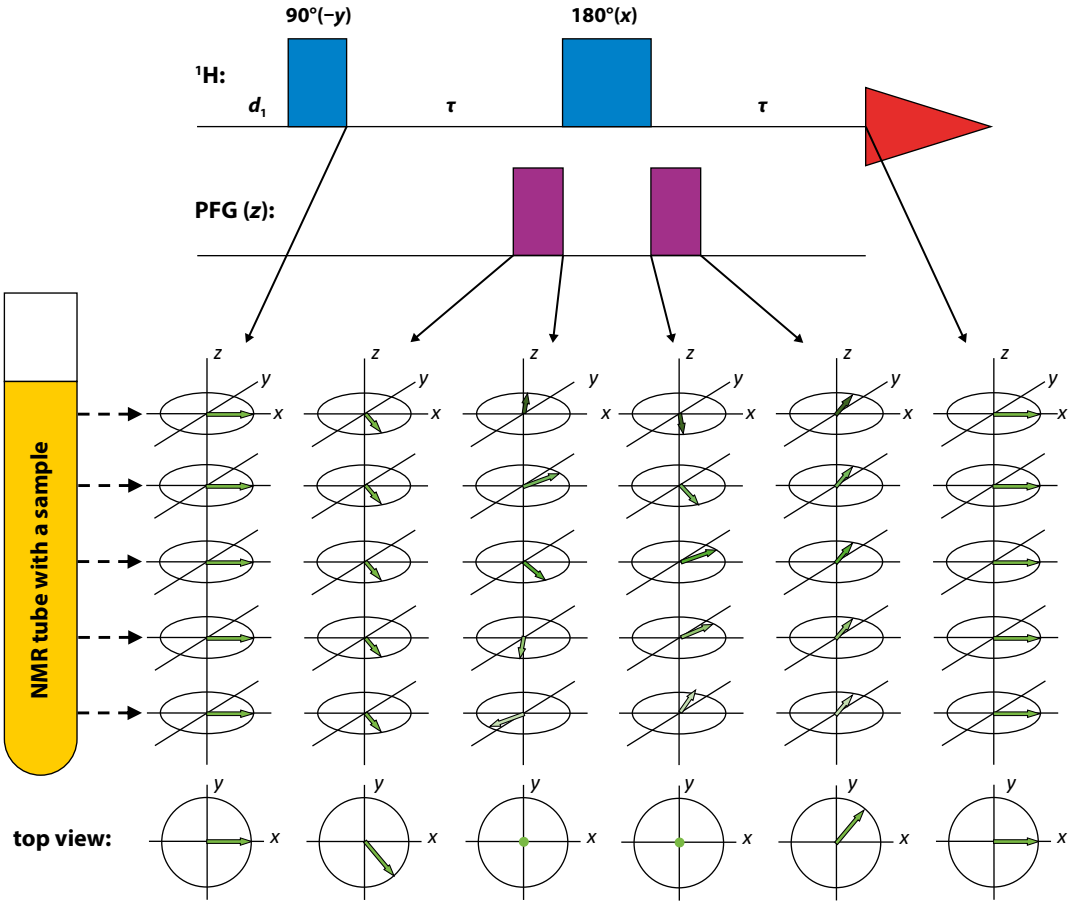

Fig. 9.1: The pulse sequence of the gradient echo (top) and the evolution of the spin system in the sample during this sequence

9.2 DOSY

For the magnetization vector to refocus during the gradient echo, it is necessary for individual molecules not to change their vertical position in the sample tube between the first- and second-gradient pulses. If a molecule changes its position along the z-axis, it is subjected to a different total magnetic field during the second-gradient pulse than during the first, and its nuclear magnetic moment rotates a different angular distance during the second-gradient pulse than during the first. At the end of the second gradient, the nuclear magnetic moment of this molecule does not refocus with the magnetic moments of the other molecules in the sample.

This dependence of the degree of magnetization-vector refocusing on the mobility of the molecules can be used to measure molecular diffusion coefficients. If the delay between the gradient pulses in the gradient echo is increased, individual molecules progressively move farther from their original position at the time of the first-gradient pulse, and their resulting magnetization

vector at the end of the echo gradually decreases. From the dependence of signal-intensity decay on the length of the delay between the gradient pulses, it is possible to calculate the diffusion coefficient of the molecule studied. An effect similar to that obtained by prolonging the delay between gradient pulses (i.e. a gradual decrease in signal intensity) can be achieved by gradually increasing the length or intensity of the gradient pulses.

The size of the diffusion coefficient depends on the size and shape of the molecule and the viscosity of the medium (e.g. according to the Stokes–Einstein equation for spherical molecules). Small molecules exhibit higher diffusion rates than larger molecules. Therefore, their signal disappears from the spectrum obtained using the gradient echo at shorter delays between gradient pulses. An example of the spectra of a mixture of substances measured with different gradient strengths is shown in **Fig. 9.2**.

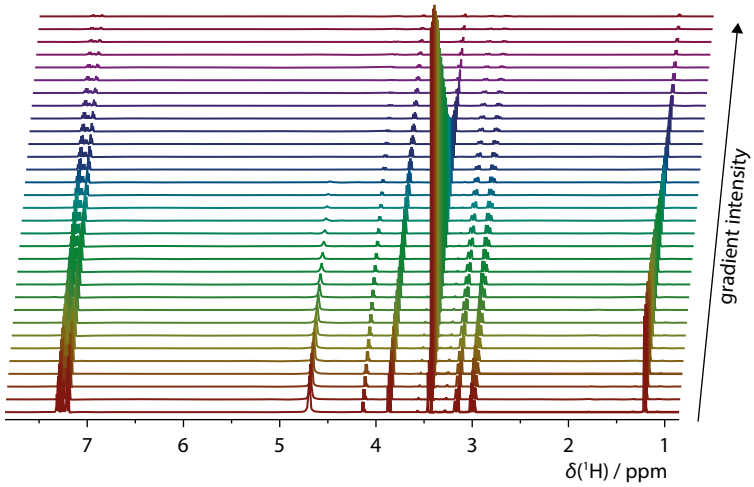

Fig. 9.2: The ^{1}H NMR spectra of a mixture of phenylalanine, threonine and glycine measured in D_2O using a gradient echo with different magnetic-field gradient strengths

In addition to measuring diffusion coefficients, the gradient echo can also be used to separate signals of different substances in mixtures. This method is called diffusion-ordered spectroscopy (DOSY). During this experiment, the gradient echo is recorded with gradient pulses of varying

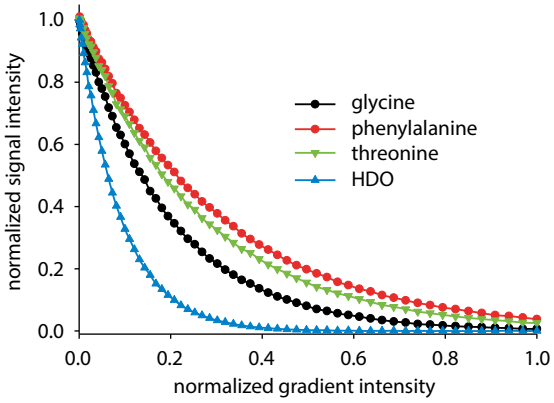

Fig. 9.3: The decay of the proton-signal intensities of individual components in a mixture of phenylalanine, threonine and glycine with increasing magnetic-field gradient strength in a gradient echo

intensity (like in **Fig. 9.2**). By means of intensity-decay analysis, it is possible to assign diffusion coefficients to individual signals (**Fig. 9.3**). All atoms in a single molecule should have the same diffusion coefficient. Consequently, based on the determined diffusion coefficients, signals can be assigned to individual molecules in the mixture. DOSY spectra are often presented as two-dimensional spectra, where the horizontal axis represents chemical shifts and the vertical axis represents diffusion coefficients (**Fig. 9.4**). Signals in the same horizontal row belong to nuclei with the same diffusion coefficients, i.e. nuclei from the same molecule. This method is advantageous, for example, in the study of dimerization or complex formation. If a dimer or complex is formed, its molecular weight is higher and its diffusion coefficient is lower. The signals of these supramolecular structures can be clearly separated from the signals of monomers or complex components in DOSY spectra.

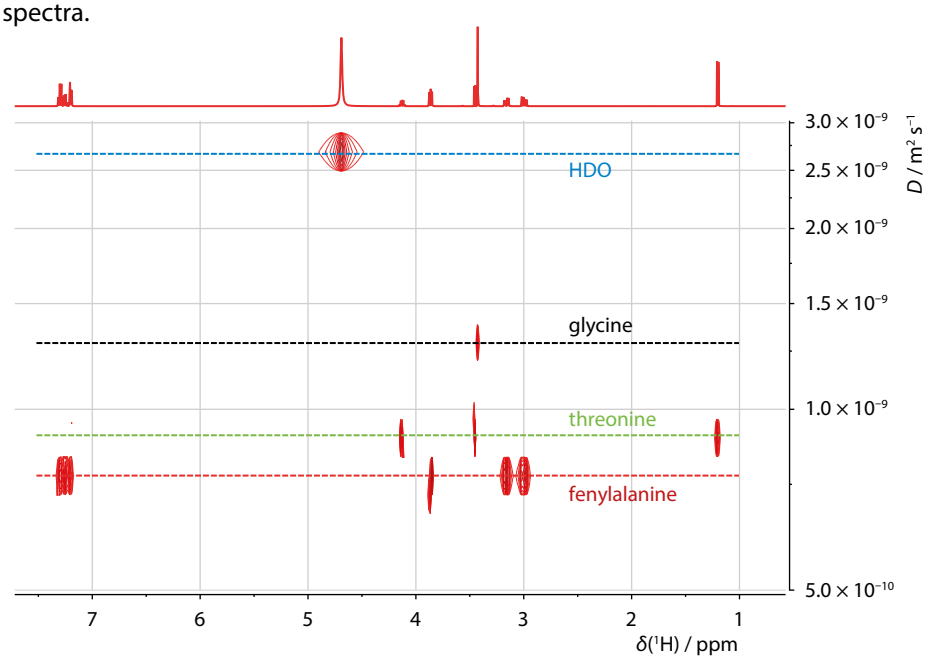

Fig. 9.4: The DOSY spectrum of a mixture of phenylalanine, threonine and glycine measured in D_2O

9.3 Magnetic Resonance Imaging (MRI)

The use of magnetic-field gradients is also the basis for magnetic resonance imaging (MRI). Consider the simplest case of one-dimensional imaging. During the gradient pulse along the *z*-axis, the resonance frequencies in different parts of the sample vary. With the application of a selective excitation pulse, the magnetization vector rotates from the *z*-axis into the *xy*-plane only for those molecules that meet the resonance condition, i.e. those that are currently in the magnetic field corresponding to the resonance frequency of the excitation pulse. In the case of a gradient field along the *z*-axis, the individual layers of the sample can be selectively excited in this way (**Fig. 9.5**).

The selective excitation of molecules in a single layer of a sample can be used, for example, to measure changes in the concentration of an active substance during the gradual dissolution of tablets. The selective excitation of individual layers is also utilized in **ultrafast 2D NMR** experiments, where individual increments (individual one-dimensional experiments, **Section 5.3**) are measured in separate layers of the sample. In these experiments, it is not necessary to wait for the relaxation of the spin system back to its equilibrium state before each increment, and the individ-

ual increments can be measured in quick succession (each in a different layer of the sample). This method allows 2D NMR spectra to be obtained within a few seconds, which is useful, for instance, in the structural characterization of unstable intermediates in chemical reactions.

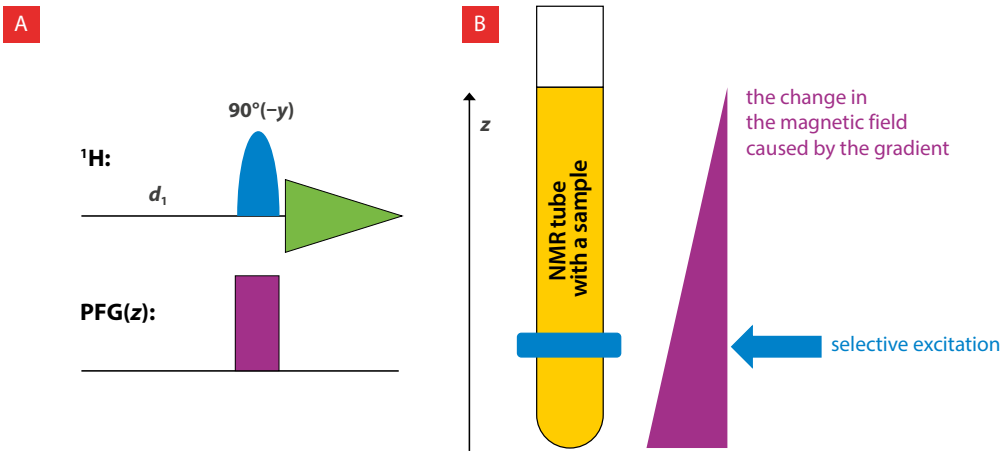

Fig. 9.5: A) The pulse sequence for the selective excitation of molecules in a single layer of a sample and **B**) a schematic representation of the selective excitation

Magnetic resonance as an imaging method (MRI) is a non-invasive imaging technique frequently used in medicine. In order to obtain a three-dimensional image, it is necessary to use magnetic-field gradients along all three axes. MRI utilizes the signal from hydrogen (^{1}H), which constitutes approximately 63% of the atoms in the human body. Since the amount of hydrogen atoms may differ in various tissues (primarily due to different amounts of water), the signal intensity varies among tissues. Additionally, the relaxation times T_1 and T_2 (**Chapter 7**) of hydrogen atoms can differ significantly in different tissues, which can be exploited to enhance contrast in the resulting image (an example is shown in **Fig. 9.6**). The contrast is further improved by the intravenous injection of contrast agents into the patient before the examination. These contrast agents are most commonly based on the presence of paramagnetic ions such as Gd^{3+}, which significantly shorten water relaxation times. Since the distribution of contrast agents in the body is uneven, it results in contrast between different tissues. Another option for obtaining contrast is the use of the different mobility of molecules (like in DOSY experiments). This method is employed in MRI angiography, which images blood vessels. Another possible application is functional brain imaging, known as functional MRI (fMRI). In fMRI, the images of the brain are taken both at rest and while performing a task (in response to stimuli, moving limbs, speaking). fMRI can thus be used to determine which areas of the brain are responsible for certain functions. The downsides of MRI examinations are the confined space in the scanner, making some people feel claustrophobic, and the significant noise during the experiment, caused by the rapid switching of gradient coils.

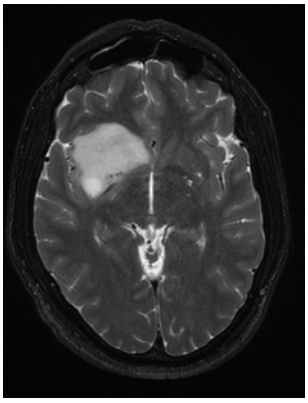

Fig. 9.6: An MRI image of the brain obtained with T_2-weighting, showing (the bright region) a diffuse astrocytoma brain tumor. The image has been provided by the Department of Radiology of the Hospital Na Homolce in Prague.

10

PRACTICAL ASPECTS OF NMR SPECTROSCOPY

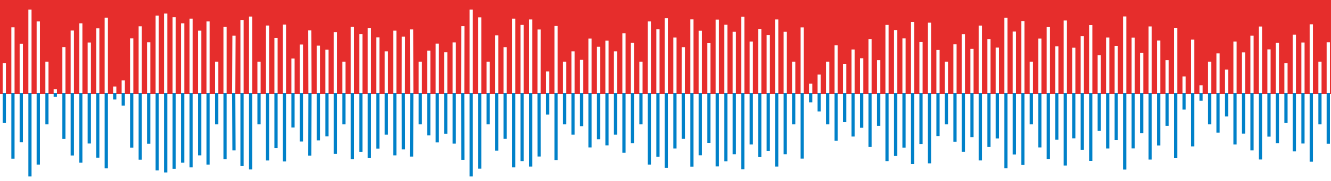

Chapter content

10.1 Spectrometer

10.1.1 Magnet

In most modern spectrometers designed for measuring the NMR of liquid samples, the magnetic field is generated by superconducting coils made of several thousand turns of special alloys. Currently available superconducting materials, capable of withstanding high magnetic fields, have a critical temperature only a few degrees above absolute zero. Therefore, the superconducting coil must be immersed in liquid helium. Since the Earth's supply of helium is limited and its cost is high, efforts are made to minimize its use. Significant savings in liquid helium have been achieved by separating the part of the magnet containing liquid helium and the superconducting coil from the environment with room temperature using a liquid nitrogen space (**Fig. 10.1**). Nitrogen is cheap and easily extracted from air. Liquid nitrogen must be refilled every one to two weeks, while liquid helium is refilled every few months. The evaporated helium can also be collected and re-liquefied. Some newer magnets even operate as closed systems, where the evaporated helium is immediately re-liquefied and returned to the magnet.

The superconducting coil carries a current of approximately 100 A. The magnetic-field induction achieved in this way is between 7 and 28 T. The field must be highly stable, because fluctuations over time lead to line broadening in the spectrum. Line broadening is also caused by insufficient homogeneity of the magnetic field—if identical nuclei in different parts of the sample experience different magnetic fields, they resonate at different frequencies. The homogeneity of the field is adjusted using a special set of spatially oriented coils where the current and thus the additional magnetic field are adjusted to make the resulting magnetic field as homogeneous as possible.

Modern NMR magnets are mostly shielded, which means that they include an additional coil that generates an opposing magnetic field to minimize the external magnetic field, preventing it from interfering with nearby devices.

If a part of the superconducting coil were to reach a temperature higher than that which allows superconductivity (for instance due to delayed or improper refilling of liquid helium), that part of the coil would lose superconductivity, gaining non-zero resistance, and the current passing through it would heat the coil. Consequently, other parts of the coil become warmer and lose superconductivity as well. The result of this chain reaction is the complete loss of the coil's superconducting properties, the conversion of electrical energy into heat (accompanied by the rapid evaporation of all helium), and the loss of the magnetic field. This undesirable process is known as NMR-magnet quenching.

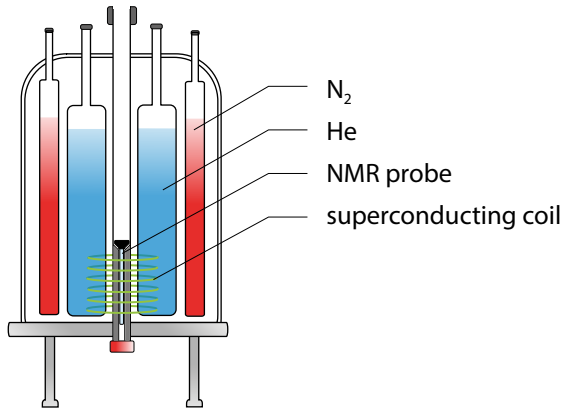

Fig. 10.1: A schematic diagram of an NMR magnet

10.1.2 Probe

The part of the NMR spectrometer that contains the receiving and transmitting coils, the coils for generating magnetic-field gradients, and the device for controlling the sample temperature is called the probe. Probes can be swapped if necessary. Some probes are designed to measure a specific type of experiment with higher sensitivity, as discussed in the case of inverse probes in **Section 5.3**. In modern spectrometers, the same coil is usually used for both pulse transmission and response detection. Additional coils may be used for the transmission of frequencies of other nuclei, such as hydrogens during decoupling.

The biggest limitation of NMR spectroscopy is its relatively low sensitivity. Each experiment requires a sufficient signal-to-noise ratio in the resulting spectra. Part of the electronic noise, called thermal noise, is caused by the random movement of electrons in any electronic device. Thermal noise is suppressed by lowering the temperature of the electronic device. In some modern probes (known as **cryoprobes**), this effect is used to increase sensitivity. The receiving coil, the wires carrying the signal, and the first signal amplifier are cooled either by helium gas at around 20 K or by nitrogen gas at around 80 K. This dramatically improves the signal-to-noise ratio (approximately fivefold for helium-cooled cryoprobes) and shortens the experimental time (a fivefold improvement in signal-to-noise ratio makes it possible to reduce the experiment duration by a factor of 25).

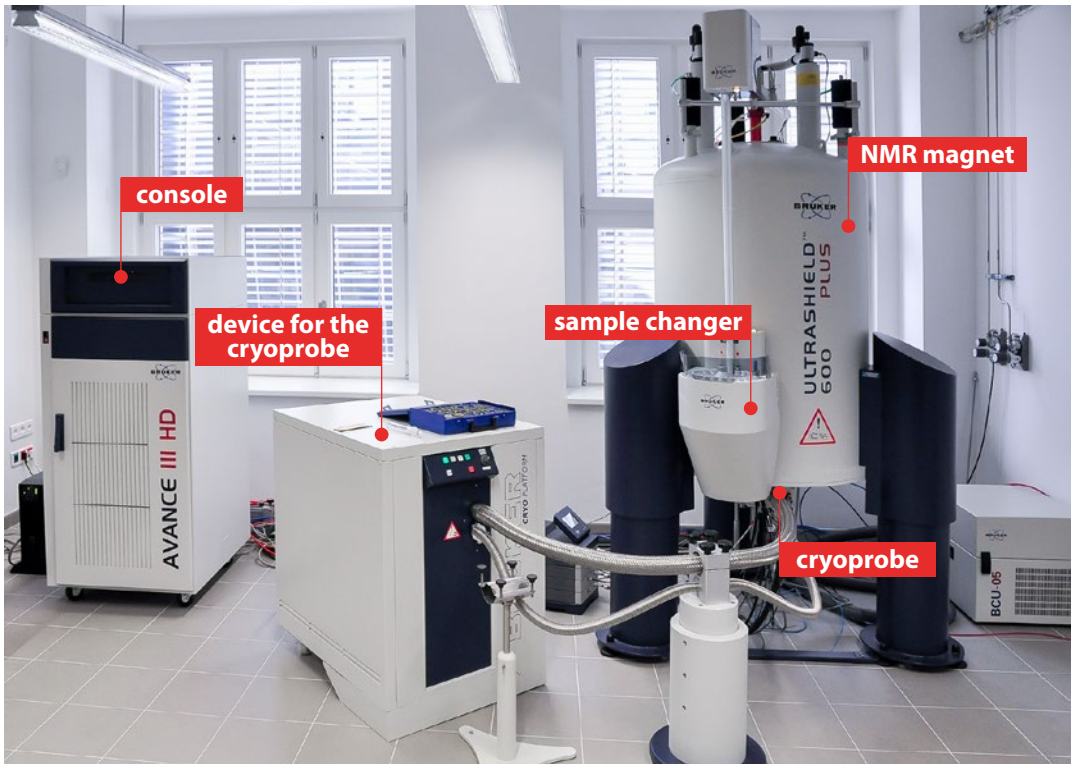

Fig. 10.2: A NMR spectrometer

10.1.3 Console

The electronic devices necessary for conducting an experiment are housed in a console. It includes a frequency synthesizer with an amplifier (transmitter) that typically produces 50–300 W

of power, capable of generating short radiofrequency pulses with precise amplitude, frequency and phase. There are usually two or more transmitters because irradiation is often applied to nuclei other than the one detected. Additionally, an independent channel is used for maintaining a stable magnetic field (lock), which typically relies on deuterium nuclei in the solvent. When the system response is detected, the coil is switched to the receiver, where the signal is amplified and digitized. The FID signal is stored in the memory of the control computer, where FID signals from individual scans are summed. The console also typically contains a temperature unit, which controls the sample temperature during the experiment. Other necessary components of the NMR spectrometer housed in the console include units for gradient-pulse control and for controlling correction coils to achieve maximum magnetic-field homogeneity.

10.2 Experiment Preparation

10.2.1 NMR Tubes

Spectra are most commonly measured using glass tubes with an outer diameter of 5 mm and a length of 15–20 cm. The sample volume typically ranges from 500 to 600 µL. However, there are also other types of tubes. For example, for measuring low-sensitivity nuclei, it is possible to use 10-mm-diameter tubes, which can hold a larger sample volume. These tubes can only be utilized with the appropriate probe. Conversely, if the sample quantity is limited, one can employ Shigemi tubes, which require only about 150–200 µL of solution, with the sample column bordered by a material with a magnetic susceptibility adjusted to match the susceptibility of the solvent. Using a regular tube with such a small amount of solution would disturb the homogeneity of the magnetic field. Tubes with an outer diameter of 3 mm (about 150 µL of sample solution) or 1.7 mm (about 35 µL of sample solution) can also be utilized for small sample quantities.

Fig. 10.3: NMR tubes: micro (**A**), standard (**B**), Shigemi (**C**)

10.2.2 Solvent and Standard

Samples are usually dissolved in deuterated solvents and transferred into a tube, which is positioned in the center of the magnet, surrounded by coils. Deuterated solvents are used because the solvent is usually present in large excess in comparison with the measured substance, as a result of which the ^{1}H signal from the solvent would be much stronger in the ^{1}H NMR spectrum than the signals from the measured substance, potentially overlapping them. However, the deuteration of solvents is never 100% complete. Therefore, the ^{1}H NMR spectra still show signals from non-deuterated or partially deuterated solvents. In ^{13}C spectra, we may observe signals from the solvent carbons, which are split into multiplets due to spin–spin couplings with deuterium (**Fig. 10.4**). **Table 10.1** summarizes the chemical shifts of the hydrogen and carbon atoms for the most commonly used deuterated solvents.

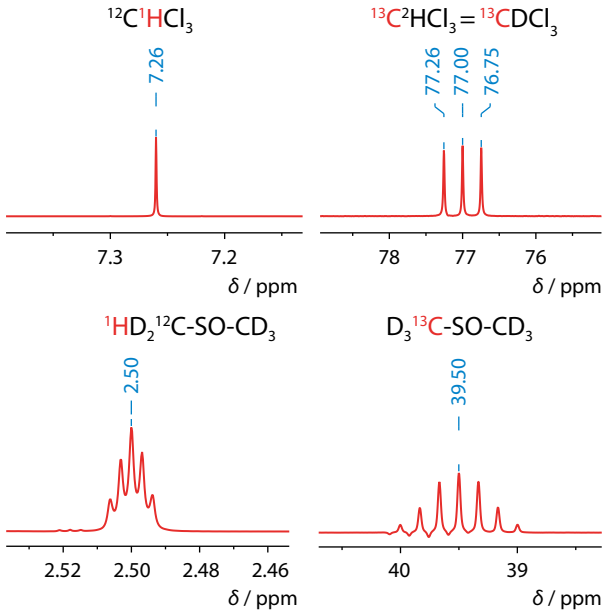

Fig. 10.4: The top left shows the ^{1}H spectrum of residual non-deuterated chloroform, whereas the top right shows the ^{13}C spectrum of deuterated chloroform. The signal is split into three equally intense lines due to the spin–spin interaction between the ^{13}C nucleus and the deuterium nucleus, which has a spin quantum number $I = 1$, giving three magnetic quantum states $m = -1, 0, 1$. The bottom row of the Figure shows the ^{1}H and ^{13}C spectra of deuterated dimethyl sulfoxide with traces of incompletely deuterated molecules. The splitting in the ^{1}H spectrum is caused by the interaction of ^{1}H with two deuterium nuclei, while the splitting in the ^{13}C spectrum is a result of the couplings of ^{13}C with three deuterium nuclei.

Table 10.1: The chemical shifts of the residual ^{1}H signals from non-deuterated fractions of the solvents commonly used for NMR measurements and the ^{13}C chemical shifts of the respective deuterated solvents

Solvent	Formula	$\delta(^{1}H)$ / ppm	$\delta(^{13}C)$ / ppm
Chloroform	$CDCl_3$	7.26	77.0
Benzene	C_6D_6	7.27	128.0
Acetonitrile	CD_3CN	1.94	1.3 (CD_3), 118.2 (CN)
Acetone	CD_3COCD_3	2.05	29.8 (CD_3), 206.3 (C=O)
Dimethyl sulfoxide	CD_3SOCD_3	2.50	39.5
Methanol	CD_3OD	3.31	49.0
Water	D_2O	~4.8	–

Deuterium from the solvents is used during experiments to **lock the magnetic field**. The spectrometer continuously monitors the resonance frequency of the deuterium signal and adjusts the stability of the magnetic field accordingly. If the magnetic field in the spectrometer were not constant, the resonance frequency would shift during the experiment (see the resonance condition, **Section 2.2**). The moving ferromagnetic-material objects nearby (such as elevators, cars, and lab carts) can also affect the induction of the superconducting magnet. To eliminate such influences as well as other fluctuations in the magnetic field, a correction coil is automatically activated to generate an additional magnetic field, ensuring that the deuterium resonance frequency remains constant. This guarantees the stability of the magnetic field for the duration of any experiment, regardless of its length.

The absolute value of the chemical shift δ is difficult to determine for technical reasons. Therefore, it is essential to use a suitable standard with a single, easily identifiable line in the spectrum. It is added directly to the measured substance (internal standard) or placed in a sealed capillary in the sample tube (external standard). The standard frequently used for ^{1}H NMR spectra is tetramethylsilane (TMS), $(CH_3)_4Si$, with twelve equivalent hydrogen atoms. In the spectrum, its signal is a singlet, usually located farthest to the right. Tetramethylsilane is insoluble in water; in aqueous solutions, it is thus necessary to use other standards, such as 1,4-dioxane, with a ^{1}H chemical shift of 3.75 ppm, or the sodium salt of 4,4-dimethyl-4-silapentane-1-sulfonic acid (DSS, **Fig. 10.5**). For ^{1}H spectra measured in water, it is not advisable to utilize the residual signal of the non-deuterated fraction of water (HDO) as a reference, because the chemical shift of water depends on temperature, pH, and ionic strength. For ^{13}C NMR spectra measured in carbon-containing solvents, it is common to use the solvent signal with the corresponding shift (**Table 10.1**).

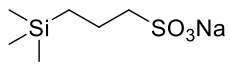

Fig. 10.5: The structure of the sodium salt of 4,4-dimethyl-4-silapentane-1-sulfonic acid (DSS), used as an internal standard in the NMR spectra of aqueous solutions

The measurement of NMR spectra in deuterated solvents is sometimes not feasible or appropriate, for example when the sample is taken directly from a reaction mixture where deuterated solvents are not used or when a deuterated solvent is not available for the specific experiment. Another case concerns experiments in protic solvents, where all exchangeable hydrogens would be replaced by deuterium. This would cause their signals to disappear from the ^{1}H NMR spectra, making the interpretation of the experiment more challenging. This is typical with peptides and proteins dissolved in water. In D_2O, amidic hydrogens are not observable, which is problematic for structural determination because these are the only hydrogens on peptide bonds linking individual amino acids. The solution in such cases is to measure NMR in non-deuterated solvents and suppress the intense solvent signal (explained below). However, a small amount of deuterated solvent (around 10%) is usually added to ensure the stability of the magnetic field using the lock.

Several methods have been developed to suppress solvent signals. The simplest is presaturation, where during the relaxation delay d_1, the solvent signal is irradiated with low-power electromagnetic radiation, which equalizes the populations (saturation) of the spin states of ^{1}H nuclei in the solvent and thus suppresses its signal intensity (**Fig. 10.6**). Other methods use NMR relaxation, such as the inversion-recovery pulse sequence (**Section 7.1**), where the delay between the 180° and 90° pulses is set such that the solvent magnetization is zero immediately before the 90° pulse, which results in the solvent signal being suppressed in the final spectrum.

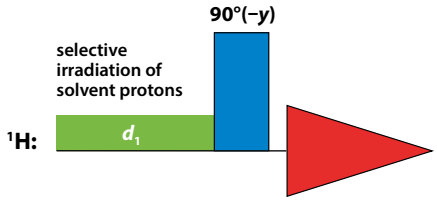

Fig. 10.6: The pulse sequence for solvent-signal suppression using presaturation

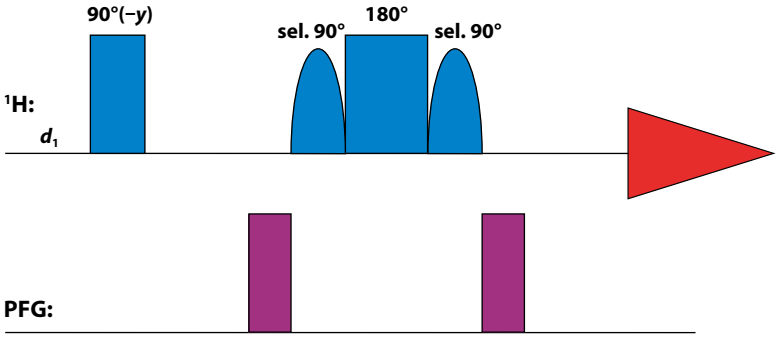

Fig. 10.7: The pulse sequence for solvent-signal suppression combining gradient-echo (**Section 9.1**) and selective pulses. Selective pulses rotate only the magnetization vector of the chosen solvent. In the middle of the pulse sequence, a 360° pulse is applied to the solvent nuclei, preventing the solvent signal from refocusing at the end of the gradient echo. All other nuclei experience only a 180° pulse between the gradient pulses, so that their signals refocus at the end of the gradient echo.

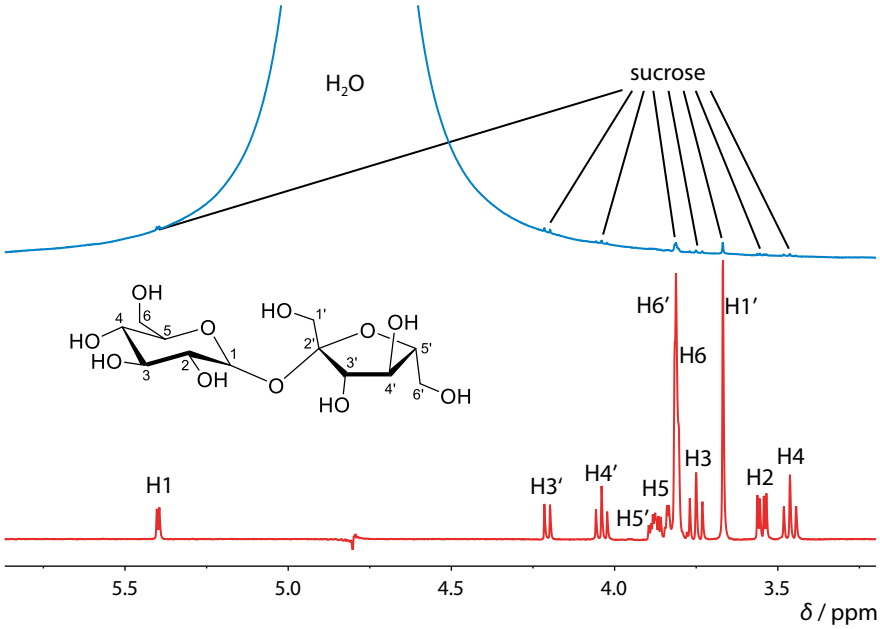

Fig. 10.8: The ^{1}H NMR spectrum of sucrose measured in a mixture of 90% H_2O + 10% D_2O without solvent-signal suppression (top) and using the modified WATERGATE method (bottom)

Modern methods for solvent-signal suppression combine gradient and selective pulses. These methods are based on the WATERGATE pulse sequence, designed to suppress the water signal in biomolecule measurements (**Fig. 10.7**). This pulse sequence has been developed by the prominent Czech spectroscopist Vladimír Sklenář. **Fig. 10.8** shows the spectrum of sucrose measured in a mixture of 90% of H_2O + 10% of D_2O without solvent-signal suppression and using the modified WATERGATE method.

10.2.3 Tuning the Resonance Circuit

For the resonance circuit of an NMR spectrometer to be able to emit and receive signals, it must be tuned to the corresponding resonance frequency. The tuning process is similar to how radios used to be tuned to a specific frequency (i.e. a specific station) by means of variable capacitors or coils. Nowadays, this process can be fully automated. The resonance circuit needs to be retuned with any change of the isotope to be irradiated or detected. For example, if we measure ^{13}C nuclei and then ^{31}P nuclei, the resonance circuit must be retuned between these measurements. The magnetic susceptibility of the solvent in the sample tube also affects the resonance circuit. Therefore, it is advisable to fine-tune the circuit even when conducting the same experiment but with a sample in a different solvent.

10.2.4 Sample Rotation

Some inhomogeneities in the magnetic field in the *xy*-plane can be eliminated by rotating the sample tube along the *z*-axis, as each nucleus passes through different regions of the magnetic field during the rotation. However, inhomogeneities in the *xy*-plane can lead to the formation of rotational sidebands (**Fig. 10.9**) when the sample is rotated. Sample rotation is not recommended for two- and multidimensional experiments because mechanical vibrations caused by the rotation can deteriorate the quality of the spectra.

10.2.5 Tuning the Magnetic-Field Homogeneity (Shim)

For NMR measurements, as already mentioned, the magnetic field must be as homogeneous as possible. If different parts of the sample tube experience different external magnetic fields, identical nuclei in molecules located in different parts of the tube have different resonance frequencies. In practice, this often leads to broadened and irregularly shaped signals (**Fig. 10.9**). The integral intensity (signal area) remains the same, but the broader signals are lower and thus have a worse signal-to-noise ratio. Consequently, poor magnetic-field homogeneity leads to a loss of resolution (as broad signals tend to overlap) and sensitivity.

Magnetic-field inhomogeneities are corrected using a set of several dozen correction coils, which create an additional magnetic field in such a way that the resulting overall magnetic field is as homogeneous as possible across the entire volume of the measured sample; this procedure is called "**shimming**". In modern spectrometers, magnetic-field homogeneity can be automatically shimmed without user intervention.

10.2.6 Temperature

Air (or nitrogen gas) of a specific temperature constantly flows around the sample tube in the probe, allowing the sample to be kept at a predetermined temperature. Some probes make it

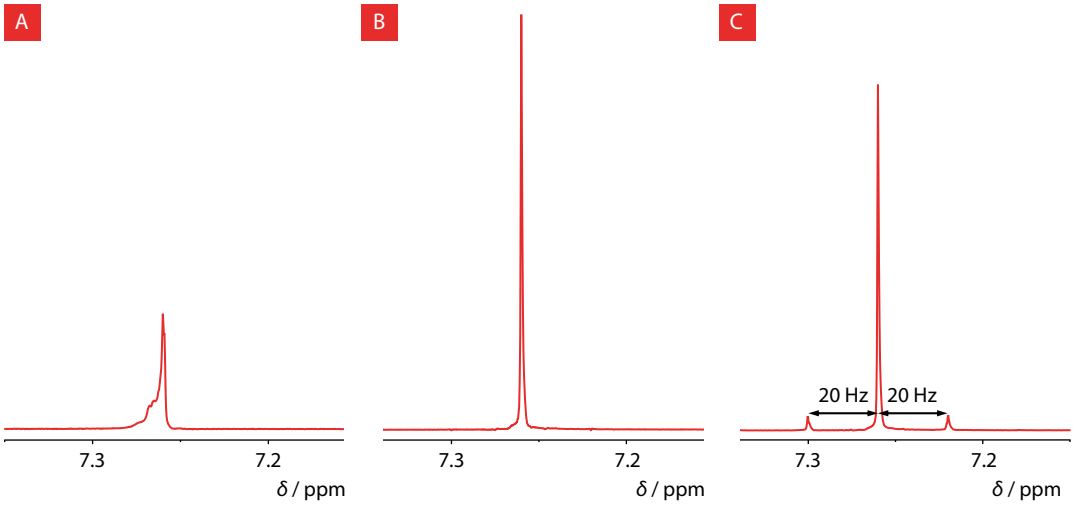

Fig. 10.9: The ^{1}H NMR spectrum of chloroform measured with poor magnetic-field homogeneity (**A**), good magnetic-field homogeneity (**B**), and good *z*-axis-field homogeneity but poor *xy*-plane homogeneity (**C**). In spectrum C, it is possible to see rotational sidebands, separated from the central line by 20 Hz, as the sample was rotating along the *z*-axis with this frequency during the measurement.

possible to measure spectra over a wide range of temperatures, for example from −150°C to +150°C. Although the temperature of the flowing air is measured by a sensor near the sample, the actual sample temperature in the tube may differ slightly from the measured temperature. If precise sample temperature is needed (e.g. when measuring reaction kinetics), this temperature must be calibrated. For low temperatures, calibration is performed using methanol, measured just before or after the experiment. Methanol has two signals in the ^{1}H spectrum (OH and CH_3), and the chemical shifts of these signals change with temperature (especially the OH signal, because higher temperatures result in the weakening of intermolecular hydrogen bonds). From the difference in the chemical shifts of these two signals, it is possible to calculate the exact temperature of the methanol sample. For higher temperatures, calibration can be done using ethylene glycol, which also has two signals in its ^{1}H spectrum, whose positions depend on temperature.

10.3 Experiment Parameters

The outcome of an NMR experiment can be influenced by several parameters. Some of these, such as the power and duration of the 90° pulse, are regularly calibrated by the NMR spectrometer manager and do not need to be optimized for routine measurements. This text discusses only the parameters related to the observed range of resonance frequencies and the resolution of signals in the resulting spectrum.

The range of resonance frequencies that can be observed in an NMR spectrum is called the **spectral window** or spectral width. Typically, the center of the spectrum and the spectral width are chosen. For example, when measuring ^{1}H spectra, we can choose a spectrum center at 7 ppm and a spectral window of 16 ppm. This ensures that the resulting spectrum includes all signals in the range from −1 ppm to 15 ppm. This spectral window is sufficient for most organic compounds. However, if the measured molecule contains a very strong intramolecular hydrogen bond, the chemical shift of the hydrogen involved in this bond may be as high as 20 ppm, which means that its signal would not appear in the spectrum with the previously mentioned spectral window. In

some types of experiments, signals outside the spectral window may "fold" into the spectral window used. The signal is then visible in the spectrum, but its chemical shift does not correspond to the actual chemical shift of the atom.

The spectral-window range, $\Delta\nu$, indicates the difference between the highest and lowest frequency in the spectrum. On NMR spectrometers, it is referred to as SW ("spectral width" or "sweep width"). If a 500-MHz spectrometer measures a ^{1}H NMR spectrum with a spectral width of 16 ppm, it is easy to calculate that $\Delta\nu = 16 \times 500$ Hz = 8,000 Hz.

The FID signal is recorded digitally as a series of points separated by a certain time interval. Mathematically, it can be shown that to record all the frequencies of a given spectral window, we must sample at least $2 \times \Delta\nu$ points per second. The total time over which we measure the FID is called the **acquisition time**, t_A (on NMR spectrometers sometimes denoted as AT). The number of digitally sampled points is given by $N = 2\,\Delta\nu \times t_A$.

The digital-resolution parameter, $\Delta\nu_{DR}$ (or simply DR), measured in Hz, indicates how much of the spectral range corresponds to one point in the FID. The lower its value, the higher the density of spectral points, and thus the better the signal resolution. The digital resolution can be calculated using the formula $\Delta\nu_{DR} = 2\,\Delta\nu\,/\,N$, which, after substitution, becomes $\Delta\nu_{DR} = 1\,/\,t_A$. From the last formula, it follows that the spectrum is better resolved the longer the acquisition time. However, it is pointless to prolong the acquisition time beyond the point where all signals have relaxed. In other words, it makes no sense to record the FID if it contains only noise.

10.4 NMR-Data Processing

NMR-data processing refers to all the manipulations performed on the FID signal, including Fourier transform, phase and baseline correction, referencing, peak picking, integration, and the visualization of the resulting spectrum.

A common procedure for improving the quality of the final spectrum is FID multiplication by a weighting function, also known as **apodization**. As mentioned in **Section 2.5**, the width of the signals in the spectrum is related to the rate of decay of the FID signal, which is tied to the relaxation time T_2. The faster the FID diminishes, the broader the signals in the spectrum. If it is desirable to narrow the signals in the spectrum, for instance, to read small coupling constants, the FID can be multiplied by a weighting function that gives more weight to the end of the signal, resulting in a slower FID decrease (**Fig. 10.10B**). This manipulation narrows the signals in the spectrum but worsens the signal-to-noise ratio (SNR) because more weight is given to the part of the FID with more noise and less signal. This approach is most commonly used in ^{1}H NMR because hydrogen nuclei (^{1}H) are very sensitive in NMR measurements and the deterioration of the SNR is usually not a significant issue. Moreover, the information contained in ^{1}H,^{1}H coupling constants is crucial for structural analysis, making it desirable to extract as many coupling constants as possible from the spectrum.

In contrast, ^{13}C nuclei are much less sensitive than ^{1}H nuclei, so it is generally undesirable to narrow their signals at the expense of the SNR. Furthermore, in the spectra of small to medium-sized organic molecules, the signals of non-equivalent carbons are often well-separated singlets (due to the broadband decoupling of hydrogen), which do not need to be narrowed using the aforementioned manipulation. Instead, it is usually advantageous to improve the SNR—even at the cost of signal broadening. For this purpose, the ^{13}C FID is multiplied by an exponential function (**Fig. 10.10C**), which gives more weight to the beginning of the FID, where there is more signal and less noise. This accelerates the FID decrease and broadens the signals in the spectrum.

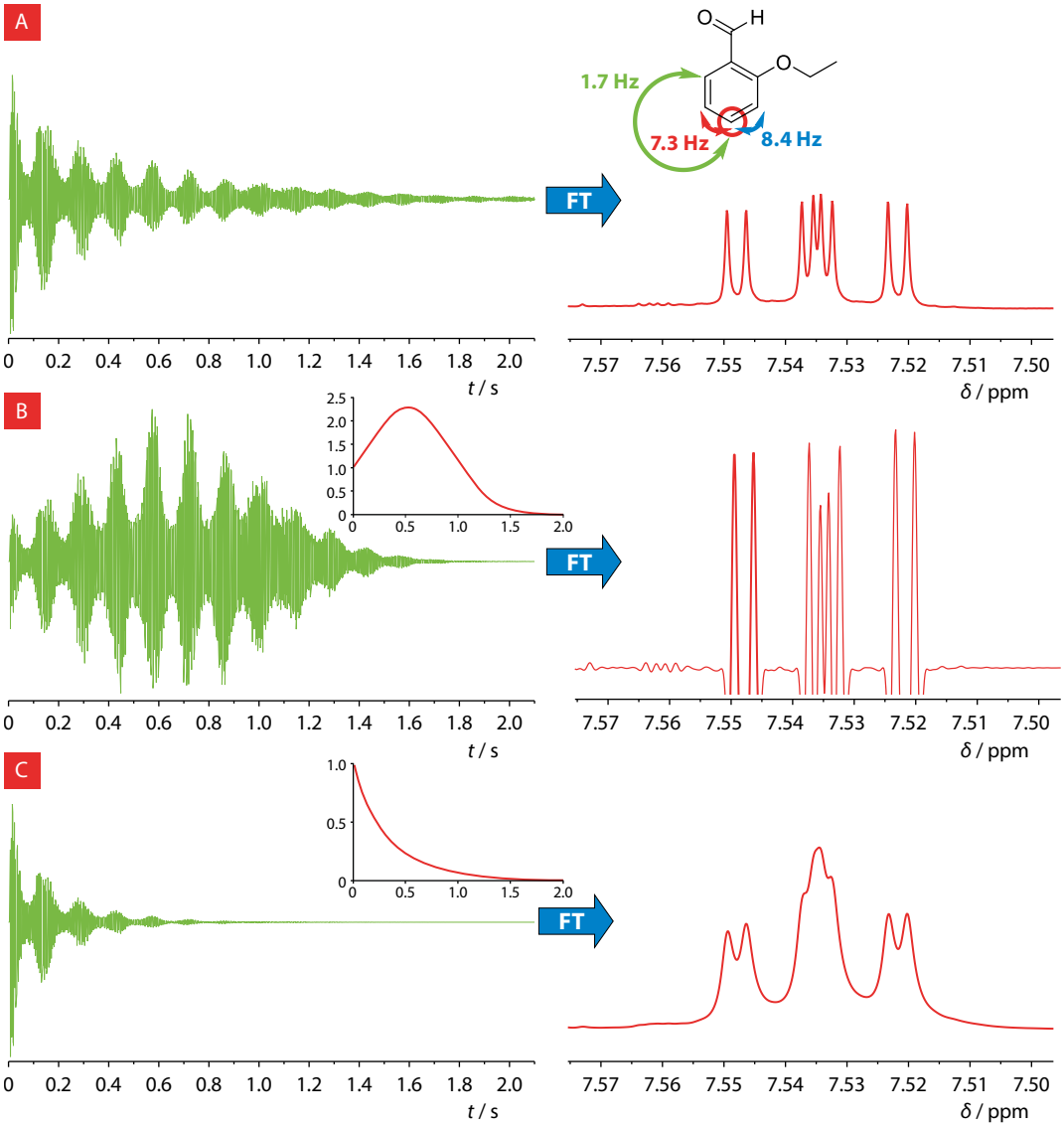

Fig. 10.10: (**A**) ^{1}H FID recording of 2-ethoxybenzaldehyde and the signal of the hydrogen H4 in the resulting spectrum
(**B**) The same FID and signal after the application of a weighting function to narrow the signals
(**C**) The same FID and signal after the application of an exponential weighting function to improve the SNR and broaden the signals. The weighting functions used are shown in the inset.

Another important parameter that affects the appearance of the spectrum is the **number of points in the spectrum**. This number can be lower than the number of sampled FID points, but this leads to a loss of spectral resolution. Conversely, the number of points can be higher than the number of FID points, which results in a visual improvement in the spectrum because the spectral points are closer to each other, making the signals appear smoother. Increasing the number of points in the spectrum is also called **zero-filling** because this process is analogous to the extension of the measured FID with additional points that have a value of zero. As mentioned earlier, **digital resolution** improves (i.e. the DR value decreases) with longer acquisition times.

Zero-filling mathematically extends the FID, reducing the distance between individual points in the spectrum. However, it is important to note that zero-filling only enhances the visual quality of the spectrum (**Fig. 10.11**). If the number of actually measured FID points is insufficient, zero-filling alone cannot achieve better signal resolution in the final spectrum.

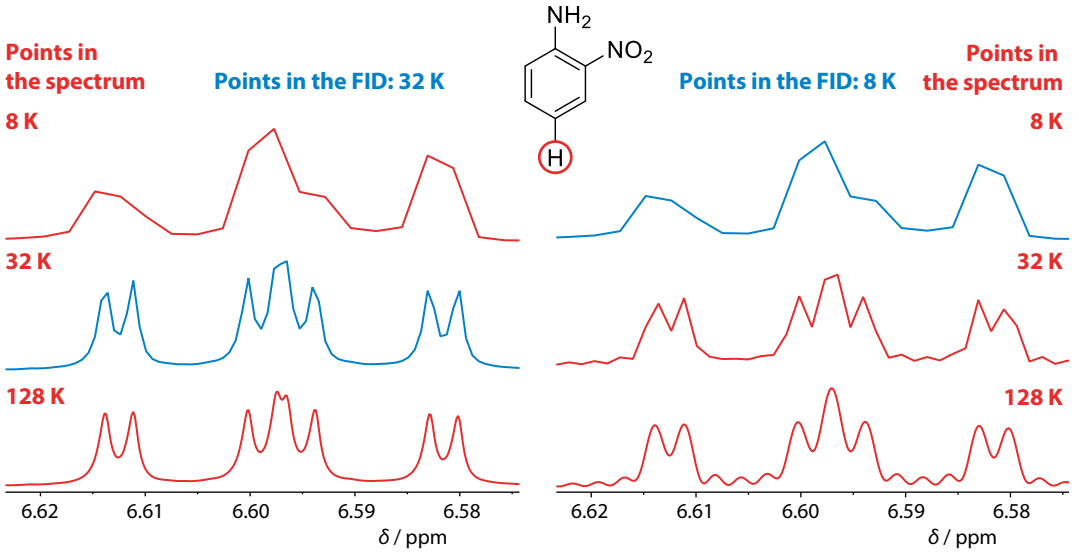

Fig. 10.11: The signal of the hydrogen H4 from 2-nitroaniline in the ^{1}H NMR spectrum. The experimental FID is identical in each column (left N = 32,768 points = 32 K points, right N = 8,192 points = 8 K points). The spectra differ in the number of spectral points (the number of points is given for the entire spectrum, not only for the displayed section). The total spectrum width is 10,000 Hz.

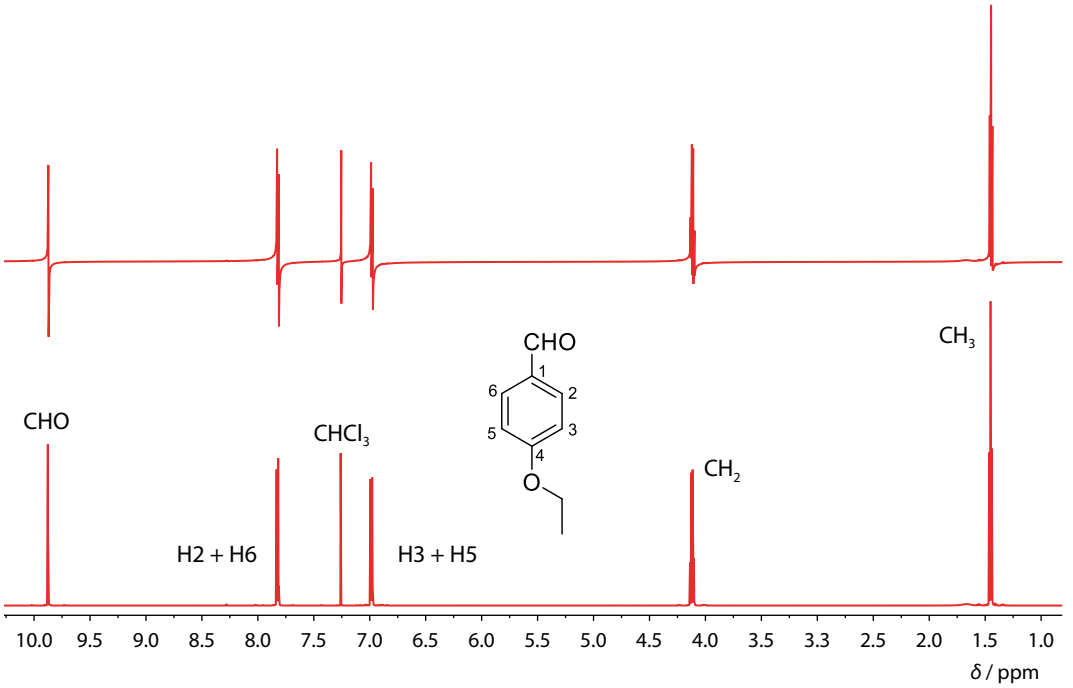

Fig. 10.12: An example of the ^{1}H NMR spectrum of 4-ethoxybenzaldehyde with incorrect (top) and correct (bottom) phase

Before interpreting and potentially presenting the NMR spectrum, it is usually necessary to perform several additional procedures, which can often be done automatically using data-processing software. One of these procedures is **phase correction**. Various factors related to the properties of the NMR spectrometer and the specific experiment can lead to incorrect phasing of the spectrum, where signals do not have the expected absorptive shape (**Fig. 10.12**). Phase correction results in a spectrum with absorption-shaped signals. It is also often necessary to perform **baseline correction**. Another step is the assignment of a chemical-shift value to a chosen standard (for example, the assignment of 0 ppm to the signal of tetramethylsilane) or to the solvent signal, a process known in practice as **referencing**. Some spectra (typically one-dimensional ^{1}H spectra) can also be integrated, which means that it is possible to determine the relative amounts of different non-equivalent atoms in the sample. Furthermore, the chemical-shift values or frequencies (in Hz) can be added to selected signals (peak picking).

Scientific journals often require that ^{1}H and ^{13}C NMR spectra be presented for all newly synthesized compounds as proof of their identity and purity. Moreover, it is customary to describe the measured NMR spectra in the experimental section of scientific publications to facilitate the verification of the compound's structure when reproducing synthetic experiments. The format for describing NMR spectra is determined by the conventions of the specific journal. As an example, here is a description format used in journals published by the American Chemical Society:

2-Nitroanilin. ^{1}H NMR (DMSO-d_6, 500.0 MHz): 7.94 (1H, dd, $J_{3,4}$ = 8.7, $J_{3,5}$ = 1.6, H3), 7.41 (2H, bs, NH_2), 7.37 (1H, ddd, $J_{5,6}$ = 8.5, $J_{5,4}$ = 6.8, $J_{5,3}$ = 1.6, H5), 7.01 (1H, dd, $J_{6,5}$ = 8.5, $J_{6,4}$ = 1.3, H6), 6.60 (1H, ddd, $J_{4,3}$ = 8.7, $J_{4,5}$ = 6.8, $J_{4,6}$ = 1.3, H4); ^{13}C NMR (DMSO-d_6, 125.7 MHz): 146.4 (C1), 135.9 (C5), 130.5 (C2), 125.6 (C3), 119.4 (C6), 115.7 (C4).

11

DYNAMIC PROCESSES

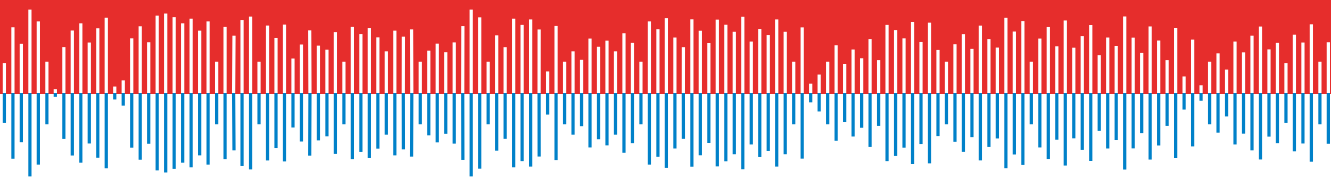

Chapter content

A possible change in the chemical environment of the observed nuclei during the NMR measurement can significantly affect the resulting spectra. Changes in the chemical environment may occur during chemical reactions, which alter the constitution of the molecule, but also during the changes of conformation, configuration, protonation/deprotonation or tautomeric form. In terms of their impact on NMR spectra, it is useful to distinguish between irreversible changes (e.g. irreversible chemical reactions) and equilibrium processes (often referred to as chemical exchange).

11.1 Chemical Reactions

When an irreversible chemical reaction occurs in the sample tube, its progress can be monitored by repeated NMR measurements. At the beginning of the reaction, the spectrum is dominated by signals from the starting material; their intensity gradually decreases, whereas the intensity of signals from the products (or intermediates) increases. The most suitable spectra for monitoring chemical reactions are hydrogen spectra because ^{1}H nuclei are the most sensitive in NMR measurements. If the concentrations of the components of the reaction mixture are not significantly lower than the typical concentrations for NMR measurements, a hydrogen experiment can be completed within a few seconds. The experiment can also be repeated quickly, enabling the monitoring of relatively fast reactions. Commonly measured hydrogen spectra can be quantified using signal integration; from these data, it is possible to obtain kinetic parameters of the reaction.

An example of an irreversible chemical reaction monitored using ^{1}H NMR spectra is shown in **Fig. 11.1**. This is the isomerization of a derivative of bicyclohexadiene (Dewar benzene), a constitutional isomer of benzene that has significant internal strain due to the fusion of two cyclobutene rings. Dewar benzene can spontaneously isomerize into benzene via a conrotatory mechanism. Because of the high energy barrier for this isomerization, Dewar benzene is surprisingly stable at room temperature. The progress of this reaction has thus been monitored at a temperature of 145°C.

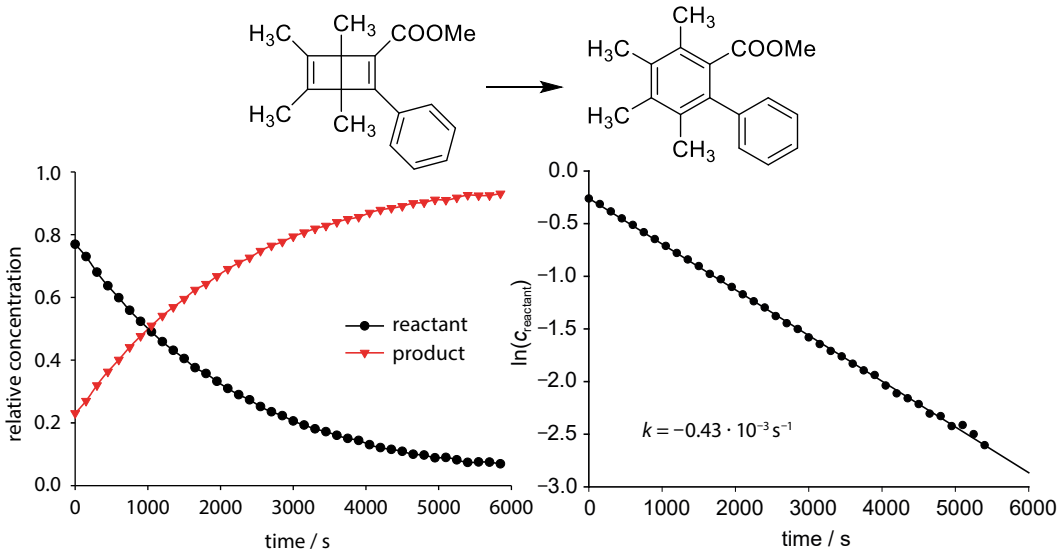

Fig. 11.1: The progress of Dewar benzene isomerization into benzene monitored using ^{1}H NMR spectra. The integration of the signals from the starting material and from the product enables the quantification of the concentrations of reaction-mixture components. The linear time dependence of the logarithm of the reactant concentration confirms that this is a first-order reaction, and the slope of this dependence is the reaction rate constant *k*.

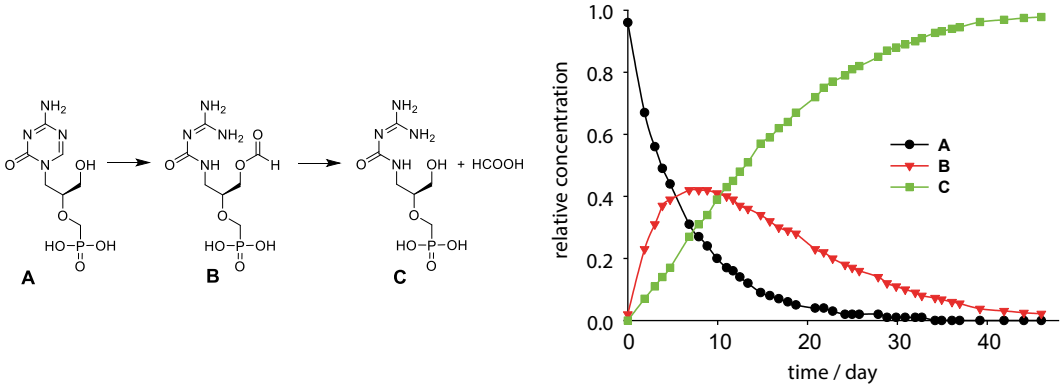

Fig. 11.2: The progress of the decomposition of an azacytosine derivative A monitored using ^{1}H NMR spectra

Another example of an irreversible chemical reaction is shown in **Fig. 11.2**. This involves the decomposition of an azacytosine derivative **A**, which first forms an intermediate **B**, further hydrolyzing into the final product **C**. The integration of hydrogen spectra again allows for the quantification of these reactions, enabling the determination of the rate constants for both processes.

An advantage of monitoring reaction kinetics using NMR spectroscopy is that spectra can be measured over a wide temperature range. From the temperature dependence of the rate constants, it is possible to determine activation enthalpy and entropy using the Eyring equation. If the molecules monitored contain fluorine or phosphorus, these nuclei can also be used to monitor the progress of chemical reactions, because ^{19}F and ^{31}P nuclei are highly sensitive. Additionally, molecules typically contain only a few fluorine or phosphorus atoms, which usually leads to clear NMR spectra with little signal overlap.

11.2 Chemical Exchange

Chemical exchange is an equilibrium process that occurs during an NMR experiment. It can be an equilibrium chemical reaction or any other equilibrium process that leads to changes in the chemical environment of the observed nuclei.

A typical example of chemical exchange is hindered rotation around the C–N bond in amides. The order of this bond is usually higher than one, which can be explained by the presence of a mesomeric form of the amide bond (**Fig. 11.3**). The partial double bond between carbon and nitrogen leads to a higher energy barrier for rotation around this bond. At low temperatures, rotation around this bond is slow; in the case of *N*,*N*-dimethylformamide, shown in **Fig. 11.3**, we observe two non-equivalent methyl groups in the NMR spectra (the red CH_3 group is in the *cis* position relative to the oxygen, while the blue is in the *trans* position, which means that they have different chemical environments and are not chemically equivalent). At higher temperatures, the rate of rotation around the C–N bond increases, leading to an averaging of the shielding of both methyl groups, which then appear as equivalent in the NMR spectra—producing a single signal.

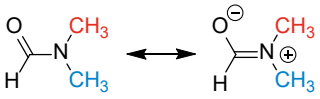

Fig. 11.3: Possible mesomeric structures of *N*,*N*-dimethylformamide

The appearance of an NMR spectrum of a substance with chemical exchange depends not only on the rate of the exchange process, which is determined by the energy barrier and temperature, but also on the resonance frequency of individual signals. An example of such spectra, which could be recorded on a 500-MHz spectrometer, is shown in **Fig. 11.4**. The spectra were simulated for a substance undergoing chemical exchange of hydrogens with chemical shifts of 1.00 and 1.05 ppm. On a 500-MHz spectrometer, the difference in resonance frequencies between these signals is $\Delta\nu = 0.05 \cdot 500 = 25$ Hz. If the exchange rate were zero (for example at very low temperature), there would be two sharp signals, namely at 1.00 and 1.05 ppm. At a higher temperature, when the exchange rate increases, both signals broaden. At a certain exchange rate, the two signals merge into one, which is a phenomenon known as **coalescence**, and the temperature at which this occurs is called the coalescence temperature T_C (in **Fig. 11.4**, this happens at an exchange rate of approximately $k = 50\ s^{-1}$). As the exchange rate increases further (with increasing temperature), the newly formed signal narrows, until, at very high exchange rates, we observe one sharp signal.

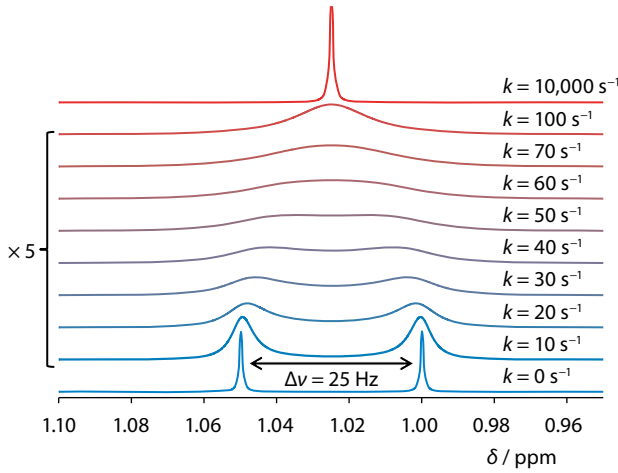

Fig. 11.4: Simulated ^{1}H NMR spectra of a substance with chemical exchange between two signals separated by 25 Hz in the slow-exchange regime. The operating frequency of the spectrometer is 500 MHz. The intensity of the marked spectra has been increased fivefold to make the signals clearly visible.

If the exchange rate were the same but the difference in resonance frequencies were different from 25 Hz, the resulting spectra would look different. **Fig. 11.5** shows the spectra of a substance with chemical exchange between two hydrogens, whose difference in resonance frequencies is 15 Hz. In this case, it is evident that coalescence occurs earlier—at an exchange rate of approximately $k = 30\ s^{-1}$. Conversely, if the difference in resonance frequencies were larger, coalescence would occur at a higher exchange rate (**Fig. 11.6** depicts spectra with a 50-Hz difference in resonance frequencies between signals). This figure also shows that the signals near coalescence can be very broad. This can be particularly problematic in carbon spectra, where very broad (and thus low) signals can easily be lost in the noise. The fact that the coalescence of signals with a larger difference in resonance frequencies occurs at higher exchange rates is also the reason why coalescence occurs at a higher temperature on a spectrometer with a higher operating frequency than on one with a lower frequency. The difference in resonance frequencies depends on the operating frequency of the spectrometer. For instance, if we measured the exchange process shown in **Fig. 11.4** on a spectrometer with double the operating frequency, the difference in resonance frequencies would also double (0.05 ppm · 1000 MHz = 50 Hz), and coalescence would thus occur only at exchange rates higher than $100\ s^{-1}$ (**Fig. 11.6**).

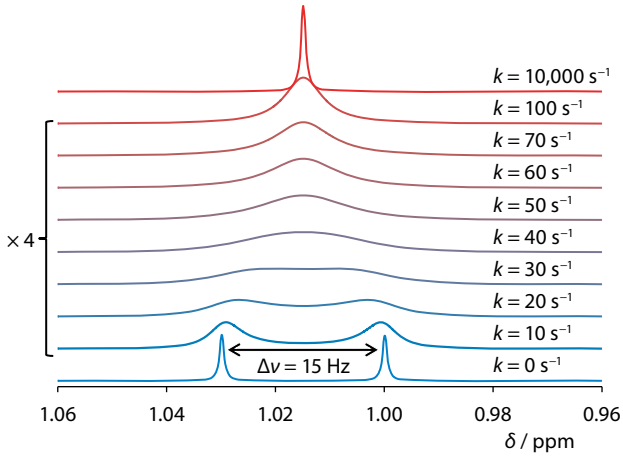

Fig. 11.5: Simulated ^{1}H NMR spectra of a substance with chemical exchange between two signals separated by 15 Hz in the slow-exchange regime. The operating frequency of the spectrometer is 500 MHz. The intensity of the marked spectra has been increased fourfold to make the signals clearly visible.

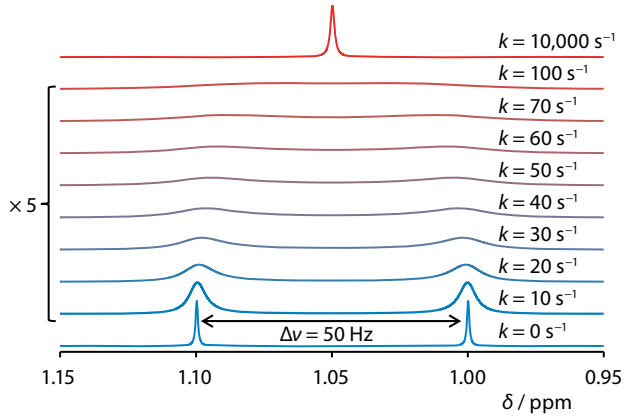

Fig. 11.6: Simulated ^{1}H NMR spectra of a substance with chemical exchange between two signals separated by 50 Hz in the slow-exchange regime. The operating frequency of the spectrometer is 500 MHz. The intensity of the marked spectra has been increased fivefold to make the signals clearly visible.

In the NMR spectra of amides with different substituents on nitrogen, depending on the rate of rotation around the C–N bond (and thus the temperature), we can observe either two sets of signals corresponding to the two rotamers around the C–N bond, broad signals near coalescence (or even the absence of certain signals in carbon spectra, as they may be below the noise level), or one set of signals corresponding to the averaged shielding of nuclei during rapid rotation. The temperature range in which we observe the broad signals near the coalescence point is often referred to as the region of intermediate exchange.

At the point of coalescence, we can estimate the chemical-exchange rate from the NMR spectra using the formula $k_C = 2.22\ \Delta\nu$, where $\Delta\nu$ is the difference in the resonance frequencies of the exchanging atoms. In the entire temperature region of intermediate exchange, it is possible to determine the exchange rate by comparing simulated spectra with experimental ones, a process known as complete lineshape analysis.

An example of experimental spectra with chemical exchange is provided in **Fig. 11.7**, showing the spectra of the dithiocarbamate at different temperatures. The N–C(S) bond has partial

double-bond character, similar to amides. The left side of **Fig. 11.7** shows the region of the CH_2 groups. At low temperatures, it is possible to see two quartets, corresponding to two non-equivalent CH_2 groups. The splitting of the signals into quartets is a result of the coupling with the neighboring CH_3 group. At higher temperatures, the signals broaden, but the solvent used ($CDCl_3$) does not allow the temperature to be increased up to the coalescence point. The right side of **Fig. 11.7** depicts the signals of the methyl groups. Each is split into a triplet as a result of coupling with the CH_2 group. However, the signals of both methyl groups have similar chemical shifts, leading to partial overlap of the two triplets. As the temperature increases, both methyl signals broaden until they coalesce. At high temperatures, we observe a single sharp triplet. Lineshape analysis makes it possible to determine the rate of rotation around the C–N bond at each temperature. Plotting the logarithm of k/T against $1/T$ (the Eyring plot, **Fig. 11.8**) enables the determination of the activation enthalpy and entropy for rotation around this bond.

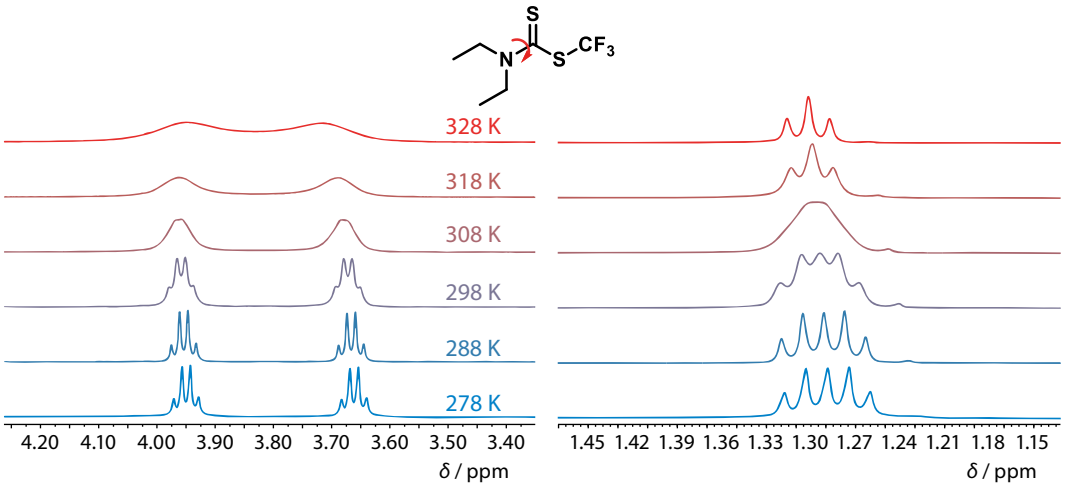

Fig. 11.7: The ^{1}H NMR spectra of the shown dithiocarbamate measured at different temperatures in $CDCl_3$

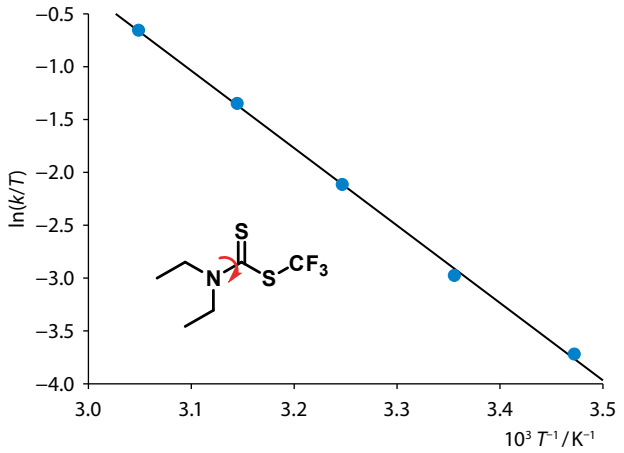

Fig. 11.8: The Eyring plot obtained from the rate constants for rotation around the C–N bond in the displayed dithiocarbamate

We can encounter chemical exchange in various processes, not only in the case of hindered rotation around a partial double bond. Another typical example is the inversion of a six-membered ring in a chair conformation. During slow inversion, the hydrogen atoms in axial and equatorial

positions are not equivalent, which means that they have distinct signals. With faster inversion, the signals of the axial and equatorial hydrogens merge. In the ^{1}H NMR spectra of cyclohexane measured at room temperature, we thus observe only a single singlet.

Another example is the inversion of configuration at nitrogen. If the nitrogen in amines has three different substituents, the nitrogen atom can act as a chiral center because the formal fourth substituent is the lone pair of electrons. However, nitrogen commonly undergoes rapid configuration inversion, leading to the loss of chirality. Hydrogens in neighboring CH_2 groups can either be diastereotopic or enantiotopic, depending on the rate of the inversion of nitrogen configuration. NMR spectra with chemical exchange can also be used to study tautomeric equilibria or valence-isomer equilibria.

11.3 NMR Titration

NMR titration is a technique used to study interactions between molecules or to monitor chemical changes, such as protonation and deprotonation. It is particularly useful for the analysis of binding interactions, reaction kinetics, and the pH-dependent behavior of molecules.

The determination of pK_A values using NMR spectroscopy takes advantage of the fact that the NMR chemical shifts of certain atoms in a molecule can change as the molecule undergoes protonation or deprotonation. By systematically varying the pH of the sample and observing the shifts in NMR signals, it is possible to track the extent of protonation at different pH levels and calculate the pK_A, i.e. the pH at which half of the molecules are protonated and half are deprotonated. Close to the pK_A value of the protonation/deprotonation reaction, the protonated and deprotonated forms of the studied compounds usually interconvert rapidly and average chemical shifts can be observed.

For example isocytosine, a structural isomer of the natural nucleobase cytosine, exists at low pH as a cation, is a neutral molecule in an intermediate pH range, and becomes deprotonated at high pH values (**Fig. 11.9A**). Furthermore, neutral isocytosine can exist in two tautomeric forms, which interconvert rapidly. The pK_A values of the acido–basic reactions can be determined by NMR titrations. The dependence of chemical shifts on the pH (**Fig. 11.9B**) reveals the pH regions of protonated, neutral and deprotonated isocytosine, which makes it easy to determine pK_A values.

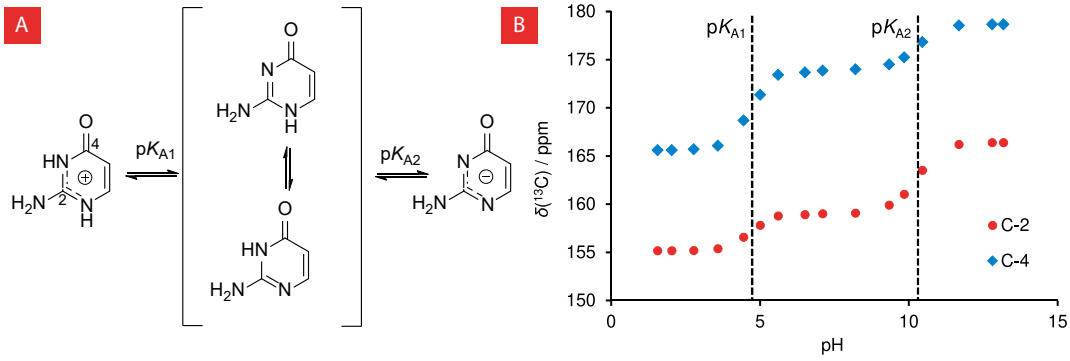

Fig. 11.9: A) The protonation/deprotonation and tautomeric equilibria of isocytosine and **B)** the pH dependence of C2- and C4-carbon chemical shifts of isocytosine

12

OTHER COMMONLY MEASURED NUCLEI (^{19}F, ^{31}P, ^{15}N, ^{2}H)

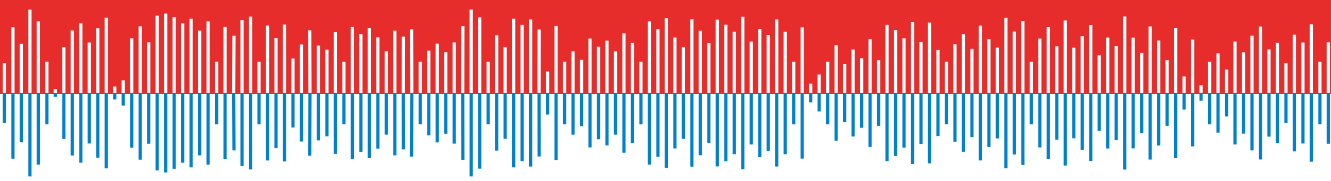

Chapter content

This chapter discusses other nuclei that are commonly found in organic molecules and whose NMR spectra are frequently measured, such as fluorine, phosphorus and nitrogen. Additionally, the chapter covers deuterium, which is indirectly significant for NMR spectroscopy (as part of solvents), although its NMR spectra are rarely measured due to its low sensitivity. Organic compounds may also contain several other elements, most commonly oxygen, sulfur, chlorine, bromine and iodine. Unfortunately, none of these elements has an isotope with a spin quantum number $I = ½$, which makes it practically impossible to measure their high-resolution NMR spectra.

12.1 Fluorine

Fluorine naturally consists of 100% of the isotope ^{19}F, which has a spin quantum number of ½ and a high gyromagnetic ratio (γ), close to that of ^{1}H-hydrogen nuclei (on a 500-MHz spectrometer, the resonance frequency of ^{19}F is approximately 470 MHz). These properties enable high sensitivity in fluorine NMR experiments. Additionally, fluorine chemical shifts cover a broad range of several hundred ppm. $CFCl_3$ is used as a standard with a chemical shift $\delta = 0$. Fluorine chemical shifts in organic molecules are typically found in the range from 0 to −300 ppm (**Fig. 12.1**). Due to this wide range, individual signals from non-equivalent fluorine atoms in spectra are usually well-separated and can be interpreted quite easily.

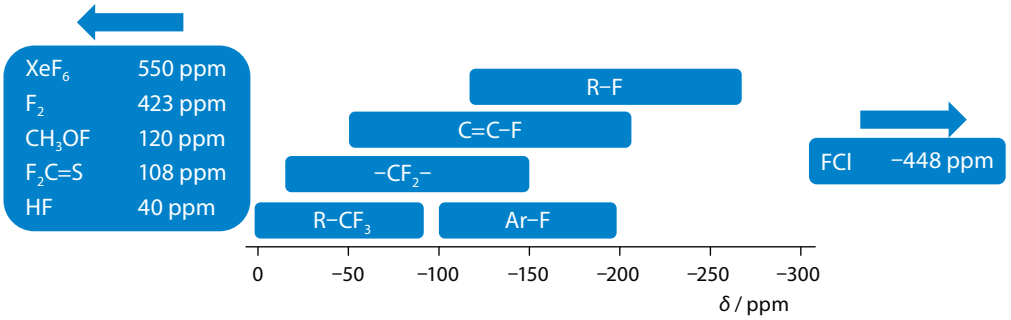

Fig. 12.1: Typical chemical-shift ranges for ^{19}F nuclei

Since all fluorine nuclei are magnetically active, fluorine spectra show mutual indirect spin–spin interactions between non-equivalent fluorine nuclei. The magnitude of these interactions depends not only on the number of bonds between the nuclei but also on their spatial proximity. When two fluorine atoms are close in space, it is often possible to observe an unusually large indirect spin–spin coupling between them, even if they are formally separated by a greater number of covalent bonds. These interactions are called "**through-space**" couplings. Nevertheless, it is important to remember that indirect spin–spin interactions are mediated by electrons, which means that they are not a direct interaction between the nuclear magnetic moments. The "through-space" couplings have been explained by interactions mediated by overlapping fluorine lone electron pairs. Selected typical values of indirect spin–spin coupling constants are shown in **Fig. 12.2**.

In fluorine and hydrogen spectra, it is also possible to observe couplings between ^{1}H and ^{19}F. Their magnitude again depends on both the number of bonds between the interacting atoms and their spatial proximity. For vicinal-coupling constants (^{3}J), there is a similar dependence on torsion angles as for interacting hydrogens (the Karplus curve, **Section 4.8.2**), but the absolute magnitude of the couplings between ^{1}H and ^{19}F is larger than in the case of interacting hydro-

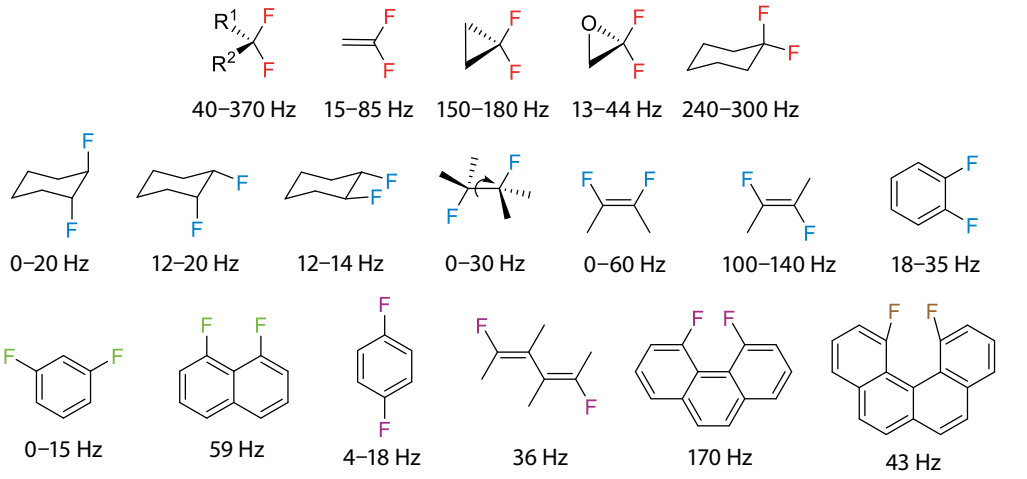

Fig. 12.2: Typical values of indirect spin–spin couplings between fluorine nuclei over two (^2J), three (^3J), four (^4J), five (^5J) and six (^6J) bonds. The figure shows the absolute values of coupling constants.

gens. Typical values of the indirect spin–spin coupling constants between fluorine and hydrogen nuclei for selected structural motifs are shown in **Fig. 12.3**.

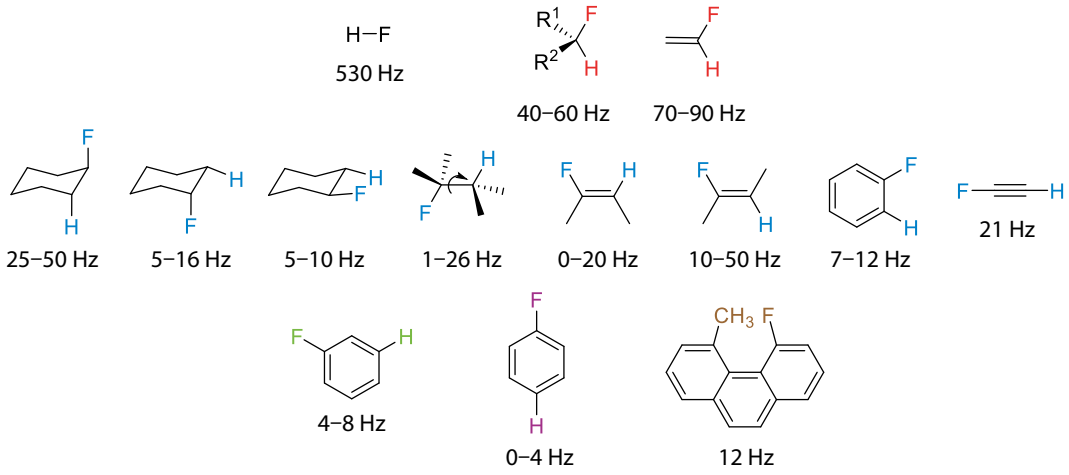

Fig. 12.3: Typical values of the indirect spin–spin coupling constants between fluorine and hydrogen nuclei over one (^1J), two (^2J), three (^3J), four (^4J), five (^5J) and six (^6J) bonds. The figure shows the absolute values of the coupling constants.

In carbon spectra, it is also possible to observe signal splitting caused by $^{13}C,^{19}F$ couplings. The magnitude of these couplings over one bond ranges from 150 to 380 Hz, over two bonds from 10 to 100 Hz, and over three bonds from 1 to 25 Hz. In fluorine spectra, couplings with carbon nuclei are observed only as ^{13}C satellites (**Section 2.6**) due to the low natural abundance of the ^{13}C isotope.

Figures 12.4 through **12.7** show the spectra of 2,2,2-trifluoroethanol measured for ^1H, ^{19}F and ^{13}C. When measuring the hydrogen spectrum using the simplest pulse sequence containing only one excitation pulse, the resulting spectrum shows couplings between the hydrogen and fluorine atoms. These couplings can be suppressed by decoupling the ^{19}F nuclei (**Fig. 12.4**). However, not all NMR probes allow for the detection of hydrogen nuclei with simultaneous decoupling of fluo-

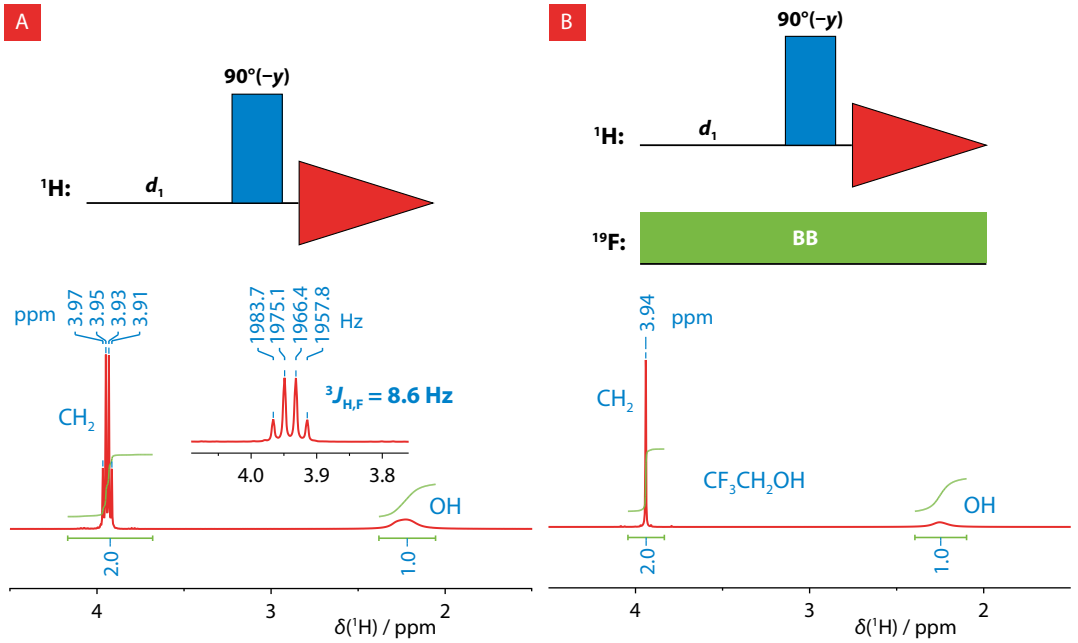

Fig. 12.4: The pulse sequence and hydrogen spectra of 2,2,2-trifluoroethanol measured without decoupling (**A**) and with ^{19}F decoupling (**B**)

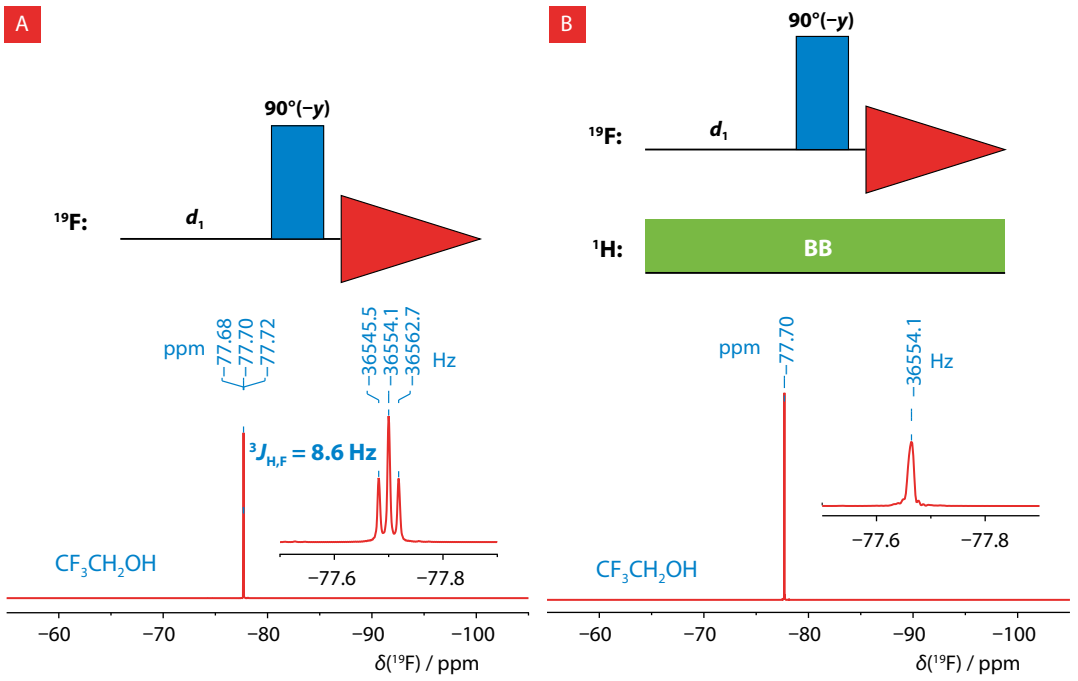

Fig. 12.5: The pulse sequence and ^{19}F spectra of 2,2,2-trifluoroethanol measured without decoupling (**A**) and with ^{1}H decoupling (**B**)

rine due to the close resonance frequencies of both nuclei. In common probes, the excitation and detection of both nuclei are performed using the same coil, which can be tuned either to ^{1}H or ^{19}F frequency, excluding the possibility of simultaneous irradiation of both nuclei. In fluorine spectra measured without decoupling, it is possible to observe the same ^{1}H,^{19}F couplings as in hydrogen spectra; these interactions can again be suppressed by hydrogen decoupling (**Fig. 12.5**).

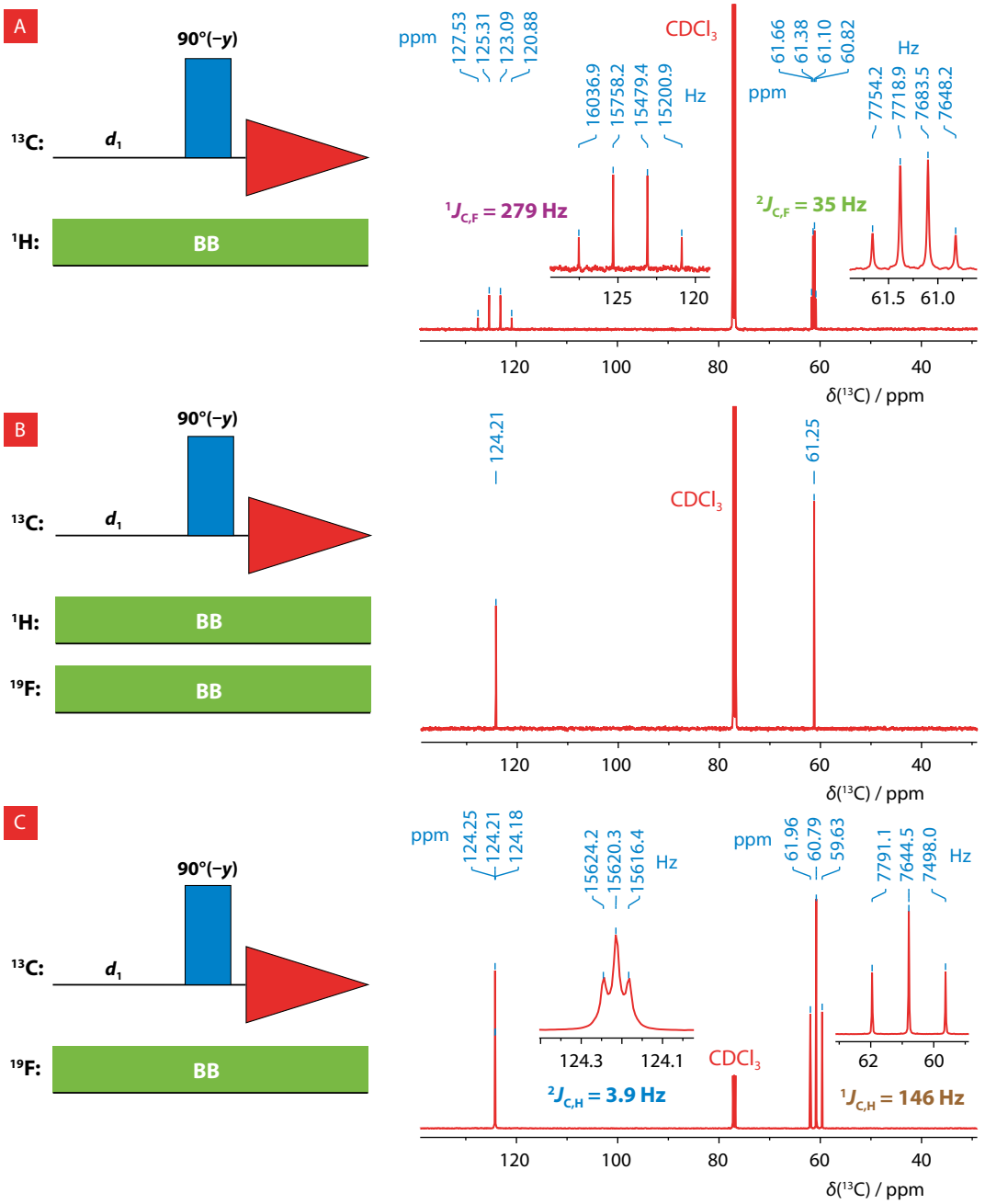

Fig. 12.6: The pulse sequence and ^{13}C spectra of 2,2,2-trifluoroethanol measured with ^{1}H decoupling (**A**), with ^{1}H and ^{19}F decoupling (**B**), and with only ^{19}F decoupling (**C**)

Carbon spectra are commonly measured with hydrogen decoupling. In such spectra, the splitting is caused by interactions with ^{19}F nuclei (**Fig. 12.6A**). If carbon spectra are measured with the simultaneous decoupling of ^{1}H and ^{19}F, there is no signal splitting (**Fig. 12.6B**). However, such an experiment requires a special probe that enables simultaneous manipulation of hydrogen and fluorine spin states. In special cases, it may be of interest to measure the carbon spectra with the decoupling of only ^{19}F nuclei. In such spectra, there are couplings between ^{13}C and ^{1}H (**Fig. 12.6C**), but the coupling with ^{19}F has been removed. For completeness, **Fig. 12.7** also shows a ^{13}C spectrum of 2,2,2-trifluoroethanol measured without decoupling. In this spectrum, the signal splitting is caused by the interactions of ^{13}C with ^{1}H and ^{19}F. The CF_3 carbon signal is split into a quartet of triplets, whereas the CH_2 carbon signal is split into a triplet of quartets.

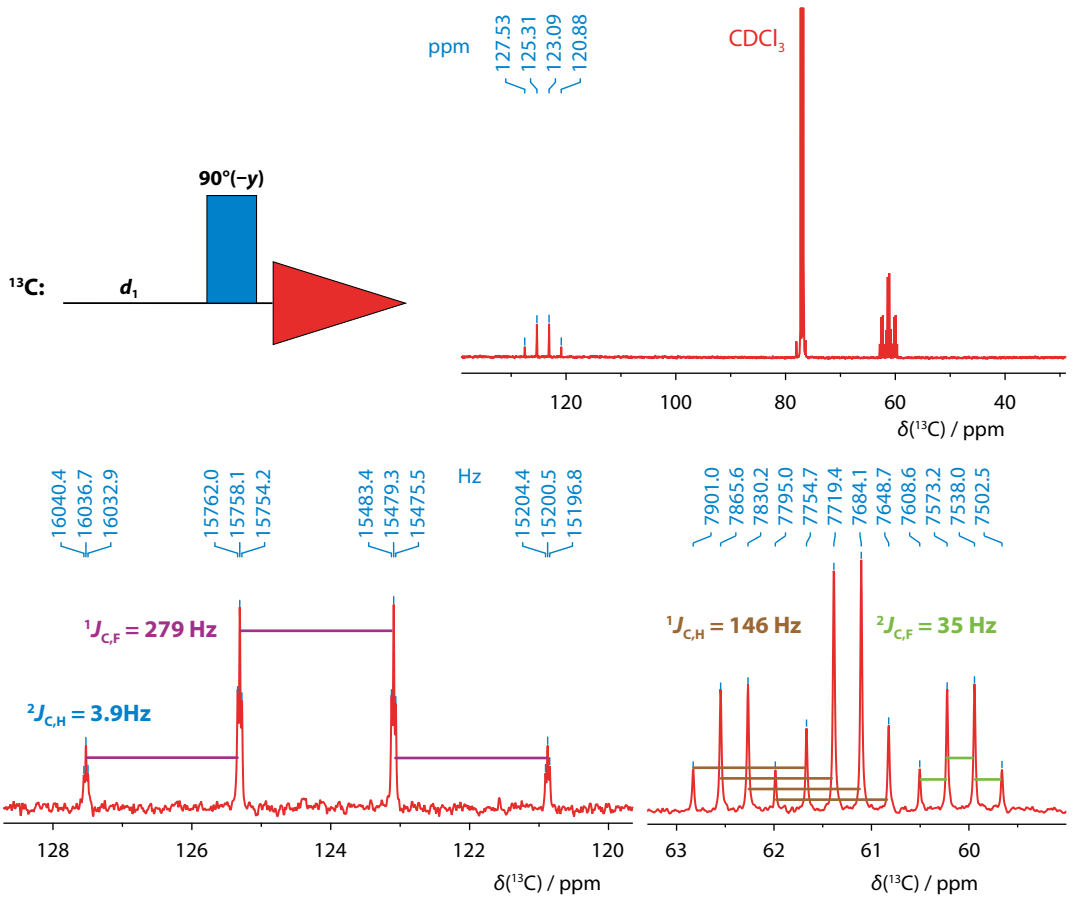

Fig. 12.7: The pulse sequence and ^{13}C spectrum of 2,2,2-trifluoroethanol measured without decoupling

12.2 Phosphorus

Phosphorus has 100% natural abundance of the isotope ^{31}P, which has a nuclear-spin quantum number $I = ½$ and a relatively high gyromagnetic ratio. In terms of NMR spectroscopy, phosphorus nuclei are thus suitable for high-resolution spectrum measurements, whose sensitivity is high. The resonance frequency of ^{31}P nuclei on a 500-MHz spectrometer is approximately 202 MHz.

The chemical shifts of phosphorus occur in a very broad range exceeding 1,000 ppm. Phosphorus spectra are referenced against 85% phosphoric acid, used as an external standard. The chemical shift of phosphorus in compounds depends on its oxidation state and coordination number. Typical ranges of chemical shifts for phosphorus coordinated from single to six-fold are shown in **Fig. 12.8**.

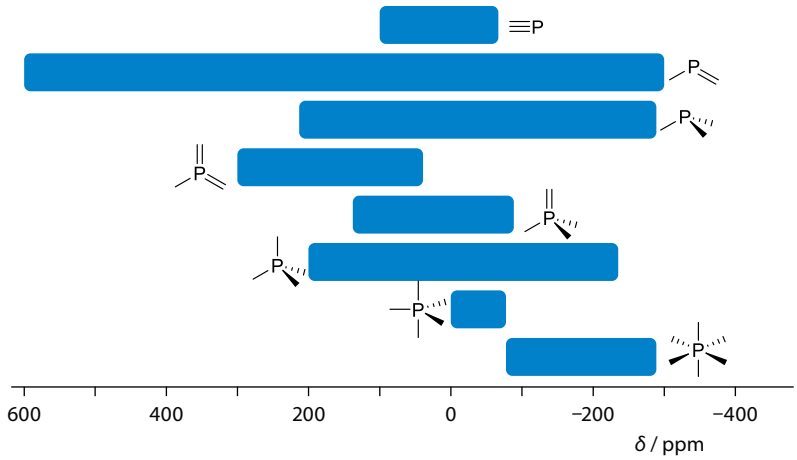

Fig. 12.8: Typical ranges of the chemical shifts of ^{31}P nuclei

The magnitudes of $^{31}P,^{31}P$ indirect spin–spin coupling constants also span a wide range of values (from zero to several thousand Hz) and primarily depend on the number of bonds between the coupled atoms, the oxidation state, and the coordination number of phosphorus. For example, **Fig. 12.9** shows the spectra of adenosine-5'-monophosphate (AMP), adenosine-5'-diphosphate (ADP), and adenosine-5'-triphosphate (ATP). Since these spectra have been measured with proton decoupling, the observed signal splitting is caused by indirect spin–spin coupling between phosphorus nuclei. The AMP spectrum shows a singlet, because the molecule contains only one phosphorus atom. In the ADP spectrum, on the other hand, we observe two doublets with a coupling

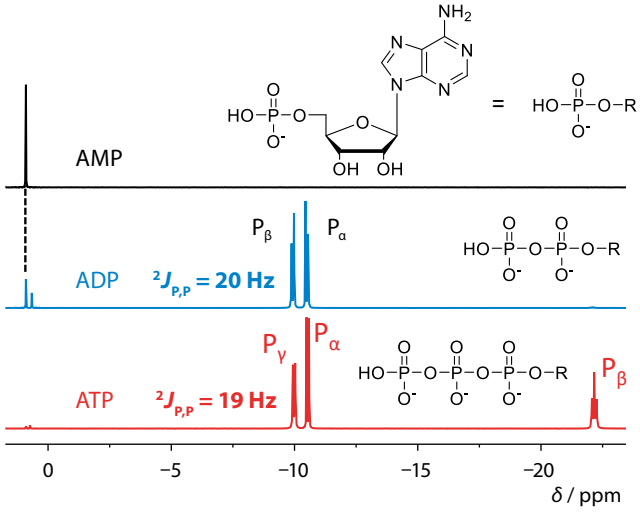

Fig. 12.9: The ^{31}P spectra of AMP, ADP and ATP, measured with proton decoupling. In the ADP sample, the terminal phosphate unit has partially hydrolyzed.

constant ^2J(P–O–P) = 20 Hz. In the ADP sample, the terminal phosphate unit has been partially hydrolyzed. The spectrum also contains signals of AMP and phosphoric acid, which have formed due to this hydrolysis. In the ATP spectrum, there are two doublets, corresponding to the terminal phosphate groups P_α and P_γ, and one triplet, corresponding to the middle phosphate group P_β.

Phosphorus–hydrogen and phosphorus–carbon couplings can also be commonly observed in the spectra of phosphorus-containing compounds. **Fig. 12.10** shows the measured coupling constants between phosphorus and hydrogen and between phosphorus and carbon in a model dinucleotide.

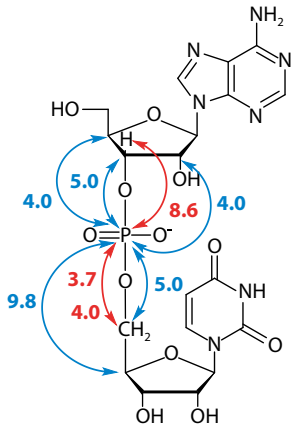

Fig. 12.10: The absolute values of the indirect spin–spin coupling constants ***J*(H,P)** and ***J*(C,P)** in the displayed dinucleotide. The magnitudes of the coupling constants across three bonds depend on the dihedral angle between the interacting atoms and can be used to determine molecular conformation.

12.3 Nitrogen

Nitrogen has two stable isotopes. The isotope ^{14}N has a spin quantum number $I = 1$; despite its high natural abundance (99.63%), it is not suitable for the measurements of high-resolution spectra, because the electric-quadrupole moment associated with ^{14}N nuclei leads to rapid relaxation of its spin states, resulting in very broad signals. The isotope ^{15}N, on the other hand, has a spin quantum number $I = ½$ and a natural abundance of only 0.37%. Unlike ^{14}N, however, the ^{15}N nuclide provides narrow signals and makes it possible to identify signals from molecules with several nonequivalent nitrogen atoms in the spectra. Unfortunately, ^{15}N also has a very low gyromagnetic ratio, with a resonance frequency approximately ten times lower than that of ^1H nuclei in the same magnetic field. As a consequence, the sensitivity of ^{15}N for NMR spectroscopy with natural isotopic abundance is about $4{\cdot}10^6$ times lower than that of ^1H. Another complication in ^{15}N measurements is that the gyromagnetic ratio of ^{15}N has the opposite sign to most other nuclei, including ^1H. This results in the nuclear Overhauser effect (NOE), induced by irradiating ^1H nuclei during ^{15}N measurements with proton decoupling, being negative for small organic compounds, which reduces signal intensities and further lowers measurement sensitivity for ^{15}N.

When measuring ^{15}N nuclei in non-enriched samples, polarization-transfer methods are most commonly used to shorten the duration of the experiment significantly. The most frequent experiments are ^1H,^{15}N-HSQC and ^1H,^{15}N-HMBC, which (like their ^{13}C counterparts) directly detect protons, whereas nitrogen chemical shifts are detected in the indirect dimension. For very con-

centrated or isotope-enriched samples, direct ^{15}N detection is possible. In such cases, the pulse sequence shown in **Fig. 12.11** is used with decoupling only during acquisition in order to collapse the multiplets caused by couplings with protons, leaving only singlets in the spectrum. During the preparation period d_1, decoupling is not used to prevent the nuclear Overhauser effect and, consequently, to avoid reduced signal intensity. For biomacromolecules, biochemical procedures for ^{15}N-enrichment based on gene expression are commonly used today, allowing the study of proteins and oligonucleotides.

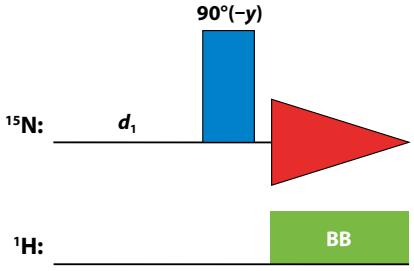

Fig. 12.11: The pulse sequence used for the direct detection of ^{15}N nuclei of small compounds

Nitrogen chemical shifts span a broad range of several hundred ppm. Various compounds (nitromethane, liquid ammonia, NH_4Cl, urea, dimethylformamide) have been used as standards for referencing nitrogen chemical shifts. Unfortunately, this leads to discrepancies in the reported chemical shifts for identical substances in the literature, which can vary by several hundred ppm. When using literature data, it is important to pay attention to the standard used and the sign convention. **Fig. 12.12** shows the nitrogen chemical-shift ranges for selected types of compounds, with all values in the figure being referenced relative to liquid ammonia. If nitromethane were used as the standard (assigned $\delta = 0$ ppm), all nitrogen shifts would be 381.7 ppm lower.

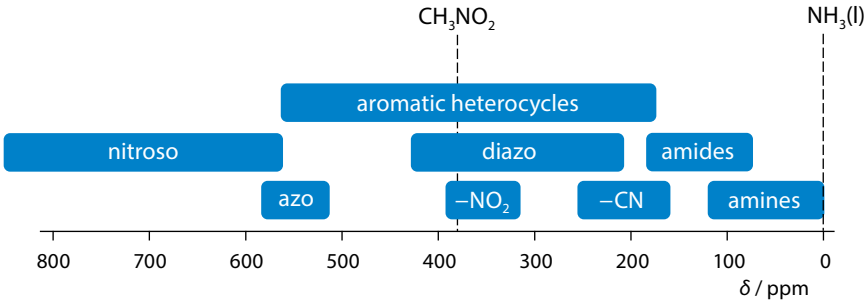

Fig. 12.12: The typical ranges of ^{15}N chemical shifts relative to liquid ammonia

Indirect spin–spin couplings between ^{15}N nuclei can only be observed in isotope-enriched samples. One-bond coupling constants, $^1J(N,N)$, have values of 2–5 Hz. The couplings between ^{15}N and ^{13}C nuclei can also only be observed in isotope-enriched samples. Typical absolute values of coupling constants are $^1J(N,C) = 0–50$ Hz, $^2J(N,C) = 0–11$ Hz, and $^3J(N,C) = 0–5$ Hz. Couplings with protons (^1H) can be observed in the ^{15}N spectra of naturally abundant samples or in both ^1H and ^{15}N spectra of isotope-enriched samples. The information about spin–spin couplings between hydrogen and nitrogen nuclei is used, for example, to determine the site of protonation or to study tautomeric equilibria. Absolute one-bond coupling constants, $^1J(N,H)$, range from 50 to 130 Hz, whereas two- and three-bond couplings are significantly lower: $^2J(N,H) = 0–16$ Hz and $^3J(N,H) = 0–7$ Hz.

Nitrogen atoms are often involved in hydrogen bonding. In NMR spectra, it is possible to observe spin–spin couplings through a hydrogen bond. An example of such interactions is shown in **Fig. 12.13** for a substituted phenylazopyrimidine containing three nitrogen atoms (circled in the figure) selectively labeled with the ^{15}N isotope. Since the depicted azopyrimidine exists in solution as a mixture of two rotamers, which slowly interconvert, the signals for each are observed separately (i.e. there is no averaging of signals due to rapid chemical exchange). In the nitrogen spectrum measured with proton decoupling, the signals of the amino-group nitrogens involved in intramolecular hydrogen bonds are observed as doublets, split by interaction with azo nitrogens through the hydrogen bond. Similarly, in proton spectra, the splitting of the signals of the amino-group protons involved in hydrogen bonding is observed due to interaction with the azo nitrogen. The letter "h" in the coupling-constant name (e.g. ^{2h}J(N,N) indicates coupling through a hydrogen bond, such as spin–spin coupling between the nitrogens involved in an N–H···N hydrogen bond.

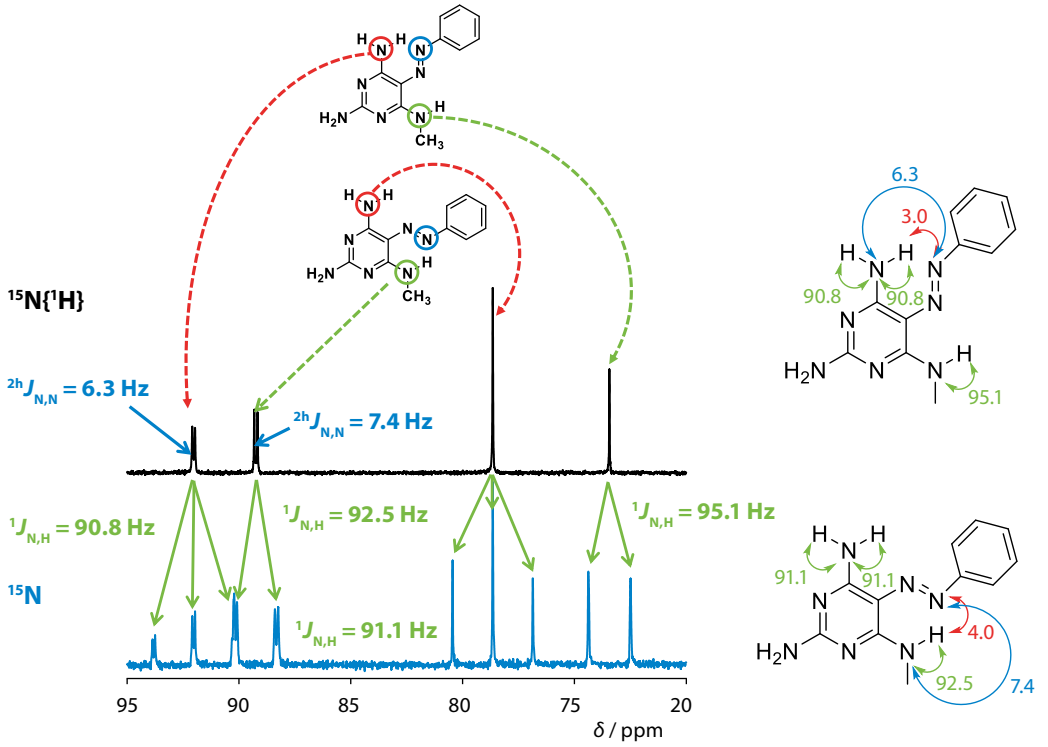

Fig. 12.13: The ^{15}N spectrum with proton decoupling (black) and without decoupling (blue) for the depicted azopyrimidine, which exists as a mixture of two rotamers. On the right: the values of ^{1}J(N,H) and couplings through the hydrogen bond (^{1h}J(N,H) and ^{2h}J(N,N))

12.4 Deuterium

Deuterium ^{2}H is an isotope of hydrogen with a low natural abundance (0.02%) and a gyromagnetic ratio approximately 6.5 times lower than that of the hydrogen ^{1}H. The resonance frequency of ^{2}H nuclei on a 500-MHz spectrometer is approximately 77 MHz. Deuterium has a spin quantum number $I = 1$, making it a quadrupolar nucleus. However, the quadrupole moment of deuterium is relatively small, and the relaxation via the quadrupolar mechanism (**Section 7.3**) is not as rapid as in other quadrupolar nuclei; therefore, it is possible to obtain ^{2}H spectra with good resolution. The

significance of deuterium for NMR spectroscopy is immense, albeit primarily indirect; because of the low sensitivity of ^{2}H nuclei, ^{2}H NMR spectra themselves are not routinely measured.

In NMR spectroscopy, deuterated solvents are commonly used both to suppress the solvent signal in ^{1}H NMR spectra and to "lock" the magnetic field during experiments (**Section 10.2**). In deuterated protic solvents, the hydrogen atoms of OH, SH and NH groups are exchanged for deuterium, thereby simplifying ^{1}H NMR spectra (**Section 4.5**). The rate of ^{1}H exchange with deuterium can be used to determine the accessibility of solvent to individual functional groups. **Fig. 12.14**, for instance, shows that the hydrogen of an amino group involved in a strong intramolecular hydrogen bond is exchanged significantly more slowly than the same hydrogen not participating in a hydrogen bond.

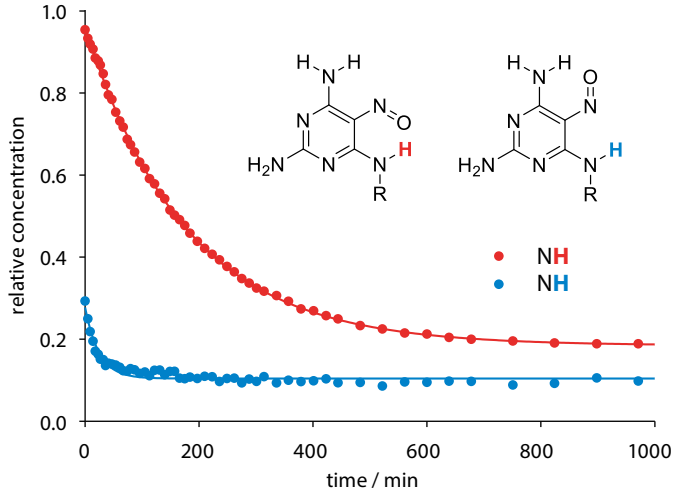

Fig. 12.14: The progressive decrease of the ^{1}H signal in two rotamers of the same compound. Measured in a mixture of CD_3SOCD_3:CD_3OD in a ratio of 9:1

In certain compounds (such as C-acids), hydrogen atoms bound to carbon may also be exchanged for deuterium. In carbon spectra with proton decoupling, this results in the appearance of a carbon CD triplet instead of a CH singlet, which is caused by interaction with deuterium (the spin quantum number $I = 1$ corresponds to three magnetic states). In attached-proton test (APT) experiments, the replacement of hydrogen with deuterium causes a change of signal orientation (a positive signal changes to negative). **Fig. 12.15**, for example, shows the carbon spectra of a mixture of undeuterated and deuterated chloroform ($CHCl_3$ + $CDCl_3$). In the ^{1}H-decoupled carbon spectrum, the $CHCl_3$ signal appears as a singlet, whereas the $CDCl_3$ signal is split into three equally intense lines. The chemical shifts of carbon in $CHCl_3$ and $CDCl_3$ are not identical (δ_{CHCl3} = 77.2 ppm, δ_{CDCl3} = 77.0 ppm). The slight change in chemical shift is caused by the altered vibrational behavior of molecules when the ^{1}H isotope is replaced with the heavier ^{2}H isotope. In the APT spectrum, the $CHCl_3$ signal points downward, like all CH and CH_3 carbons (**Chapter 5**). However, the $CDCl_3$ signal points upward, as the carbon in $CDCl_3$ bears no ^{1}H and thus behaves like a quaternary carbon in the APT experiment.

The chemical shifts of ^{2}H are nearly identical to the chemical shifts of ^{1}H, because the nuclear shielding is determined by electrons, and the electron structure of molecules is only slightly dependent on particular isotopes of the atoms. In certain cases, it is possible to observe small changes in chemical shifts, again due to the different vibrational behavior of molecules with iso-

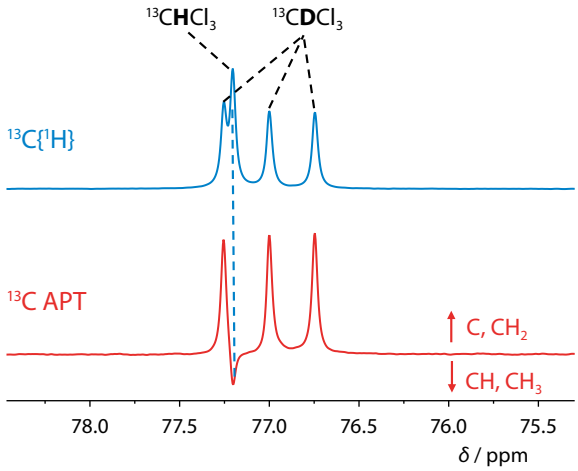

Fig. 12.15: The carbon spectrum with ^1H decoupling (top) and the ^{13}C APT spectrum (bottom) of a $CHCl_3$ and $CDCl_3$ mixture

topes of different masses. ^1H and ^2H spectra for ethanol are compared in **Fig. 12.16**. ^2H,^2H coupling constants are approximately forty times smaller than ^1H,^1H coupling constants (because of the ratio of the squares of the gyromagnetic ratios of ^1H and ^2H nuclei), as a result of which they are usually not observed in deuterium spectra.

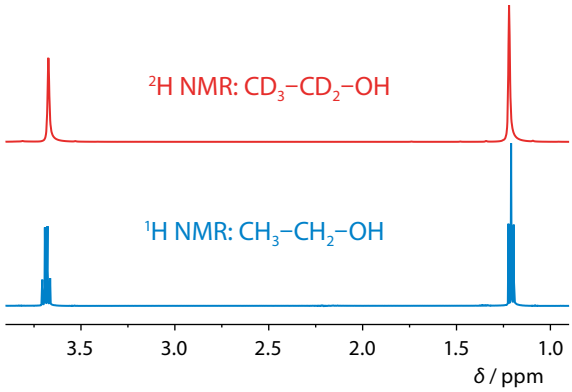

Fig. 12.16: The ^2H spectrum of deuterated ethanol (top) and the ^1H spectrum of ethanol (bottom)

^2H NMR spectroscopy plays a special role in verifying the authenticity of foods and beverages. This verification is based on a method that measures the isotopic ratio ^2H:^1H, which is specific to products with different chemical, botanical and geographical origins. This method, for example, can distinguish between fermented and synthetic ethanol and even determine the geographical origin of fermented ethanol. It is also able to reveal the addition of sugar to fruit juices, wine and honey, as well as to identify the origin of vanillin.

Another hydrogen isotope is ^3H (tritium); it is radioactive (half-life of 12 years) and occurs only in trace amounts in nature. Tritium labeling is used, for example, in drug development—radioactive labels allow for tracking the accumulation of substances in different tissues. Tritium has a spin quantum number $I = ½$ and the highest gyromagnetic ratio among all known isotopes. On a 500-MHz spectrometer, its resonance frequency is 533 MHz. The measurement of ^3H spectra requires specialized probes. An example of spectra from selectively isotope-labeled uracil is provided in **Fig. 12.17**.

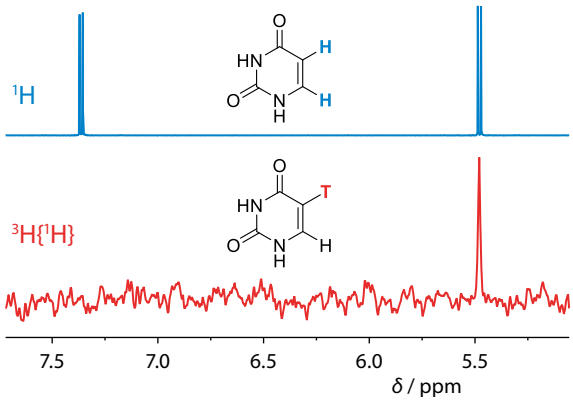

Fig. 12.17: The aromatic hydrogen region in the ^{1}H spectrum of uracil (top) and the ^{3}H spectrum of selectively isotope-enriched uracil with ^{1}H decoupling (bottom)

13

NMR SPECTRUM PREDICTION

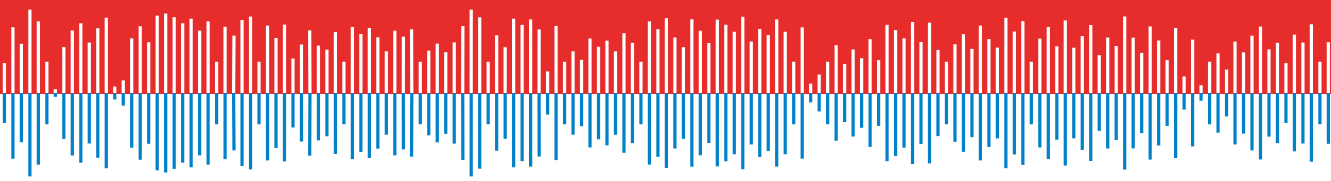

Chapter content

To facilitate the interpretation of NMR spectra, it is useful to have a good idea of what the spectrum of a substance with an assumed structure would look like. A comparison of this predicted spectrum with the actual measured spectrum can assist in signal assignment and also serve as supporting evidence to confirm or disprove the proposed structure. NMR spectra can be predicted using three fundamentally different approaches: analogy, empirical correlations, or quantum-chemical calculations.

13.1 Analogy

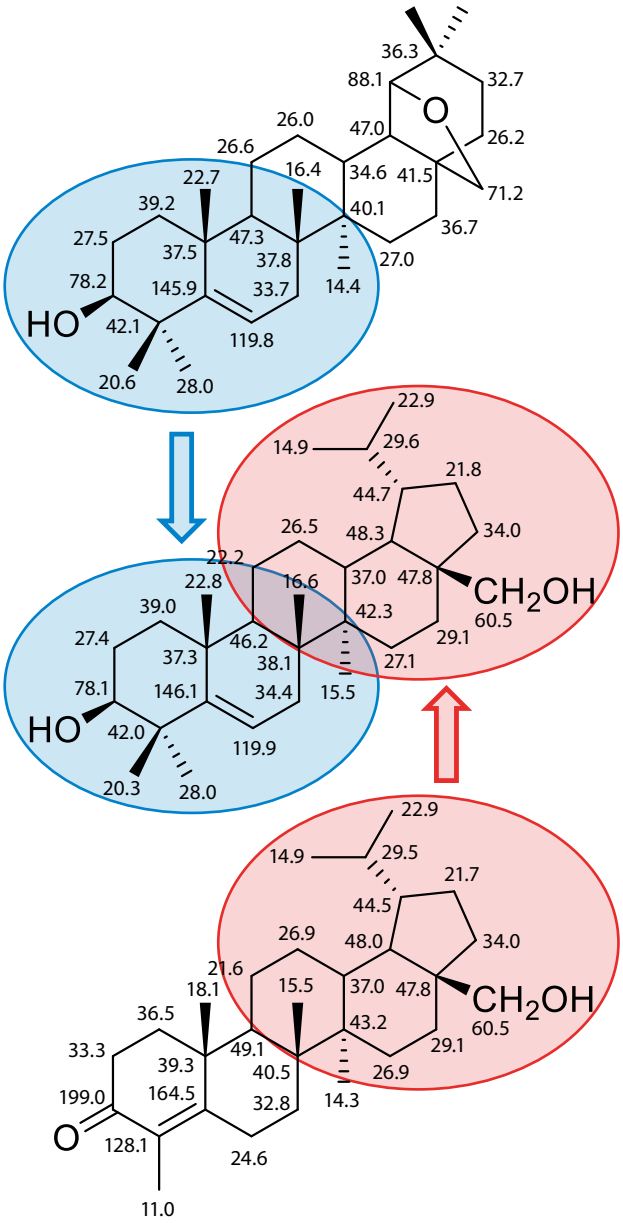

Fig. 13.1: The assignment of carbon signals for a newly synthesized compound (in the center) based on analogy with two compounds with known carbon spectra (the experimental values of ^{13}C chemical shifts are indicated by the numbers in the structures).

NMR parameters primarily reflect the local structure (the immediate environment) of the observed nuclei. Therefore, in larger molecules, changes in one part of the molecule usually do not significantly affect the chemical shifts or other parameters in more distant parts. This can be utilized in predicting chemical shifts and assigning signals if an assigned spectrum of a similar molecule is available. As an example, **Fig. 13.1** illustrates how carbon signals of a newly synthesized triterpenoid can be assigned using the known signal assignments of similar structures measured in the same solvent. The figure shows that a change in the chemical structure at one end of the molecule only leads to minor changes in the carbon chemical shifts in the opposite part of the molecule.

Of course, this approach cannot be used when the structural change leads to, for example, more extensive conformational changes, significantly different interactions with the solvent, or the formation of dimers or other supramolecular structures. Signal assignment based on analogy can also sometimes fail in the case of solid-phase NMR spectra, where chemical shifts are significantly affected by the crystalline environment (see **Chapter 14**).

13.2 Empirical Correlations

Since the early development of NMR spectroscopy, it has been clear that the chemical shifts of individual atoms are not random but reflect the molecular structure. As the amount of experimental data has increased, correlations between structure and chemical shifts have been revealed. In the mid-20th century, James Shoolery published a series of rules for calculating ^{1}H chemical shifts based on empirical correlations. For example, the chemical shifts of hydrogens in substituted methane can be calculated using the formula:

$$\delta_H = 0.23 + a^1 + a^2 + a^3$$

where a_1–a_3 are substitution coefficients, listed in **Table 13.1**. For chloroform, for example, this formula would give an approximate hydrogen-shift value of $\delta_H = 0.23 + 3{\cdot}2.53 = 7.82$. The experimental chemical shift of chloroform ranges between 7 and 8 ppm, depending on the solvent used (it is lower in aromatic solvents). Similar empirical relationships have been proposed for hydrogens in other types of compounds, such as hydrogens on double bonds or aromatic hydrogens.

Table 13.1: Substitution coefficients for determining approximate values of ^{1}H chemical shifts in substituted methane

Substituent R_i	a_i	Substituent R_i	a_i
–H	0	–OH	2.56
$-CH_3$	0.47	$-OC_6H_5$	3.23
$-CF_3$	1.14	$-NR_2$	1.57
–C=C	1.32	–CO–R	3.13
–C≡C	1.44	–Cl	2.53
$-C_6H_5$	1.83	–Br	2.33
–SR	1.64	–I	1.82

The relationships between structure and chemical shifts have also been observed for carbon atoms. The best-known are the empirical rules proposed by Grant and Pauli for alkanes. The chemical shift of carbon is calculated using the formula:

$$\delta_C = -2.3 + 9.1n_\alpha + 9.4n_\beta - 2.5n_\gamma + 0.3n_\delta + 0.1n_\varepsilon + S + K,$$

where n_α–n_ε are the numbers of carbon atoms in the positions α–ε relative to the predicted atom, S is the steric correction factor obtained from **Table 13.2**, and K is the conformational correction factor. For freely rotating bonds in alkanes, K is equal to zero. For 2-methylbutane, it is possible to determine, for example, these approximate chemical shifts for the carbons:

$$\delta_{C1} = -2.3 + 9.1 \cdot 1 + 9.4 \cdot 2 - 2.5 \cdot 1 + 0.3 \cdot 0 + 0.1 \cdot 0 - 1.1 + 0 = 22.0 \text{ ppm}$$

$$\delta_{C2} = -2.3 + 9.1 \cdot 3 + 9.4 \cdot 1 - 2.5 \cdot 0 + 0.3 \cdot 0 + 0.1 \cdot 0 - 3.7 + 0 = 30.7 \text{ ppm}$$

$$\delta_{C3} = -2.3 + 9.1 \cdot 2 + 9.4 \cdot 2 - 2.5 \cdot 0 + 0.3 \cdot 0 + 0.1 \cdot 0 - 2.5 + 0 = 32.2 \text{ ppm}$$

$$\delta_{C4} = -2.3 + 9.1 \cdot 1 + 9.4 \cdot 1 - 2.5 \cdot 2 + 0.3 \cdot 0 + 0.1 \cdot 0 + 0.0 + 0 = 11.2 \text{ ppm}$$

Table 13.2: The values of steric correction factors used in predicting ^{13}C chemical shifts in alkanes

Observed ^{13}C	The most branched carbon atom in α position to the observed atom			
	CH_3	CH_2	CH	C
methan	0.0	0.0	0.0	0.0
CH_3	0.0	0.0	−1.1	−3.4
CH_2	0.0	0.0	−2.5	−7.5
CH	0.0	−3.7	−9.5	−15.0
C	−1.5	−8.4	−15.0	−25.0

The predicted and experimental values of the carbon chemical shifts for 2-methylbutane are shown in **Fig. 13.2**.

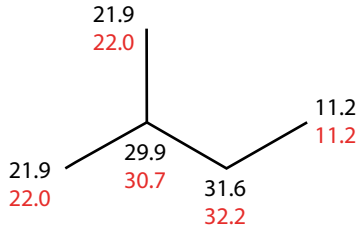

Fig. 13.2: The observed (in black) and predicted (in red) values of ^{13}C chemical shifts in 2-methylbutane

13.3 NMR Predictors

NMR predictors are software tools that predict the appearance of NMR spectra based on the structure of substances. Some programs predict NMR spectra solely based on the previously described (or similar) empirical correlations between structure and chemical shifts, or even coupling constants. These predictions are fairly reliable when the studied structure is similar to those for which empirical correlations have been developed. For example, the chemical shifts predicted for ^{13}C in saturated hydrocarbons are likely to align well with experimental values. However, if the studied structure contains less common structural fragments or if intramolecular or intermolecular interactions play a crucial role in the resulting NMR spectrum, predictors based on empirical correlations can be highly unreliable, with errors in ^{13}C chemical-shift predictions reaching several dozen ppm.

More sophisticated NMR predictors utilize not only empirical correlations but also an internal database of compounds for which NMR parameters are known. When a spectrum is predicted for a particular structure, the predictor searches this database for similar molecules or structural

fragments. The proposed chemical shifts are usually based on a combination of both approaches—empirical correlations and analogy. However, it still holds that if the studied structure or part of it is unusual, NMR predictors may fail catastrophically in predicting chemical shifts.

13.4 Quantum-Chemical Calculations

Quantum-chemical calculations can be used to compute NMR parameters for any structure, even for those that do not exist in reality. There is thus no need to know any experimental data about the substance studied or analogous compounds. A detailed discussion of quantum-chemical methods and their principles goes far beyond the scope of this textbook. Generally, the methods most commonly used for calculating NMR parameters now are based on *density functional theory* (DFT). Quantum-chemical methods can calculate not only chemical shifts but also scalar coupling constants and other molecular properties. If necessary, it is also possible to model dynamic molecular behavior and its effect on NMR parameters (e.g. relaxation times or coalescence temperature). Additionally, one can study intermolecular interactions and their influence on NMR spectra.

To perform a calculation, the molecular structure is required, along with keywords indicating the chosen method and the properties to be computed. Parameters are calculated for the given structure. Therefore, in order to achieve calculated values close to the experimental ones, the input structure should be as close as possible to the actual structure of the substance in the sample. Before the calculation, the geometry of the studied molecule is thus typically optimized to find the molecular geometry with the lowest energy. This can be particularly challenging for flexible molecules or those with more complex conformational equilibria.

An example of a structural problem that can be elegantly solved using quantum-chemical calculations is shown in **Fig. 13.3**. Sulfur in the depicted bicyclic monosaccharide derivative can easily be oxidized to sulfoxide. However, this oxidation results in two diastereomeric sulfoxides, differing in the orientation of the oxygen attached to the sulfur; sulfur in these sulfoxides serves as a chiral center (as it is attached to three different substituents, with a lone electron pair acting as the fourth substituent). Using NMR spectroscopy alone to determine the configuration at the sulfur atoms in the resulting sulfoxides is very difficult—it is not possible to utilize any indirect spin–spin interactions or NOE. Nevertheless, the oxidation of sulfide to sulfoxide leads to significant changes $\Delta\delta$ in the chemical shifts of neighboring carbon atoms. **Fig. 13.3** shows the observed $\Delta\delta(^{13}C)$ values and those calculated using DFT. By comparing experimental and calculated values, the configuration of the individual sulfoxides can be unequivocally determined.

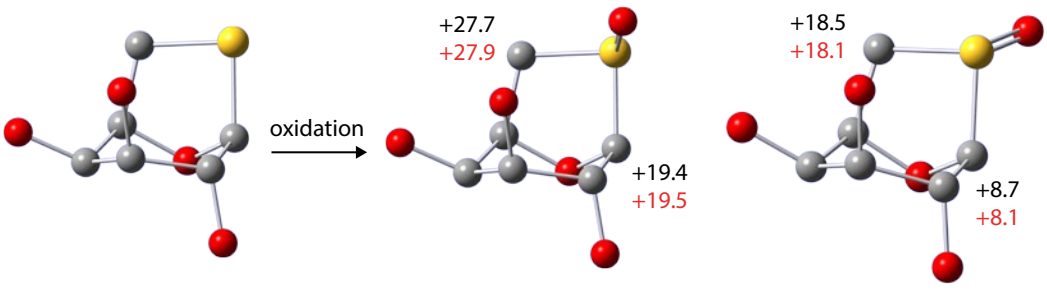

Fig. 13.3: Changes in the carbon chemical shifts $\Delta\delta$ induced by the oxidation of sulfide to sulfoxide. By comparing the experimental values (in black) with the calculated values (in red), the structure can be unambiguously assigned to individual diastereomers (for clarity, hydrogen atoms are not shown; the color coding of the atoms: carbon = **gray**, oxygen = **red**, sulfur = **yellow**)

13.5 Machine-Learning Predictions of Chemical Shifts

Machine learning (ML) has recently become a powerful tool for predicting NMR parameters. ML models for predicting chemical shifts use large datasets of known experimental chemical shifts or calculated shieldings as training data. ML models, once trained, can quickly predict chemical shifts for new molecules. This is particularly valuable for large molecules such as proteins, where computational-chemistry methods are slow. High-quality, experimentally-verified NMR data are crucial for training, but such data can be limited, especially for less common elements or complex molecular environments. Furthermore, like empirical correlations, ML models may struggle with generalizing to molecules that are very different from those in the training set, especially in terms of electronic environments or unusual chemical motifs. An example of a web application that can be used for the online ML predictions of ^{1}H and ^{13}C chemical shifts can be found at **https://nova.chem.colostate.edu/cascade/predict/**.

13.6 Spectrum Simulation

Using all the aforementioned types of calculations, we can predict chemical shifts and other NMR parameters for a given structure. However, this is not sufficient for simulating spectra that resemble real NMR spectra. The simulations must also incorporate signal linewidths caused by T_2 relaxation, multiplet-shape simulation (e.g. the roof effect in an AB spin system), and the influence of dynamic processes on the resulting spectrum. It is even more complicated to simulate NMR spectra for solids, where it is necessary to consider, in addition to isotropic chemical shifts, also chemical-shift anisotropy, direct dipole–dipole interactions, quadrupolar interactions of nuclei with spin quantum numbers greater than ½, as well as the speed of magic-angle spinning and the orientation of individual crystallites in a powdered sample. NMR spectra can be simulated using specialized software tools based on the given parameters.

14

NMR SPECTROSCOPY OF SOLIDS

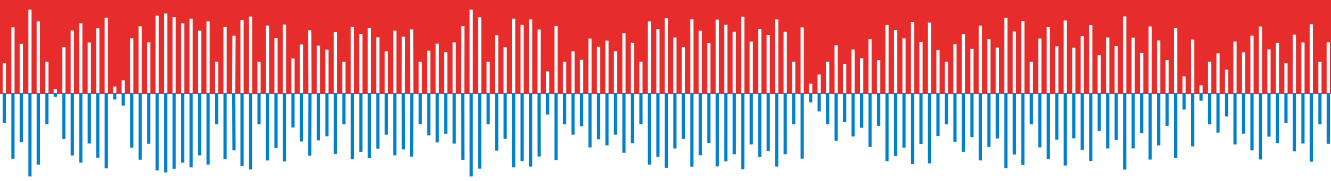

Chapter content

The entire previous text focused on experiments and data interpretation for substances in solution. However, NMR spectroscopy also enables the measurement of gaseous and solid samples. The measurement technique for gaseous samples is similar to that for solutions. The only difference lies in sample handling, such as the use of pressure NMR tubes. For gaseous samples, we can even use the same probes as for solution measurements.

The measurement of solid samples in NMR, however, is significantly different from experiments with solutions or gases. The rapid reorientation of molecules in solution suppresses certain electromagnetic interactions, which simplifies the spectra. In solids, molecular movement is restricted, and spectra measured similarly to those in solutions result in very broad and difficult-to-interpret signals. Therefore, special techniques have been developed for measuring solids to narrow the signals.

The NMR spectroscopy of solids provides unique information about their structure. It is used, for example, in materials chemistry to characterize solid materials or in the pharmaceutical industry to study polymorphism (the ability of substances to crystallize in multiple crystalline structures), which is very important for the bioavailability of active pharmaceutical ingredients.

This chapter first examines the fundamental differences between the NMR spectroscopy of solutions and solids, after which it presents some examples of solid-state NMR spectroscopy.

14.1 Principles of NMR Spectroscopy of Solids

14.1.1 Chemical Shift in Solids

Nuclear shielding by electrons depends on the orientation of the molecule in the magnetic field $\boldsymbol{B}_0$. For carbon nuclei, the chemical shift can vary by several hundred ppm based on this orientation. In solution, due to the rapid isotropic reorientation of molecules, electron shielding averages, as a result of which there is a single signal for each nonequivalent nucleus in the spectra; this chemical shift is then referred to as the **isotropic chemical shift**. In solids, this rapid reorientation of molecules does not occur. If we were to measure a single crystal, the position of the signals in the spectrum would be controlled by the orientation of the crystal in the magnetic field of the spectrometer. In the vast majority of cases, however, we measure powder samples, where all possible molecular orientations are randomly represented. Each orientation contributes to the resulting spectrum, which contains very broad signals caused by the overlap of signals from molecules with different orientations in the magnetic field.

Fig. 14.1 shows the spectrum of powdered glycine. The signal of the carbonyl carbon is significantly broader than the signal of the C_α carbon, because the shielding of the carbonyl carbon is

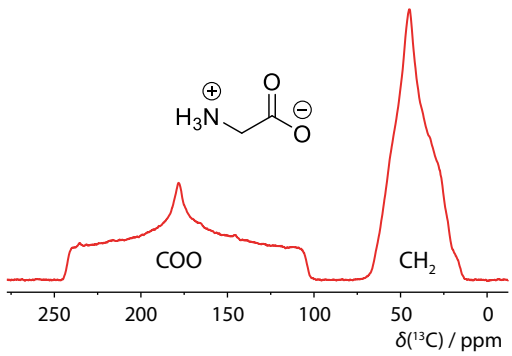

Fig. 14.1: The static ^{13}C NMR spectrum of crystalline glycine measured with ^{1}H nucleus decoupling

more dependent on the molecular orientation (the anisotropy of the chemical shielding of the carboxyl carbon is greater).

For more complex molecules, the broad individual signals measured in this way would overlap in the spectra, complicating interpretation. Therefore, solid-state NMR measurements often involve the technique of **magic-angle spinning (MAS)**, which to some extent suppresses chemical-shift anisotropy.

14.1.2 Magic-Angle Spinning

The magic angle θ_m is approximately 54.7° (the exact value is derived from the formula $3\cos^2\theta_m = 1$), which is the angle formed by the edge of a cube with its diagonal. If the sample rotates at this magic angle in a magnetic field, individual molecules assume all possible orientations relative to the magnetic field over time. Magic-angle spinning thus partially simulates isotropic molecular movement in liquids. The effect on the resulting spectrum depends on the rate of rotation (in Hz); if it is sufficiently high, only the averaged (isotropic) chemical shifts are observed and the resulting spectra resemble those of solutions. However, if the rate of magic-angle spinning is insufficient, anisotropic shielding is not completely suppressed and the spectra show spinning sidebands (see **Fig. 14.2**). The ^{13}C spectra of powdered glycine measured with different magic-angle spinning speeds contain spinning sidebands that are always a multiple of the rotation frequency away from the central isotropic signal. For example, at a rotation of 1,000 Hz, the spinning sidebands in the spectrum are exactly 1,000 Hz apart. On a 600-MHz spectrometer, operating at a working frequency of 150 MHz for ^{13}C, the sidebands are approximately 6.7 ppm apart (1,000 / 150 = 6.$\overline{6}$).

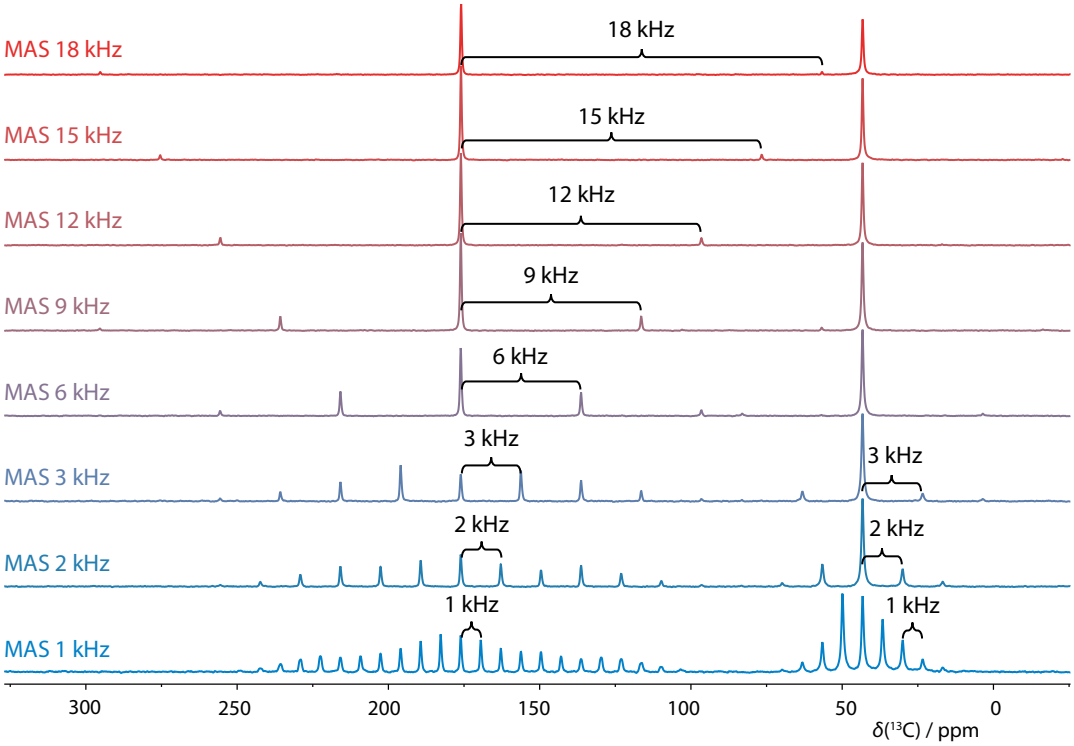

Fig. 14.2: The ^{13}C NMR spectra of crystalline glycine measured with different magic-angle spinning speeds (values in kHz for each spectrum) and with ^{1}H decoupling

The speed of magic-angle spinning required for the complete suppression of anisotropic interactions depends on the magnitude of the interaction. For example, if the chemical-shielding anisotropy is 100 ppm, it corresponds to 15,000 Hz on a 600-MHz spectrometer, which means that the rotation rate must be on the order of this value. In **Fig. 14.2**, it is evident that the anisotropy of the chemical shielding of the C_α carbon is suppressed at a lower rotation rate than that of the carbonyl carbon because the anisotropy of C_α is smaller.

Rotating a sample at speeds on the order of kilohertz is technically quite demanding. Samples are placed in rotors made of durable materials (such as ZrO_2) because significant centrifugal forces act on the rotor walls during the rotation. The rotor is sealed on one side with a cap containing a "turbine," and the sample is spun by a stream of air or nitrogen directed at this turbine. The maximum rotation rate is determined by the outer diameter of the rotor to ensure that the surface of the rotor does not exceed the speed of sound in the air. **Fig. 14.3** shows examples of rotors with different diameters and their corresponding maximum magic-angle spinning speeds. For instance, rotors with an outer diameter of 3.2 mm, which are among the most commonly used, achieve a maximum rotation rate of 24 kHz, which is sufficient to suppress the chemical-shielding anisotropy of ^{13}C nuclei.

An interesting fact is that rotors for solid-state NMR spectroscopy are among the fastest man-made rotating macroscopic objects with a practical purpose. The second-fastest rotating macroscopic objects are parts of dental drills, but even the fastest of these rotate at speeds about ten times slower than the rotors used in NMR.

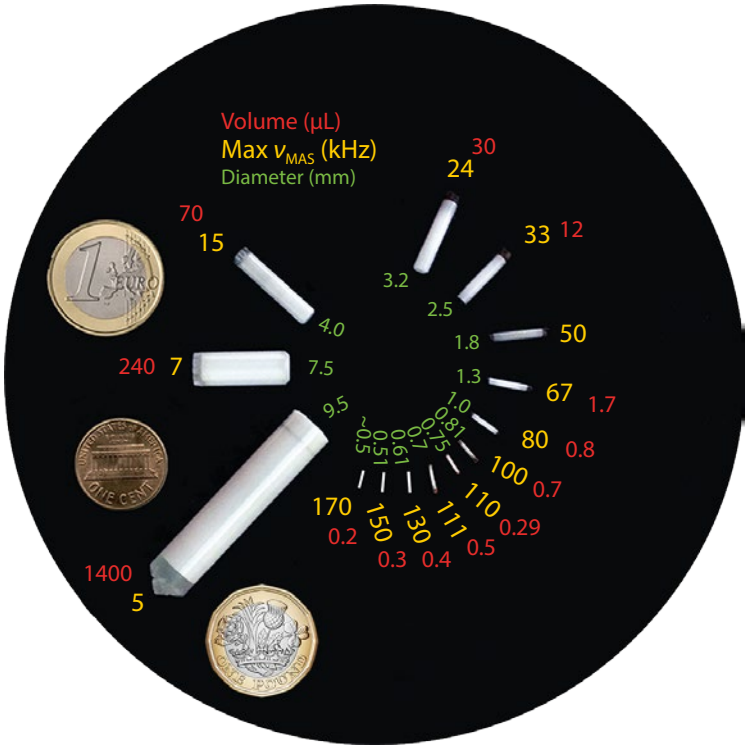

Fig. 14.3: The rotors with different outer diameters used for measuring solid-state NMR spectra. The image shows the sample volume (in µL, **red** numbers), the maximum magic-angle spinning speed (in kHz, **orange** numbers), and the outer rotor diameter (in mm, **green** numbers). Some common coins are included for comparison. The picture has been provided by Prof. J. Lewandowski (University of Warwick)

14.1.3 Direct Dipole–Dipole Interactions

In Section 2.6, it was mentioned that there are two types of interactions between nuclear spins—direct and indirect. Direct spin–spin interactions (or dipole–dipole, dipolar interactions) are interactions through space, and their magnitude depends on the distance between the interacting nuclei, the gyromagnetic ratios of the interacting nuclei, and the orientation of the vector connecting these nuclei with respect to the magnetic field $\boldsymbol{B}_0$. In solution, due to isotropic molecular motion, this interaction averages out to a mean value of zero. Therefore, in the context of the NMR spectroscopy of solutions, this interaction could be entirely neglected, and it was only mentioned as one of the important relaxation mechanisms (Section 7.3).

Nevertheless, in solid-state NMR measurements, dipolar interactions are extremely important. Heteronuclear dipolar couplings, similarly to indirect heteronuclear coupling, can be suppressed by broadband decoupling. All the carbon spectra of glycine shown in Figures 14.1 and 14.2 have been measured with proton decoupling. When measuring the proton spectra of solids, however, dipolar couplings pose a problem. Homonuclear dipolar ^{1}H,^{1}H interactions cannot be removed by broadband decoupling, and the strength of dipolar couplings between closely spaced hydrogen nuclei can reach tens of kHz. Therefore, the removal of these couplings using magic-angle spinning requires higher spinning speeds than the suppression of chemical-shielding anisotropy. For proton-spectrum measurements, it is necessary to use rotors with small outer diameters. It is con-

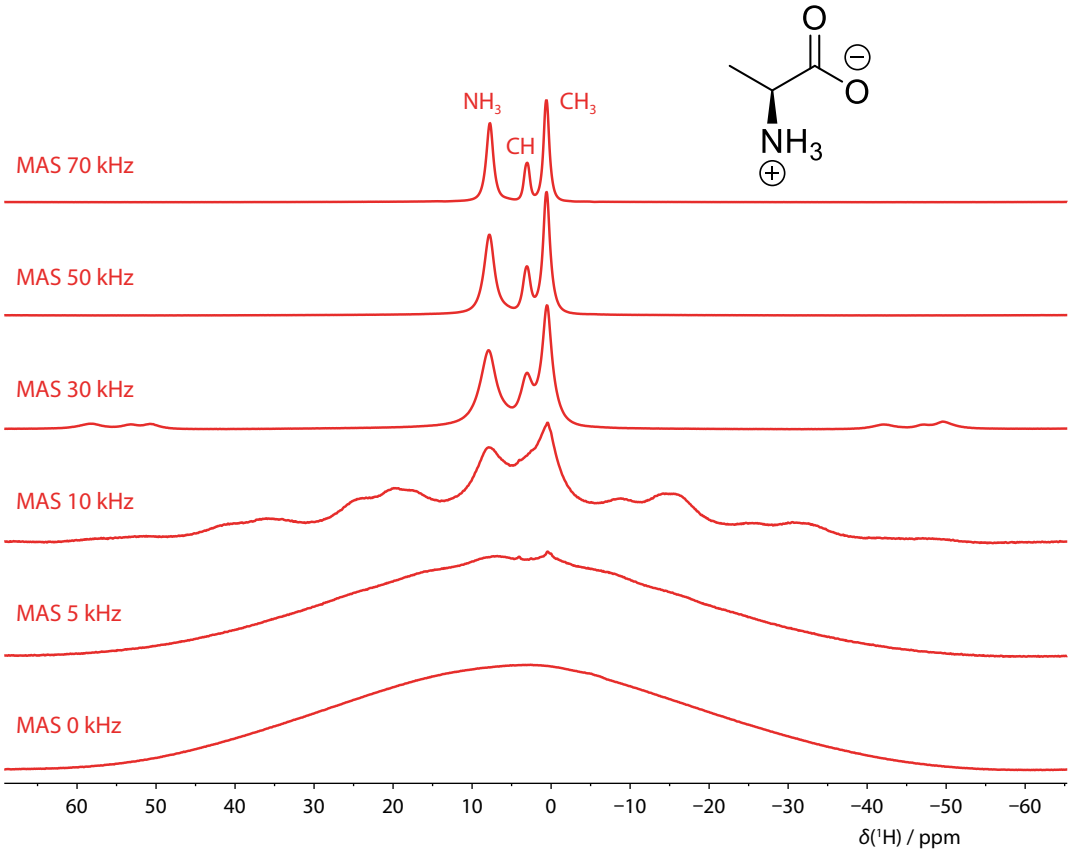

Fig. 14.4: The proton spectra of solid alanine measured at different spinning speeds at the magic angle (values in kHz next to individual spectra)

siderably more difficult to handle these rotors, including their filling and cleaning, than to work with larger rotors. Even at high spinning speeds, the signals in the ^{1}H spectra of solids are significantly broader than those in solution spectra. **Fig. 14.4** shows the proton spectra of crystalline alanine measured without spinning and with magic-angle spinning at speeds from 5 to 70 kHz.

Dipole–dipole interactions can also be utilized in solution measurements. As mentioned earlier, upon isotropic molecular motion in solution, dipolar interactions average out to zero. However, if molecular motion is restricted, dipolar couplings are not completely suppressed and can be detected. Since the magnitude of the dipolar coupling depends on the distance between the interacting atoms, it is possible to use the values obtained from **residual dipolar coupling** (RDC) constants to determine molecular conformation or configuration. This technique involves measuring NMR spectra in an anisotropic medium, such as liquid crystals or gels formed by certain polymers. In these environments, molecular motion is not isotropic, and dipolar interactions are not fully suppressed in the spectra.

14.1.4 Indirect Spin–Spin Interactions

Indirect spin–spin interactions, i.e. magnetic interactions between nuclei mediated by electrons, are of great importance in solution NMR spectroscopy (**Section 2.6**), where the size of coupling constants is one of the most important tools for determining molecular structures. However, indirect homonuclear spin–spin interactions in the ^{1}H spectra of solids are practically inaccessible, as their values are much smaller than the linewidths of spectral lines. Indirect heteronuclear $^{13}C,^{1}H$ interactions in carbon spectra are removed along with dipolar $^{13}C,^{1}H$ interactions by decoupling. As a result, indirect spin–spin interactions are utilized less frequently in solid-state spectra measurements than in solution. Only at very high magic-angle spinning speeds, where direct dipolar interactions are suppressed, it is possible to use indirect interactions for measuring $^{13}C,^{1}H$ correlation spectra (HSQC-type spectra, **Section 5.3**). More commonly, direct spin–spin interaction is employed to measure $^{13}C,^{1}H$ correlations. It is important to bear in mind that the direct spin–spin interaction is a through-space interaction leading to correlations between spatially close nuclei, whereas the indirect spin–spin interaction is a through-bond interaction.

14.1.5 Quadrupolar Interactions

When measuring solid-state NMR spectra, it is also necessary to consider quadrupolar interactions. These are the interactions between the electric quadrupole moment of a nucleus and the electric-field gradient created by surrounding nuclei and electrons. These interactions occur during the measurement of quadrupolar nuclei, i.e. nuclei with a spin quantum number greater than ½. Their magnitude again depends on the orientation of the molecule relative to the magnetic field, and in solution, they average out to a mean value of zero. Quadrupolar interactions significantly contribute to the relaxation of spin states in solution (**Section 7.3**). In the solid-state spectra of quadrupolar nuclei, quadrupolar interactions lead to line broadening; in many cases, this broadening is greater than that caused by chemical-shielding anisotropy, with linewidths reaching several thousand ppm. Quadrupolar interactions cannot be completely removed by magic-angle spinning.

An example of a quadrupolar-nucleus spectrum is the ^{2}H spectrum of the crystalline sodium salt of guanine-5'-monophosphate hydrate recrystallized from D_2O (**Fig. 14.5**). Note that the spectrum spans several thousand ppm, even though deuterium chemical shifts in solutions are observed in the same region as ^{1}H shifts, i.e. approximately from 0 to 10 ppm (**Section 12.4**).

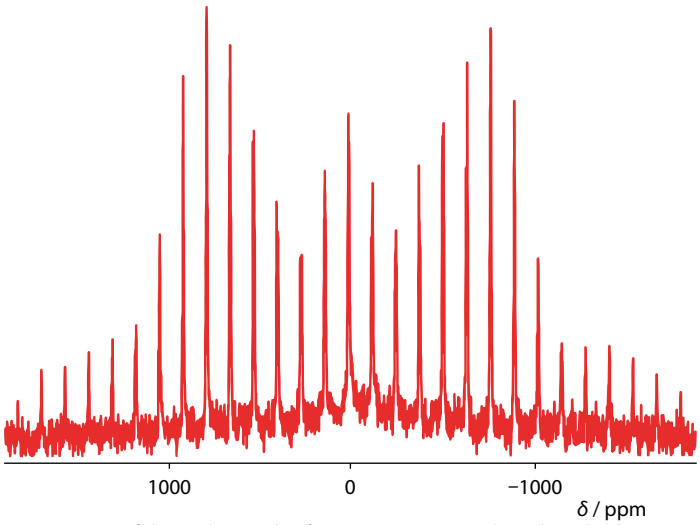

Fig. 14.5: The ^{2}H NMR spectrum of the sodium salt of guanine-5'-monophosphate hydrate recrystallized from D_2O. The spectrum has been measured with magic-angle spinning at 12 kHz.

14.1.6 Cross Polarization

Cross polarization (CP) is a commonly used technique in solid-state NMR spectroscopy, where polarization is transferred from sensitive nuclei with high natural abundance and large gyromagnetic ratios γ (most commonly protons, ^{1}H) to less sensitive nuclei (such as ^{13}C). Polarization transfer is achieved by simultaneously irradiating both nuclei with radiofrequency radiation at precisely defined intensities, causing the magnetization vectors of both the hydrogen and carbon nuclei to precess at the same rate (the Hartmann-Hahn condition). In addition to enhancing the sensitivity of carbon-nucleus measurements by transferring polarization from protons, the advantage of cross polarization is that the repetition time of the experiment is determined by the relaxation time T_1 of the ^{1}H nuclei rather than the ^{13}C nuclei. Proton nuclei usually relax more rapidly than carbon nuclei.

Routine measurement of carbon spectra in solids use a combination of these techniques: magic-angle spinning (to suppress nuclear-shielding anisotropy), broadband proton decoupling (to eliminate both direct and indirect $^{13}C,^{1}H$ spin–spin interactions), and cross polarization (to enhance sensitivity).

14.2 Examples of the Use of Solid-State NMR Spectroscopy – NMR Crystallography

Crystallography is primarily associated with X-ray structural analysis. By measuring the diffraction of X-rays caused by the presence of electrons, it is possible to determine the crystal structure, which is easiest when a sufficiently high-quality single crystal of the studied substance is available. Determining the crystal structure of microcrystalline substances (powdered samples) is significantly more difficult and, in many cases, impossible. Additional challenges for X-ray structural analysis are posed by crystalline substances with disordered parts or amorphous materials.

Solid-state NMR spectroscopy makes it possible to obtain important structural information about both crystalline and amorphous substances without the need for a long-range order (regularly repeating identical structural units, unit cells), because NMR spectra primarily reflect the local

structure. Furthermore, NMR experiments are suitable for studying dynamic processes in solid materials, such as the mobility of solvent molecules in solid solvates. NMR spectroscopy is thus, to some extent, complementary to X-ray structural analysis. Let us consider several phenomena commonly encountered when measuring solid-state spectra.

14.2.1 Polymorphism

Polymorphism is the ability of substances to crystallize in multiple crystal structures. Some substances are known to have more than ten different crystal structures. Crystal structure significantly influences the properties of solid substances. Polymorphs of the same substance can differ in color, melting point, dissolution rate, and other properties. Polymorphism plays a crucial role in the pharmaceutical industry, because, for example, different dissolution rates affect the bioavailability of pharmaceutically active substances.

The diverse crystal structures in polymorphs result in different nuclear shielding, which leads to distinct NMR spectra. Using NMR spectroscopy, we can easily monitor the polymorphic purity of solid substances; the great advantage is that it enables tracking polymorphic forms of substances even in tablets, where they are mixed with other compounds. An example of a carbon spectrum of a polymorph mixture is shown in **Fig. 14.6**.

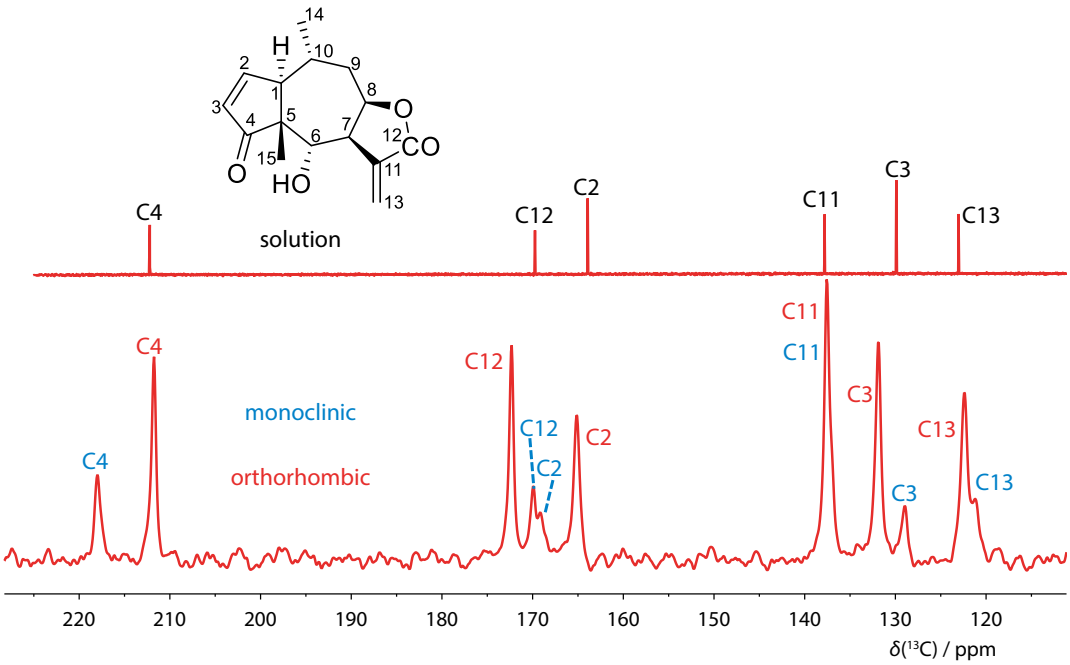

Fig. 14.6: A part of the ^{13}C NMR spectrum of a mixture of monoclinic and orthorhombic polymorphs of helenalin, measured with magic-angle spinning at a speed of 13 kHz. The ^{13}C spectrum of the same substance in solution is also shown for comparison.

14.2.2 Solvates

Solid-state NMR spectra can be influenced not only by polymorphism but also by the presence of solvent molecules in the crystal lattice. Solvates (including hydrates), where the solvent is present in the crystal lattice, are sometimes described using the term pseudopolymorphism. **Fig. 14.7** shows the carbon spectra of a substance obtained in its monohydrate and anhydrous forms.

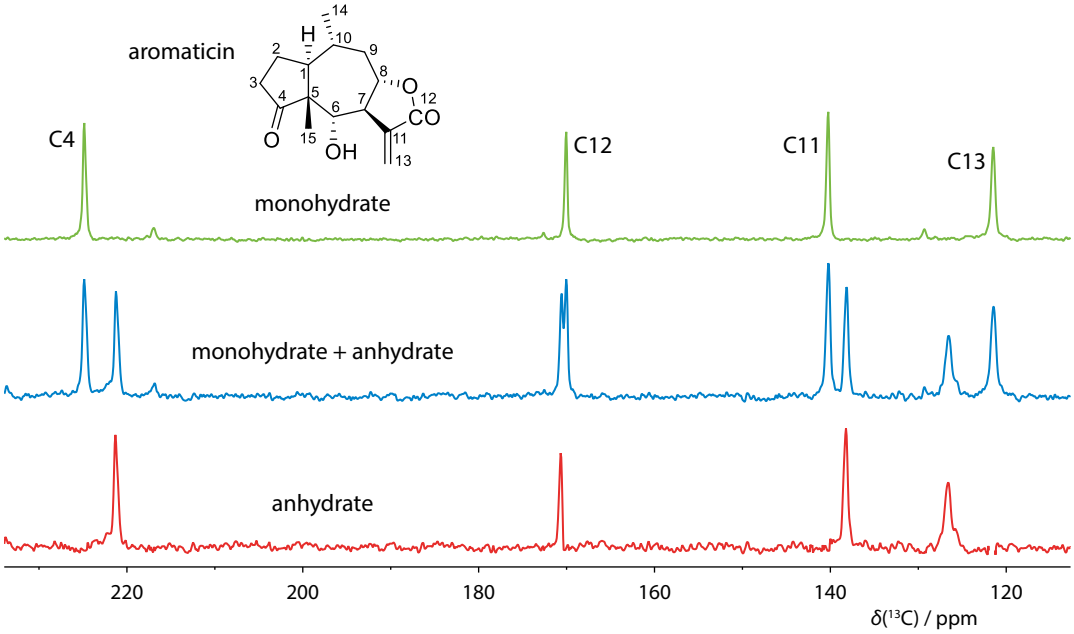

Fig. 14.7: A part of the ^{13}C NMR spectra of the displayed substance, which has been crystallized as a monohydrate (top), anhydrate form (bottom), and as a mixture of monohydrate and anhydrate forms (middle)

14.2.3 The Presence of Multiple Molecules in an Asymmetric Unit

Crystalline substances may contain multiple crystallographically nonequivalent molecules of a single substance (one chemical entity), which differ in their crystal environment. When such a substance is dissolved, the NMR spectrum shows one set of signals. On the other hand, in the spectra of solid substances, each crystallographically nonequivalent molecule has its own set of signals. An example is shown in **Fig. 14.8**, depicting the spectrum of crystalline leucine, which has two nonequivalent molecules in its crystal lattice.

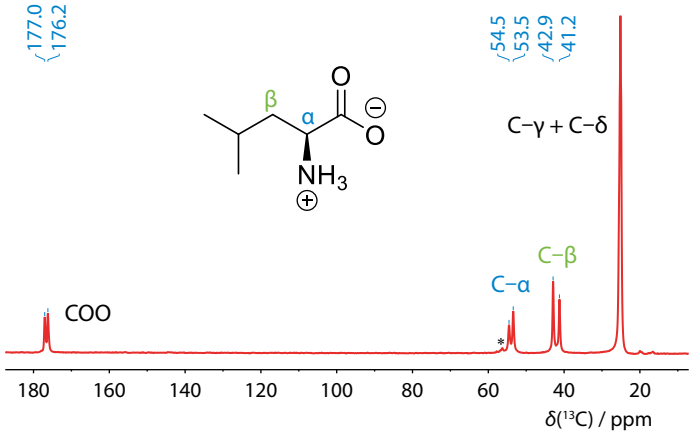

Fig. 14.8: The ^{13}C NMR spectrum of crystalline leucine with two crystallographically nonequivalent molecules in the crystal structure. A spinning sideband of the carbonyl carbon is marked with an asterisk. Measured with magic-angle spinning at a speed of 18 kHz

MATERIALS FOR FURTHER STUDY

This textbook by no means covers the full breadth and depth of the science of NMR spectroscopy. Only the basic concepts most commonly encountered by the chemist-user of NMR spectroscopy have been introduced. Moreover, only minimal space has been devoted in this textbook to practicing the solution of structures of unknown substances from spectra. Yet for the interpretation of NMR spectra, it is true (as in any field) that practice makes perfect. The reader/student who would like to practice solving the structures of unknown substances from one- and two-dimensional spectra using simple examples should visit the interactive webpage **nmr-challenge.com** with more than 200 spectral assignments measured for real samples.

For readers whose interest in NMR spectroscopy has been sparked by this book, the following is a selection of textbooks that may serve as excellent resources for further study. While not exhaustive, this list reflects, in part, the author's personal preferences and experience.

Textbooks of NMR spectroscopy

H. Friebolin: *Basic One- and Two-Dimensional NMR Spectroscopy*. 5th edition, Wiley-VCH, Weinheim, 2010. ISBN-13: 978-3527327829

H. Günther: *NMR Spectroscopy: Basic Principles, Concepts and Applications in Chemistry*. 3rd edition, Wiley-VCH, Chichester, 2013. ISBN-13: 978-3527330003

J. Keeler: *Understanding NMR Spectroscopy*. 2nd edition, John Wiley & Sons, Chichester, 2010. ISBN-13: 978-0470746080

M. H. Levitt: *Spin Dynamics: Basics of Nuclear Magnetic Resonance*. 2nd edition, John Wiley & Sons, Chichester, 2008. ISBN-13: 978-0470511176

T. D. W. Claridge: *High-Resolution NMR Techniques in Organic Chemistry*. 3rd edition, Elsevier Science, Oxford, 2016. ISBN-13: 978-0080999869

D. C. Apperley, R. K. Harris, P. Hodgkinson: *Solid-State NMR: Basic Principles and Practice*. Momentum Press, New York, 2012. ISBN-13: 978-1606503508

P. J. Hore, J. A. Jones, S. Wimperis: NMR: THE TOOLKIT: *How Pulse Sequences Work*. 2nd Edition, Oxford University Press, Oxford, 2015. ISBN-13: 978-0198703426

Exercise book for solving NMR spectra

L. D. Field, H. L. Li, A. M. Magill: *Organic Structures from Spectra*. 6th edition, John Wiley & Sons, Chichester, 2020. ISBN-13: 978-1119524809